Enzyme Assays in Assessing Respiratory Metabolism in Marine Plankton.

The development of a new CO_2-production proxy and further applications of respiratory enzymatic assays in oceanography

Doctoral dissertation
for the Ph.D. degree in Oceanography and Global Change

Maria Teresa Tames Espinosa

Instituto de Oceanografía y Cambio Global
Universidad de Las Palmas de Gran Canaria
Las Palmas de Gran Canaria

15 May 2019

D. SANTIAGO HERNÁNDEZ LEÓN COORDINADOR DEL PROGRAMA DE DOCTORADO DE OCEANOGRAFÍA Y CAMBIO GLOBAL DE LA UNIVERSIDAD DE LAS PALMAS DE GRAN CANARIA,

INFORMA,

Que la Comisión Académica del Programa de Doctorado, en su sesión de fecha veinticuatro de mayo de dos mil diecinueve tomó el acuerdo de dar el consentimiento para su tramitación, a la tesis doctoral titulada "Enzyme Assays in Assessing Respiratory Metabolism in Marine Plankton. The development of a new CO_2-production proxy and further applications of respiratory enzymatic assays in oceanography" presentada por la doctoranda Dª María Teresa Tames Espinosa y dirigida por la Dra. May Gómez y el Dr. Theodore T. Packard.

Asimismo, se acordó el informar favorablemente la solicitud para optar a la Mención Internacional del Título de Doctor, por cumplir los requisitos reglamentarios.

Y para que así conste y a efectos de lo previsto en el Artº 11 del reglamento de Estudios de Doctorado (BOULPGC 7/10/2016) de la Universidad de Las Palmas de Gran Canaria, firmo la presente en Las Palmas de Gran Canaria, a veinticuatro de mayo de dos mil diecinueve.

Enzyme Assays in Assessing Respiratory Metabolism in Marine Plankton.

The development of a new CO₂-production proxy and further applications of respiratory enzymatic assays in oceanography

DOCTORAL DISSERTATION
for the Ph.D. degree in Oceanography and Global Change

Tesis doctoral presentada por María Teresa Tamés Espinosa
dentro del Programa de Doctorado en Oceanografía y Cambio Global

Dirigida por los Doctores
May Gómez Cabrera y Theodore Train Packard

El doctorando   El/La director/a   El/La director/a

Instituto de Oceanografía y Cambio Global
Universidad de Las Palmas de Gran Canaria

En Las Palmas de Gran Canaria a 15 de Mayo de 2019

A mis padres

Agradecimientos/Acknowledgements

Sin duda, ésta es la parte más profunda y personal de todo el documento que tienen entre manos. Es el momento en el que reflexionamos, a solas, acerca del periodo que hemos vivido en los últimos años, y prestamos atención a las personas que nos han acompañado en el camino. Curiosamente, yo lo empiezo a escribir en una cafetería de Vitoria, en un huequito que he sacado de entre las reuniones y fiestas familiares de una Navidad cualquiera. Y es que a los primeros a los que he de agradecer el haber llegado hasta aquí es sin duda a mi familia,a la más cercana, a mis padres. Creedme, soy muy consciente de que no debe ser nada fácil ver que tu única hija abandona un trabajo y un entorno seguro por culpa de una "vocación". Gracias no, GRACIAS por apoyarme en cada paso y en cada momento, aun no estando siempre plenamente de acuerdo. Asimismo, este agradecimiento no sería del todo justo si no lo extendiera a todos mis tíos y primos, que sé que siempre han estado, están y estarán ahí con nosotros. Gracias Familia.

Por otra parte, debo agradecer el ejemplo, el apoyo, el tesón, la guía y los muchos abrazos de esta otra familia, la académica, que es el grupo EOMAR. Un grupo que, bajo la dirección de la Prof. May Gómez, tiene como seña de identidad la calidad humana, tan importante en la ciencia y más en momentos como en el que nos encontramos. Gracias May por no cesar en la protección de esos valores y por tu gran fuerza y tesón para encontrar siempre nuevos caminos y salidas que, sin duda, nos hacen cada día más fuertes y mejores. Asimismo, gracias, Ted: Por ser el ejemplo perfecto de la mezcla genialidad y humanidad que sé que siempre nos guiará cuando nos sintamos más perdidos. Eres una fuente de enseñanzas, no "sólo" por los conocimientos que transmites o por los que ayudas a generar, sino por aquellos que sólo los verdaderos sabios poseen y saben fomentar. May y Ted, sin duda ha sido un lujo teneros a los dos como directores de esta tesis.

Además, debo agradecer también a nuestros compañeros "veteranos" Fede, Igor y Natalia, por mostrar unas pinceladas de la dirección que puede tomar este camino. Gracias también a Ali, sobre todo por volver, y así tener la oportunidad de conocer algo más de la persona y científica extraordinaria que eres... tu forma de trabajar unida a tu eterna sonrisa y palabras de apoyo te hacen la compañera perfecta y un modelo a seguir. En esta línea, no puedo dejar de darle las gracias también a Ico, porque sin ti a EOMAR le faltaría algo. Sin duda el trabajo en el laboratorio se vuelve fácil cuando podemos contar contigo, todos los "predoc"

estaríamos un poco más perdidos sin ti... y cabe incluso la posibilidad de que ya hubiéramos acabado con el laboratorio. Gracias también a los chicos del lab: Dani, Jorge, y el reciente Eugenio, por estar siempre dispuestos a echar una mano con una amplia y sincera sonrisa. Y por supuesto, gracias Vane: por tus locuras, tus ideas, las proteínas, tus risas, la limpieza de mesocosmos, tus viajes, el sushi, el ETS, el jazz en una azotea, la energía, las carabelas portuguesas en el aseo, la IDH, los tatuajes de henna... por una de esas amistades que espero que continúen siempre... por nuestro bien, el de la ciencia, y el de los experimentos a cuatro manos.

Asimismo, debo agradecer a todos los colaboradores de los diferentes experimentos que han permitido el desarrollo de esta tesis. En primer lugar, gracias al Dr. Melchor González Dávila, a la Dra. Magdalena Casiano Santana y a Adrián Castro Álamo. Sé que no fue fácil hacer un hueco en la agenda para nuestros experimentos y vuestra ayuda ha sido esencial para poder cerrar esta tesis con un buen resultado. Gracias. Por otro lado, debo agradecer a todos los miembros del instituto ECOAQUA y del Departamento de Biología, donde, siempre que ha habido alguna urgencia, han estado dispuestos a colaborar compartiendo equipos, tiempo o energía. No tengo duda de que la colaboración es lo que hará aún más grande la investigación en esta Universidad.

También debo dar las gracias a la propia Universidad, ya que no habría podido desarrollarse este trabajo si no fuera por sus contratos predoctorales, en concreto el PIFULPGC-2013-CIENCIAS-1. Además no puedo dejar de nombrar a la Fundación ULPGC y a los mecenas de su Programa Innova 2020, en especial a la Familia Megías Martínez y a la empresa Vidrieras Canarias. Si no hubiera sido por ellos, no habría podido comenzar la investigación tras el Máster, y probablemente no estaría hoy aquí. Gracias.

Besides, I would like to acknowledge all the colleagues at GEOMAR Helmholtz centre, Kiel. First of all, I am grateful to Prof. Ulf Riebesel for inviting me to the KOSMOS GC 2014 experiment, one of the most exciting experiences I have had during the PhD Program, and for hosting me in his laboratory some years later. I extend these thanks to Dr Silke Lischka: I would always appreciate your academic support and your personal kindness (I will learn to bake a cake for our next coffee, I promise). Allanah, Andrea, Silvana, Jan, Lenni, Veit... to all the members of the Biological Oceanography Department: it was a pleasure to share those three months and a half with you all. And last but not least, I would like to thank Roberto, Mario, my landlady Greta, and my sailing-course mates for making my stay abroad so enjoyable.

La verdad es que en estos años de doctorado, la vida también pasa. Por un lado, ¡tenemos grandes momentos de risas y alegrías! Por ello no puedo dejar de recordar a todos los compañeros del grupo "The petardest from ULPGC": ¡Qué buenos fueron los achuchones, asaderos, cenas y bailes que nos echamos! Por otro, también se dan momentos críticos en los que se tambalean hasta los principales pilares de nuestra vida. Por suerte, es justo en estos momentos cuando podemos reconocer a aquellas personas que se hacen un hueco en nuestro corazón para siempre. Gra-

Abstract

The anthropogenic CO_2 emissions have been increasing for the past 250 years. Oceans are estimated to take up nearly one third of this CO_2. However, proper assessment and understanding of the processes controlling these carbon fluxes requires, among other factors, quantifying primary production rates (CO_2 fixation) and respiration rates (CO_2 production, R_{CO2}). Direct R_{CO2} measurements are not always feasible. Often they have to be calculated from O_2 consumption (R_{O2}). To do so, respiratory quotients (RQ), reported to be variable, are needed. In addition, when assessed from potential respiration (Φ), R_{O2}/Φ ratios are also needed. In order to reduce the variability linked to the use of these ratios and quotients, this thesis is focussed on developing a more direct assessment of R_{CO2} throughout the water column. It aims to develop and use an assay for $NADP^+$-dependent isocitrate dehydrogenase (NADP-IDH) in marine plankton.

In the development process, we determined the NADP-IDH optimum concentrations of substrate and cofactors, the optimum pH, and the proper treatment conditions needed to attain the NADP-IDH maximum velocity (V_{max}). Unfortunately, NADP-IDH is not the only CO_2-producing enzyme in the cells. Thus, we also assessed the relationship between the NADP-IDH and the other CO_2-producing enzymes. After normalising their activities per NADP-IDH, we were able to develop a model to predict the potential CO_2 production in marine plankton based on NADP-IDH measurements (Ψ_{NADP}). These results were validated by comparison with R_{CO2} values calculated from Φ, after applying different R_{O2}/Φ ratios and RQs. Ψ_{NADP} always exceeded R_{CO2}. This is consistent with the theoretical arguments that any physiological response should never exceed the potential activity controlled by the underlying enzymology.

As part of our investigation, we also measured both the NADP-IDH and the R_{CO2} during incubations of two communities of the mysid *Leptomysis lingvura*. Among all the studied factors, we observed that trophic conditions before sampling affected the enzyme activities. In addition, nutrient availability had significant impacts on the physiological response. However, the R_{CO2}/NADP-IDH ratio was similar between the two different communities of *L. lingvura*, which suggests that those values would be representative of *L. lingvura'*s physiology.

Last but not least, we wanted to highlight how valuable respiratory enzyme measurements (NADP-IDH and ETS) are in assessing the catabolic metabolism in

the plankton community. To do so, we measured the Φ/Chl_a ratio in a microplankton community during the KOSMOS GC 2014 experiment (BIOACID Project from GEOMAR, Kiel, Germany). We monitored the changes as the plankton community oscillated from photoautotrophic dominance to heterotrophic dominance following an injection of nutrient-rich deep water. We were simulating an upwelling event. The lowest values were reached in a phytoplankton bloom while the highest were reached in a heterotrophic dinoflagellate bloom.

Taking everything into consideration, we believe that the development of this new enzyme assay avoids the use of the RQ while measuring R_{CO2}, thus minimising the variability of previous methodologies. In addition, the NADP-IDH facilitates development of bisubstrate enzyme kinetic models (EKM) which, based on the measurement of both the NADP-IDH and the in-cell concentration of substrates and cofactors, predict accurately the physiological response. By doing so, the quantification of the vertical carbon flux (Fc) and the role of the ocean as a CO_2 sink can be strengthened. Furthermore, the regular measurements of NADP-IDH and Φ in oceanographic campaigns, and their comparison with autotrophic parameters (e.g. Chl_a), will enhance the understanding of changes in the microplankton community and the assessment of the metabolic state of the ocean.

Resumen

Debido a las emisiones por combustión de energías fósiles, los niveles de dióxido de carbono (CO_2) atmosféricos han aumentado exponencialmente en los últimos 250 años. El océano puede considerarse un sumidero de este CO_2. Sin embargo, para estimar adecuadamente su papel, es necesario conocer tanto las tasas de producción primaria de los organismos autótrofos (fijación de CO_2), como las de respiración (producción de CO_2). La producción de CO_2 (R_{CO2}) es particularmente difícil de medir, siendo generalmente calculada a partir de mediciones de consumo de O_2 (R_{O2}) con la aplicación de cocientes respiratorios (RQ). Esta dificultad se hace mayor en los estudios del océano profundo, donde la R_{O2} es obtenida tras la medición de la respiración potencial (Φ) y la aplicación de ratios R_{O2}/Φ. Estos ratios pueden variar significativamente en función de la disponibilidad de nutrientes. A esta variabilidad, hay que añadir la existente en los RQ. Por ello, esta tesis está centrada en el desarrollo de un nuevo método que profundice en una medición más directa de R_{CO2} en toda la columna de agua.

Este nuevo método, específico para el microplacton y mesozooplancton, es una adaptación de la medición de una de las principales enzimas productoras de CO_2: la isocitrato deshidrogenasa dependiente del $NADP^+$ (NADP-IDH). Durante su desarrollo se han determinado las concentraciones de sus substratos y cofactores, su pH óptimo y las condiciones de tratamiento que permiten alcanzar la máxima actividad en muestras de la comunidad planctónica. Lamentablemente, la NADP-IDH no es la única enzima productora de CO_2 en la célula. Por ello, estudiamos su relación con las principales enzimas involucradas, de manera que, normalizando sus actividades por la NADP-IDH, desarrollamos un modelo para la predicción de la producción de CO_2 potencial máxima en la célula, basado en la medición de la NADP-IDH (Ψ_{NADP}). Una vez medida en muestras de mesozooplancton y microplancton, comparamos la Ψ_{NADP} con valores de R_{CO2} obtenidos a partir de la Φ de las mismas muestras, tras la aplicación de los principales ratios R_{O2}/Φ y RQs utilizados en la literatura. En todos los casos, Ψ_{NADP} fue superior a R_{CO2}, siendo coherente con la idea teórica de que la respuesta fisiológica nunca debe superar a la capacidad metabólica del organismo.

Además, gracias a la experimentación con distintas comunidades de *Leptomysis lingvura* pudimos comparar medidas directas de R_{CO2} con la actividad de la NADP-IDH. De entre todos los factores analizados, comprobamos que las condi-

ciones tróficas previas al muestreo tienen efectos significativos sobre sus actividades enzimáticas. Asimismo, observamos que la disponibilidad de nutrientes afecta significativamente a la respuesta fisiológica. Sin embargo, las distintas comunidades obtuvieron ratios similares de R_{CO2}/NADP-IDH, lo que sugiere que los valores obtenidos pueden ser representativos para *L. lingvura*.

Finalmente, hemos querido destacar el valor de las medidas de NADP-IDH y de Φ como indicadores del metabolismo respiratorio de la comunidad planctónica. Para ello, ahondamos en el desarrollo del ratio Φ/Chl_*a* que permitió la monitorización de los cambios metabólicos en la comunidad microplanctónica durante el experimento KOSMOS GC 2014 dentro del proyecto BIOACID. Los valores más bajos se dieron durante el desarrollo de un bloom fitoplanctónico, mientras que los más altos, durante la proliferación de dinoflagelados heterótrofos.

En conclusión, el desarrollo de un nuevo método enzimático para el análisis de la producción de CO_2 en toda la columna de agua evitar la aplicación de los RQ, reduciendo la variabilidad de los métodos usados hasta ahora. Además, permite el desarrollo de modelos cinéticos bisustrato (EKM) que, en base a la concentracion de sustratos en la célula, predicen la respuesta fisiológica. Esto tendrá un impacto muy positivo en la cuantificación de la función del océano como sumidero de CO_2 y en el estudio del flujo de carbono vertical (*Fc*) al poder obtener datos de R_{CO2} del océano profundo. Además, consideramos que la medición del metabolismo catabólico en campañas oceanográficas de manera regular, y su comparación con parámetros relacionados con la autotrofía, favorecerá la comprensión de los cambios en la comunidad microplanctónica y la estimación del estado metabólico de las distintas regiones oceanográficas.

Thesis Preview

The present dissertation entitled "Enzyme Assays in Assessing Respiratory Metabolism in Marine Plankton: the development of a new CO_2-production proxy and further applications of respiratory enzymatic assays in oceanography" has been conducted within the Doctoral Program of Oceanography and Global Change from the University of Las Palmas de Gran Canaria and has been supervised by Dr. María M. Gómez Cabrera and Dr. Theodore T. Packard. It is comprised of 4 original research articles (one of them already published) developed in the frame of the projects BIOMBA (CTM-2012-32729), granted to Dr. May Gómez. Moreover, this thesis includes samples collected during KOSMOS experiment from research project BIOACID that was granted to Dr. Ulf Riebesell. In addition, a research stay was made at the GEOMAR Helmholtz Centre for Ocean Research Kiel (Kiel, Germany) during this period. This thesis is structured in two parts. The first is divided into six chapters that encompass: a general introduction with the major objectives of the work; four original contributions in the form of scientific research articles that embed discussion sections and specific conclusions; a synthesis chapter that embeds the major conclusions of the thesis; and finally, the outline for future research. This first part is completely written in English (except for the abstracts on chapters 2 to 5, which are written in both English and Spanish), fulfilling the demands to obtain the International Doctor Mention (Real Decreto 99/2011 del 28 de enero por el que se regulan las enseñanzas oficiales de doctorado, Art.15). The second part, in turn, is written in Spanish and consists of a brief summary of the English section, with an introduction to the topic, the general material and methods, the main results and the conclusions derived from the work. This is a requirement of the PhD Thesis Regulation from the Universidad de Las Palmas de Gran Canaria (BOULPG, January 9th, 2013, modified in BOULPGC, November 4th, 2013). During the development of this research, I received financial support from University of Las Palmas de Gran Canaria (PIFULPGC-2013-CIENCIAS-1).

Presentación de la Tesis

La tesis que aquí se presenta bajo el título "Los Ensayos Enzimáticos en el Análisis del Metabolismo Respiratorio del Plancton Marino: el desarrollo de un nuevo método para medir la producción de CO_2 y nuevas aplicaciones de estas metodologías en oceanografía" se ha desarrollado dentro del Programa de Doctorado en Oceanografía y Cambio Global de la Universidad de Las Palmas de Gran Canaria y ha estado dirigida por los doctores May Gómez y Ted Packard. En ella se incluyen 4 contribuciones originales (una de ellas ya publicada) enmarcadas principalmente dentro del proyecto de investigación BIOMBA (CTM 2012-32729) otorgado a la Dr. May Gómez. Además, esta tesis incluye muestras tomadas durante el experimento KOSMOS GC 2014, dentro del proyecto BIOACID dirigido por el doctor Ulf Riebesel. Por último, durante el desarrollo de la misma se realizó una estancia en GEOMAR Helmholtz centre for ocean research en Kiel (Alemania). Esta tesis está estructurada en dos partes. La primera engloba: la Introducción con los principales objetivos del trabajo; las Contribuciones Originales en formato de artículo científico, incluyendo la discusión y conclusiones específicas; las Conclusiones Generales de la tesis; y las Futuras Líneas de Investigación. Estos capítulos están escritos íntegramente en inglés (a excepción de los resúmenes de los capítulos 2 al 5, que se han escrito en ambos idiomas), de acuerdo a la normativa para la obtención de la Mención Internacional del Título de Doctor (Real Decreto 99/2011 del 28 de enero por el que se regulan las enseñanzas oficiales de doctorado, Art.15). La segunda parte de la tesis incluye un resumen en castellano que consta de una breve introducción, el material y los métodos generales, los principales resultados y las conclusiones más relevantes del presente trabajo, cumpliéndose así los requisitos expuestos en el Reglamento de Estudios de Doctorado de la Universidad de Las Palmas de Gran Canaria (BOULPG, January 9th, 2013, and modified in BOULPGC, November 4th, 2013). El desarrollo de esta tesis no habría sido posible sin el apoyo económico recibido de la Universidad de Las Palmas de Gran Canaria en el marco del contrato predoctoral PIFULPGC-2013-CIENCIAS-1.

Contents

List of Figures

List of Tables

Chapter 1

Chapter 1. General Introduction

*Respiration is a slow combustion of carbon
and hydrogen, similar in every way to that
which takes place in a lamp or lighted
candle.
Breathing animals are active combustible
bodies that are burning and wasting away.*

Antoine Laurent Lavoisier

1.1 The role of respiration in the ocean metabolism

Ocean metabolism is one of the main biological processes that control marine
chemistry. Its anabolic facet is responsible for the carbon dioxide (CO_2) fixation and oxygen (O_2) formation. This facet creates new particulate organic matter (POC) through photosynthesis in the euphotic zone, or through widely diverse
forms of chemosynthesis throughout the water column. Metabolism's catabolic
facet is responsible for CO_2 production, O_2 consumption, nutrient remineralization, and in-cell energy production (in the form of adenosine triphosphate (ATP)
following degradative reactions that break-down POC (Nelson and Cox (2008)).
This degradative facet is mainly driven by respiration in heterotrophs, autotrophs
and mixotrophs. All cells share the same catabolic pathway, it is a ubiquitive process (Lane (2006, 2010)). del Giorgio and le B. Williams (2005) described it as the
major sink of organic matter in any ecosystem. At this scale, to understand both
the marine ecosystems and the biogeochemical relationships that impact them, a
deep knowledge of the biological transformation rates becomes mandatory. However, even though marine respiration is ubiquitous throughout the water column, it
was not until the 70's when it began to be measured in a regular basis, instead of
being estimated indirectly from the primary productivity or from biomass measurements (Packard et al. (1974)). The classic assumption of strong coupling between
both facets on a global scale supported the assessment of respiration derived from
primary production. However, since Sverdrup et al. (1942), the application of the

dynamic equilibrium concept to the O_2 distribution illustrated that both ecosystem processes often occur separated in time and space. This is because ecosystems can exchange both mass and energy with their surroundings, they are open systems. Thus, an accurate assessment of respiration in the ocean requires direct measurements not derived from primary production. In addition, direct measurements of respiration reflect the activity of organisms at a cellular level. At this scale, respiration is the pathway whereby organisms produce their vital energy in the form of ATP. Meanwhile, CO_2 is produced and O_2 is consumed.

1.1.1 Physiological O_2 consumption rates

The most commonly used techniques in respiration assessment are related to measuring O_2 consumption rates (R_{O2}) when organisms or ecosystem samples are incubated in isolation from their surroundings. Early measurements of respiration in marine organisms were carried in the 30's, by observing the decrease of O_2 content in incubations of pure, marine-bacterial cultures (Waksman and Carey (1935); Johnson (1936)) or in bottled seawater (Seiwell (1937); Seiwell and Seiwell (1938)). Since then, in addition to the Winkler method (Winkler (1888)), R_{O2} has been commonly assessed by electrodes or optodes during up-to-24h of incubation. Even though all these physiological measurements are direct, they are not flawless. Artefacts linked to the manipulation of the living organisms, to the starvation of the sample when long periods of incubation are needed, and to overcrowding in the bottle, affect the reliability of the measure as an accurate representation of what is happening in the ocean (Fernández-Urruzola et al. (2011); Williams et al. (2013); Bondyale-Juez et al. (2017)). Furthermore, many factors impact the physiological response. A few of these are: nutrient limitation, circadian rhythm, size (Marshall et al. (1935); Christensen et al. (1980); Herrera et al. (2011b); Fernández-Urruzola et al. (2011)), age (Hernández-Leon and Gómez (1996)), the reproductive state (Kiørboe et al. (1985)), sex differences (Isla and Perissinotto (2004)), and oxygen partial pressure (Salvato et al. (2001)). Besides, the respiration measurements are time-and-manpower consuming, so they usually result in low data acquisition rates, which for oceanographic purposes is a disadvantage. These measures are useful in physiology, but oceanography requires a higher data acquisition rate over time and space (think satellite mapping of phytoplankton productivity). For that reason, enzymatic assays to detect metabolism were developed as oceanographic tools in the 70's (Packard (1971); Packard et al. (1971a)).

1.1.2 Enzymatic activity: potential O_2 consumption rates

Enzymes in the electron transport system (ETS) are the major players in O_2 consumption. Most ETS enzymes are large complexes. NADH-dehydrogenase, the principle target of the ETS assay used in oceanography, is an enormous, "L"-shaped, 40 unit, superprotein complex of more than 1000 kDa. Diagonally, it is 330 Angstroms long. It is one of the largest enzymes known; containing more

than 7724 amino acids[1] (Fisher (1964); Walker (1992); Kühlbrandt (2015)). Depending on the presence or absence of inhibitors or activators, the ETS enzymes lead the respiratory physiological response of the organism, the O_2 consumption rates (R_{O2}). Thus, Packard assayed the ETS activity to measure potential respiration (Φ) in marine plankton, allowing the assessment of O_2 consumption rates even in the deep ocean (Packard (1971); Packard et al. (1971b)). When the ETS enzymes are saturated with their specific substrates, the ETS works at its maximum velocity (*Vmax*). Theoretically, this is the maximum capacity of the cell in consuming O_2 (Moran et al. (2012); Nelson and Cox (2008)). This value reflects the respiratory enzymatic structure of the cell, describing the catabolic metabolism of the organism. Thus, the ETS *Vmax* remains stable under different physiological conditions in the short term. This is because the respiratory ETS is a constitutive enzyme system. Except under long-term stress, it is maintained at a constant concentration in its membrane matrix. In contrast, R_{O2} is more variable, as it is the result of the *in vivo* ETS activity, the actual, substrate modulated, velocity of the reactions catalysed by the ETS. In detail, this physiological rate is controlled by the in-cell availability of substrates, activators and inhibitors, as well as temperature and pressure (Packard et al. (1975); King and Packard (1975); Packard et al. (1996b)).

1.1.3 The R_{O2}/Φ ratio

First attempts in proxying R_{O2} from ETS measurements involved seeking the relationship between R_{O2} and Φ. In the beginning, it was thought to be a quotient close to half Φ (Cleland (1967); Segel (1975)). Since the 80's, studies were run in different regions to assess the direct measurement of this ratio: from the Antarctic Ocean (Ikeda and Fay (1981)); from the Gulf of Maine (Packard and Williams (1981)); from the North Pacific Ocean (Ikeda et al. (2006)); and from 8 different oceanic regions (Arístegui and Montero (1995b,a, 2005)). In addition, a comparison was made between assessing R_{O2} with the He-tritium/AOU method of Jenkins (1982) and assessing R_{O2} with the ETS assay and the R_{O2}/Φ ratio (0.26) described in Packard and Williams (1981). As predicted (see section 1.1.2) variability in the ratio was found (from 0.26 to 0.53 in microplankton (Packard and Williams (1981); Gómez et al. (2011)); from 0.4 to >1 in zooplankton (Gómez et al. (2011)). R_{O2}, as any physiological rate, depends on different factors (Hernández-Leon and Gómez (1996); Fernández-Urruzola et al. (2011); Herrera et al. (2011b)), while the ETS reflecting the maximum V_{max} of the enzymatic activity, i.e., the potential O_2 consumption (Φ) is more stable. In consequence, the variations in the R_{O2}/Φ ratios depend on the same factors that impact the physiology (Hernández-Leon and Gómez (1996)). Until recently, R_{O2} has been calculated from Φ based on different biochemical hypotheses or statistically based ratios. Packard et al. (1971b) based their R_{O2} calculations on the respiratory control ratio (0.10) of Chance and

---

[1]Note the difference with other simple enzymes, such as insulin, with only 51 amino acids and a molecular weight of only 5.8 kilodaltons (kDa)

Williams (1956); Chance (1965). Later, Packard et al. (1977) solved Harmon Craig's advection-model for deep-sea R_{O2} (Craig (1971)) to derive an R_{O2}/Φ ratio suitable for the dark-ocean (0.02)[2]. Subsequent research on interpreting the meaning of Φ considered the theoretical assumption that: 1) the physiological respiratory response is half the ETS V_{max} (Cleland (1967); Segel (1975)); 2) the directly measured physiological respiratory response in a region at a certain moment is representative of that region, so the R_{O2}/Φ is developed to be applied to the Φ measurements in that region (Packard and Williams (1981); 3) an average R_{O2}/Φ for a plankton size is representative and applied to Φ measurements on that size group; and finally, 4) a linear regression with as many measures as possible throughout the whole ocean is used to derive R_{O2} from Φ (Arístegui and Montero (1995a)).

In the meanwhile, other studies were carried out in the laboratory in order to understand the variability of this ratio, which complemented oceanographic results (Hernández-Leon and Gómez (1996); Martínez et al. (2010); Herrera et al. (2011b); Osma et al. (2016a,b)). Among the variables investigated, starvation and nutrient availability resulted to be the factors which mainly drove changes in the physiological response, and so, changed the R_{O2}/Φ ratio. As enzymes are the main drivers of respiratory reactions, these results, combined with kinetics, fostered consideration of a new approach to this topic. Enzymes obey Michaelis-Menten kinetics, where substrates are the main regulators of their function, and consequently, on the physiological response. How the different environmental and physiological factors impact the intracellular substrate availability to the ETS, will lead to different R_{O2}. This conceptual idea fuelled the development of the enzyme kinetic model (EKM) in the 90's Packard et al. (1996b,a). Since Packard et al. (1996b), several studies in bacteria (Aguiar-González et al. (2012)) and in marine zooplankton (Packard and Gómez (2008); Osma et al. (2016b)) have modelled R_{O2} by measuring Φ, its intracellular substrates and applying the bisubstrate enzyme kinetics. These models were validated with direct R_{O2} measurements during the experiments, and resulted in more accurate predictions of R_{O2} than the use of simple R_{O2}/Φ ratios. Both Aguiar-González et al. (2012) and Osma et al. (2016b) demonstrated the advantage of using an EKM instead of a constant R_{O2}/Φ ratio, or the Metabolical Theory of Ecology (MTE) based on biomass.

In addition, the use of *in vivo* tetrazolium reduction in whole populations of microplankton was introduced in the last decade by Martínez-García et al. (2009) and Aranguren-Gassis et al. (2012). This method involves adding the tetrazolium salt (INT[3]) directly to bottled seawater samples containing living-organism and incubating them for various time-periods. While respiring, these organisms reduce INT to formazan by a wide variety of enzymatic and non-enzymatic reactions. Res-

---

[2]The original R_{O2}/Φ ratio of 0.05, reported in Packard et al. (1977), was based on the Packard (1971) ETS assay. Modern deep-sea ETS assays are based on the more sensitive Kenner and Ahmed (1975) ETS assay. According to Table 3 in Christensen and Packard (1979) were the ETS measurements in Packard et al. (1977) made by the Kenner and Ahmed (1975) ETS assay the R_{O2}/Φ ratio would be 0.02 rather than 0.05.

[3]2-(p-iodophenyl)-3-(p-nitrophenyl)-5-phenyl tetrazolium chloride (Nachlas et al. (1960)

piratory INT reduction, directly related to the O_2 consumption, is thought to be the dominant reaction. However, INT is toxic to whole cells (Villegas-Mendoza et al. (2015)) because it uncouples respiratory O_2 consumption from ATP production (Clark et al. (1965)). Starved for energy, the cells die during the incubation, thus the measurement represents the respiration of a dying community. Especially for long-period incubations, this toxicity will generate misleading measurements. In spite of this, a useable correlation between both measurements has been reported (Martínez-García et al. (2009); Aranguren-Gassis et al. (2012)), so this tool may be useful depending on the aim of the study. However, because Φ and in-cell substrates are the casual basis of respiration, we consider the measurement of Φ, the use of the EKM, and research into R_{O2} variability a better way to asses respiration in the ocean than *in vivo* INT reduction.

1.2 The impact of respiration on the carbon flux assessment

As the global economy is based on the combustion of fossil resources, the anthropogenic CO_2 emissions have been increasing for the past 250 years. This rise, combined with the spread of deforestation and agriculture, has resulted in the highest atmospheric CO_2 levels in the last 800000 years (400ppm) and keeps increasing up to one order of magnitude higher than one million years ago (Doney and Schimel (2007)). The oceans are estimated to take up nearly one third if this anthropogenic CO_2. Thus, the assessment and understanding of the processes that control the carbon fluxes between atmosphere, marine surface waters, the deep ocean and the benthos, have been the focus of international research programs since the 1980s (e.g. Joint Global Ocean Flux Study, JGOFS). In the ocean, the net carbon flux is controlled by three key-processes : 1) the autotrophic CO_2 fixation into POC which is mainly synthesised by autotrophs in the upper euphotic layer of the water column; 2) the POC remineralisation back to CO_2 through respiration, mainly driven by heterotrophs but also by autotrophs and mixotrophs (Redfield (1934)); and 3) the export of particulate and dissolved organic carbon (POC and DOC) to the sea bottom (Ketchum (1957); Munk (1966); Rivkin and Legendre (2001)). This transfer of organic carbon from the euphotic zone to the seafloor occur by different processes: a) gravitational sinking of particles (McCave (1975)); b) advection (Seiwell and Seiwell (1938); Redfield (1934); Riley (1951)); c) active transport by vertical migrants (Ketchum (1957); Munk (1966)); and d) isopycnal pumping (Packard et al. (1977)). Among them, the passive sinking of POC results in the main source of organic carbon in the dark ocean (Eppley and Peterson (1979); Osma et al. (2014)). A better understanding of the processes that control vertical carbon flux (F_C) requires an improvement in the knowledge of both primary production and respiration in terms of carbon. However, although respiration is the most important process involved in carbon cycling, its measurements are scarce relative to primary production. It was not until the 90's when

the first studies in carbon flow between production and respiration arose. Many of these were focused in the assessment of remineralization from sub-euphotic ETS measurements throughout the water column (Lefévre et al. (1996); Arístegui et al. (2002a); Packard and Codispoti (2007)). Furthermore, the connection between the primary production and the deep ocean carbon demands was also assessed from ETS measurements (Packard et al. (1971b, 1977); Arístegui and Harrison (2002); Arístegui et al. (2002b)). More recently, vertical active F_C was also studied by the ETS profile measurements in migrants throughout the water-column (Dam et al. (1995); Darnis and Fortier (2012); Packard and Gómez (2013); Ariza et al. (2015); Hernández-León et al. (2019)).

Finally, considering respiration as the major sink of organic matter in any ecosystem (del Giorgio and le B. Williams (2005)), many researchers have studied how respiration impacts the marine vertical passive F_C (Packard and Christensen (2004); Giering et al. (2014); Osma et al. (2014); Packard et al. (2015)). In these studies, vertical F_C was calculated assuming that the decrease in sinking POC is caused by respiratory CO_2 production. This means that the first derivative, mathematically speaking, of the F_C-depth function is the respiration depth function (Suess (1980); Martin et al. (1987); Packard and Christensen (2004)). The development of the ETS assay resulted in metabolism measurements that could be converted to respiration throughout the water-column down to the deep ocean. From these measurements, the production of CO_2 related to respiration was calculated. The CO_2 production from the bottom of the euphotic zone to the deep ocean was calculated as the integral of the CO_2 production rates at different depths (Packard and Christensen (2004); Osma et al. (2014); Packard et al. (2015)). This equalled the F_C sinking out of the euphotic zone.

1.2.1 Physiological CO_2 production rates

Even though during the last decades the CO_2-producing facet of the respiration (R_{CO2}) received more attention because of its importance in assessing the role of the ocean as an antropogenic CO_2 sink, respiration has been mainly approached by measuring R_{O2} rates. Direct physiological measurement of R_{CO2} has not been as feasible as measuring R_{O2} in the ocean, mainly because of the complexity and paucity of the available techniques to measure it and because of the buffering effect of the carbonate system.

Despite these difficulties, marine R_{CO2} rates have been assessed from different approaches since the 70's. The first marine, direct R_{CO2} rates measurements were done by following the CO_2 absorption by KOH (Rakusa-Suszczewski et al. (1976)). Since then, other studies have measured these rates by following the changes in the Total dissolved inorganic carbon (TC) as an end-point measurement after long incubations (Johnson et al. (1987, 1993)). These TC measurements involve a gas extraction of acidified seawater by coulometric titration of the acid formed by the resultant CO_2 and monoethanolamine. In addition, other studies, building on the R_{CO2} control, via Henry's Law, of the pCO$_2$ in the head space

above the respiring plankton, have assessed R_{CO2} by monitoring the changes in the pCO_2 by infrared detection (2000μm of absorption peak). These studies used a Micro-Oxymax respirometer (www.colinst.com) (Berdalet et al. (1995a); Packard et al. (1996a); Romero-Kutzner et al. (2015)). More recently, the development of infrared spectrometry has allowed not only the TC measurement but also the δ^{13}C and δ^{18}O stable isotopic composition determination (Yakir and da SL Sternberg (2000); Braden-Behrens et al. (2017)). This new approach has already facilitated the continuous measurement of these parameters in terrestrial ecosystems during time, assessing the separation of the net CO_2 exchange into photosynthetic and respiration components (Braden-Behrens et al. (2017)). However, its application on marine ecosystems is still under development (Smajgl et al. (2018)). Finally, the improvement of pCO_2 optodes may also become a proper tool to measure R_{CO2}. However, even though they have provided accurate and precise measurements, they still require strong calibration and preconditioning to the high salinity of marine ecosystems (Atamanchuk et al. (2014)). In addition, the CO_2 produced by respiration enters the surrounded water and participates in the equilibrium processes as in Eq.1.1 (Millero (2006)):

(1) $[CO_2] + H_2O <\text{->} H^+ + [HCO_3{}^-]$
(2) $[HCO_3{}^-] <\text{->} H^+ + [CO_3{}^{--}]$
(3) $[Ca^{++}] + [CO_3{}^{--}] <\text{->} CaCO_3$ (s)(1.1)
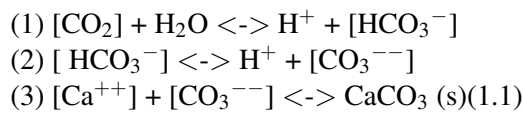
So this reaction sequence leads to pCO_2 buffering in marine waters, as equilibria is established. Thus, direct measurements of pCO_2 in the water, as those addressed by the pCO_2-optodes, are not useful to directly assess R_{CO2} rates. However, every mol of CO_2 produced by respiration adds one mol to the sum of all the inorganic carbon pool in the marine water. This is the TC, Eq.1.2:

$$TC = [CO_2] + [HCO_3{}^-] + [CO_3{}^{--}](1.2)$$

Taking this into consideration, the optode pCO_2 measurements require the conversion to TC based on pH and total alkalinity (TA) (Berggren et al. (2012)).

Due to all these constraints in determining CO_2 changes in seawater related to respiration such as: (1) the need for long incubation periods to measure TC as an end-point measurement Mayzaud et al. (2005); (2) the need for strong calibration and preconditioning to high salinity of the pCO_2 optodes (Atamanchuk et al. (2014)) and for the conversion to TC by alkalinity and pH (Berggren et al. (2012)); (3) the not-so-affordable cost of the technology linked to the infrared sensing of pCO_2 (Berdalet et al. (1995a); Packard et al. (1996a)) and of the new marine application of stable isotopes (Smajgl et al. (2018)), respiratory rates have mainly been reported as O_2 consumption in oceanography. As a result, Respiratory Quotients (RQs) ratios between mol of CO_2 produced per mol of O_2 consumed, have

been required to calculate respiratory CO_2 production rates from R_{O2}. However, these ratios are variable, not only because of different nutrient sources, but also to differences in nutrient availability (Berggren et al. (2012); Romero-Kutzner et al. (2015)). So, when assessing R_{CO2} rates, not only does the variability in the physiological R_{O2} rates affect the final measurement, but also the variability in the RQ ratios, which would bias the accuracy of the results.

To sum up, all the direct R_{CO2}-measurement techniques are currently time-and-manpower consuming and cannot be used on deep ocean communities, so they usually result in low data acquisition rates. As oceanography requires a higher data acquisition rate over time and space, an enzymatic assay related to CO_2 production would has arisen as a interesting improvement in the carbon flux assessment research.

1.2.2   Enzymatic potential CO_2 production rates

The biochemistry of respiratory CO_2 production is dominated by $NAD(P)^+$- dependent isocitrate dehydrogenase in the Krebs cycle (IDHкс in Fig. 1.1) (Nelson and Cox (2008)). In cells, other biochemical reactions produce CO_2, but their production rates can be predicted from IDHкс activity (Packard et al. (1996a); Roy and Packard (2001); Tames-Espinosa et al. (2018)). Of those linked to respiration, pyruvate dehydrogenase (PDH) serves to bridge the metabolism of glucose (glycolysis) to the Krebs cycle. Then, inside this cycle of enzyme reactions, both IDHкс and alpha-ketoglutarate dehydrogenase (KGDH in Fig. 1.1), produce CO_2, being the IDHкс activity 1.1 times the KGDH activity (Walsh and Koshland (1984), Fig.1.1). Finally, linked to, but not in the Krebs cycle, are the malic enzyme (ME in Fig. 1.1) and phosphoenol pyruvate carboxykinase (PEPCK in Fig. 1.1). They also generate CO_2 but at much reduced rates. IDHкс activity is 8.4 times greater than these activities.

IDHкс encompass two isoenzymes that catalyse the conversion of isocitrate to α - ketoglutarate in a reaction summarized in Eq.1.3 (Nelson and Cox (2008)).

$$Isocitrate + NAD(P)^+ \leftrightarrow \alpha\text{-}ketoglutarate + NAD(P)H + CO_2 (1.3)$$
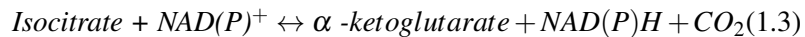
where 1 mol of CO_2 is stoichiometrically related to the production of 1 mol of NAD(P)H.

These enzymes can be either NAD^+ or $NADP^+$-dependent (NAD-IDH or NADP-IDH respectively) (Kornberg and Pricer (1951); Gálvez and Gadal (1995)). However, unlike NAD-IDH, NADP-IDH is ubiquitous in all types of organisms (from *E.coli*-like bacteria to plants and mammals); its activity has been reported to be up to 10-fold greater than NAD-IDH activity (Alp et al. (1976); Colman (1975); Denton et al. (1978)); and, unlike NAD-IDH, NADP-IDH is stable during the measurement (Plaut (1970, 1962)). Furthermore, NADP-IDH largely controls CO_2
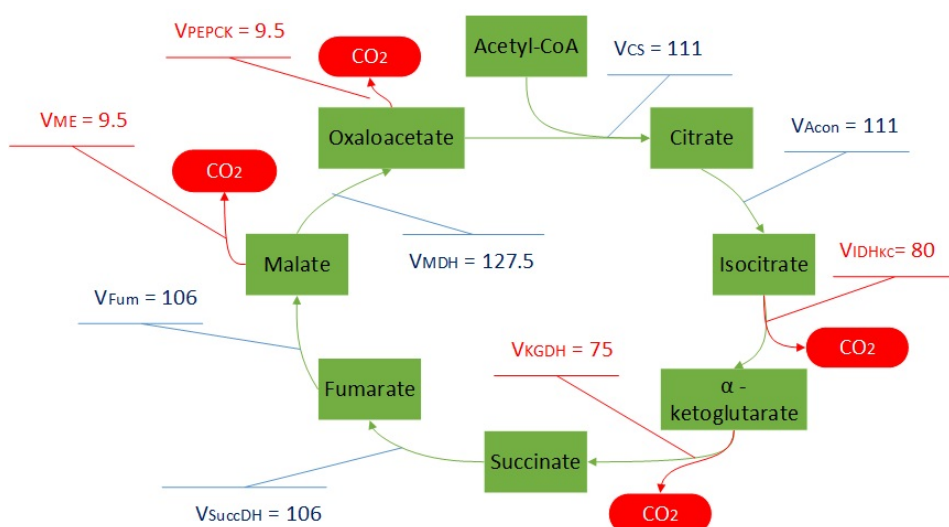
Figure 1.1: Velocities (V) through the main pathways in *E.coli* Krebs cycle (KC) in the bacterium, *Escherichia coli*, during acetate utilisation (redrawn from Walsh and Koshland (1984)). Rates are expressed in terms of mmol substrate consumed $min^{-1} L^{-1}$ of cell volume. Abbreviations in the velocity expressions are CS, citrate synthase; Acon, aconitase; IDH_{KC}, isocitrate dehydrogenase linked to the Krebs cycle; KGDH, α-ketoglutarate dehydrogrenase; SuccDH, succinate dehydrogenase; Fum, fumarase; MDH, malate dehydrogenase; ME, malic enzyme; PEPCK, phosphoenolpyruvate carboxykinase. Rates linked to CO_2 production have been highlighted in red. Not shown is the CO_2-producing enzyme, pyruvate dehydrogenase, that links glucose metabolism in the Embden-Myerhof pathway with the KC by decarboxylating pyruvate to acetyl-coenzyme A.

production in the Krebs cycle (Nicholls and Garland (1969); Walsh and Koshland (1984); Williamson and Cooper (1980)) not only because it is the more active CO_2-producing enzyme (Fig. 1.1) but also because it works as a key enzyme in the Sazanov and Jackson substrate cycle in the regulation of Krebs cycle activity (Sazanov and Jackson (1994)). In addition, mitochondrial NADP-IDH produces NADPH that is used to produce both, ATP by the electron transport system (ETS), and reduced glutathione (a reactive oxygen species (ROS) scavenger which serves as the cellular defence against oxidative stress-induced damage (Jo et al. (2001)). Moreover, cytosolic CO_2-producing NADP-IDH generates NADPH outside the mitochondria, linked to lipid synthesis (Koh et al. (2004)). Increases in its activity have been related to hypothyrodism in mammals (Czyzewska et al. (2012); Kadenbach et al. (1964)). Thus, cytosolic NADP-IDH measurements may improve the assessment of lipid production on the base of the marine food chain. Even though the main goal of this research is the development of the NADP-IDH assay for the plankton community, we firmly believe it will be useful in further research within

these diverse fields.

An early attempt to assess the relationship between CO_2 production rates and the NADP-IDH activity was made in the marine bacterium *Pseudomonas nautica* (Berdalet et al. (1995a)). From these measurements, the first steps in modelling the CO_2 production were developed (Packard et al. (1996a)). Later, this model was improved and tested in the same bacterium by making measurements of the substrates, $NADP^+$ and isocitrate (Roy and Packard (2001)). From these analyses, a factor (χ) was derived to calculate CO_2 production from NADP-IDH activity in the *P. nautica* Krebs cycle (Roy and Packard (2001)). These studies on marine bacteria were the first assessment on the NADP-IDH role in the CO_2 production in marine organisms.

However, they were focused on marine bacteria, whereas oceanography needed a plankton community tool. Thus, the first objective in the present thesis has been the development of an NADP-IDH assay in the marine plankton (Chapter 2). To do so, we considered previous studies of NADP-IDH activity in yeast, marine bacteria, and marine fish (turbot) (Berdalet et al. (1995a); Kornberg and Pricer (1951); Munilla-Moran and Stark (1989); Munilla-Moran (1994); Packard et al. (1996a); Roy and Packard (2001)). After carrying out many experiments in the laboratory, this was the first time NADP-IDH was measured in marine plankton. The new assay was published on the journal, Marine Chemistry, in 2018 (Tames-Espinosa et al. (2018)).

Although we were able to measure the NADP-IDH activity, the potential CO_2 production in the cells involves also the CO_2 produced by other respiratory and non-respiratory enzymes. Thus, we work on the second objective of this thesis in Chapter 3: modelling the potential CO_2 production based on NADP-IDH in marine plankton, taking into account the main CO_2-producing enzymes in the cells.

1.2.3 The R_{CO2}/NADP-IDH ratio

One of the main advantages of the NADP-IDH assay for the plankton community is the possibility of proxying the R_{CO2} from these measurements throughout the water-column. The development of these ratios reduces the variability linked to the estimations of R_{CO2} from R_{O2} by using RQ, particularly in water-column studies, where R_{O2} is also derived from Φ at depth. However, as in the case of the R_{O2}/Φ ratios, we expect the plankton physiological rate to be variable whereas the enzymatic measurements would remain more stable in the short term. In previous studies on the marine bacterium *Pseudomonas nautica* the carbon-source depletion induced these differences between R_{CO2} and NADP-IDH in the short term (Berdalet et al. (1995a); Packard et al. (1996a); Roy and Packard (1998, 2001)).

Thus, the use of such an ocenographic tool would require the following research:

- From a physiological point of view, we should improve the current knowledge about the influence of different factors on the performance of the CO_2 producing enzymes, their kinetics and their in-cell substrates availability. Here, in chapter 3, we have attempted for the first time how the sex-differences and starvation may impact this ratio in *Leptomysis lingvura*.

- On a short time-scale, we should measure and develop R_{CO2}/NADP-IDH ratios that describe an specific region, at a certain time for a size-fractioned plankton community, so that the ratios can be considered representative for communities under similar environmental conditions in that region. In chapter 3, we measured the *L. lingvura* R_{CO2}/NADP-IDH ratio in two communities from different years, leading to similar representative results.

- In the long run, when many ratios were measured, we tried to assess an average ratio (or a linear regression between R_{CO2} and NADP-IDH measurements). However, we have to bear in mind that this kind of approach may greatly deviate from the actual measurement at an instantaneous time-scale. Unfortunately, we will have to wait until widespread use of this tool before we can properly define an average relationship between both parameters.

- Finally, an accurate model for proxying R_{CO2} from NADP-IDH, isocitrate and $NADP^+$ measurements in plankton communities should be developed. To do so, the same theoretical bases of the bisustrate kinetics models would be applied, as done on *P. nautica* (Packard et al. (1996a); Roy and Packard (2001)).

1.3 Further applications of respiratory enzymatic measurements

In the previous sections, we presented the valuable role of the respiratory enzymatic measurements to assess R_{O2} and R_{CO2} and the factors that affected their variability. However, we should keep in mind that they are the reflection of an inherent characteristic of the community: its metabolism. Several studies took this into consideration and, after applying not-so-difficult mathematical models, they were able to asses other parameters in the ecosystem that were not previously studied.

The next subsections describe several examples of how the combination of metabolic measurements, mathematics, and the relationship with other oceanographic parameters may improve the marine research and the study of the aquatic ecosystems.

1.3.1   Carbon flux and Nutrient regeneration efficiency

Vertical carbon flux (F_C) in the ocean can be assessed from the vertical profiles of R_{CO2}. Conceptually, "planktonic R_{CO2} in a seawater cube is considered equivalent to the difference between the total F_{C1} through the top of the cube (z_0) and total F_{C2} through the bottom of the cube (z)" (Packard et al. (2015)). F_C changes in that depth layer are related to the loss of carbon by respiration between the boundaries of that layer. This is the integral of R_{CO2} between them. So, the first step in this assessment requires the development of the vertical profile of R_{CO2} (see Fig.1.2).
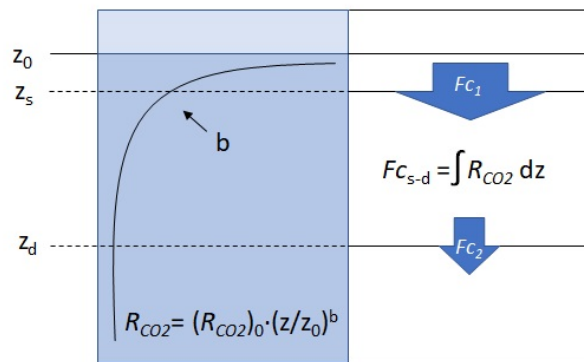
Figure 1.2: Diagram of the vertical profile of R_{CO2} and its relationship with vertical F_C. Light blue illustrates the euphotic zone whereas dark blue represents the aphotic zone.

In Packard et al. (2015), the respiration-depth profile was obtained by modelling R_{CO2} from microplankton Φ. Then, the power function that describes these depth profile (Eq. 1.4) was developed (see Fig.1.2).

$$R_{CO2} = (R_{CO2})_0 \cdot (z/z_0)^b \quad (1.4)$$

where $(R_{CO2})_0$ is the R_{CO2} at z_0 and b (always negative) is the exponent that defines the curvature of the vertical profile. The larger |b| is, the lower F_C is from the epipelagic ocean. It is the opposite when |b| is low.

Then, to calculate F_C from any depth in the water column (z_s) down to a deeper one (z_d), the mathematical vertical profile of R_{CO2} between those two depth was integrated (Eq. 1.5, Fig.1.2) (Packard et al. (2015))).

$$F_{Cs-d} = \int_{Zs}^{Zd} R_{CO2} dz$$

$F_{Cs-d} = \int_{Zs}^{Zd} (R_{CO2})_0 \cdot (z/z_0)^b \, dz$

$F_{Cs-d} = \{(R_{CO2})_0/[(b+1)z_0^b]\} (z_s^{b+1} - z_d^{b+1})$ (1.5)

Note that z_s is a depth between z_0 and z_d ($z_0 \leq z_s \leq z_d$).

In addition, the nutrient retention efficiency (NRE), described as the nutrient remineralization rate within an ocean layer (Packard and Gómez (2013); Osma et al. (2014); Packard et al. (2015)), can be also calculated from both a profile of plankton respiration, or as the inverse of the F_C transfer efficiency below the euphotic zone(Buesseler and Boyd (2009)). In Packard et al. (2015), the NRE was assessed as the R_{CO2} within an ocean layer per the F_C into that layer, expressed as a percentage.

NRE$=R_{CO2} \cdot \Delta z/F_C$ (1.6)

Note that R_{CO2} was reported in mol CO_2 d^{-1} m^{-3} and F_C in mol C d^{-1} m^{-2}. Since the Redfield N=C or P=C ratio is applied for both parts of the ratio in Eq.1.6, the NRE is unitless and can be expressed as a percent.

Taking all into consideration, plankton respiration depth-profiles from ETS measurements allowed the assessment of the nutrient retention capacity of a plankton community and its variability throughout a geographical section (Packard et al. (2015)). In addition, the use of mathematical analyses highlighted that both the water column NRE, and the F_C are controlled by the curvature of the vertical R_{CO2} profile (|b| in the depth-profile power function).

1.3.2   Heterotrophic energy production

The energy and carbon flux are terms commonly used in ecology to describe the main processes in the ecosystem (solar energy capture, organic matter production or energy dissipation through the food chain in form of heat). However, despite the fact the carbon flux has been widely addressed, the measurement of the energy flow has been rarely assessed (Karl). Surprisingly, even though all life forms live on a complex network of energy flow, the quantification of its capture, transformation and dissipation is not entirely well-known. In 2014, Karl pointed out this lack of knowledge, highlighting the already-existing pioneering methods that could have also been calibrating to assess these energy transformations, instead of just estimating living carbon and oxygen consumption. He was referring, among others, to the Packard's ETS method, the measurement of potential respiration (Φ) (Packard (1971)).

As it has been said before, Φ is a measurement of the mitochondrial electron transport system (ETS) in terms in O_2 consumption. Thus, R_{O2} is coupling with the oxidative phosphorylation of the adenosine diphosphate (ADP). This process results in energy production in the form of ATP (Ochoa (1943)). While measuring

Φ (or R_{O2}), the potential capacity (or actual capacity, respectively) of producing heterotrophic energy by the community can be assessed.

Considering this theoretical basis, Packard et al. (2015) addressed the heterotrophic energy production (HEP) in the microplankton community from Φ measurements, after converting them to R_{O2}). To do so, they related the R_{O2} to energy as expressed in Eq. 1.7:

$$HEP = R_{O2} \cdot 2 \cdot 2.5 \cdot 48 \quad (1.7)$$

where 2 are the number of pairs of electrons ($2e^-$) needed to reduce O_2 to H_2O ($O_2 + 2e^- + 2H^+ \leftrightarrow H_2O$); 2.5 is the number of molecules of ATP generated by the ATP synthase per pair of electrons (ATP/$2e^-$, Ferguson (2010)); and 48 is the Gibbs Free Energy (ΔG) in J per mmol of ATP (Alberty and Goldberg (1992)).

So, with this equation, after considering Karl's suggestion in 2014, Packard calculated the heterotrophic energy transformation from existint ETS data in 2015. In oxic waters, when R_{O2} was expressed in mmol O_2 per time and volume, it was directly converted to J per time and volume (Eq.1.7).

1.3.3   Use of respiratory enzymes as a proxy of the catabolic metabolism in the oceans

The measurement of the enzymes that drive respiration, i.e., their activity (Fruton and Simmonds (1958); Kornberg (1991)), reflects the catabolic metabolism in the plankton community that is used to obtain energy from organic matter. It is the biochemical basis of Harmon Craigâs Deep Metabolism (Craig (1971)) and the driving force for Walter Munk's Abyssal Recipes (Munk (1966)) that was recognized and used by Packard et al. (1971b). Comparison with other oceanographic parameters, linked to anabolic processes such as Chl_a and ^{14}C uptake in photosynthesis, facilitates the assessment of the level of autotrophy or heterotrophy of the community at a certain moment.

However, despite the fact that many oceanographic studies have measured both Chl_a and Φ (Packard et al. (1974); Packard (1979); Packard and Williams (1981); Packard et al. (2000); Packard and Christensen (2004)), only a few assessed the relationship between both parameters (Packard et al. (1974); Martinez et al. (1990); Martinez (1991); Bangqin et al. (2005)). After analysing the reported values and its relationship we observed a Φ/Chl_a ratio variability ranging from 0.3 $\mu LO_2 h^{-1} (\mu g \ Chl\_a)^{-1}$ in eutrophic waters (Packard et al. (2000)) or in the maximum Chl_a depth (Martinez et al. (1990)), to 5 $\mu LO_2 h^{-1} (\mu g \ Chl\_a)^{-1}$ in oligotrophic regions (Martinez et al. (1990)). This variability seems to be related to the dominance of autotrophs or heterotrophs in the community in different regions during certain moments.

In 2014 we participated in a mesocosm experiment where the oligotrophic community was monitored before, during and after a simulated upwelling of en-

riched deep-water. After measuring Φ and having access to the Chl_a measurements we assessed the Φ/Chl_a ratio and monitored the changes in the community metabolisms towards a pure-autotrophic community during the phytoplankton bloom, its shift towards a more heterotrophic one due to the proliferation of heterotrophic dinoflagellates or the moments where mixotrophs (or a mixed community) dominated. Here, we present our results in Chapter 5.

The definition of the values related to a more autotrophic or more heterotrophic community makes the Φ/Chl_a an useful oceanographic tool to determine the metabolic state of the ocean at a certain moment. The measurement of both parameters in a regular basis in oceanography may lead to a further knowledge about the ecosystem, specially in the open ocean.

1.4 Thesis objectives and outline

Taking all into consideration, the present dissertation is, firstly, focused on the development of a new enzymatic assay for $NADP^+$-dependent isocitrate dehydrogenase (NADP-IDH) to facilitate the assessment of the potential CO_2 production in marine plankton. To do so, the following objectives were addressed.

- Objective 1: The development of an assay for marine NADP-IDH activity because this activity is one of the main reactions for the CO_2 production in cells. From existing NADP-IDH assays in yeast, bacteria and fish, a new, composit NADP-IDH assay was adapted to the microplankton and mesozooplankton (Chapter 2).

- Objective 2: The assessment of mesozooplankton potential CO_2 production from NADP-IDH measurements. The relationships among NADP-IDH and all the others CO_2-producing enzymes in the Krebs cycle was assessed in planktonic cells taking into account the studies from Walsh and Koshland (1984) and Alp et al. (1976) (Chapter 3). This approach led to the normalisation of every enzyme activity by the NADP-IDH. Total CO_2 production is the sum of all the CO_2-producing enzymes.

- Objective 3: The assessment of the relationship between R_{CO2} and NADP-IDH activity (Chapter 4). R_{CO2} was measured by following the TC increase in *L. lingvura* incubations. With the collaboration of members of the QUIMA research group. NADP-IDH was determined with the marine plankton NADP-IDH assay.

These three objectives led to a methodological improvement in the assessment of respiration and its impact on the vertical carbon flux in the water column. Furthermore, it allowed a direct measurement of the CO_2 production facet of respiration. This is particularly important in the deep-water studies. It facilitates an improvement in the knowledge of metabolism in bathypelagic organisms and ecosystems.

In addition, a fourth objective was also pursued. It was as an example of how metabolic assays, as oceanographic tools, can improve marine research.

- Objective 4: Use of an enzymatic tool to assess variations in the autotrophy versus heterotrophy state of the microplankton community in the oligotrophic Atlantic ocean during time (Chapter 5). Here, the assesment of the metabolic state is done by measuring Φ per mg of Chl_a during 55 days under the effects of a simulated enriched-deep-water upwelling. Furthermore, the effects of acidification on the former community and its metabolic state, were also studied.

Chapter 2

Chapter 2. NADP$^+$-dependent isocitrate dehydrogenase activity in marine plankton

The existence of atoms and molecules is dominated by 'attractions', 'repulsions', 'wants' and 'discharges', to the point that it becomes virtually impossible to write about chemistry without giving in to some sort of randy anthromorphism.

Nick Lane

RESUMEN: En este capítulo se recoge cómo se ha medido la NADP$^+$-isocitrato deshidrogenasa, una de las principales enzimas productoras de CO_2, en el plancton marino. Para ello, se ha adaptado la metodología a las fracciones de 0,7-50μm, 50-200μm, y 200-2000μm de la comunidad planctónica de las Islas Canarias. Durante el proceso se estudió la variabilidad de la actividad de la NADP-IDH en relación con el pH, temperatura, dilución de la muestra, centrifugación o la concentración de sustratos. En nuestras condiciones de trabajo, la velocidad máxima de reacción (V$_{max}$) se alcanzó en un buffer fosfato 0,1M, con un pH 8,2 (*pKa$_1$*=7,6 y *pKa$_2$*=8,8), añadiendo 6mM de MgCl$_2$, 0,3mM de NADP$^+$ y 2mM de isocitrato DL-trisódico. La temperatura óptima de reacción para el mesozooplancton subtropical fue 28°C, con una energía de activación de Arrhenius (*Ea*) de 20,4 Kcal mol^{-1} (85,4J mol^{-1}), y un factor de frecuencia de colisión (*A*) de 2,9·10^{11} mol NADPH s^{-1} (Kg of protein)$^{-1}$. Las constantes de Michaelis-Menten (*Km*s), que muestran la afinidad de la enzima con sus sustratos a pH 8,5 y 18°C fueron 271$\pm$63 μM para el isocitrato y 18$\pm$3 μM para el NADP$^+$. Esta enzima, aparte de ser una de las principales responsables de la producción de CO_2, puede utilizarse para el estudio de: (1) la respiración en muestras marinas; (2) el flujo de carbono en la columna de agua; (3) las adaptaciones metabólicas de los organismos ante cambios medioambientales; (4) el pa-

pel de los distintos componentes de la comunidad planctónica en la cadena
trófica; y (5) la capacidad de mitigación de las especies de oxígeno reactivo
(ROS) de los recursos planctónicos marinos.

ABSTRACT: NADP$^+$-isocitrate dehydrogenase (NADP-IDH), as one of the
most active intracellular CO_2-producing enzymes, was measured in marine
plankton by adapting an enzyme assay to the 0.7-50μm, 50-200μm, and
200-2000μm size fraction of the Canary Islands coastal plankton commu-
nity. The variability of NADP-IDH activity in relation to pH, temperature,
dilution of the sample, centrifugation or substrates was measured. In our
hands, the maximum NADP-IDH activity (V_{max}) in marine plankton samples
was attained in 0.1M phosphate buffer at pH 8.2 (pKa_1=7.6 and pKa_2=8.8),
by adding 6mM $MgCl_2$, 0.3mM NADP$^+$ and 2mM DL-trisodium isocitrate.
The optimum temperature in these subtropic mesozooplankton samples was
28°C, with an Arrhenius energy of activation (*Ea*) of 20.4 Kcal mol^{-1} (85.4J
mol^{-1}), and an Arrhenius collision frecuency factor (*A*) of 2.9·10^{11} mol
NADPH s^{-1} (Kg of protein)$^{-1}$. The apparent Michaelis-Menten *Km* values
for the substrates in crude homogenates at pH 8.5 and 18°C were 271$\pm$63
μM for isocitrate and 18$\pm$3 μM for NADP$^+$. This enzyme, in addition to its
high CO_2-producing activity, can be used to calculate: (1) respiration in ma-
rine samples; (2) carbon flux in the water column; (3) metabolic adaptations
to environmental changes; (4) roles of the plankton components of the food
chain; and (5) the reactive oxygen species (ROS) scavenging capacity of the
marine plankton resources.

2.1   Introduction

Here, we propose the first step of a further enzymatic assessment of the CO_2 pro-
duction related to the marine plankton respiration. To do so, we have developed an
oceanographic tool to accurately measure the activity of NADP$^+$- dependent isoc-
itrate dehydrogenase (NADP-IDH, Eq. 1.3) and characterize the properties of this
enzyme in the marine plankton. We have considered previous studies of NADP-
IDH activity in yeast, marine bacteria, and marine fish (turbot) (Berdalet et al.
(1995a); Kornberg and Pricer (1951); Munilla-Moran and Stark (1989); Munilla-
Moran (1994); Packard et al. (1996a); Roy and Packard (2001)). This is the first
time NADP-IDH has been measured in marine plankton. Thus, in order to make
this assay sensitive to all its components, we fractionated plankton samples into
three separated size-fractions. We measured NADP-IDH activity in the Canarian
microplankton (0.7 to 50μm), microzooplankton (50 to 200μm,), and mesozoo-
plankton (200-2000μm). These microplankton samples are mixed communities
with heterotrophic organisms (procaryotes, nanoflagellates and also small dinoflag-
ellates) and also autotrophs (cyanobacteria, other eukaryotic picoplankton, au-
totrophic nanoflagellates and some diatoms) (Schmoker et al. (2013)). The micro-
zooplankton community around the Canary Islands is dominated by heterotrophs

(large ciliates and dinoflagellates). Finally, Canarian mesozooplankton is also dominated by heterotrophs, largely crustacean copepods (Hernández-León et al. (2007)).

In summary, here we propose a new method to assess NAPD-IDH activity in the marine plankton community. This tool may be useful in further studies on CO_2 production in the water column, lipid synthesis in the base of the food chain, and in studies on the ROS scavenging capacity of the marine plankton resources.

2.2 Material and Methods

Assessing NADP-IDH activity, accurately and reproducibly, requires determinations of the optimum substrate concentration, optimum cofactor concentration (sections 2.2.4 and 2.3.1), and optimum pH (sections 2.2.5 and 2.3.2). Also, the nature of the temperature dependence (sections 2.2.6 and 2.3.3) and the biomass linearity (sections 2.2.8 and 2.3.4) need to be determined (Suelter et al. (1985)). In addition, other factors such as the optimum time and speed of centrifugation (sections 2.2.7 and 2.3.5); as well as the stability of the enzyme preparation (sections 2.2.9 and 2.3.6), were assessed. Quantifying these factors not only makes the assay accurate and reproducible, but it stimulates the reaction to emit its maximum signal. Other factors that enhance the assays accuracy have been included in the Appendix A. These include: buffer sensitivity (Appendix A.1); extinction coefficient (Appendix A.2); precision (Appendix A.6); and spectrophotometric response (Appendix A.7).

2.2.1 Plankton sampling procedures

Zooplankton were collected off the north coast of Gran Canaria Island (GCI) from the upper 10m of the euphotic zone, stored alive in plastic containers until fractionated through 2000μm, 200μm, and 50μm nets in the laboratory, and finally stored for less than 3 months in 2mL microcentrifuge tubes at -80°C until enzyme analysis (Ahmed et al. (1976)). Microplankton were sampled from Alcaravaneras Beach, GCI. Seawater samples were stored in 25L high-density polyethylene containers until they were filtered through a 50μm net and then through a 0.7μm glass fiber filter (GF/F) in the laboratory. Note that the use of a 0.7μm filter instead of a 0.2μm, means a large percentage of the bacterial and archaeal community were not included in this measurement. After being blotted to remove excess seawater, all samples were stored, for less than 3 months, on the GF/F filters, in 2mL microcentrifuge tubes, at -80°C until analysis (Ahmed et al. (1976)).

2.2.2   Crude homogenate preparations and protein determination

The zooplankton samples from above, were homogenized in 0.1M phosphate buffer
(0.1M Na$_2$HPO$_4$, 0.1mM KH$_2$PO$_4$, 75μM MgSO$_4\cdot$ 7H$_2$O, PVP (1.5mg mL^{-1}),
TRITON X-100) (Appendix A.1), by sonication for 45sec at 70% amplitude in a
Vibracell VCX 130 Sonics$^{\circledR}$ ultrasonic processor maintained at 0-4°C. Zooplank-
ton homogenates ranged from 1.2 to 15mL. Microplankton samples were homog-
enized at 0-4°C in the same 0.1M phosphate buffer, with a Teflon$^{\circledR}$ 2mL-pestle
PYREX$^{\circledR}$ Potter-Elvehjem tissue grinder at 2600rpm for 2 min. Microplankton
homogenate volumes ranged from 1.0 to 1.2mL. Homogenate volume (V_t) was
measured to 50μL. Crude homogenates were centrifuged in 2mL microcentrifuge
tubes at 0-4ºC and 4000rpm in an 8.4cm-radius centrifuge rotor (giving 1500 g)
for 10 min. Biomass, as mg of protein, was determined from subsamples of the
crude homogenate. The protein method of Lowry et al. (1951) modified by Rutter
(1967) was used. Bovine serum albumin was the standard.

2.2.3   NADP-IDH assay

NADP-IDH activity was measured kinetically by following the time dependent
production of NADPH (Δ_{NADPH}) at 340nm (Δ_{340}) and 18°C in a 1cm plastic cu-
vette (l) in a Cary 100 U-V visible spectrophotometer for 1000sec. To be clear,
Δ_{340} is the time-dependent absorbance increase at 340nm of the reaction in the
spectrophotometer. [NADPH], at any time, was determined by the Beer-Lambert
law (2.1) from the absorbance (A_{340}), the molar absorption coefficient for our re-
active solution (ε), and the optical pathlength of the cuvette (l) (see Appendix
A.2).

A_{340}=$l\cdot\varepsilon\cdot$[NADPH] (2.1)

So, transposing and using 5.42 absorbance units mL μmol^{-1}cm^{-1} for ε, we ob-
tained Eq.2.2 for the calculation of NADPH in mmol^{-1} mL^{-1}:

[NADPH]=A_{340}/(5.42$\cdot l$) (2.2)

If A_{340} is followed kinetically over time (t), then the slope (A_{340}) becomes
Δ_{340} and Eq.2.2 becomes: [Δ_{NADPH}]= Δ_{340}/(5.42$\cdot l$). The reaction was carried
out in 0.5mL of 0.1M phosphate buffer (pH 8.5), with 6 mM MgCl$_2$ (PANREAC
#131396), 2.1 mM DL-trisodium-isocitrate (SIGMA #I1252; which, from here on,
we will call, isocitrate) and 0.3 mM β-NADP$^+$ (SIGMA #N0505; which, from
here on, we will call, NADP$^+$) in the cuvette. The blank assay (B$_{340}$) controlled
for the background activity of other enzymes and the non-enzymatic reduction of
NADP$^+$. It lacked isocitrate. Occasionally, to check for contamination and to as-
sess any non-enzymatic reaction between NADP$^+$ and isocitrate, an assay was run
without homogenate. Normally, contamination and any non-enzymatic reaction

between $NADP^+$ and isocitrate are negligible. For all assays and blanks, the reaction volume in the cuvette (V_c) was maintained at 0.5 mL with buffer. The assay consisted of sequential additions of 0.3mL of a solution containing 10mM $MgCl_2$ and 3.5mM isocitrate, 0.1 mL homogenate (V_h), and 0.1mL of 1mM $NADP^+$ to a 1mL cuvette. $NADP^+$ started the reaction. After 3 min, the linear signal (Δ_{340}) represented the NADP-IDH activity. Δ_{340} depended on V_c. To relate Δ_{340} per mL of the solution to the original homogenate which represents the sample (V_s), Δ_{340} must be multiplied by the factor, ($V_s \cdot V_c/V_h$) (Eq.2.3). Since the original units of Δ_{340} are $cm^{-1} sec^{-1}$, it must be multiplied by 60 sec min^{-1}, multiplied by 1 cm (pathlength), and divided by 5.42 absorbance units mL $\mu mol^{-1} cm^{-1}$ (ε) (Eq.2.3) (Appendix A.2). This calculation is for the production of NADPH per time, per sample:

$$\Delta_{NADPH} = ((\Delta_{340} - B_{340}) \cdot 60 \cdot V_s \cdot V_c)/(5.42 \cdot V_h) \quad (2.3)$$

A unit analysis of Eq.2.3 is:

Δ_{NADPH} [$\mu mol\ min^{-1}\ mL^{-1}$] = ($\Delta_{340}$-$B_{340}$) [absorbance units $cm^{-1}\ sec^{-1}$]·60 [$sec\ min^{-1}$]·V_s [mL]·V_c [mL]/(5.42 [absorbance units $cm^{-1}(\mu mol \cdot mL^{-1})^{-1}$]·$V_h$ [mL])

Since CO_2 is produced stoichiometrically 1:1 with NADPH, this results in NADP-IDH activity in units of mM $CO_2\ min^{-1}$ per sample. Note that, to promote oceanographic significance, we do not follow the biochemical convention of enzyme units. The NADP-IDH activity could be reported for microplankton in terms of seawater volume; for zooplankton field samples in terms of net-haul volume, or for physiological/biochemical experiments in terms of protein.

2.2.4   Kinetic properties of NADP-IDH activity

The affinity between substrates and the mineral cofactor (Mg^{2+}) and NADP-IDH was determined in the three plankton size-fractions (Section 2.3.1). Their optimum concentrations, their effective Michaelis-Menten constants (K_ms) and the NADP-IDH maximum velocity (V_{max}) were calculated from Michaelis-Menten and Hanes-Woolf plots (Suelter et al. (1985)). First, using the same homogenate at pH 8.5 and 18°C, NADP-IDH activity was measured, in triplicate, for ten different concentrations of isocitrate. These ranged from 0.002 to 2.1mM in the cuvette, while $MgCl_2$ and $NADP^+$ were held constant at 2mM and 0.3mM, respectively. Second, NADP-IDH activity was measured in the same homogenate, at the same conditions as above, but with isocitrate being held at its optimum, 2.1mM, while 10 concentrations of $NADP^+$ from 0.4 to 400μM in the cuvette, were tested. Finally, to determine the optimum concentration of $MgCl_2$, the same procedure was followed. NADP-IDH activity was measured in the same homogenate, at the same conditions as above, with 2.1mM isocitrate, and 0.3mM $NADP^+$ (its optimum), while 9 concentrations of $MgCl_2$ from 0.05 to 12mM, were tested. Before each experiment, pilot experiments were performed in order to determine the concentra-

tion ranges needed to minimize errors in the linearisation of the Michaelis-Menten equations.

We tried three linearisation techniques to evaluate the K_ms (Appendix A.3). Hanes-Woolf linearisation was the most precise for our data base ($p<0.001$ in the whole community). In Hanes-Woolf plots, substrate concentration [S] was plotted against the ratio of concentration to enzymatic activity ([S]/V). The V_{max} was the inverse of the slope (a) (i. e., $V_{max} = 1/a$), whereas K_ms were equal to the ratio of the Y intercept (y_0) and a ($K_m = y_0/a$) (Suelter et al. (1985)).

2.2.5   pH optimum

The effect of pH on NADP-IDH activity was determined on mesozooplankton samples at 18°C. Assays were run using phosphate buffer at eleven levels of pH from pH 5.5 to pH 11 (Section 2.3.2 and Appendix A.4). The buffer solution was the same as used for homogenization, reagent solutions, and the kinetic assay. Assays were done kinetically, in quintuplicate, with 0.2mM NADP$^+$, 2.1mM isocitrate and 2mM MgCl$_2$ in the cuvette.

2.2.6   Temperature dependence

The temperature (T) dependence of activity in NADP-IDH in crude mesozooplankton homogenates and in pure NADP-IDH from porcine heart (Sigma Aldrich #I2002) was determined at pH 8.5 (Section 2.3.3). Assays were conducted, in triplicate, under optimum conditions, at nine temperatures ranging from 5 to 60°C. The Arrhenius equation describes the temperature dependence of chemical reaction rates (Eq.2.4 (Arrhenius (1889)):

$$k_{IDH}=A\cdot exp^{(-E_a/(R\cdot T))} \quad (2.4)$$

where: k_{IDH} is NADP-IDH activity; A is the preexponential frequency factor in the same units as k_{IDH}. It is a unique value for each chemical reaction and is related to the collision frequency when reactants are in the correct orientation. Ea is the energy of activation in Kcal mol^{-1}; T is the absolute temperature in °K and R is the universal molar gas constant in Kcal mol^{-1} °K^{-1} (1.9872· 10^{-3} Kcal mol^{-1} °K^{-1}). The Ea and A were obtained from the Arrhenius plot (Fig. 2.3). Eq.2.5 describes the linear regression from this Arrhenius plot (y=a·x +y_0), where x is 1/T, the slope (a) is -Ea/R, and y intercept (y_0) is ln$A$:

$$\ln(k_{IDH})=\ln(A)-(E_a/R)\cdot(1/T) \quad (2.5)$$

The enthalpy of activation (ΔH^*), in Kcal mol^{-1}, for 25°C was calculated from the E_a according to Eq.2.6 (Low et al. (1973)):

$$\Delta H^*=E_a-R\cdot T \quad (2.6)$$

Here, T is expressed in °K (298°K).

The effect of T on NADP-IDH was also assessed by measuring the Q_{10} temperature coefficient, a unitless factor by which the activity increases for every 10-degree rise in T (Przibram (1923)). Q_{10} was measured according to Eq.2.7, where NADP-IDH$_{T2}$ was the NADP-IDH activity at T_2 (T_2=25°C), and NADP-IDH$_{T1}$ was the NADP-IDH activity at T_1 (T_1=15°C).

$$Q_{10}=(\text{NADP-IDH}_{T2}/\text{NADP-IDH}_{T1})^{10/(T2-T1)} \quad (2.7)$$

2.2.7 Centrifugation studies

Homogenate centrifugation separates cell membranes and organelles from the cytosol, it clarifies the homogenate, and increases assay sensitivity. Effects of centrifugation on NADP-IDH activity were analysed at pH 8.5 and 18°C. Five experimental conditions were tested: (1) a blank without centrifugation, where activity was measured after 8min of gravitational sinking; (2) 2min at 1000 rpm (375 g); (3) 2min at 2000rpm (750 g); (4) 2min at 4000rpm (1500 g); (5) 10min at 4000 rpm (1500 g). Measurements were made in quintuplicate. NADP-IDH activity was reported in units of μmol NADPH min^{-1}(mL of homogenate)$^{-1}$ units and normalized by V$_{max}$ to give a percentage.

2.2.8 Linearity with enzyme concentration and limit of detection

Establishing linearity with enzyme concentration in crude homogenates is essential for any enzyme assay. Here, it was tested for microplankton and mesozooplankton by diluting original homogenates (Section 2.3.4). Protinaceous biomass was simultaneously diluted and proxied for NADP-IDH concentration. Seven dilutions from 5% (4μg protein mL^{-1}) to 100% (83μg protein mL^{-1}) of the original were made for microplankton and nine dilutions, from 0.39% (3μg protein mL^{-1}) to 100% (684μg protein mL^{-1}) were made for the mesozooplankton. Activity was measured at 18°C, with the optimised assay. The limit of detection was determined by plotting the NADP-IDH activity against the homogenate protein (Fig.2.4), as the lowest biomass with a standard deviation lower than 50% of the NADP-IDH activity.

2.2.9 Stability of the crude homogenate

Stable enzyme activity in crude homogenates promotes ease, flexibility and dependability of analysis. We assessed NADP-IDH activity stability in Mysids (*Leptomysis lingvura*). Samples were collected off Taliarte, GCI by scuba using an 8$''$ net, transferred to the lab as were the zooplankton (above), gently pipetted into 2mL microcentrifuge tubes, and stored at -80°C until analysis. Mysids were homogenized by sonication as explained above. The homogenate was always main-

tained on ice. Loss of NADP-IDH activity per time after homogenisation was measured at 18°C, under optimum assay conditions (above). Activity was measured in triplicate, every 90min, for 8h; and was reported in μmol NADPH min^{-1}(mL of homogenate)$^{-1}$. Then it was normalized by V$_{max}$ to give a percentage of maximum activity (Section 2.3.6).

2.2.10 Statistics of the substrate and temperature kinetics

In substrate kinetic studies (Section 2.3.1), *F* tests (Pentecost (1999)) quantified the differences between the logarithmically transformed Michaelis-Menten curves (lnV vs ln[S]). *F* tests were also used with the Arrhenius plots (Section 2.3.3). The *t* test (Sachs (2012)) quantified differences between the regression coefficients of the Arrhenius plots.

2.3 Results

2.3.1 Kinetic properties

Substrate, cofactor and effector concentrations were determined to optimize the conditions of the enzyme assay. As standard practice in developing an enzyme assay, NADP-IDH kinetic constants were calculated from Michaelis-Menten plots (Fig.2.1 and Appendix A.3) and Hanes-Woolf linearisation. The average K_ms were 271$\pm$63μM for isocitrate, and 18$\pm$3μM for NADP$^+$. For the metal cofactor MgCl$_2$, that stimulated NADP-IDH activity following a rectangular-hyperbola, its concentation at 1/2 V$_{max}$ was 3060$\pm$643μM (Appendix A.3). For isocitrate, V$_{max}$ was 0.038 in mesozooplankton; 0.031 in microzooplankton; and 0.002 in microplankton. For NADP$^+$, V$_{max}$ was 0.029 in mesozooplankton; 0.019 in microzooplankton; and 0.001 in microplankton. For MgCl$_2$, V$_{max}$ was 0.010 in mesozooplankton; 0.009 in microzooplankton; and 0.00002 in microplankton. V$_{max}$ is in μmol NADPH min^{-1} (mL homogenate)$^{-1}$ units.

The optimal values to measure NADP-IDH activity (100% V$_{max}$ in Fig.2.1) in this community are 2mM for isocitrate and 0.3mM for NADP$^+$ (Fig.2.1). By inspection of Fig.2.1c, we conclude that, although 4mM of MgCl$_2$ would be enough to reach the V$_{max}$ in the zooplankton fractions, an optimal value of 6mM for MgCl$_2$, is needed to ensure that all the community reaches 100%V$_{max}$.

[a]

[b]

[c]
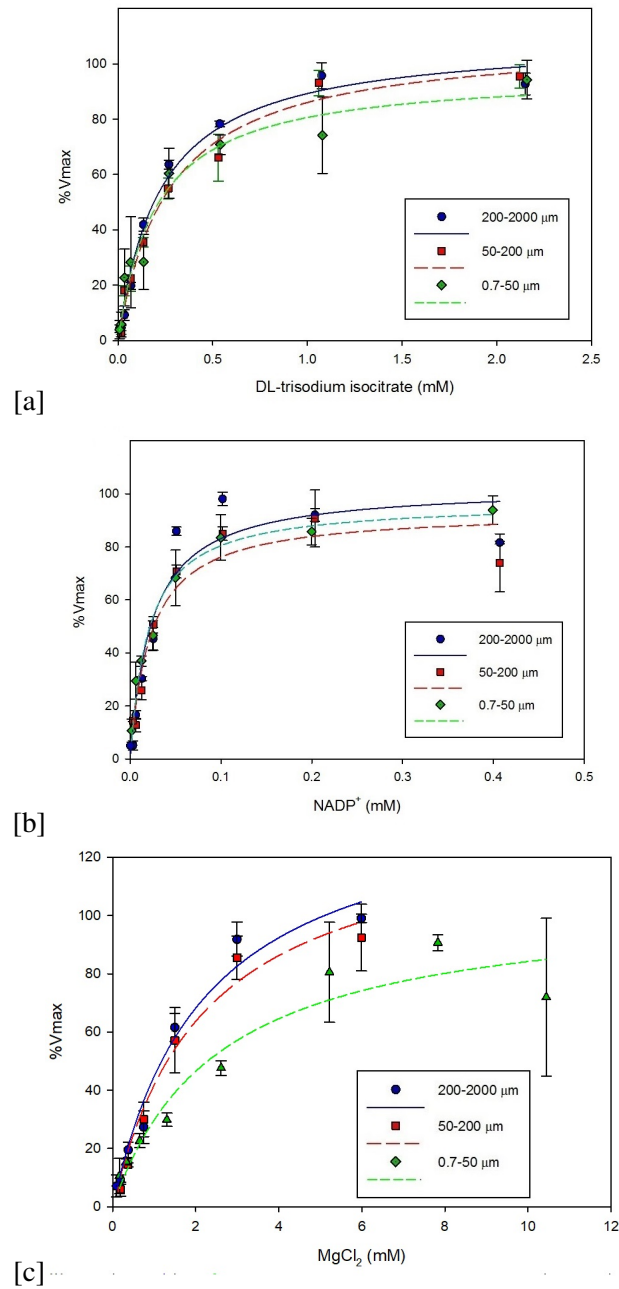
Figure 2.1: Michaelis-Menten plots to determine the NADP-IDH K_m and optimum values for isocitrate, NADP$^+$ and MgCl$_2$ for different plankton community size fractions. (a) Affinity between NADP-IDH and isocitrate. (b) Affinity between NADP-IDH and NADP$^+$. (c) Affinity between NADP-IDH and Mg^{2+}.

2.3.2   Effect of pH

The effect of pH on the catalytic activity of the NADP-IDH was measured on phosphate buffer at 18°C, with the same concentration of ligands. In our hands, the maximum activity was obtained at pH 8.19 (Fig.2.2), whereas measurements below pH 7.62 and above pH 8.75 led to activities lower than 50% of its V$_{max}$ (*pKa*s) (Appendix A.4).
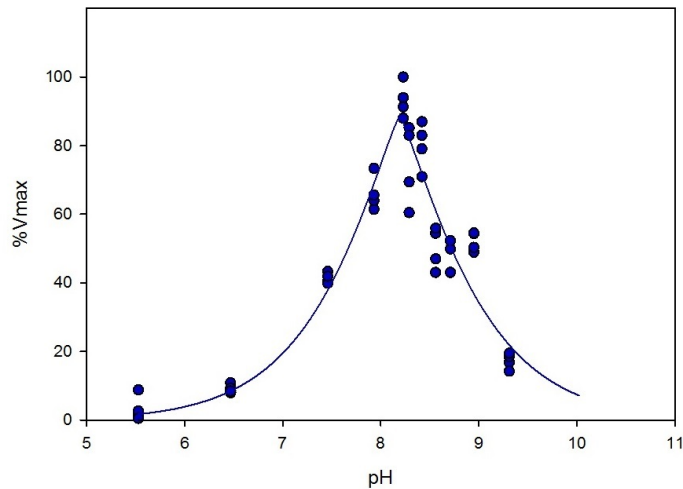
Figure 2.2: pH effects on mesozooplankton NADP-IDH activity, where V$_{max}$ was 0.027 μmol NADPH min^{-1} (mg protein)$^{-1}$.

2.3.3   Effect of Temperature

The relationship between NADP-IDH activity and temperature was studied on mesozooplankton samples and compared to the results from pure porcine-heart NADP-IDH (Fig.2.3). Both activities increased with temperature before reaching an optimum temperature, 27.6°C on the subtropical mesozooplankton samples, and 38.6°C on the pure porcine-heart NADP-IDH ones. At higher temperatures, the activity decreased. Besides, Q_{10} between 15°C and 25°C was 1.98 for mesozooplankton samples. Although this value is higher than the NADP-IDH in turbot larvae between 20-35°C (1.74) (Munilla-Moran (1994)), it is consistent with the Q_{10} for respiratory rates in epipelagic marine copepods (1.8-2.1) (Ikeda et al. (2001)). From this data set, the Arrhenius energy of activation (*Ea*) had a value of 20.4 Kcal mol^{-1} for the subtropical mesozooplankton samples and 21.40 Kcal mol^{-1} for the pure enzyme from porcine heart; the Arrhenius frequency factor (*A*) was 2.19·10^{11} mol NADPH s^{-1} (kg of protein)$^{-1}$ for the mesozooplankton samples and 1.60·10^{13} for the pure porcine heart NADP-IDH; and finally, the Arrhenius enthalpy of activation at 25°C (ΔH*) was 19.81 Kcal mol^{-1} for the mesozooplankton

samples and 20.76 Kcal mol^{-1} for the porcine heart NADP-IDH. These results suggested that, for NADP-IDH, although the frequency factor (A) was different (F test, $F_{(2,37)}$=4.64, p=0.05), Ea and ΔH* were not significantly different between the two types of organisms (t test, $t(39)$=0.0773, p=0.05).

This permits the development of a common Arrhenius equation for both types of NADP-IDH. When the in-situ T (T_i) is different from T during the assay (T_m), the measured NADP-IDH activity needs to be corrected for the difference. The in-situ activity (NADP-IDH(T_i)) is calculated using the Arrhenius equation (Atkin and de Paula (2006), Appendix A.5), based on Arrhenius Ea (Eq.2.8):

$$\text{NADP-IDH}(T_i) = \text{NADP-IDH}(T_m) \cdot exp^{((20.39/R) \cdot (1/T_m - 1/T_i))} \quad (2.8)$$

where: NADP-IDH(T_i) is NADP-IDH activity at T_i; NADP-IDH(T_m) is NADP-IDH activity at T_m; and R is 1.9872$\cdot$10^{-3} Kcal mol^{-1} $^{\circ}$K^{-1}.
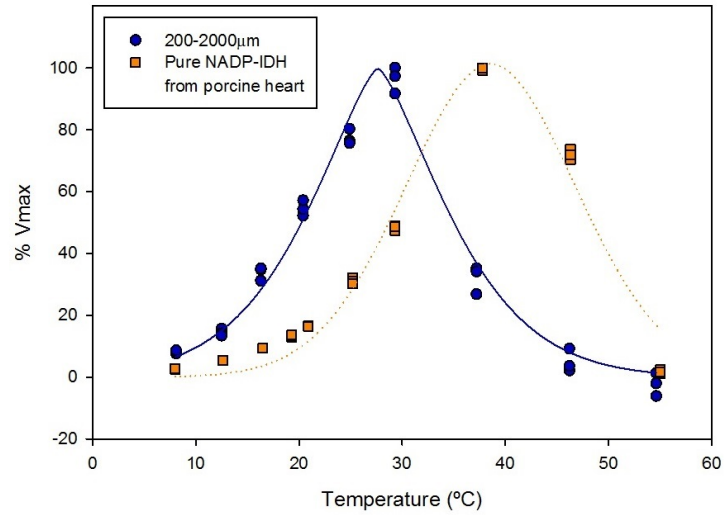
[a]
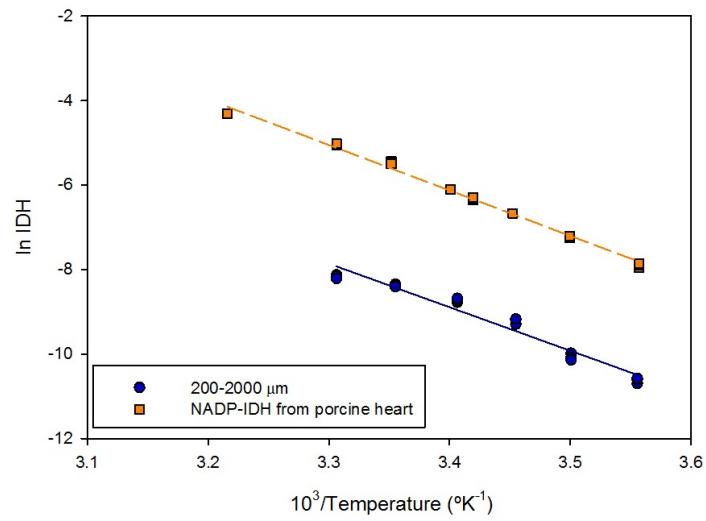
[b]

Figure 2.3: Temperature dependence of NADP-IDH activity. (a) Temperature impact on NADP-IDH activity, where V$_{max}$ was 0.018μmol NADPH min^{-1} (mg of protein)$^{-1}$ in mesozooplankton and 0.808μmol NADPH min^{-1} (mg of protein)$^{-1}$ in pure porcine heart enzyme. (b) Arrhenius plot, where ln(k_{IDH}) is plotted against 1/T and T is in $^{\circ}$K units.

2.3.4   Biomass linearity and limit of detection

Once optimum conditions were applied, the NADP-IDH could be measured with an standard deviation less than 3.5% on every ten duplicates (Appendix A.6). To determine the limit of detection, NADP-IDH was measured in seven different dilutions using both the mesozooplankton and the microplankton homogenates. The linearity in Fig.2.4, shows that the relationship between NADP-IDH and biomass holds even when samples are diluted to 1% of the original strength. The limit of detection for mesozooplankton samples was $10\pm2\mu$g protein mL^{-1} and for microplankton samples, it was $8\pm2\mu$g protein mL^{-1}.
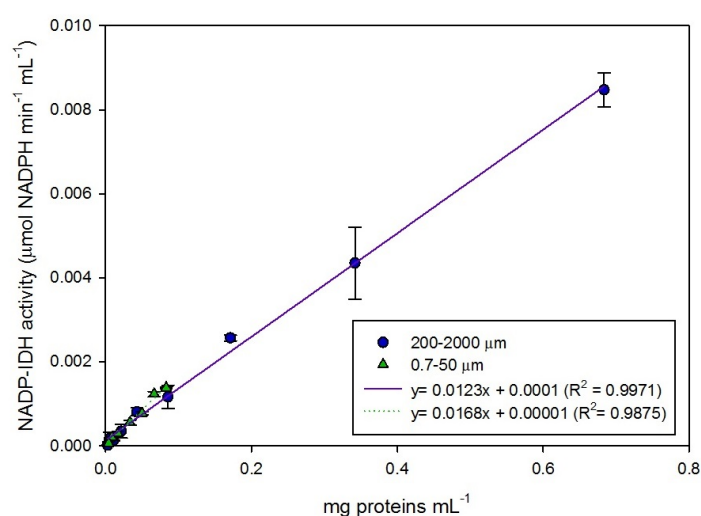
Figure 2.4:   Biomass linearity of marine-microplankton and marine-mesozooplankton NADP-IDH. Enzyme activity as a function of protein in the homogenate.

For microplankton samples under oligotrophic conditions, this biomass can be attained by filtering 4L through 0.7 GF/F glass fiber filters, whereas during eutrophic conditions, 2.5L were enough. In deep water samples, more volume will be required (10L or even 20L) to stay above the limit of detection. For unknown conditions, and also for mesozooplankton samples, pilot measurements to determine the optimum seawater volume needed should be made (see Section 2.2).

2.3.5   Effect of centrifugation

GF/F filtered samples (microplankton, green columns in Fig.2.5) need centrifugation greater than 1500g for 2min to achieve the maximum NADP-IDH activity and a low standard deviation (12.6 % of the activity). Note that without centrifugation the signal is obscured by the turbidity of the filter fibers.
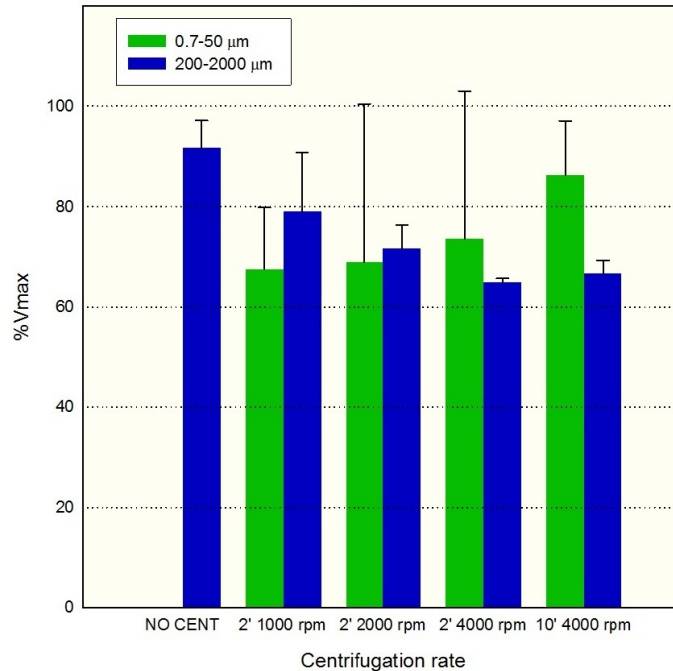
Figure 2.5: Centrifugation effects on NADP-IDH activity, where V$_{max}$=0.0073 in mesozooplankton and 0.0008 in microplankton. V$_{max}$ is in μmol NADPH min^{-1} (mL homogenate)$^{-1}$ units. Note that, for our centrifuge, a force of 375g was achieved at 1000rpm; 750g was achieved at 2000rpm; and 1500g was achieved at 4000rpm.

Sonicated samples (mesozooplankton, blue columns in Fig.2.5), on the other hand, are not improved by centrifugation. However, part of the activity reached without centrifugation is related to a negative blank, which may indicate that either other enzymes are consuming NADPH or that particle sinking has interfered with the signal. As both problems are solved by centrifugation, we argue that sonicated samples should be centrifuged at a minimum of 375g for 2min.

2.3.6 Stability of the enzyme preparation from mysid samples

NADP-IDH activity decreased continuously (Fig.2.6) during the 500min experiment. However, the regression coefficient of 0.109 (r^2=0.9771, p<0.0001) indicates an average loss of 1.1% of NADP-IDH activity per 10min. This means that only 3% of the activity is lost if analyses are run within half-hour after centrifugation.
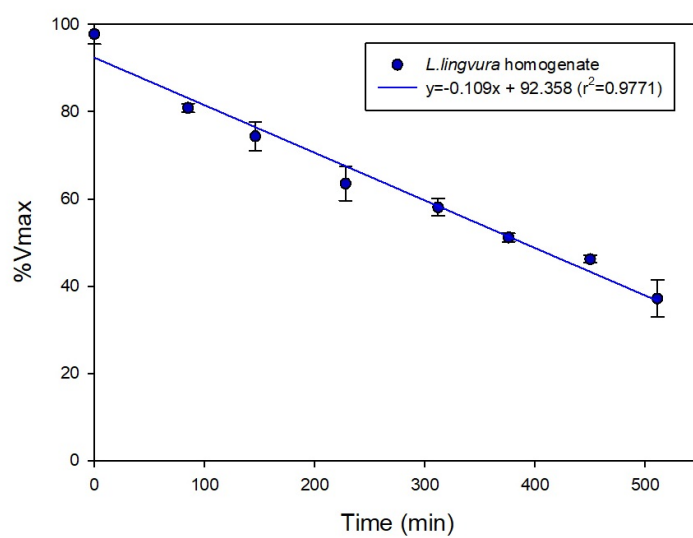
Figure 2.6: Stability of the enzyme preparations from *L. lingvura* samples, where V_{max}=0.0085μmol NADPH min^{-1} (mL homogenate)$^{-1}$. T_0 is the end of the centrifugation process.

2.4 Discussion

2.4.1 What does the development of the assay reveal about plankton NADP-IDH?

While determining the conditions for assaying the V$_{max}$ of NADP-IDH, we also determined the K_m for isocitrate, NADP$^+$ and MgCl$_2$ (Fig. 2.1, Appendix A.3). Earlier research on IDH in marine bacteria cultures developed mathematical models to determine the physiological R_{CO2} (Roy and Packard (2001); Packard et al. (1996a)), but the research was not extended to ocean microplankton and zooplankton. Here, the older IDH assay (Berdalet et al. (1995b)) has been revised, modified, and updated for ocean plankton samples. As always in science, additional research is still needed. However, we predict that, given this updated assay, new models based on measurements of NADP-IDH, isocitrate and NADP$^+$ in marine plankton will result in improved assessment of marine R_{CO2}. In addition, being able to measure NADP-IDH opens up new research avenues for plankton research. For example, cytosolic NADP-IDH measurements may facilitate the assessment of lipid synthesis at the base of the marine food chain (Koh et al. (2004)). Also, because Wieckowski et al. (2009) have greatly improved the isolation of mitochondria from cytosol, mitochondrial NADP-IDH measurements may proxy the ROS scavenging capacity of cells (Jo et al. (2001)).

On marine plankton samples, NADP-IDH measurements should be done maintaining the buffer, pH levels, and the Arrhenius relationship developed in this study. If these conditions are changed, the K_ms would need to be reassessed (Olano et al. (1995)). In our hands, isocitrate, NADP$^+$ and MgCl$_2$ K_ms were up to one order of magnitude higher than other reported values (Munilla-Moran (1994)). These differences can be attributed to our specific chemical conditions (buffer, pH, T) that are likely responsible for the variations in the affinity between enzymes and their substrates (Olano et al. (1995)).

Michaelis-Menten constants are affected by pH levels that impact ionisation around the enzyme active site. Our results, with an optimum pH of 8.2 (section 2.3.2), are consistent with those reported in turbot larvae (optimum pH between 7.8 and 9.0) (Munilla-Moran (1994)). The pK_as of 7.62 and 8.75, which are close to the optimum value, indicate a high enzyme sensitivity to pH changes. As the pH involved in the reaction is intracellular, it is controlled by cellular membranes so slight environmental pH changes are unlikely to affect the intracellular enzymatic activity (Simčič and Brancelj (2006)). However, the influence of pH on the metabolic response (in the short, medium and long term) of the plankton community should be assessed in further research, particularly in the current scenario of increasing ocean acidification.

Another key factor that impacts enzyme kinetics is temperature (T). The NADP-IDH activity in the subtropical mesozooplankton drops as T rises above 27.6^{o}C, whereas in pure NADP-IDH from porcine heart, this occurs above 38.6^{o}C. This

decreasing activity can be related: (1) to denaturation of the enzyme; (2) to a direct effect of T on the collision history at any stage of the reaction (formation of the enzyme-substrate complex; conversion of the enzyme-product complex; or dissociation of the product); (3) or to the ionisation of the different groups comprising the active site. This will change the substrates' K_ms even under the same pH conditions (Dixon and Webb (1979)). Under a global warming scenario, further research on the T effects on plankton metabolism and the biochemical response will improve our knowledge about the magnitude and reversibility of the negative high-temperature effects on respiratory metabolism and physiology. These future studies will be relevant for poikilotherms, taking into account that environmental temperatures higher than the optimum (25-30°C for subtropical mesozooplankton) will affect the enzymatic structure that supports the metabolism of these organisms. High-latitude plankton communities, likely with a lower optimum T, should be particularly studied. In the case of homoeothermic samples (from porcine heart) the optimum T is around ten degrees higher than in poikilothermic samples. However, Ea and ΔH^* are not significantly different, being also consistent with Ea reported by Munilla-Moran for NADP-IDH in turbot (around 23.5 Kcal mol^{-1} on turbot liver and 23.3 Kcal mol^{-1} for turbot larvae) and by Moon and Hochachaka for cold-adapted and warm-adapted NADP-IDH in rainbow-trout liver (18 Kcal mol^{-1}) (Munilla-Moran (1994); Munilla-Moran and Stark (1989); Moon and Hochachka (1971)). Thus, although there seems to be an adaptation to homoeothermic conditions allowing high activity at higher temperatures, a common basic structure seems to have been maintained even after differences in evolution.

2.4.2   Why should this metabolic assay be measured kinetically?

While studying enzyme activities, two approaches can be used: (1) Two point measurements (endpoint); and (2) time-course monitoring (kinetics). Endpoint measurements are only feasible, with reliable results, when the reaction is linear, and this condition must be frequently validated (Škorjanc and Pette (1998)) unless the behaviour of the sample is well-known. Here, all measurements were made kinetically, and even though the linear relationship was well maintained for more than 1000s, we realise that some conditions, such as low and high biomass samples, the lag until thermal equilibrium in the cuvette, or the blank signalling may change the linearity of the reaction (see Appendix A.7), rendering endpoint detection unsuitable. From these different observations we conclude that by measuring the A_{340} kinetics for 1000 seconds, the NAPD-IDH activity can be determined with confidence. This time-course analysis demonstrates the impact of pH, T, dilution, substrate concentration, biomass and centrifugation (see Appendix A.7). This visualisation, not detected by end-point approach, lends itself to modifying assay conditions when needed. Thus, we recommend using kinetics for measuring NADP-IDH in oceanographic research.

2.5   Conclusions

- An enzyme assay for IDH (NADP-IDH) in zooplankton and microplankton, based on the reduction of NADP$^+$ has been developed.

- The apparent Michaelis-Menten constants for the substrates were 271 ± 63 μM for isocitrate and 18 ± 3 μM for NADP$^+$.

- The rates of NADPH formation (μmol NADPH min^{-1} mL^{-1}) are obtained kinetically at 340nm. Activities in μmol of NADPH were based on a molar extinction coefficient (ε) of 5.42 mL μmol^{-1}cm^{-1}.

- Each laboratory should verify ε for their solutions and laboratory conditions to reduce error.

- Arrhenius plots for NADP-IDH in mesozooplankton samples and porcine heart yielded similar Energies of activation, 20.4 Kcal mol^{-1} and 21.4 Kcal mol^{-1}, respectively.

Chapter 3

Chapter 3: The Potential Respiratory CO_2 Production from $NADP^+$-dependent isocitrate dehydrogenase in marine plankton.

> *Biochemistry asks how the remarkable properties of living organisms arise from the thousands of different biomolecules.*
>
> Albert L.Lehninger

RESUMEN: En este capítulo se ha medido la producción de CO_2 potencial máxima de las fracciones 0,7-50μm y 200-2000μm del plancton en la costa de las Islas Canarias, en base a la actividad de la NADP-IDH. Esta enzima es una de las principales responsables de la producción de CO_2 en la célula, pero no es la única. Por ello, tras considerar todas las enzimas productoras de CO_2 y normalizar su actividad por la de la NADP-IDH, la producción potencial máxima de CO_2 (Ψ_{NADP}) del organismo resultó 2.94·NADP-IDH. Además, se definieron doce escenarios teóricos para el análisis de la relación entre las tasas fisiológicas de producción de CO_2 (R_{CO2}) y Ψ_{NADP}. Los ratios R_{CO2}/Ψ_{NADP} obtenidos variaron entre 0,24 y 0,66 para el mesozooplancton y entre 0,15 y 0,28 para el microplancton. En base a nuestros resultados del Atlántico Nordeste Subtropical, predecimos que los ratios R_{CO2}/Ψ_{NADP} para el mesozooplancton en el océano abierto variarán entre 0,33 y 0,44, mientras que en el microplancton variarán entre 0,15 y 0,27. Consideramos que el uso de los ratios R_{CO2}/Ψ_{NADP} puede ser una herramienta muy útil en oceanografía. Podrían incrementar la eficiencia de las campañas aumen-

CHAPTER 3. Chapter 3: The Potential Respiratory CO_2 Production from
NADP$^+$-dependent isocitrate dehydrogenase in marine plankton.

36

tando la tasa de obtención de datos, y con ello, el conocimiento asociado.
Estos ratios pueden ser especialmente interesantes en los estudios del flujo
de carbono vertical, el estudio de la capacidad de secuestro de carbono del
océano, la respiración celular, las adaptaciones metabólicas de los organis-
mos ante cambios ambientales, y el papel de la comunidad planctónica en la
cadena trófica.

ABSTRACT: Potential CO_2 production of the 0.7-50μm and of the 200-
2000μm fraction from the Canary-Island coastal-plankton community was
measured by an enzyme assay based on the NADP$^+$-dependent isocitrate de-
hydrogenase (NADP-IDH). This enzyme plays a key role in the metabolism
as one of the most active CO_2-producing enzymes in the cell. Thus, con-
sidering all the CO_2-producing enzymes and normalising their activities by
NADP-IDH activity, the potential CO_2 production (Ψ_{NADP}) was calculated
as 2.94·NADP-IDH. The development of R_{CO2}/Ψ_{NADP} ratios obtained from
twelve different theoretical scenarios, led to a range of R_{CO2}/Ψ_{NADP} ratios
which spans from 0.24 to 0.66 for the mesozooplankton community and
from 0.15 to 0.27 for the microplankton community. We predict that, from
our NADP-IDH measurements in the North Eastern Subtropical Atlantic,
the R_{CO2}/Ψ_{NADP} ratios for open ocean mesozooplankton will fall between
0.33 and 0.44, and will be between 0.15 and 0.27 in the case of the mixed
microplankton community. We propose the use of R_{CO2}/Ψ_{NADP} ratios as a
powerful tool in oceanographic research. They can be used to improve the
efficiency of oceanographic field experiments and the knowledge that they
yield. Specifically, NADP-IDH measurements can be used in studies of ver-
tical carbon flux, sequestering capacity for anthropogenic CO_2 in plankton
communities, cellular respiration in marine samples, metabolic adaptations
to changes in environmental conditions, and the role of plankton community
in the food chain.

3.1 Introduction

Global climate change and marine acidification linked to the emission of green-
house gases are leading the marine scientific community to develop new method-
ologies that advance our knowledge of carbon flux (Cflux), its relationship with
biogeochemical processes and, particularly, the importance of the ocean,s role as
a carbon sink (Packard et al. (2015); Giering et al. (2014); Ducklow and Doney).

Among biogeochemical processes, technical limitations on the assessment of
marine respiration in terms of carbon dioxide production (R_{CO2}), have restricted
its direct measurement to the upper water column. Furthermore, these respira-
tion measurements are derived largely from the product of respiratory oxygen con-
sumption rates (R_{O2}) and a theoretical Respiratory Quotient (RQ, Mayzaud et al.

(2005); Berggren et al. (2012); Romero-Kutzner et al. (2015)). Thus, the calculation of R_{CO2} is based firstly, on the circumstantially variable R_{O2}. It depends on, e.g., the physiological, nutritional and life-cycle state of the organism, and also on the effects of sampling and incubation (Herrera et al. (2011b); Fernández-Urruzola et al. (2011); Osma et al. (2016a); Ferguson et al. (1984)). Secondly, it also depends on the RQ. Even though RQ has been widely used so far, not only does the type of consumed organic matter effect on its variability, but the nutritional state of the organism also affects it (Romero-Kutzner et al. (2015)). Here, we propose new methodology which avoids the variability associated with the RQ by measuring the enzymatic maximum velocity (V_{max}) of a key CO_2-producing enzyme, the $NADP^+$-dependent isocitrate dehydrogrenase (NADP-IDH) (Tames-Espinosa et al. (2018)), inherent to the plankton community metabolic apparatus. This kind of measurements, once optimized, describes the organisms' maximum capacity which, as a stable characteristic, remains so, even when environmental or circumstantial events modify the physiological response (Herrera et al. (2011b); Fernández-Urruzola et al. (2011); Osma et al. (2016a)). Although this methodology is based on the complex enzymology of the underlying biochemical processes that control the physiological CO_2 production (R_{CO2}), we have developed a functional linear predictive model based on the measurement of the activity of NADP-IDH, one of the key enzymes involved.

Here, we assess the relationships among different CO_2-producing enzymes in the marine plankton samples, to develop a basic model to evaluate the potential CO_2 production of the plankton community.
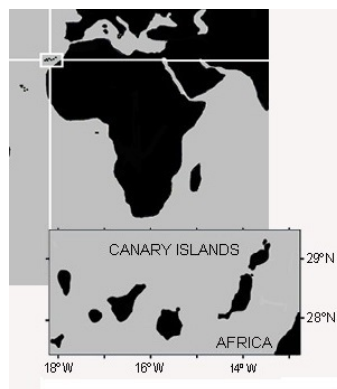
Figure 3.1: Canary Islands Archipelago, surrounded by waters of the North Eastern Subtropical Atlantic Ocean where most of the samples in this paper were taken.

To do this, we collected plankton samples from the coastal waters around Gran Canaria in the Canary Islands archipelago. In the Canary Current System that flows South through the islands (Fig.3.1), microplankton from 0.7 to 50μm is composed of heterotrophic prokaryotes, heterotrophic and autotrophic nanoflagellates, and autotrophic picoplankton (eukaryotic and the cyanobacteria *Prochlorococcus and Synechococcus*). All share the same Krebs cycle (Fig.1.1). In addition, diatoms of

the genera *Rhizosolenia, Chaetoceros* and *Navicula* and small dinoflagellates of the
genera *Gymnodinium, Gynodinium, Amphidinium, Cochlodinium* and *Torodinium*
are also present within this fraction (Schmoker et al. (2013)). The 200-to-2000μm
size-fraction of zooplankton is dominated by minute crustaceans, specially cope-
pods (Hernández-León et al. (2007)). The most abundant species reported at our
sampling depths (less than 20m) were *Oithona plumifera, Nannocelanus minor* and
Temora stylifera throughout the year, and also *Acartia negligens* during spring and
summer, the seasons when our sampling was accomplished (Corral (1970)).

To calculate these communities' CO_2 production from NADP-IDH activity,
we derive a factor, χ, obtained from the analysis of the rates of different CO_2 pro-
duction enzymes in the Krebs cycle (Walsh and Koshland (1984)). However, the
potential CO_2 production in the cells also involve non-respiratory CO_2 production.
To ensure that our modelled CO_2 production predicts the potential, we have to take
into account the non-respiratory CO_2 producing enzymes as well as the respiratory
CO_2 producing enzymes. The potential CO_2 production model is based princi-
pally on NADP-IDH activity (Ψ_{NADP}). However, it is developed by combining
the CO_2 production rate analysis with the relationship between maximum activi-
ties of citrate synthase (CS), NAD-IDH and NADP-IDH in crustacean organisms.
These relationships are based on enzyme analysis in crustaceans (Alp et al. (1976))
(Tables 3.2 and 3.3).

Finally, we develop an experimental base for a CO_2 production proxy (Eq.3.14,
Table 3.4). We have assessed the R_{CO2} theoretically to develop R_{CO2}/Ψ_{NADP} ratios
that range from 0 to 1. Thus, Ψ_{NADP} resulted comparable to measurements of
the potential CO_2 production of the plankton community. This approach is the
second step in developing a chemically-based proxy to rapidly detect the rate of
respiratory CO_2 production on oceanographically relevant time and space scales
(sensu Sverdrup et al. (1942)).

3.2 Material and Methods

3.2.1 Plankton sampling procedures

Mesozooplankton size fraction samples (200-2000μm) were collected from the
shallow waters of Sardina del Norte (Gáldar, Gran Canaria island) by three scuba
divers dragging a WP2 net horizontally in the upper 10m of the euphotic zone
(Fig.3.2). After being stored in plastic containers, the samples were fractionated
through 2000μm and 200μm nets at laboratory. Pilot measurements to determine
the optimum seawater volume needed were made to obtain biomass higher than
10$\pm$2 μg protein mL^{-1} (Tames-Espinosa et al. (2018)). Phytoplankton size frac-
tions (from 0.7 to 50μm) were sampled from Alcaravaneras Beach (Las Palmas de
Gran Canaria, Gran Canaria island). Seawater samples (4L per filter) were stored
in 25L plastic containers and later passed through a 50μm net and 0.7μm non-
combusted 25mm Glass Fiber Filter (GF/F) in the laboratory. Then, all samples
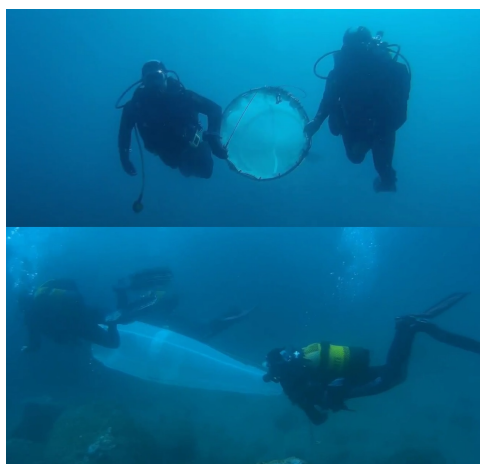
Figure 3.2: Sampling in the coastal waters of Gran Canaria using the WP2 net dragged by scuba divers during spring-bloom conditions.

were stored in 2mL microcentrifuge tubes at -80°C until analysis.

3.2.2 Preparations for kinetic enzyme activity measurements

The 200-2000μm plankton samples were homogenated in 0.1M phosphate buffer (0.1M Na_2HPO_4, 0.1mM KH_2PO_4, 75μM $MgSO_4$ $7H_2O$, PVP (1.5mg mL^{-1}), TRITON X-100 (2mL L^{-1})), by sonication for 45sec at 70% amplitude in a Vibracell VCX 130 Sonics® ultrasonic processor. On the other hand, the 0.7-50μm plankton samples were homogenized at 0-4ºC in the same 0.1M phosphate buffer, by a Teflon® 2mL-pestle PYREX® Potter-Elvehjem tissue grinder (homogenizer) at 2600rpm for 2 min. Then, crude homogenates were centrifuged (0-4°C) at 4000rpm for 10 min.

The supernatant aliquot was assayed for NADP-IDH activity following the Tames-Espinosa et al. (2018) method (Tames-Espinosa et al. (2018), see Chapter 2). NADP-IDH activity was measured kinetically by following the time-dependent production of NADPH (Δ_{NADPH}) at 340nm (Δ_{340}) and 18°C in a 1cm UV-transparent plastic cuvette in a Cary 100 U-V visible spectrophotometer for 1200 sec. β-NADP$^+$ (SIGMA #N0505; from here on we will call NADP$^+$) was reduced by NADP-IDH to NADPH while decarboxyled the DL-trisodium-isocitrate (SIGMA #I1252; from here on we will call isocitrate) to α-ketoglutarate. Control assays (blanks) lacked isocitrate. The reaction was started by adding the NADP$^+$ solution. After 3 min, the slope of the linear time-course signal was considered the IDH activity. A molar extinction coefficient (ε) of 5.42 absorptivity units mL μmol^{-1}cm^{-1} was obtained for NADPH under these conditions (Tames-Espinosa et al. (2018)). NADP-IDH activity was reported in μmol NADPH min^{-1} (mL of homogenate)$^{-1}$ units.

3.2.3   Potential respiration (Φ)

For 0.7-50μm samples, potential respiration (Φ) was determined from ETS activity
(Packard (1971)) incorporating the modifications described in Kenner and Ahmed
(1975) and Gómez et al. (1996) on the same centrifuged supernadant aliquotes
on which NADP-IDH was also measured. For the 200-2000 μm size-fractionated
plankton samples, after centrifugation, the supernatant aliquot was assayed for ETS
activity following Owens and King (1975).

   The absorbance increase of the INT-formazan at 490nm was continuously mon-
itored at 18ºC in 1cm path-length cuvettes for 8min. The regression line of ab-
sorption versus time was used to estimate the ETS activity and potential respira-
tion rates (Φ) after Packard and Williams (1981). The tetrazolium salt, INT (p-
Iodonitrotetrazolium Violet, Sigma #I8377) was reduced by the respiratory ETS
enzymes, replacing O_2 as the electron acceptor. The INT accepts two electrons
whereas the O_2 would accept four. Thus, the INT-formazan production rate is sto-
ichiometrically related by a factor of 2 to ETS activity and by a factor of 0.5 to Φ.
Blanks were run without the ETS substrates in order to subtract the contribution
of the background non-enzymatic and enzymatic reduction of the INT (Maldonado
et al. (2012)). Φ was reported in μmol O_2 min^{-1}(mL of homogenate)$^{-1}$ units. To
convert to μLO_2 min^{-1}(mL of homogenate)$^{-1}$, multiply by 22.4 μL μmol^{-1}.

3.2.4 R_{O2} calculations from Potential respiration (Φ) measurements

When direct measurements of R_{O2} are not available, reported ratios are commonly
used to calculate R_{O2} from Φ in the micro- and mesozooplankton community.
Calculations of this type (Cleland (1967); Hernández-Leon and Gómez (1996);
Packard and Codispoti (2007); Osma et al. (2016c)) have been done before by
applying a R_{O2}/Φ ratio for the determination of R_{O2} (Eq.3.1). Here, we have
applied three different zooplankton R_{O2}/Φ ratios from the literature (Tables 3.1)
in Eq.3.1 (Section 3.3.2, Fig.3.3), developing three scenarios: (A) 0.50, the ratio
when standard physiological rates, governed by enzyme activities, operate at one-
half their potential capacity (Cleland (1967)); (B) 0.57, the ratio characteristic for
the mesotrophic ocean conditions around the Canary Islands (Osma et al. (2016c));
and (C) 0.77, the ratio that exemplifying the late-winter bloom conditions in the
waters around the Canary Islands (Hernández-Leon and Gómez (1996)). In the
case of the 0.7-50μm size-fractionated plankton community, a fourth scenario (D)
was developed using a R_{O2}/Φ ratio of 0.26 (Packard and Christensen (2004); Osma
et al. (2014)) (Tables 3.1). In all of them, the equation for calculating R_{O2} from Φ
is:

$R_{O2}= \Phi \cdot R_{O2}/\Phi$ (3.1)

   where R_{O2} is the physiological O_2 consumption rate, and Φ is the potential O_2
consumption, both are in in μmol of O_2 min^{-1} mL^{-1}.

3.2.5 R_{CO2} calculations from R_{O2}

From the R_{O2} values obtained as above, R_{CO2} was calculated by Eq.3.2, applying Redfield ratios (Packard and Gómez (2013)) or different Respiratory Quotients (RQ) (Romero-Kutzner et al. (2015); Berggren et al. (2012)), describing a wide range of different marine scenarios (Section 3.3.2,Fig. 3.3). Such calculations have been done in the literature when physiological measurements are not available. In Packard and Gómez (2013) (Packard and Gómez (2013)) the physiological measurements were not available so the Redfield ratio, C/O in the cells (122/172), was used with natural samples to convert R_{O2} into R_{CO2}. In other studies, this type of respiration measurements have been also derived from the product of R_{O2} and the theoretical RQ (Mayzaud et al. (2005)). Here, the plankton community was sampled during the spring-bloom when the organisms were likely to have been well-fed, a condition described by normal RQ ranging from 0.7 to 1.2 (Romero-Kutzner et al. (2015); Berggren et al. (2012)). Thus, in Table 3.1 we have applied in Eq.3.2 three different conversion factors ($R_{CO2:O2}$) for every physiological condition described in Section 3.2.4. These factors were: (1) the Redfield ratio (0.71), as a standard value related to an unknown nutrient composition of the zooplanktonic diet (Packard and Gómez (2013))(note that this value is close to the RQ = 0.7 linked to lipid consumption (Berggren et al. (2012))); (2) an average value of 0.87 obtained for copepods (Mayzaud et al. (2005)); (3) a mean value of RQ = 1.3 linked to a net-heterotrophic system (Berggren et al. (2012)) (note that this value is close to the RQ = 1.2 linked to a carboxylic acid nutritional source (Berggren et al. (2012)), Table 3.1). An RQ value of 0.7 is also used as a low theoretical RQ for phytoplankton, assuming that it is constituted mainly by oxygen-poor components (lipids and proteins) (Takahashi et al. (1985); Berggren et al. (2012)).

$R_{CO2} = R_{O2} \cdot R_{CO2:O2}$ (3.2)

where $R_{CO2:O2}$ is the applied conversion in every scenario from Table 3.1.

3.2.6   Biomass

Biomass content was determined from samples kept for enzyme activities by the protein method of Lowry *et al.* (1951) (Lowry et al. (1951)) modified by Rutter (1967) (Rutter (1967)) using bovine serum albumin (BSA) as standard. Biomass was reported in mg of protein.

3.2.7   Data analysis and Statistics

ANOVA and *t* tests were used to analyse the differences between the linear regressions from the NADP-IDH activity and Φ, in the two different size-fractionated plankton samples (Section 3.4.1) (Pentecost (1999)) in an attempt to assess the differences between a pure heterotrophic plankton community and a mixed plankton community.

Table 3.1: Different scenarios designed to develop the R_{CO2}/Ψ_{NADP} ratios from the Φ and Ψ_{NADP} measurements, using conversion ratios reported in the literature. Scenarios 2.2 and 3.2 describe the natural conditions of our 200-2000 μm zooplankton samples, and 4.1 describes the natural conditions in our 0.7-50μm samples.

Scenario	R_{O2}/Φ	Conditions	$R_{CO2:O2}$	Conditions
A1	0.5	Ratio for standard physiological rates	0.71	Standard natural sample conditions (Redfield)
A2	0.5	Ratio for standard physiological rates	0.87	RQ in samples dominated by copepods
A3	0.5	Ratio for standard physiological rates	1.3	RQ in net-heterotrophic microplankton samples
B1	0.57	Ratio for mesotrophic conditions in waters around the Canary islands	0.71	Standard natural sample conditions (Redfield)
B2	**0.57**	**Ratio for mesotrophic conditions in waters around the Canary islands**	**0.87**	**RQ in samples dominated by copepods**
B3	0.57	Ratio for mesotrophic conditions in waters around the Canary islands	1.3	RQ in net-heterotrophic microplankton samples
C1	0.77	Ratio for late winter-bloom conditions in waters around the Canary islands	0.71	Standard natural sample conditions (Redfield)
C2	**0.77**	**Ratio for late winter-bloom conditions in waters around the Canary islands**	**0.87**	**RQ in samples dominated by copepods**
C3	0.77	Ratio for late winter-bloom conditions in waters around the Canary islands	1.3	RQ in net-heterotrophic microplankton samples
D1	**0.26**	**Ratio for a mixed microplanktonic community**	**0.71**	**Standard natural sample conditions (Redfield)**
D2	0.26	Ratio for a mixed microplanktonic community	0.87	RQ in samples dominated by copepods
D3	0.26	Ratio for a mixed microplanktonic community	1.3	RQ in net-heterotrophic microplankton samples

3.3   Results

3.3.1   Potential CO_2 production from NADP-IDH measurements

Although we propose NADP-IDH activity as a proxy for plankton respiratory CO_2 production, the total CO_2 production of the cell is closer to the CO_2 production of all the enzymes associated with the Krebs cycle (KC_{CO2}). This is the sum of the activities of five enzyme activities, pyruvate dehydrogenase (PDH_{CO2}); α-ketoglutarate dehydrogenase ($KGDH_{CO2}$); malic enzyme (ME_{CO2}); phosphoenolpyruvate carboxykinase ($PEPCK_{CO2}$); and all the isocitrate dehydrogenase isoenzymes that work within the Krebs cycle ($IDH_{KC_{CO2}}$) (Packard et al. (1996a)). This summation is represented by Eq.3.3.

KC_{CO2}=PDH_{CO2} + $IDH_{KC_{CO2}}$ + $KGDH_{CO2}$ + ME_{CO2} + $PEPCK_{CO2}$ (3.3)

To develop a model based on the NADP-IDH measurements, the CO_2 production of these other enzymes needs to be related to NADP-IDH activity. The contribution of every enzyme of the Krebs cycle linked to the CO_2 production, normalized by NADP-IDH activity, can be obtained from the reported rates in *E.coli* (Fig.1.1) (Walsh and Koshland (1984)), assuming that the *E.coli* Krebs cycle is equivalent to the Krebs cycle in other prokaryotes and also to the mitochondrial Krebs cycle in eukaryotes. Accordingly, the relationship between the CO_2 production of the above-mentioned five-enzymes and the IDH activity in the Krebs cycle (IDH_{KC}) can be obtained as follows:

- Pyruvate dehydrogenase (EC 1.2.4.1, PDH). For plankton on a carbohydrate -based diet, PDH bridges glycolysis and the Krebs cycle. In the transfer process between these two metabolic pathways, one mole of CO_2 is produced for every mole of acetyl-CoA generated (El-Mansi and Holms (1989)). Then, in the beginning of the Krebs cycle, citrate synthase (EC 2.3.3.1, CS) takes this acetyl-CoA, and generates the six-carbon tricarboxylic acid, citric acid. These acids are normally found in the cell in their sodium or potassium salt forms (Walsh and Koshland (1984)). According to Walsh and Koshland (1984) in Fig.1.1, in order to obtain an IDH_{KC} activity of 80moles isocitrate min^{-1} L^{-1} , CS must react at an activity of 111moles min^{-1} L^{-1} of acetyl-CoA. As this acetyl-CoA is being produced by PDH, one mole of CO_2 per mole of acetyl-CoA is also being produced. This means that, according to Fig.1.1, 111 moles of CO_2, related to the PDH activity, will be produced when 80 moles of CO_2 are produced by IDH_{KC}. Thus, the ratio of CO_2 produced by PDH to CO_2 produced by IDH_{KC} is 1.39. Thus, PDH_{CO2}=1.39·$IDH_{KC_{CO2}}$.

- Isocitrate dehydrogenase (both EC 1.1.1.41, NAD-IDH; and the mitochondrial EC 1.1.1.42, NADP-IDH_{mit}) in the Krebs cycle (IDH_{KC}). This enzyme is the third Krebs-Cycle reaction. It is the oxidation and decarboxylation of isocitrate, producing α-ketoglutarate, NAD(P)H and CO_2 (Eq.1.3). As we

are normalizing by this rate in our model, the CO_2 production ratio here is 1 in the Krebs cycle (IDH$_{KC}$).

- α-ketoglutarate dehydrogenase (EC 1.2.4.2, KGDH). This enzyme is the 4th Krebs-Cycle reaction. In this reaction, α-ketoglutarate undergoes oxidative decarboxylation, producing succinyl-CoA, NADH and CO_2. As explained above, according to the rates in Fig.1.1, 75moles of CO_2 were produced by KGDH for every 80 moles of CO_2 produced by IDH$_{KC}$; so, the ratio between the two enzyme activities is 0.94. Thus, KGDH$_{CO2}$=0.94·IDH$_{KC_{CO2}}$.

- Cytosolic malate dehydrogenase (EC 1.1.1.40, ME). Malate dehydrogenase (MDH, EC 1.1.1.37) in the Krebs-Cycle proper, does not produce CO_2. However, part of the malate, generated by fumarase (EC 4.2.1.2) in the Krebs cycle, is transported outside to the decarboxylating malate dehydrogenase (EC 1.1.140) in the cytosol (MacDonald (2002)). There, it is decarboxylated to pyruvate, producing NADPH and CO_2. In this case, from Fig.1.1, 9.5 moles of CO_2 are produced by this enzyme per 80 moles produced by IDH$_{KC}$; so, the ratio between ME and IDH$_{KC}$ is: 0.12. Thus, ME$_{CO2}$=0.12·IDH$_{KC_{CO2}}$.

- Phosphoenolpyruvate carboxykinase (EC 4.1.1.49, PEPCK). This enzyme shunts part of the oxaloacetate produced in the Krebs cycle to the cytosol. There, it is decarboxylated to phosphoenolpyruvate and CO_2. Here, according to Fig.1.1, 9.5 moles of CO_2 are produced by PEPCK per 80 moles produced by IDH$_{KC}$; so, the ratio between both enzyme activities is 0.12. Thus, PEPCK$_{CO2}$=0.12·IDH$_{KC_{CO2}}$.

So, assuming all the IDH activity is related to the Krebs cycle, the Krebs cycle CO_2 production, normalized by IDH$_{KC}$ would be:

$$KC_{CO2}=1.39 \cdot IDH_{KC_{CO2}}+1 \cdot IDH_{KC_{CO2}}+0.94 \cdot IDH_{KC_{CO2}}+0.12 \cdot IDH_{KC_{CO2}}+0.12 \cdot IDH_{KC_{CO2}} \quad (3.4)$$

Or, after combining terms algebraically:

$$KC_{CO2}=3.57 \cdot IDH_{KC_{CO2}} \quad (3.5)$$

However, depending on the type of organism, the IDH$_{KC}$ activity is not directly equal to NADP-IDH measurement as explained below. While applying the NADP-IDH activity to calculate the potential CO_2 production, two facts must be taken in account:

1. In prokaryotes, the IDH$_{KC}$ is only NADP$^+$-dependent:

   $$IDH_{KC} = NADP\text{-}IDH \quad (3.6)$$

   There is no NAD$^+$-dependent IDH. However, in the case of eukaryotes, not only is there a mitochondrial-based NADP$^+$-dependent IDH reaction, but there is, also inside the mitochondria, a NAD$^+$-dependent IDH reaction (Gálvez and Gadal (1995)). There is an isoenzyme of IDH using the other

pyridine nucleotide! So, in the case of eukaryotes, IDH_{KC} must be defined as:

$$IDH_{KC} = NADP\text{-}IDH_{mit} + NAD\text{-}IDH_{mit} \quad (3.7)$$

2 Secondly, in eukaryotes, not only is the mitochondrial enzyme being measured, but the isoenzymes located outside the mitochondria are also being measured. These include the isoenzymes in the cytosol, and even the NADP-IDH located in the chloroplasts and the peroxysomes of photosynthetic organisms (Gálvez and Gadal (1995)). So, our NADP-IDH measurements included NADP-IDH isoenzymes from both the inside and outside of the mitochondria. This is expressed in Eq.3.8:

$$NADP\text{-}IDH = NADP\text{-}IDH_{out} + NADP\text{-}IDH_{mit} \quad (3.8)$$

Returning to prokaryotes, the specific IDH isoenzymes related to the Krebs cycle, will be purely NADP-IDH, as in Eq.3.6.

Zooplankton are eukaryotes, mainly crustaceans. In a study of muscles from six different crustaceans, Alp et al. (1976) reported maximum activities of CS (a purely Krebs cycle enzyme), NAD-IDH (specifically located in mitochondria), and NADP-IDH (located inside and outside the mitochondria) (Table 3.2). Combining these rates with the rates of CS and Krebs cycle IDH as reported by Walsh and Koshland (1984) (Fig. 1.1), we determined the proportions of NADP-IDH related to the Krebs cycle and related to other metabolic pathways.

Accordingly, we know that, for 111 moles of substrate consumed by CS, IDH_{KC} consumes 80 moles of isocitrate (Fig.1.1). So, the activities of CS and IDH_{KC} are related as in Eq.3.9.

$$CS = 1.39 \cdot IDH_{KC} \quad (3.9)$$

Rearranging and solving for IDH_{KC}, Eq.3.9 is transformed into: $IDH_{KC} = 0.72 \cdot CS$. Thus, from the CS, NADP-IDH and NAD-IDH activities in crustacean samples reported by Alp et al. (1976) (Table 3.2) we can again calculate IDH_{KC}. Then, to obtain the NADP-IDH inside and outside the mitochondria we transformed and combined Eq.3.7 and Eq.3.8 as follows:

$NADP\text{-}IDH_{mit} = IDH_{KC} - NAD\text{-}IDH$, from Eq.3.7; and $NADP\text{-}IDH_{out} = NADP\text{-}IDH - NADP\text{-}IDH_{mit}$ from Eq.3.8. So, combining these transformations, we obtained Eq.3.10:

$$NADP\text{-}IDH_{out} = NADP\text{-}IDH - (IDH_{KC} - NAD\text{-}IDH) \quad (3.10)$$

The results of these calculations are shown in Table 3.2.

Table 3.2: Enzyme activities in crustacean samples, in μmol substrate min^{-1} (g fresh weight)$^{-1}$. IDH$_{KC}$ activity was calculated as expressed in Eq.3.9; NADP-IDH$_{mit}$ activity was calculated as expressed in Eq.3.7; and NADP-IDH$_{out}$ activity was calculated as expressed in Eq.3.10. In each case, the activities of CS, NADP-IDH and NAD-IDH in crustacean samples from Alp et al. (1976) were used.

Organism	CS	IDH$_{KC}$	NADP-IDH	NAD-IDH	NADP-IDH$_{mit}$	NADP-IDH$_{out}$
Lobster	1	0.72	1.1	0.1	0.62	0.48
Lobster	1.1	0.79	1.1	0.1	0.69	0.41
Squad lobster	3.4	2.45	3.5	0.1	2.35	1.15
Swimming crab	7	5.04	6.5	1	4.04	2.46
Edible crab	2.4	1.73	3	0.1	1.63	1.37
Pedunculate barnacle	1.2	0.86	2.3	0.1	0.76	1.54
Hose-shoe crab	17.4	12.53	10.2	0.6	11.93	0
Average	4.79	3.45	3.96	0.3	3.15	1.06
Standard deviation	5.95	4.28	3.31	0.36	4.06	0.83

From the enzyme activity in Table 3.2, the ratios of NAD-IDH, NADP-IDH$_{mit}$, NADP-IDH$_{out}$ activities were calculated as a fraction of NADP-IDH activity. Table 3.3 was then constructed from these ratios.

Table 3.3: Ratios of NAD-IDH, NADP-IDH$_{mit}$ and NADP-IDH$_{out}$ activities to NADP-IDH activity. These ratios are needed for the calculation of total potential CO_2 production (Eq. 3.12).

Organism	NAD-IDH/ NADP-IDH	NADP-IDH$_{mit}$ / NADP-IDH	NADP-IDH$_{out}$/ NADP-IDH
Lobster	0.09	0.56	0.44
Lobster	0.09	0.63	0.37
Squad lobster	0.03	0.67	0.33
Swimming crab	0.15	0.62	0.38
Edible crab	0.03	0.54	0.46
Pedunculate barnacle	0.04	0.33	0.67
Horse-shoe crab	0.06	1.17	0
Average	**0.07**	**0.65**	**0.38**
Standard deviation	0.04	0.26	0.20

Eq.3.5 describes the CO_2 production related to the Krebs cycle (KC$_{CO2}$), however, the total potential CO_2 production of the cell (Ψ), from both the mitochondria and the cytosol, will be:

$$\Psi = KC_{CO2} + \text{NADP-IDHout}_{CO2} \quad (3.11)$$

Combining Eq.3.11 with Eq.3.5 yields Eq.3.12

$$\Psi = 3.57 \cdot (\text{NADP-IDH}mit + \text{NAD-IDH}) + \text{NADP-IDH}out \quad (3.12)$$

Where all terms are defined in Table 3.2. From the average activity ratios in Table 3.3 (in bold), applied to Eq.3.12, we calculated the total potential CO_2 production normalized by NADP-IDH (Ψ_{NADP}), as in Eq.3.13:

Ψ_{NADP}= 3.57·(0.65·NADP-IDH+0.07·NADP-IDH)+0.38·NADP-IDH(3.13)
    Condensing Eq.3.13, yields Eq.3.14

Ψ_{NADP}= 2.94·(NADP-IDH)(3.14)

    Note that the NADP-IDH activity should be in molar CO_2 units rather than molar NADPH units. This is because the stoichiometry of the reaction (Eq.1.3) indicates that 1 mole of CO_2 is produced for every mole of NADPH produced. To change to volume units we simply need to remember that 1 mole of CO_2 is equivalent to 22.4L of CO_2.

    Eq.3.14 is equivalent to the Roy and Packard (2001) equation (R_{CO2} = χ· $V_{NADP-IDH}$, where χ=3) that they used to calculate R_{CO2} production from modelled *in vivo* NADP-IDH activity in bacterial cultures ($V_{NADP-IDH}$). In bacteria the physiological R_{CO2} was equal to 3 times modelled *in vivo* NADP-IDH activity when the nutrient source was based on carbohydrates (Roy and Packard (2001)), so the activity of the PDH was being considered. In our case, it is not the *in vivo* NADP-IDH activity but the V_{max} what is being measured. Thus, using our V_{max} in the Roy equation, would yield the potential R_{CO2}.

    Here, we will use Eq.3.14 to calculate potential CO_2 in crustacean-dominated zooplankton samples. However, in the case of a more heterogeneous community, for example, the 0.7-50μmm size-fractionated plankton, other types of organisms such as prokaryotes and photoautotrophs may dominate the community. In a prokaryotic community, all the NADP-IDH is related to the Krebs cycle, so the total CO_2 production can be calculated directly from Eq.3.5, where χ is 3.57 (instead of 2.94, the value calculated for crustaceans). In the case of photoautotrophs, where the NADP-IDH fraction that is not related to the Krebs cycle, the NADP-IDH_{out} could be greater than it is in crustaceans. This is because the NADP-IDH in photoautotrophs is also located in the cytosol, peroxisomes and chloroplasts (Gálvez and Gadal (1995)). Values of χ lower than 2.94 are expected to be found if additional experiments were performed on photoautotrophs. If the kind of experiment, similar to the one performed by Alp et al. (1976), were conducted on photoautotrophs, it would facilitate an analysis similar to the one we made on crustacean enzyme activities (Tables 3.2, 3.3). This would lead to a better relationship between Ψ and NADP-IDH activity, in photoautotrophs.

    As the 0.7-50μm samples are from a heterogeneous community, the prokaryotic part will have χ values higher than 2.94, whereas the photoautotrophic part will have lower χ values. Accordingly, we suggest using χ = 2.94, as an average, being aware that this will underestimate potential CO_2 production by prokaryotes, and will overestimate potential CO_2 production by photoautotrophs.

3.3.2   Physiological rates from Φ measurements

After being normalized by protein, Φ was used to calculate R_{O2} for different physiological conditions as described in section 3.2.4 (Table 3.1). R_{O2}/Φ ratios from sce-

narios A-C were applied to the mesozooplankton samples, where $\Phi=26.6\pm4.8\cdot10^{-3}$ μmol O_2 min^{-1} (mg protein)$^{-1}$. Besides, the ratio for condition D is specific for microplankton, where $\Phi=42.7\pm9.1\cdot10^{-3}$ μmol O_2 min^{-1} (mg protein)$^{-1}$.

Results were plotted in Fig.3.3a, where a high R_{O2} occurred related to the late-winter bloom conditions in the Canary Islands (scenario C in Fig.3.3a, and Table 3.1). Values between scenario C and B (from $15.2\cdot10^{-3}$ to $20.5\cdot10^{-3}$ μmol O_2 min^{-1} (mg protein)$^{-1}$ respectively) were likely to reflect the physiological state of our Canary-Island mesozooplankton samples, as they were taken during the spring bloom. Scenario D ($R_{O2}=11.1\pm2.4\cdot10^{-3}$ μmol O_2 min^{-1} (mg protein)$^{-1}$) reflected the R_{O2} related to mixed microplankton. Besides, R_{CO2} was calculated applying different Respiratory Quotients (RQ) to R_{O2}, as described in section 3.2.5 (Table 3.1). This assessment results in twelve different scenarios, nine related to mesozooplankton communities (from A1 to C3 in Fig.3.3b and Table 3.1), and three related to mixed microplankton communities (from D1 to D3 in Fig.3.3b and Table 3.1). As a result, the highest R_{CO2} production rate occurred in scenario C3 ($26.6\pm4.8\cdot10^{-3}$ μmol CO_2 min^{-1} (mg protein)$^{-1}$, Fig.3.3b), during a late-winter bloom condition, considering that these mesozooplankton samples were similar to a net-heterotrophic microzooplankton community (Section 3.2.5, Table 3.1). However, as our mesozooplankton samples were composed mainly of copepods during the spring, the R_{CO2} rates were likely to be between scenarios B2 and C2 (from $13.2\pm2.4\cdot10^{-3}\mu$mol CO_2 min^{-1} (mg protein)$^{-1}$) to $17.8\pm3.2\cdot10^{-3}\mu$mol CO_2 min^{-1} (mg protein)$^{-1}$) (Fig. 3.3). This corresponds to copepods under mesotrophic conditions or under late-winter bloom conditions respectively, as represented in Fig. 3.3b and Table 3.1. In the case of microzooplankton samples, a value between scenario D1 and D3 (between $7.9\pm1.7\cdot10^{-3}$ μmol CO_2 min^{-1} (mg protein)$^{-1}$) related to the phytoplankton community (Takahashi et al. (1985); Berggren et al. (2012)), and $14.4\pm3.1\cdot10^{-3}$ μmol CO_2 min^{-1} (mg protein)$^{-1}$, related to a net-heterotrophic community is likely representative of the mixed- microzooplankton sample (Fig.3.3).
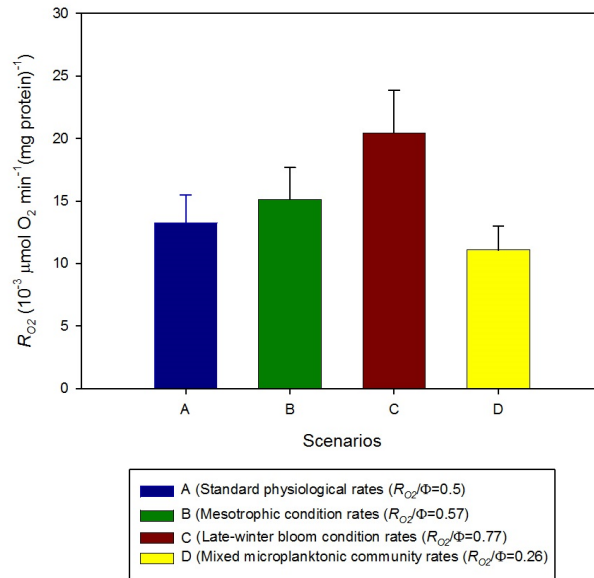
[a]
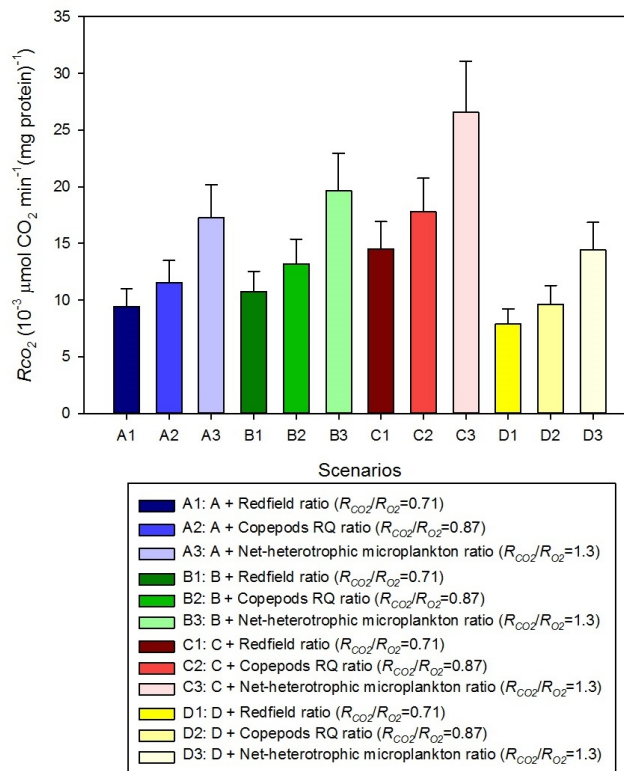
[b]

Figure 3.3: Physiological rates under different scenarios. (a) R_{O2} rates obtained from Φ under four different scenarios. (b) R_{CO2} rates obtained from R_{O2} resulting in twelve different physiological conditions.

3.3.3   Variability of R_{CO2}/Ψ_{NADP} ratios

Taking into account Section 3.3.1, we applied Eq.3.14 to the NADP-IDH results obtained from both the mesozooplankton and the microzooplankton samples (Fig.3.4) in order to calculate Ψ_{NADP}. After normalizing the Ψ_{NADP} results by biomass, we obtained the average values of Ψ_{NADP} for both types of zooplankton samples in 10^{-3} μmol CO_2 min^{-1} (mg protein)$^{-1}$ (Table 3.4).

Table 3.4: Results in Ψ_{NADP} (in 10^{-3} μmol CO_2 min^{-1} (mg protein)$^{-1}$), in R_{CO2} (also in 10^{-3} μmol CO_2 min^{-1} (mg protein)$^{-1}$ units) and in the R_{CO2}/Ψ_{NADP} ratios for every scenario. Values that likely represent the actual conditions of our mesozooplankton samples (between scenarios B2 and C2) and microzooplankton samples (scenario D1 and D3) have been highlighted in bold text.

		Ψ_{NADP}	R_{CO2}	R_{CO2}/Ψ_{NADP}
12[2]*Scenarios	A1	42.1±10.9	9.4±1.7	0.24±0.07
	A2	42.1±10.9	11.6±2.1	0.29±0.03
	A3	42.1±10.9	17.3±3.1	0.43±0.13
	B1	42.1±10.9	10.8±1.9	0.27±0.08
	B2	42.1±10.9	13.2±2.4	**0.33±0.10**
	B3	42.1±10.9	19.7±3.5	0.49±0.15
	C1	42.1±10.9	14.5±2.6	0.36±0.11
	C2	42.1±10.9	17.8±3.2	**0.44±0.14**
	C3	42.1±10.9	26.6±4.8	0.66±0.20
	D1	53.5±9.5	7.9±1.7	**0.15±0.03**
	D2	53.5±9.5	9.7±2.1	0.18±0.03
	D3	53.5±9.5	14.4±3.1	**0.27±0.05**

The highest R_{CO2}/Ψ_{NADP} ratio was 0.7, attained under C3 conditions. In this case, a late-winter bloom scenario in which the RQ was close to a net-heterotrophic microplankton community (RQ = 1.3) was represented. This RQ was also close to that based on carboxylic acid nutritional source (RQ=1.2) (see Section 3.2.5, Table 3.1) (Berggren et al. (2012)). However, our mesozooplankton samples were composed mainly by copepods, and were sampled during spring. Thus, a value between 0.3 and 0.4 (B2 and C2 in Table 3.4 respectively) would be expected to be more representative for these specific conditions in the Canary Islands.

In the case of the microplankton community, values between 0.2 and 0.3 (scenario D1, related to the phytoplankton community, and D3, related to a net-heterotroph community respectively), would be representative for a mixed community.

3.4 Discussion

3.4.1 What is the relationship between potential CO_2 production and potential O_2 consumption?

Cellular respiration has four components: (1) CO_2 production; (2) organic carbon oxidation; (3) O_2 consumption; (4) ATP production. Here, CO_2 production was assessed from NADP-IDH measurements, considering them as a proxy of the CO_2-producing apparatus in the cells. Besides, potential respiration, Φ, was considered also a proxy of the O_2-consuming apparatus in the cells.

Relationship between NAP-IDH activity and Φ

In an attempt to assess variations between autotrophic and heterotrophic metabolic pathways, we analysed both NADP-IDH and Φ (Fig.3.4) on 0.7-50μm and 200-2000μm samples.
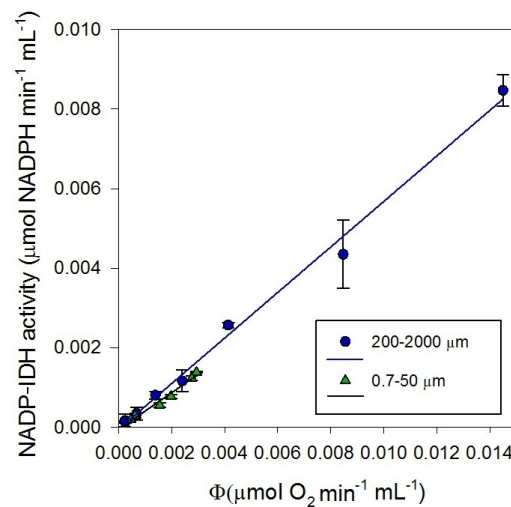
Figure 3.4: Relationship between NADP-IDH and Potential Respiration (Φ) in mesozooplanton (200-2000μm; y=0.5723x-4.4$\cdot 10^{-5}$, r^2=0.994, $p<0.0001$) and microplankton (0.7-50μm; y=0.46x-5$\cdot 10^{-5}$, r^2=0.9749, p=0.0002).

The slope of the linear regressions in Fig.3.4 reflects a zooplankton NADP-IDH activity of 57.23% of Φ. In the microplankton community (Fig.3.4), this activity reached 46.00% of Φ. ANOVA and a t test demonstrated that there was no significant difference between the two samples. Specifically, neither the linear regressions (ANOVA, $F_{(2,38)}$=2.15, p=0.01), nor the regression coefficients (t test, t(40)=1.34, p=0.01), were significantly different.

Relationship between Ψ_{NADP} and Φ

In eukaryotes, the respiratory CO_2 production occurs both in the cytosol, associated with PDH, and in the mitochondrial matrix, associated directly with IDH$_-$KC and KGDH, and indirectly with ME and PEPCK. In prokaryotes,the respiratory CO_2 production also occurs in the cytosol. However, the O_2 consumption and ATP production occur in the inner mitochondrial membrane of eukaryotes and in the plasmalemma membrane of prokaryotes (Nelson and Cox (2008)).

   Total CO_2 production, Ψ_{NADP}, (Eq.3.13), not only involves the respiratory CO_2 production (as above and in Eq.3.15) to be considered, but also the CO_2 production due to other metabolic pathways, such as fatty acid synthesis (biosynthetic CO_2 production, Eq.3.16). When compared to Φ, total potential CO_2 production was up to 1.7 times potential O_2 consumption in the mesozooplankton community (Fig.3.5(a), based on the slope of the linear regression (r^2=0.994, p<0.0001)).

   However, being able to calculate separately the respiratory potential CO_2 production facilitates a new estimation of the plankton carbon cycling related to the ATP production. The other part of the total potential CO_2 production is linked to biosynthesis.

   For the zooplankton community, composed mainly of crustaceans, we can estimate these values using Eq.3.13. By just extracting the CO_2 production related to the NADP-IDH activity outside the mitochondria, we can express the respiratory potential CO_2 production, normalized per NADP-IDH, as Eq.3.15. The biosynthetical CO_2 production can be expressed as Eq.3.16:

Respiratory Ψ_{NADP}= 2.57·NADP-IDH(3.15)

Biosynthetic Ψ_{NADP}= 0.38·NADP-IDH(3.16)

   Thus, respiratory Ψ_{NADP} is 1.47 greater than Φ in the crustacean community (Fig.3.5(b), based on the slope of the linear regression (r^2=0.9940, p<0.0001)). In effect, this means that the RQ for the potential respiratory metabolism would be 1.47. However, assuming total potential CO_2 production (Ψ_{NADP}) and O_2 consumption (Φ), we would expect an RQ even higher when biosynthesis and growth occur, because of the CO_2 production related to the pentose phosphate pathway, as well as to the fatty acid synthesis repeating reaction sequence (Nelson and Cox (2008)), which could not be estimated in this study. Note that physiological RQ could still reach higher values than 1.47 if physiological CO_2 production rates were close to the Ψ_{NADP} or the O_2 consumption rates were far from Φ. If compared with the cellular respiration reaction (Eq.3.17), this value of 1.47 is higher than the average as calculated from the stoichiometry of the cellular respiration equation.

$C_6H_{12}O_6 + 6 \cdot O_2 \rightarrow 6 \cdot CO_2 + 6 \cdot H_2O$ + heat (3.17)

   This may mean that the enzymatic pathways that supply the ETS are prepared to produced more NAD(P)H than is needed. This may be advantageous when, eventually, the organism has a high energy requirement. Once this requirement

is over, NAD(P)H excess may be redirected to biosynthesis by the IDH substrate cycle of Sazanov and Jackson (1994).

[a]

[b]
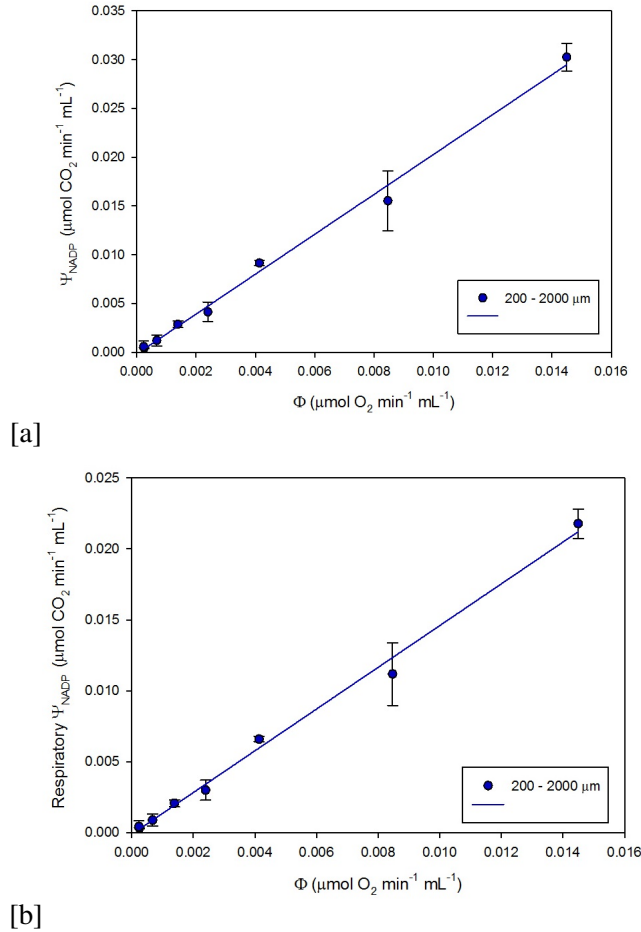
Figure 3.5: Relationship between potential CO_2 production (NADP-IDH based model) and O_2 consumption (ETS-based model) in the mainly crustacean 200-2000μm size-fractionated plankton community. (a) Total Ψ_{NADP} (Eq.3.14) vs Φ (y=1.68x-0.0001, r^2=0.994, p<0.0001). (b) Respiratory Ψ_{NADP} (Eq.3.15) vs Φ (y=1.47x-0.0001, r^2=0.994, p<0.0001)

.

3.4.2   What is the relationship between R_{CO2} and Ψ_{NADP}?

Carbon flux, when not measured directly by sediment traps, can be indirectly calculated from ETS activity or R_{O2} in the ocean water column (Osma et al. (2014); Packard et al. (2015)). However, using measurements of respiratory oxygen consumption entails the use of an RQ, and R_{O2}/Φ ratio particularly in the deep water samples, in the calculation of R_{CO2} (Osma et al. (2014)). Here, we propose the

CHAPTER 3. Chapter 3: The Potential Respiratory CO_2 Production from
NADP$^+$-dependent isocitrate dehydrogenase in marine plankton.

54

measurement of Ψ_{NADP} as a direct proxy for R_{CO2} and, by doing so, we eliminate the need for the RQ and all its variability (Romero-Kutzner et al. (2015); Berggren et al. (2012); Mayzaud et al. (2005)). With physiological measurements of CO_2 production (R_{CO2}), its ratio to potential CO_2 production can be determined (R_{CO2}/Ψ_{NADP}). Once this ratio is calculated for a station in an oceanographic region, it may be used to obtain the actual R_{CO2} for other samples of the NADP-IDH activity from the same region. Integrating R_{CO2} will yield a mathematical model of carbon flux in carbon units. Furthermore, measuring Ψ_{NADP} as a R_{CO2} proxy will improve data acquisition on oceanographic expeditions, and it will increase the sensitivity in detecting deep water CO_2 production. Thus, Ψ_{NADP} may be a powerful tool for calculating vertical carbon flux in the ocean in the short term. This approach requires calibration of Ψ_{NADP} with another measure of R_{CO2} which, currently, is extremely challenging in all but the most eutrophic conditions.

Thus, we recommend the direct measurement of R_{CO2} if possible. However, as we have just noted, this is inconvenient, impractical or impossible in the open ocean (Mayzaud et al. (2005)). That is why we have modelled the Ψ_{NADP} from the NADP-IDH measurements and the other CO_2-producer enzyme activities in the literature (Section 3.3.1). Here, the physiological R_{CO2} were not available, so we made a first step in determining R_{CO2}/Ψ_{NADP} ratio from the R_{CO2} obtained by ETS activity (Φ) (Fig. 3.3). We found that in all cases the results were between 0 and 1 (Table 3.4, Section 3.3.3). This means that in any scenario Ψ_{NADP} exceeded physiological R_{CO2} rate, validating the reliability of the Ψ_{NADP} measurements as a measurement the potential CO_2 production in the cells. Even under the scenario with highest R_{CO2} (C3 for zooplankton samples and D3 for microplankton in Table 3.4), suggesting a plankton community grown up under eutrophic or late winter-bloom conditions, the value R_{CO2}/Ψ_{NADP} is still below 1 (R_{CO2}/Ψ_{NADP}= 0.7 in zooplankton communities, 0.3 in heterogeneous microplankton communities, Table 3.4). This argues that Ψ_{NADP} accurately measures potential CO_2 production for these communities. As no physiological R_{CO2} measurements are available in the case of our zooplankton samples, and assuming they are composed mainly by copepods grown during the spring bloom around the Canary island, we suggest that scenarios B2 and C2 (Table 3.1) would be the most representative. Accordingly, an R_{CO2}/Ψ_{NADP} ratio between 0.3 and 0.4 approximates the range of the actual ratio (Table 3.4). In the case of the microplankton community, a value between 0.2 and 0.3, related to the scenarios D1 and D3 (Tables 3.1, 3.4), is a likely approximation for a mixed microplankton community.

However, we suggest to use these ratios as a guideline when R_{CO2} measurements are not available. To develop an accurate R_{CO2}/Ψ_{NADP} ratio, further experiments using physiological R_{CO2} methods (Mayzaud et al. (2005)), need to be done for every case. As RQ has been demonstrated to be variable depending on the conditions of the community growth phase, composition and starvation level (Berggren et al. (2012); Romero-Kutzner et al. (2015)), we suggest avoiding the use of these values, particularly when a more accurate measurement of R_{CO2} is available.

3.5   Conclusions

- A linear model for potential CO_2 production in zooplankton was developed from a measurement of NADP-IDH activity and related CO_2-producing enzymes:

  Ψ_{NADP}=2.94·NADP-IDH in μmol CO_2 min^{-1} mL^{-1} units.

- The ratio between the purely respiratory CO_2 production (Respiratory Ψ_{NADP}) and the potential O_2 consumption is 1.47 (Fig.3.5), indicating that the enzymatic pathways related to the organic carbon oxidation phase of cellular respiration is prepared to exceed the requirements of the ETS. This may serve as an advantage when, eventually, the organism has a high energy requirement. Once this requirement is met, NAD(P)H excess may be redirected to biosynthesis by the IDH substrate cycle of Sazanov and Jackson.

- This also means that RQ between the potential respiratory metabolism responses would be 1.47. However, assuming potential CO_2 production and O_2 consumption, we would expect an RQ even higher when biosynthesis and growth occur. This is because the CO_2 production is related to the pentose phosphate pathway, as well as to the fatty acid synthesis, which could not be completely estimated in this study. Note that the physiological RQ could still reach higher values than 1.47 if physiological CO_2 production rates were close to the Ψ_{NADP} or if the O_2 consumption rates were far lower than Φ.

- Ψ_{NADP} is a useful tool to assess R_{CO2} after applying R_{CO2}/Ψ_{NADP} ratios. Its utility will be amplified when used to calculate vertical carbon flux in the open ocean. In both cases it eliminates the use of the RQ.

- We predict that, from our measurements in the North Eastern Subtropical Atlantic, the R_{CO2}/Ψ_{NADP} ratios for open ocean zooplankton samples will fall between 0.3 and 0.4, whereas the ratios for a mixed microplankton community will fall between 0.2 and 0.3. However, we recommend the use of physiological R_{CO2}, if available, to develop accurate R_{CO2}/Ψ_{NADP} ratios for every region, experiment or case.

- From our calculations, Ψ_{NADP} always exceeded the physiological R_{CO2} rate. This is in harmony with theory because the physiological rate should not exceed the potential. Thus, it reinforces the concept of using Ψ_{NADP} measurements as a tool to assess potential CO_2 production in the marine plankton community.

Chapter 4

Chapter 4: Impact of sex differences and starvation on respiratory metabolism: CO_2 production on marine mysid *Leptomysis lingvura.*

Scientific physiology has the task of determining the functions of the animal body and deriving them as a necessary consequence from its elementary conditions.

Carl Ludwig

RESUMEN: En este capítulo se ha medido la tasa de producción de CO_2 (R_{CO2}) en *Leptomysis lingvura* para compararla con la producción máxima de CO_2 asociada a la actividad de la $NADP^+$-dependiente isoc-itrato deshidrogenasa (NADP-IDH). Tanto las medidas de respiración fisiológicas (R_{CO2}, R_{O2}), su ratio (RQ) como la actividad enzimática (NADP-IDH y Φ) se midieron en dos comunidades de *L. lingvura*: una en estado de florecimiento (bloom), y otra es un estado posterior al florecimiento (post-bloom). En ellas pudimos analizar la variabilidad de la respiración dada por diferencias en el sexo, por la inanición, y por el estado trófico original de la comunidad. Las hembras de la comunidad en "bloom" mostraron actividades enzimáticas significativamente mayores que las hembras de la comunidad en "post-bloom" (Φ=1.04±0.14 versus 0.58±0.12 μmol O_2 h^{-1} (mg of protein)$^{-1}$, respectivamente; y NADP-IDH=1.96±0.09 versus 0.97±0.19 μmol CO_2 h^{-1} (mg of

protein)$^{-1}$, respectivamente). Por el contrario, no se observaron diferencias entre ambas comunidades en términos de producción de CO_2. Por lo tanto, un ratio R_{CO2}/NADP-IDH de 0.12±0.05 representaría con precisión la respuesta fisiológica de una comunidad de *L. lingvura* bien alimentada. El cociente entre NADP-IDH y Φ fue 1.8±0.4 en las hembras y 1.6±0.4 en los machos. A parte de esto, no encontramos otras diferencias asociadas al sexo en R_{O2}, R_{CO2}, RQ, Φ o NADP-IDH. Por el contrario, la inanición fue el factor con mayor impacto en la respuesta fisiológica. La limitación en la disponibilidad de alimento hizo que el ratio R_{O2}/Φ descendiera de 0.35±0.02 a 0.27±0.08. Sin embago hizo que el ratio R_{CO2}/NADP-IDH aumentara de 0.12±0.04 a 0.16±0.06. Por ello, el RQ fue casi el doble en los misidáceos en condiciones de inanición que en aquellos que habían sido bien alimentados. Esto puede reflejar que, en condiciones de inanición, los nutrientes se utilizan para el mantenimiento de la estructura celular en vez de para la generación de energía. Finalmente, las tasas de R_{CO2}/NADP-IDH fueron más bajas en aquellas incubaciones que duraron más de 12h, lo que sugiere que los ritmos circadianos de *L. lingvura* afectan en las incubaciones de larga duración. Por ello, recomendamos incubaciones menores a las 6h para futuros estudios de *L. lingvura*.

ABSTRACT: CO_2 production rates (R_{CO2}) were measured in *Leptomysis lingvura* to compare with the potential CO_2 production rates, proxied here for the first time by the NADP$^+$-dependent isocitrate dehydrogenase activity (NADP-IDH). Both respiratory physiological rates (R_{CO2}, R_{O2}), their ratio (RQ), and enzymatic potential respiration rates (NADP-IDH and Φ) were measured in a bloom and in a post-bloom community of *L. lingvura*. This way, we were able to assess the respiratory variability linked to sex differences, to starvation (nutrient-limitation), and to differences in the previous trophic state of the community. Bloom-community females showed significantly higher respiratory enzyme activity than post-bloom-community females (Φ=1.04±0.14 versus 0.58 ±0.12 μmol O_2 h^{-1} (mg of protein)$^{-1}$, respectively; NADP-IDH=1.96 ±0.09 versus 0.97±0.19 μmol CO_2 h^{-1} (mg of protein)$^{-1}$, respectively). In contrast, the physiological CO_2 production was the same in the two communities. Thus, an average ratio, R_{CO2}/NADP-IDH, of 0.12±0.05 accurately characterized the well-fed *L. lingvura*, being only slightly higher in nutrient-limited mysids (0.16±0.06). The NADP-IDH/Φ ratio was 1.8±0.4 in females and 1.6±0.4 in males. Besides, we did not find significant differences in R_{O2}, R_{CO2}, RQ, Φ or NADP-IDH between sexes. In contrast, starvation was the most impacting factor on the physiological response. It reduced the R_{O2}/Φ ratio from 0.35±0.02 to 0.27±0.08, but increased the R_{CO2}/NADP-IDH ratio from 0.12±0.04 to 0.16±0.06. The RQ was almost double in nutrient-limited

mysids than in well-fed mysids. This may reflect the diversion of nutrients to cell maintenance and anti-oxidation from energy generation. Finally, lower physiological rates on samples incubated longer than 12h suggested circadian-rhythm which argues for incubation periods shorter than 6h in future *L. lingvura* studies.

4.1   Introduction

As it was said in the General Introduction (Chapter 1.1), even though during the last decades the CO_2-producing facet of the respiratory process (R_{CO2}) arose in assessing the role of the ocean as an antropogenic CO_2 sink, respiration has been mainly approached by assessing R_{O2} rates. Direct physiological measurement of R_{CO2} is not as feasible as measuring R_{O2} in the ocean, mainly because of the buffering effect of the carbonate system and the complexity and paucity of the available techniques to measure it. Thus, these rates have usually been derived from R_{O2} measurements by using the Respiratory Quotient ratios between moles of CO_2 produced per moles of O_2 consumed (RQ). These ratios are variable, not only because of different nutrient sources, but also to differences in nutrient availability (Berggren et al. (2012); Romero-Kutzner et al. (2015)). So, when assessing R_{CO2} rates, not only affects the variability in the physiological R_{O2} rates the final measurement, but the variability of RQ ratios would also bias the accuracy of the results. Here, we propose assessing the R_{CO2} production rates in the marine peracardian mysid *Leptomysis lingvura* by the development of physiological versus enzymatic ratios. *L. lingvura* is a mesozooplankton species found on the sandy bottoms of the East Coast of Gran Canaria (Spain). It has been proved to adapt well to lab cultures, even completing its life cycle in captivity (Herrera et al. (2011a)). Thus, it has been considered suitable for several enzymatic and physiological studies (Herrera et al. (2011b); Fernández-Urruzola et al. (2011)). Mysids are abundant in coastal regions, although they can also be found in the pelagic waters throughout the water column (Jumars (2007)). Being omnivorous, they usually feed on phytoplankton, zooplankton (copepods, tinntinids) seagrasses, macroalgae or detritus (Jumars (2007); Herrera et al. (2011a)), although they may switch to cannibalism in cultures when there is not enough food available (Laboratory observations; Domingues et al. (1999); Herrera et al. (2011a)). As they are part of the food chain and are hunted by many benthic, coastal and pelagic fishes, mammals, cephalopods and decapods (Mauchline (1980); Castro (1995); Jumars (2007); Kitsos et al. (2008)), strengthening the knowledge about their metabolism and the physiological responses may improve the assessment of both their roles and impacts on the ecosystem and their use as prey in aquaculture (Woods (2005); Otero-Ferrer et al. (2012)). In this study, we worked

with two communities of *L. lingvura*. The first one was sampled in Taliarte
(Telde, Gran Canaria) at the beginning of November 2017. Even though autumn is the most oligotrophic season in the Canaries (Barton et al. (1998)),
mysids were forming 300-500 individuals per group at the moment, as if
they were under bloom conditions (where "bloom" refers to a surge in the
mysid population), and were found together with the mysid *Siriella armata*
(SCUBA observations). On the other hand, the individuals sampled at the
end of November 2018, 48h after a storm, were found in 20-50 individuals
per group, as if they were under post-bloom conditions (SCUBA observations). The impact of the previous trophic conditions, sex differences, starvation, and the potential effect of a dial rhythm on the CO_2-producing facet
of respiration was assessed as follows:

– First, we set out to measure the relationship between the changes in
total inorganic carbon (δTC) over up-to-24h incubations (to assess
R_{CO2}), and the activity of the $NADP^+$-dependent isocitrate dehydrogenase (NADP-IDH), one of the most important cellular CO_2-producing
enzymes.

– Secondly, in order to understand the variability in this relationship:

1. We assessed the enzymatic activities (Φ and NADP-IDH) directly related to respiratory metabolism in bloom and post-bloom communities of *L. lingvura*.

2. We studied the differences in the physiological response and
the R_{CO2}/NADP-IDH ratios between females and males in the same
community.

3. We studied the differences between well-fed and nutrient-limited
females.

4. Finally, we studied the potential effect of a circadian rhythm on
these ratios in up-to-24h incubations.

In addition, all these data were compared with the results on the R_{O2} and
R_{O2}/Φ in the same organisms. Thus, we assess both the viability of the
development of R_{CO2}/NADP-IDH as a proxy of R_{CO2}, and the differences
between these two physiological responses of respiration to starvation, sex
differences or the circadian rhythm.

4.2   Material and Methods

4.2.1   *Leptomysis lingvura* sampling and cultures

This work was conducted on the mysid *L. lingvura*, sampled in two different
life-cycle modes. The first occurred during the middle of a mysid bloom in
early November 2017. The second occurred during the post-bloom phase at

the end of November 2018. Samples were collected off the port of Taliarte (Telde, East coast of Gran Canaria) by scuba-diving at a 5-10m depth. The mysids were swarming over shallow sandy bottoms closed to the rocky edge, in warm seawater at $20^o \pm 1^o$C. Plankton nets with a mesh size of 500μm were used to captured them, and plastic containers with a mesh cover (to ensure the sea-water flow during sampling time) were used to store them. The samples were taken directly to the laboratory in the plastic containers with an air pump to avoid O_2 depletion during transport. Two species were identified: *S. armata* and *L. lingvura*. The experiments were carried out only on *L. lingvura* because its survival rate, in culture, is higher (Herrera et al. (2011a)) and because other physiological and enzymatic studies, related to O_2 consumption and NH_4^+ excretion (Fernández-Urruzola et al. (2011); Herrera et al. (2011b); Fernández-Urruzola et al. (2016); Osma et al. (2016b)), have been already done. Afterwards, the mysids were maintained at 19.5 ± 1.5^oC (in situ temperature) and on a 11:13h light:dark cycle, in a culture system according to Herrera et al. (2011a). The system consisted of four 40L-glass aquariums connected to a temperature-controller, 70 L biological filtration system (BIO DIGEST ©). The 19.5^o seawater flowed through the system at a velocity of 6L h^{-1}. The levels of NH_4^+, NO_2^- and NO_3^- are kept below 0.1, 0.02 and 0.2 mg L^{-1} by both a biological filtration system and a mechanical one (mini-filters in every aquarium) (Lussier et al. (1988)). In addition, every week, 25% of the volume of sea-water was replaced by fresh filtered seawater. Mysids were fed twice a day on *Artemia sp.* >72h nauplii, at a daily dose of 100 Artemia mysid^{-1} d^{-1} from secondary cultures (Domingues et al. (1999); Fernández-Urruzola et al. (2011); Herrera et al. (2011b); Osma et al. (2016b)). After an acclimation period of one week, the healthiest mature males and females were selected for experimentation:

- On the samples from 2017, the influence of the incubation time on the physiology of well-fed females was assessed. Incubation for CO_2 production ranged from 4h to 24h (4h, 8h, 12h, 16h and 24h). Every incubation was carried out in triplicate with samples of 10 mysids.

- On the samples from 2018, the influence of sex and starvation on the physiology of well-fed and 12h-starved females (well-fed: WF-F, nutrient-limited (starved): S-F) and well-fed males (well-fed: WF-M) was assessed. Every 6h-incubation was carried out in triplicate with samples of 10 mysids for CO_2 production and with 3 mysids for O_2 consumption.

For the well-fed mysid experiments, before incubations, the mysids were placed, for two hours, in filtered sea water containing 72h artemia-nauplii at a concentration of 50 artemia mysid^{-1}. After 2h of feeding, they were sieved out and placed in filtered seawater for the two types of respiration measurements. For the nutrient-limited-mysid experiments, before incuba-

tions, the mysids were placed, for two hours, in filtered sea water containing 72h artemia-nauplii at a concentration of 50 artemia mysid^{-1} (exactly as were the well-fed mysids). After 2h of feeding, they were sieved out and placed in filtered seawater for 12 h. Then they were pipeted out, with a basting pipet, and placed in new filtered seawater for the two types of respiration measurements.

A parallel experiment with 12h-starved males that were fed on 50 artemia mysid^{-1} for 2h just before a 4h-incubation was also carried out on the 2018 community (non-starved males: NS-M). After every incubation, mysids were sieved through a 50μm mesh and frozen at -80°C with a freezing container Nalgene© Mr Frosty. Samples were stored in Microvials® 2mL-tubes at -80°C until enzyme and protein analyses.

4.2.2 NADP-IDH activity: potential CO_2 production

Samples were homogenised in 0.1M phosphate buffer (0.1M Na$_2$HPO$_4$, 0.1mM KH$_2$PO$_4$, 75μM MgSO$_4\cdot$7H$_2$O, PVP (1.5mg mL^{-1}), TRITON X-100 (2mL L^{-1})), by sonication for 45sec at 70% amplitude in a Vibracell VCX 130 Sonics® ultrasonic processor. Then, crude homogenates were centrifuged (0-4^{o}C) at 4000rpm (1500 g) for 10 min. An aliquot of the supernatant fluid was assayed for NADP-IDH activity following Tames-Espinosa et al. (2018). The activity was measured kinetically by following the time-dependent production of NADPH at 340nm and 20^{o}C in a 1cm UV-transparent plastic cuvette in a Cary 100 U-V visible spectrophotometer for 1200 sec. One mol of β-NADP$^+$ (SIGMA #N0505; from here on we will call NADP$^+$) was reduced by NADP-IDH to NADPH while decarboxylating the DL-trisodium-isocitrate (SIGMA #I1252; from here on we will call isocitrate) to α-ketoglutarate and producing 1 mol of CO_2 (Eq.4.1).

Isocitrate + NADP$^+$ $\leftrightarrow$ α -*ketoglutarate* + *NADPH* + *CO2* (4.1)

Control assays (blanks) lacked isocitrate. Occasionally, to check for contamination and to assess any nonenzymatic reaction between NADP$^+$ and isocitrate, an assay was run without homogenate. Normally, contamination and any non-enzymatic reaction between NADP$^+$ and isocitrate are negligible. The reaction was started by adding the NADP$^+$ solution. After 3 min, the slope of the linear time-course absorbance signal was considered the IDH activity. A molar extinction coefficient (ε) of 5.42 absortivity units mL μmol^{-1}cm^{-1} was obtained for NADPH under these conditions (Tames-Espinosa et al. (2018)). As 1 mol of NADPH is produced, 1 mol of CO_2 is generated, NADP-IDH activity was reported in μmol CO_2 h^{-1} (mg of protein)$^{-1}$ units. To convert to volume units (μLCO$_2$ h^{-1}(mg of proteins)$^{-1}$), multiply by 22.4 μL μmol^{-1}.

4.2.3 Electron transport system (ETS) activity: potential O_2 consumption

Potential respiration in terms of O_2 consumption (Φ), was determined from the electron transport system activity (ETS) by the in vitro tetrazolium reduction method (Packard (1971)). After centrifugation, the supernatant aliquot was assayed for ETS activity following Owens and King (1975) and Gómez et al. (1996). The absorbance increase of the INT-formazan at 490nm was continuously monitored at 18°C in 1cm path-length cuvettes for 8min. A molar extinction coefficient (ε) of 12.8 absortivity units mL μmol^{-1}cm^{-1} was obtained for tetrazolium salt, INT (p-Iodonitrotetrazolium Violet, Across #122400010) under these conditions. The regression line (slope) of absorption versus time was used to estimate the ETS activity and potential respiration rates (Φ) after Packard and Williams (1981). The INT was reduced by the respiratory ETS enzymes, replacing O_2 as the electron acceptor. The INT accepts two electrons whereas O_2 would accept four. Thus, the INT-formazan production rate (i.e., 1μmol formazan mL^{-1} h^{-1}) is stoichiometrically related by a factor of 2 to ETS activity (i.e., 2μmol e$^-$ mL^{-1} h^{-1}) and by a factor of 0.5 to Φ (i.e., 0.5μmol O_2 mL^{-1} h^{-1}). Note that in terms of electrons transferred, the three rates are equivalent. Blanks were run without the ETS substrates in order to subtract the contribution of the background non-enzymatic and enzymatic reduction of the INT (Maldonado et al. (2012)). Occasionally, to check for contamination and to assess any nonenzymatic reaction between the ETS substrates, an assay was run without homogenate. Normally, contamination and any non-enzymatic reaction between the ETS substrates are negligible. Φ was reported in μmol O_2 h^{-1}(mg of protein)$^{-1}$ units. To convert Φ to μLO_2 h^{-1}(mg of proteins)$^{-1}$, multiply it by 22.4 μL μmol^{-1}.

4.2.4 Physiological O_2 consumption rates (R_{O2}) in *L. lingvura* incubations

O_2 consumption rates (R_{O2}) were measured by incubating three mysids in a 60mL bottle per triplicate with a 1-Channel Fibox 4 optode (Presens$^{®}$) with four PSt3 sensors following Bondyale-Juez et al. (2017). Three sensors measured the O_2 concentration [O_2] in three bottles containing 3 mysids per bottle in filtered seawater, whereas the fourth was used in the blank bottle, filled only with filtered seawater. As this system was limited to one measurement at a time, to ensure the measurement every 15 min, we moved the probe from bottle to bottle, for 120min. [O_2] was expressed in μmol O_2 L^{-1} units. These measurements, according to Bondyale-Juez et al. (2017), are in agreement with (and comparable to) the results obtained from the Winkler method and from the Strathkelvin 928 O_2-electrode system. The negative slope (α)

of the regression line of $[O_2]$ per time, after the first 30min, is directly related
to the O_2 consumption per time in the bottle (which is expressed in μmol O_2
L^{-1} min^{-1} units). To convert this result to the mysids' respiration rates in
μmol O_2 h^{-1} units, we used the incubation bottle volume (V) in L units, as
expressed in Eq.4.2:

R_{O2} = - (α) · V · 60 (4.2)

Where α is the slope of the obtained linear regression of $[O_2]$ per min, V
the incubation bottle volume in L units, and 60 the minutes in one hour.
Thus, R_{O2}, per bottle, is expressed as μmol O_2 h^{-1}. Combined with the
biomass measurements, per bottle, for the same samples, R_{O2} may also be
expressed in μmol O_2 h^{-1} (mg of protein)$^{-1}$. This facilitates the direct com-
parison of Φ to R_{CO2}. For further comparison, to convert to μLO_2 h^{-1}(mg
of proteins)$^{-1}$, multiply by 22.4 μL μmol^{-1}.

4.2.5 Physiological CO_2 consumption rates (R_{CO2}) in *L. lingvura* incubations

Total dissolved inorganic Carbon (TC) measurements require bigger vol-
umes (250mL per measurement) than the O_2 optode method. Thus, we as-
sessed the R_{CO2} as an end point measurement for the increase in TC (δ_{TC})
of ten-mysids, incubated (in triplicate) in 1L-bottles, for an incubation pe-
riod that ranged from 4h to 24h. The length of this period depended on
the aim of the experiment. Initial TC was measured, in triplicate, in bottles
filled with filtered seawater at the beginning of the incubation (TC_0). For the
respiration measurements, each bottle contained ten mysids in filtered sea-
water. Then, after the incubation, the TC was measured (TC_e). Finally, TC
was measured in the blank bottles incubated with filtered seawater, over the
same period, ($TC_{e-blank}$). TC was determined in every case together with the
total alkalinity (TA, μmol L^{-1}) by the VINDTA 3C coulometric detection
method (Mintrop et al. (2000)). The titration of certified reference material
for oceanic CO_2, CRMs 117, was used to test the performance of the equip-
ment. Measurements of CRMs were within ± 1.0 μmol kg^{-1} of the certified
value for TC and ± 2 μmol kg^{-1} for TA. Thus, it had a precision of ± 1 μmol
TC L^{-1} and ± 2 μmol kg^{-1} for TA (www.MARIANDA.com). Once the TC
concentration in every bottle was measured, the rate of TC increase (δ_{TC})
was calculated as in Eq.4.3:

δ_{TC} = ((TC_e-TC_0)-($TC_{e-blank}$-TC_0))·V/t (4.3)

Where V is the volume of the incubation bottle in liters (which was 1L during
the entire study) and t the incubation time expressed in h. Thus, δ_{TC} is
expressed in μmol TC h^{-1}.

Note that TC does not include the inorganic carbon that has been converted into $CaCO_3$ (carbonate sequestration, Eq.1.1). This value can be measured by the assessment of the increase in TA. In our hands, TA remained constant within the average standard deviation of the method (± 2 μmol kg^{-1}). Thus, we assume the carbonate sequestration was not significant in this experiment during the incubation periods.

Therefore, as the production of one mol of CO_2 impacts directly on the TC by adding one mol to the total inorganic carbon in sea water, the increase in TC is directly related to the CO_2 production (Eq. 4.4).

$R_{CO2} = \delta_{TC}$ (4.4)

Where R_{CO2} is expressed in μmol CO_2 h^{-1}. R_{CO2} may be also expressed in μmol CO_2 h^{-1} (mg of protein)$^{-1}$ when normalized by the biomass measurements in the same sample. This normalization facilitates the direct comparison of IDH to R_{CO2}. For further comparison, using volume units (i.e., (μLCO_2 h^{-1}(mg of proteins)$^{-1}$), one simply multiplies by 22.4 μL μmol^{-1}.

4.2.6 Respiratory Quotient (RQ) calculations

The respiratory quotient (RQ) is a dimensionless ratio of the CO_2 produced to the O_2 consumed. Here, in Eq. 4.5, we assessed the RQ as the ratio between R_{CO2} (expressed in μmol CO_2 h^{-1} (mg of protein)$^{-1}$) and the R_{O2} (expressed in μmol O_2 h^{-1} (mg of protein)$^{-1}$) in samples related to the same incubation conditions (e.g. well-fed females, well-fed males, nutrient-limited females, and non-nutrient-limited males).

RQ = R_{CO2}/R_{O2} (4.5)

4.2.7 Biomass

Proteinaceous biomass was determined on aliquots from sample homogenates preserved for enzyme activities. We assayed the protein with the method of Lowry et al. (1951) as modified by Rutter (1967) and Markwell et al. (1981) using bovine serum albumin (BSA) as the standard. Biomass was reported in mg of protein (mL of homogenate)$^{-1}$. It may also be reported in mg of protein L^{-1}, knowing the homogenate volume and the sea-water volume of the sample. To facilitate further comparison, protein (P) can be converted into dry weight (DW), by using the ratio from Herrera et al. (2011a), where 1mg of DW corresponds to 0.74$\pm$0.05 mg protein. Taking this into account, the relation between DW from P would be expressed as Eq.4.6.

DW=P$\cdot$1.35 (4.6)

4.2.8   Statistical Analysis

In every experiment, the Student´s t-test (Sachs (2012)) was applied to quantify the differences between pairs of datasets (e.g. females and males, well-fed and nutrient-limited females, bloom and post-bloom conditions) by the t-test function of the CRAN R Stats package (v.3.4.2, Eddelbuettel et al. (2011)).

4.3   Results and Discussion

4.3.1   Impact of trophic conditions on potential respiration (Φ and NADP-IDH) and R_{CO2}/NADP-IDH ratios in ovigerous females of two communities of *L. lingvura*

The trophic conditions under which the community had been raised had an impact on the development of the catabolic metabolism enzymes (Fig.4.1), as the respiratory enzymatic activities normalised per biomass were significantly higher (p<0.001) in those females that belonged to a bloom community than those that belonged to a post-bloom community.

[a]

[b]
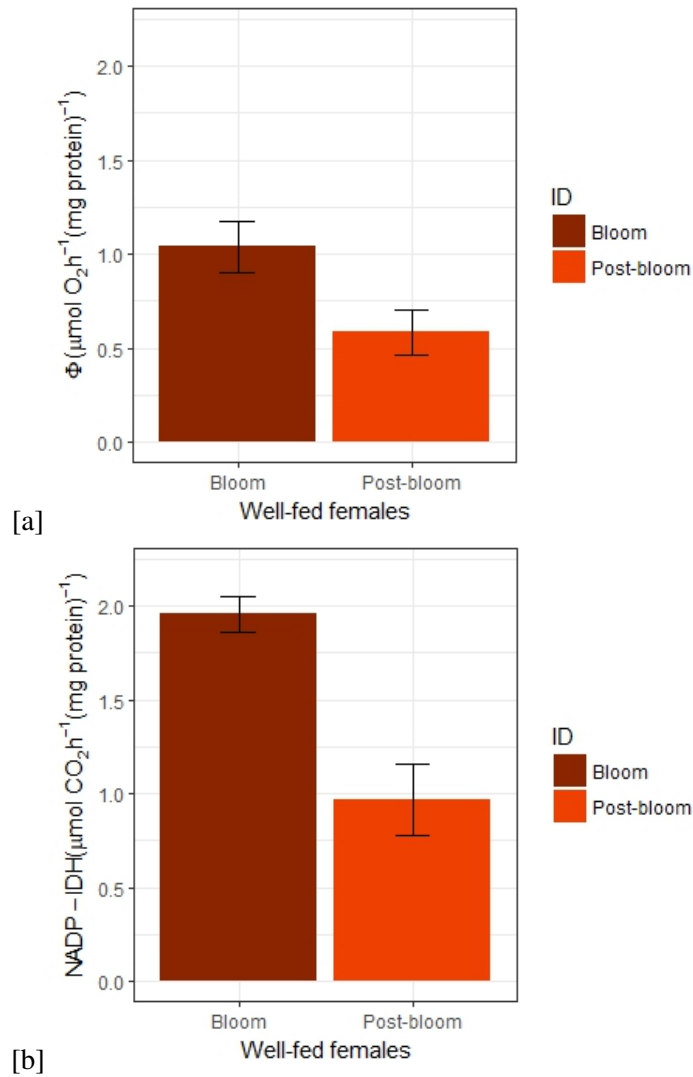
Figure 4.1: Differences in normalised respiratory enzymatic activities in well-fed females of *L. lingvura* from a bloom and from a post-bloom community. Note that Φ represents the potential O_2 consumption of the mysids and NADP-IDH is the potential CO_2 production of the NADP-IDH enzyme in the mysids.

The variability of Φ between bloom females (1.04 ± 0.14 μmol O_2 h^{-1} mg of protein^{-1}), and post-bloom females (0.58 ± 0.12 μmol O_2 h^{-1} mg of protein^{-1}) is consistent with the variability of Φ in other studies of *L. lingvura*. They are from 30 to 60% lower than those reported by Herrera et al. (2011b) (1.53 ± 0.43 μmol O_2 h^{-1} mg of protein^{-1}), which were sampled under mesotrophic conditions during spring. On the other hand, they are 2 to 4-fold higher than the values obtained on samples from October 2015 (0.25 ± 0.06 μmol O_2 h^{-1} mg of protein^{-1}) (Bondyale-Juez et al. (2017)), during the warmest and most oligotrophic season in the year (Jurado-Ruzafa et al. (2019)). Furthermore, our results fall within the range (1.47 ± 0.76 μmol O_2 h^{-1} mg protein^{-1}) of the Canarian mesozooplankton (500-1000μm) reported by Osma et al. (2016c).

The variability of NADP-IDH, based on the CO_2-producing enzyme NADP-IDH, was similar. It was significantly higher (p<0.001) in female mysids raised under bloom conditions (1.96 ± 0.09 μmol CO_2 h^{-1} mg of protein^{-1}) than in the post-bloom females (0.97 ± 0.19 μmol CO_2 h^{-1} mg of protein^{-1}). These are the first NADP-IDH measurements on two different communities of *L. lingvura*.
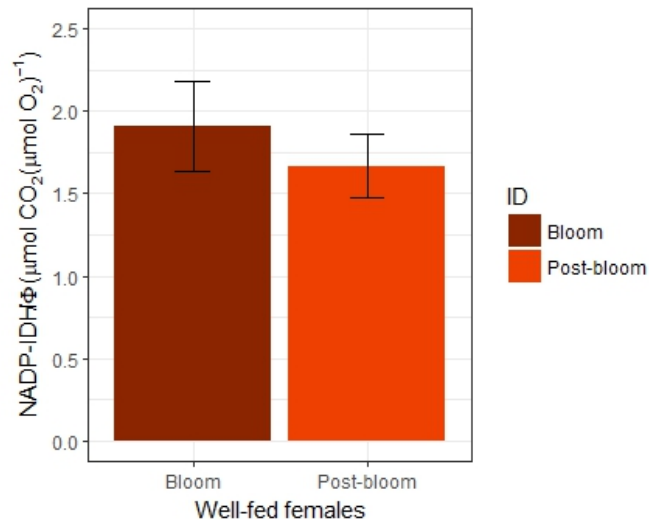
Figure 4.2: NADP-IDH to Φ proportion in well-fed females of *L. lingvura* belonged to a bloom and to a post-bloom community. Note that Φ represents the potential O_2 consumption of the mysids and NADP-IDH is the potential CO_2 production of the NADP-IDH enzyme in the mysids.

Besides, the ratio between NADP-IDH and Φ allows the assessment of the relationship between the decarboxylating facet and the ATP-producing-O_2-consuming facet in respiration. Both communities followed a similar pattern (Fig. 4.2), where NADP-IDH ranged between 1.5 and 2.2 times Φ activ-

ity. These results suggest that the enzymatic pathways related to the organic carbon oxidation phase of cellular respiration are prepared to exceed the demands of the ETS. This may serve as an advantage when, eventually, the mysid has a high energy requirement. Once this requirement is met, NADPH excess may be redirected to lipid synthesis by the NADP-IDH substrate cycle (Sazanov and Jackson (1994)). There was still a slight difference between both communities (p=0.1098) that may be related to the differences in the intensity of the reproductive activity that females were experiencing during the moment of collection. Higher results in the NADP-IDH/Φ ratio in the bloom females may be linked to higher lipid demands during gametogenesis, egg production, and breeding (Lawrence (1976); Lee et al. (2006)).
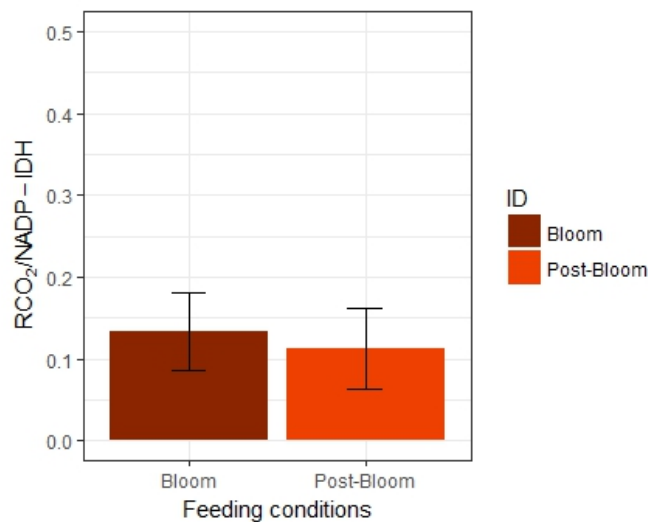
Figure 4.3: R_{CO2}/NADP-IDH ratio in well-fed females of *L. lingvura* belonged to a bloom and to a post-bloom community.

Whereas the enzymatic activities were higher in bloom females than in post-bloom females, the R_{CO2}/NADP-IDH ratio was not significantly different between the two communities (p=0.5623) (Fig. 4.3). Thus, we suggest that an average ratio of 0.12 ± 0.05 would accurately characterize the physiological response for CO_2 production in well-fed females in *L. lingvura* communities (Fig.4.3). Bloom females had slightly, but not significantly, higher values than did post-bloom females (0.13 ± 0.05 and 0.11 ± 0.05 respectively). These results are lower than expected in comparison with the average O_2 consumption ratios in the literature (0.81 in Bondyale-Juez et al. (2017); from 0.66 to 1 in Herrera et al. (2011b) for those mysids assessed close to dawn). However, they were close to the obtained ratios related to the excretion metabolism during the first 18h of starvation (0.11 ± 0.05 in Fernández-Urruzola et al. (2011)).

4.3.2   Impact of sex differences and starvation on potential respiration (Φ and NADP-IDH)

Neither the O_2 consumption, the CO_2 production, nor the enzymatic activities showed significant differences between sexes (p=0.1299 in Φ between well-fed females and males; and p=0.6126 in NADP-IDH between well-fed females and males), resulting in an average Φ of 0.6$\pm$0.12 μmol O_2 h^{-1} mg of protein^{-1} and an average NADP-IDH of 0.95$\pm$0.17 μmol CO_2 h^{-1} mg of protein^{-1} (Fig. 4.4).

[a]

[b]
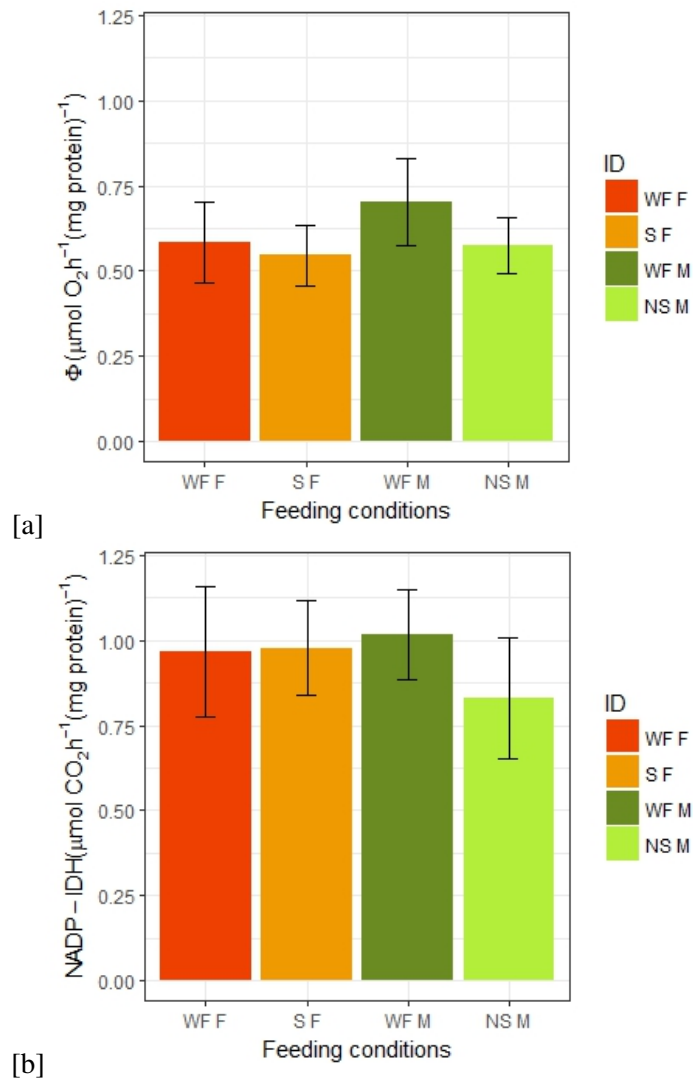
Figure 4.4:   Differences in normalised respiratory enzymatic activities in well-fed and nutrient-limited (starved) females (WF F & S F) and well-fed and non-starved males (WF M & NS M) from the post-bloom community. Note that Φ is the potential O_2 consumption and NADP-IDH is the potential CO_2 production of the NADP-IDH enzyme in the mysid.

These similarities also occurred between nutrient-limited females and the
non-starved males which, after 12h of starvation were fed for two hours
(p=0.5409 in Φ between nutrient-limited females and non-starved males, and
p=0.1398 in NADP-IDH between nutrient-limited females and non-starved
males). However, starvation seemed to have a slightly higher impact on
males than on females, as the reduction of the metabolic activities in both
Φ and NADP-IDH after starvation was slightly greater (p=0.070382 in Φ
between well-fed and non-starved males whereas p=0.5333 in Φ between
well-fed and nutrient-limited females).
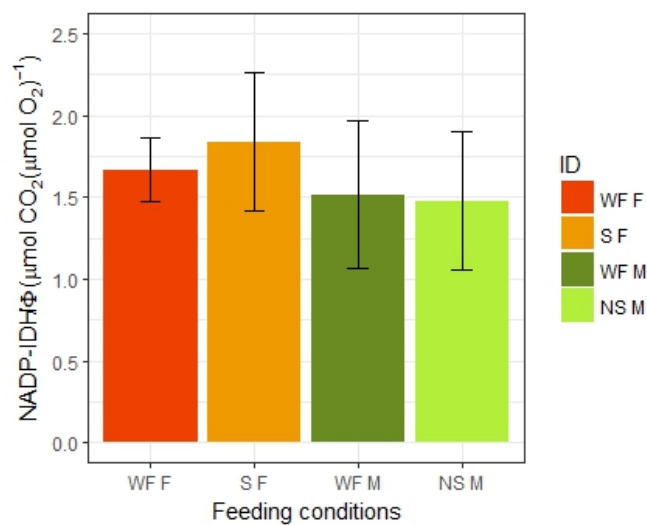
Figure 4.5: NADP-IDH to Φ proportion in well-fed and nutrient-limited (starved)
females (WF-F & S-F) and well-fed and non-starved males (WF-M, NS-M) from
the post-bloom community.

These slight differences between sexes were even smaller in relation to the
NADP-IDH/Φ proportion (p=0.4784 between sexes in well-fed mysids, p=0.1688
between sexes in nutrient-limited mysids), resulting in NADP-IDH being
1.63$\pm$0.4 times Φ (Fig.4.5). However, starvation produced a higher differ-
ence in this ratio between sexes (NADP-IDH/Φ=1.48$\pm$0.42 in males, whereas
NADP-IDH/Φ=1.84$\pm$0.42 in females). These results may imply that oviger-
ous nutrient-limited females tend to protect their lipid synthesis pathways for
gametogenesis, egg production, and breeding (Lawrence (1976); Lee et al.
(2006).

On the other hand, the difference between well-fed and nutrient-limited mysids
was not significant (p=0.4006 in females, and p=0.8762 in males).

4.3.3 Impact of sex differences and starvation on the R_{O2}/Φ and R_{CO2}/NADP-IDH ratios

Results with the R_{O2}/Φ ratio were not significantly different between sexes in the same post-bloom community of *L. lingvura* (p=0.7435 between well-fed females and males and p=0.9466 between nutrient-limited females and males, Fig.4.6). In contrast, the R_{O2}/Φ ratio in well-fed mysids was 0.35±0.07, whereas in nutrient-limited mysids was slightly lower (0.27±0.08). For the R_{CO2}/NADP-IDH ratio, lower values were obtained. They ranged from 0.06 up to 0.25, without significant differences between sexes (p=0.7592 between well-fed females and males). As in the case of the enzymatic activity, the physiological response of the non-starved males was similar to those females that were in starvation (p=0.7564). This is coherent with the results in R_{O2} reported by Osma et al. (2016b), where after having fed the nutrient-limited mysids, the R_{O2} slightly increased during the first hours. The highest R_{O2} values were attained 6 hours later, being still lower than the well-fed mysids' respiratory rates. Thus, we analysed these results assuming that non-starved males are behaving more likely nutrient-limited mysids than well-fed mysids. The R_{CO2}/NADP-IDH ratio in well-fed mysids was 0.12±0.04, whereas in nutrient-limited mysids it was only slightly higher, 0.16±0.06. The R_{CO2}/NADP-IDH ratio in the well-fed females from the bloom community was also around 0.12. Thus, this value seems to accurately describe the R_{CO2}/NADP-IDH ratio in a well-fed community of *L. lingvura*.

Starvation differently affected the physiological O_2 consumption and CO_2 production facets of respiration. Although the differences between well-fed and nutrient-limited mysids cannot be considered statistically significant (p=0.3480 in females (n=6) and p=0.4176 in males (n=6)), there is a clear trend in both cases (Fig.4.6). Whereas the decrease in food availability reduced both the R_{O2} and the R_{O2}/Φ ratio, the R_{CO2} and R_{CO2}/NADP-IDH increased in both males and females. Note that this experiment was carried out in the same circadian time, as all the incubations began around three hours after dawn on mysids which had been adapted to culture conditions for more than one week.

Due to this imbalance between the physiological responses, the RQ was almost double in nutrient-limited mysids than in well-fed individuals (Fig.4.7). The RQ tended to increase during the first 12-18h of starvation, although the difference could not be considered statistically significant (p=0.1592 between well-fed and nutrient-limited females, and p=0.1526 between well-fed and non-starved males). The increase in these results during starvation is consistent with Romero-Kutzner et al. (2015)'s findings in bacteria, where the highest RQ resulted during the first hours of nutrient depletion. In addition, Mayzaud et al. (2005) reported lower RQ in Euphausiids *Meganyctiphanes norvegica* sampled during the late winter (March 2001) in

[a]

[b]
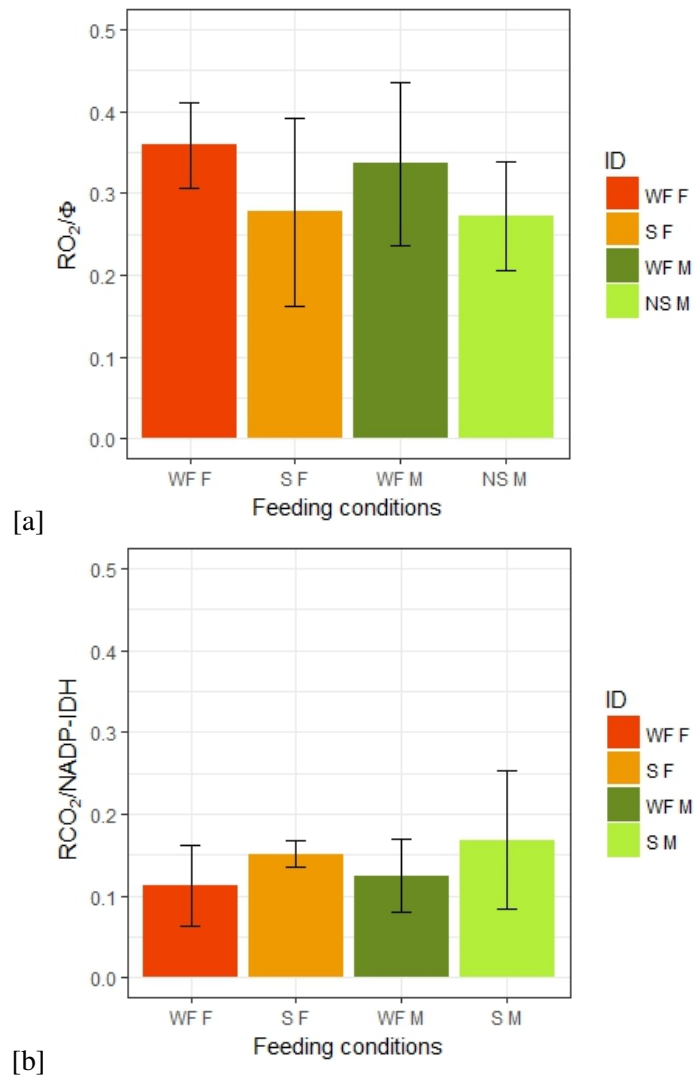
Figure 4.6: Effects of starvation and sex differences on the ratios of respiration to enzymatic activity in well-fed and nutrient-limited females (WF-F & S-F) and well-fed and non-starved males (WF-M & NS-M) from the post-bloom community

the North Atlantic than in those sampled during the more oligotrophic summer (September 2001) (1.29±0.1 versus 1.62±0.23 respectively). Besides, after converting their Euphasiids R_{CO2} from $\mu L\ CO_2 h^{-1} (mg\ DW)^{-1}$ to $\mu mol\ CO_2 h^{-1} (mg\ protein)^{-1}$ units, we found that the average *L. lingvura* R_{CO2} of $0.13\pm0.04\ \mu mol\ CO_2 h^{-1} (mg\ protein)^{-1}$ was similar to the average R_{CO2} in *M. norvegica* $(0.13\pm0.03\ \mu mol\ CO_2 h^{-1} (mg\ protein)^{-1})$. Furthermore, in the terrestrial Arthropoda Lepidoptera, an averaged RQ of 1.5-1.6 under starvation was reported, with a maximum of 2.09 (Kozhantshikov (1938)). This author also reported a peculiar reduction of O_2 consumption related to an
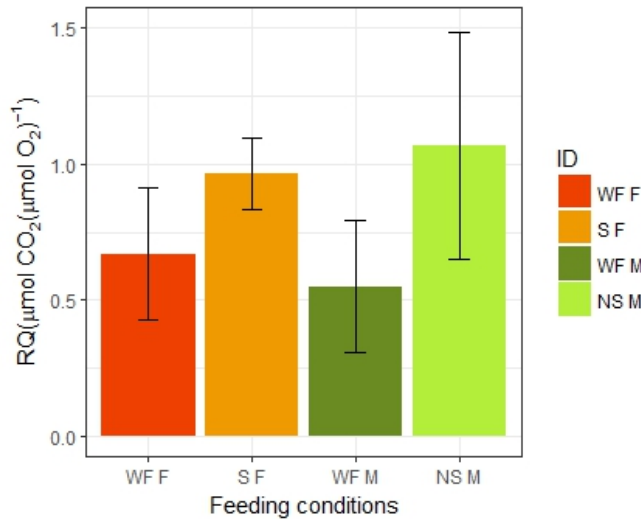
Figure 4.7: Effects of starvation and sex difference on the respiratory quotient (RQ) in well-fed and nutrient-limited (starved) females (WF-F & S-F) and well-fed and non-starved males (WF-M & NS-M) from the post-bloom community.

increase of fat synthesis from carbohydrates. As O_2 is produced during this process, the O_2 consumption related to respiration is reduced.

Besides, the enzyme NADP-IDH is also linked to lipid synthesis as one of the cellular sources of NADPH. An increase in CO_2 production during starvation is consistent with other findings in the literature that assess lipogenesis during starvation. Lipid synthesis was not reduced in mice during the first 18h of starvation (Jansen et al. (1966)). In nutrient-limited eels an increase occurs in the activity of the tricarboxylate carrier that exports citrate from the mitochondria to the cytosol (Zara et al. (2000)). In the liver of these nutrient-limited fish, the cytosolic IDH is thought to be the main source of NADPH, as it is the receptor of carbon flowing from this extramitochondrial citrate towards isocitrate (Aster and Moon (1981)). This increase in cytosolic isocitrate during starvation would drive the enzyme NADP-IDH to generate both NADPH and CO_2 while increasing lipid synthesis.

Taking all this into consideration, we hypothesized that during starvation in *L. lingvura*, nutrients are diverted to the maintenance of cell structures instead of to energy generation. This is consistent with the upregulation of metabolic marks linked to gluconeogenesis and the use of stored lipids reported by Teruya et al. (2019) during fasting in humans. In addition, as NADP-IDH is also related to the production of reduced glutathione, involved in the reactive oxygen species (ROS) scavenging (Jo et al. (2001)), the slight increase in the R_{CO2} (from 0.11 ± 0.01 μmol CO_2h^{-1}(mg protein)$^{-1}$ in well-fed mysids to 0.14 ± 0.04 μmol CO_2h^{-1}(mg protein)$^{-1}$ in nutrient-limited

mysids) may reflect that anti-oxidation is a principal response to fasting
Teruya et al. (2019).

Thus, we suggest that the increase in RQ during starvation is related to:

- The CO_2 production during carbohydrate catabolism to produce NADPH,
  which is diverted from energy generation to the structural lipid synthe-
  sis and the production of the ROS scavenger reduced glutathione.

- The O_2 consumption linked to the ATP production is limited because
  the in-cell ATP requirements are minimised.

- Finally, an O_2 production linked to the lipid synthesis reduced the R_{O2}
  during starvation.

4.3.4   Impact of long-term incubations on R_{CO2}/NADP-IDH ratios in females of *L. lingvura*
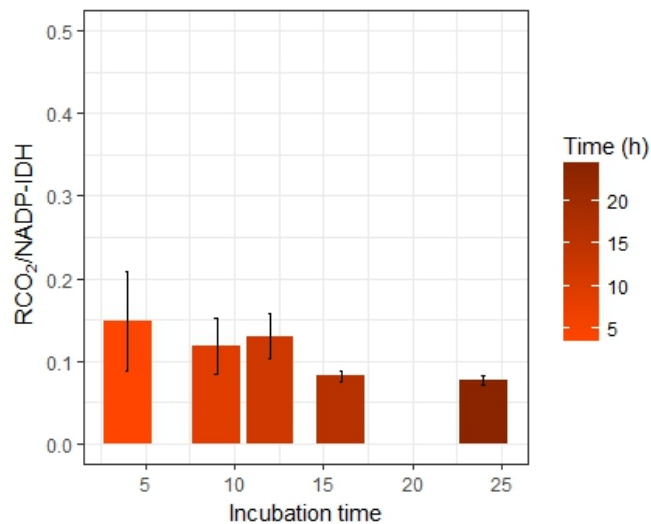
Figure 4.8: R_{CO2}/NADP-IDH ratio variability during long-term incubation peri-
ods.

We assessed the impact of long-term incubations on well-fed females. In
previous subsections, R_{CO2}/NADP-IDH ratios were measured at the same
circadian time and, in the first hours after feeding, were lower than those
measured after 12h of starvation. Here, we measured the average ratio dur-
ing the whole incubation period (from 4h to 24h) beginning after feeding.
R_{CO2}/NADP-IDH remained around 0.13 ± 0.04 during the first 12 hours of in-
cubation but, unlike other experiments made at the same circadian time, here
the measurements dropped to less than 0.1 in longer incubations (0.08 ± 0.01)
(Fig.4.8). As *L. lingvura*'s metabolism has a circadian rhythm (Herrera et al.

(2011b)), we hypothesized that the lower values in those periods longer than 12h were driven by lower activity conditions linked to those circadian rhythms. Thus, we recommend incubation periods shorter than 6h in future *L. lingvura* studies.

4.4 Conclusions

– Nutrition prior to sampling, has a significant impact on the respiratory enzymatic activity of *L. lingvura*. Higher activities normalised per biomass were found in bloom communities than in post-bloom communities.

– An average R_{CO2}/NADP-IDH ratio of 0.12 was obtained on well-fed mysids from both communities. This result was only slightly higher in nutrient-limited mysids (0.16). This value accurately characterized the physiological response of *L. lingvura*.

– Sex difference did not significantly impact enzymatic activities nor the ratios of respiratory physiology to enzyme activity.

– Starvation for longer than 12h decreased the R_{O2}/Φ ratios, whereas it increased the R_{CO2}/NADP-IDH ratios, leading to higher RQs. Our interpretation is that energy production is diminished whereas lipid synthesis and anti-oxidation are strengthened.

– Incubation of mysids longer than 12h mixes starvation and circadian effects. We recommend incubations between 4 and 6 hours in future ecophysiological studies.

Chapter 5

Chapter 5: Metabolic responses of subtropical North Atlantic microplankton after a simulated deep-water upwelling event.

*We cannot solve our problems with
the same thinking we used when we
created them.*

Albert Einstein

RESUMEN: Durante el otoño de 2014 se instalaron nueve mesocosmos en las aguas oligotróficas del Nordeste del Atlántico subtropical, en Gran Canaria, con el objetivo de estudiar el impacto de la acidificación en una comunidad planctónica bajo la influencia de un afloramiento simulado de aguas profundas ricas en nutrientes. Entre otros parámetros, se midieron la Clorofila *a* (Chl_*a*), la Respiración Potencial (Φ) y la biomasa (B) en el microplancton (0.7-50μm) tanto durante la fase oligotrófica (Fase I), como durante el bloom fitoplantónico (Fase II) y durante la fase posterior al bloom (Fase III). En este capítulo hemos analizado el ratio Φ/Chl_*a* para monitorizar los cambios en el metabolismo de la comunidad microplanctónica. Cuando la comunidad estuvo dominada por los fotoautrótrofos se obtuvieron valores < 2,5μLO$_2$h^{-1} μg Chl_*a*$^{-1}$ (siendo incluso <1,7μLO$_2$h^{-1} μg Chl_*a*$^{-1}$ durante el bloom fitoplantónico). Cuando los valores se situaron entre 2,5-7μLO$_2$h^{-1} μg Chl_*a*$^{-1}$ reflejaron una comunidad mixta o dominada por mixótrofos. Además, los ratios Φ/Chl_*a* fueron > 7μLO$_2$h^{-1} μg Chl_*a*$^{-1}$ cuando proliferó el microzooplancton (llegando a 10μLO$_2$h^{-1} μg Chl_*a*$^{-1}$ en el momento del bloom de dinoflagelados heterótrofos). Utilizando la

CHAPTER 5. Chapter 5: Metabolic responses of subtropical North Atlantic
microplankton after a simulated deep-water upwelling event.

80

primera derivada de la biomasa se ha observado una productividad neta
máxima entre uno y dos días antes del pico de Chl_a^{-1}, mientras que la
mayor pérdida de biomasa se dió en las 24h siguientes. Siguiendo este
mismo análisis, no hubo una productividad neta significativa ni durante
la fase I ni durante la fase III. El análisis de la integral de Φ, Chl_a y
B, por fase y mesocosmos, mostró una relación positiva entre Φ y los
niveles de pCO$_2$ durante la fase II, y una relación positiva entre Chl_a
y pCO$_2$ durante la fase III. Como a partir del final de la fase II proliferó
una especie de alga tóxica (*Vicicitus globosus*) en los mesocosmos con
mayor nivel de acidificación, la comunidad fue afectada: el microzoo-
plancton no proliferó, y el tiempo de retención de la Chl_a aumentó. En
estas comunidades los ratios Φ/Chl_a (4,1±1,5μLO$_2$h^{-1} μg Chl_a^{-1})
fueron similares a los de una comunidad mixta o mixótrofa. Esto, unido
a que *V. globosus* tiene un sistema fotosintético ineficiente a los nive-
les de pCO$_2$ actuales (carece de pirenoide) y la capacidad de cambiar de
una forma flagelada a una forma ameboide, parece indicar que *V. globo-
sus* es más un mixótrofo que un fotoautótrofo, y que su crecimiento se
refuerza cuando los niveles de pCO$_2$ son altos. Esto favorece la relación
positiva entre Chl_a^{-1} y pCO$_2$ observada en el experimento. Teniendo
en cuenta todo podemos concluir que los ratios Φ/Chl_a refuerzan el
conocimiento sobre el metabolismo de la comunidad, no sólo a nivel
del ecosistema, sino también a nivel de especies.

ABSTRACT: In the autumn of 2014, as part of the German KOSMOS
research program, nine large mesocosms were deployed in the olig-
otrophic sub-tropical North-eastern Atlantic close to the island of Gran
Canaria. Their deployment was designed to address the acidification ef-
fects on a plankton community experiencing upwelling of nutrient-rich
deep water. Among other parameters, chlorophyll a (Chl_a), poten-
tial respiration (Φ), and biomass (B) were measured in the microplank-
ton community (0.7-50μm) during the oligotrophic phase (Phase I),
the phytoplankton-bloom phase (Phase II) and the post bloom phase
(Phase III). Here, we explored using the Φ/Chl_a ratio to monitor shifts
in the microplankton community metabolism. Φ/Chl_a values below
2.5μLO$_2$h^{-1} μg Chl_a^{-1} indicated a community dominated by pho-
toautotrophs. The ratio reached lows below 1.7μLO$_2$h^{-1} μg Chl_a^{-1}
during the phytoplankton bloom. When the Φ/Chl_a ratios ranged be-
tween 2.5-7μLO$_2$h^{-1} μg Chl_a^{-1}, they indicated a mixed community
or a mixotroph dominance. When these ratios rose above 7μLO$_2$h^{-1} μg
Chl_a^{-1}, microzooplankton proliferated. In a heterotrophic dinoflagel-
late bloom, the Φ/Chl_a ratios rose as high as 10μLO$_2$h^{-1} μg Chl_a^{-1}.
Here, in our data analysis, we explored using Leibnizian differential
and Newtonian integral analysis to elucidate plankton dynamics from
time-courses of static biomass parameters. Derivative analysis of B re-
vealed maximum net productivity occurring between one and two days
before the Chl_a peak, whereas net maximum loss occurred 24h after
this peak. According to this analysis, no significant net productivity oc-
curred either on Phase I nor during Phase III. The integral analysis of
Φ, Chl_a and B, per phase and mesocosms, reflected a positive rela-

tionship between Φ and pCO_2 during Phase II and between Chl_a and pCO_2 during Phase III. At the end of Phase II, a harmful algal species, *Vicicitus globosus* bloomed in the high pCO_2 mesocosms and the community was disrupted. In these mesocosms, microzooplankton did not proliferate, and Chl_a retention time in the water column increased. In these communities, the Φ/Chl_a ratios ($4.1\pm1.5\mu LO_2h^{-1}\,\mu g\,\text{Chl}\_a^{-1}$) were similar to those in a mixed plankton community. These values, combined with the knowledge of *V. globosus*' inefficient photosynthetic system at current pCO_2 levels (it lacks pyrenoid bodies) and the knowledge of its ability to quickly shape-shift from a flagellate-shaped microorganism to an amoeboid-shaped one, suggest that *V. globosus* is more a mixotroph than a photoautotroph. Its proliferation is enhanced when high pCO_2 levels occur, resulting in positive Chl_a to pCO_2 relationships. All in all, the combined use of Φ/Chl_a ratios, Leibnizian differential, and Newtonian integral analysis strengthens our understanding of plankton community dynamics, not only at an ecosystem scale, but also at a species scale.

5.1 Introduction

The global economy, based on the combustion of fossil resources, has caused the increase in anthropogenic carbon dioxide (CO_2) emissions over the past 250 years. This rise, combined with the spread of deforestation and agriculture, has resulted in the highest atmospheric CO_2 levels (400ppm) in the last 800,000 years and keeps increasing up to one order of magnitude faster than it increased over the previous millions of years (Doney and Schimel (2007)). Oceans are taking up nearly one third of the anthropogenically produced CO_2, leading to effects on seawater carbonate chemistry, now denominated, the ocean acidification (OA) (Doney et al. (2009)). Even when positive impacts on photosynthetic carbon fixation have been reported when nutrients are available (Riebesell et al. (2007)), the resulting organic matter with low nutritional value may affect the rest of the community (Doney et al. (2009)). Under eutrophic conditions, these changes had different effects. In the most acidified environments, picophytoplankton growth is stimulated, and excreted dissolved organic carbon (DOC) becomes an important fraction of the organic matter. The shift to more DOC reduces the carbon flux, meaning that there is less sinking material in the water column (Paul et al. (2015)).

For 55-days, a KOSMOS mesocosm experiment (Taucher et al. (2017)) was conducted, in the subtropical North-Atlantic coastal waters off Gran Canaria, in order to reveal the effects increasing pCO_2 would have on the oligotrophic plankton community that was simultaneously experiencing an upwelling event. After 24 days of Oligotrophy (Phase I), an upwelling event

CHAPTER 5. Chapter 5: Metabolic responses of subtropical North Atlantic
microplankton after a simulated deep-water upwelling event.

82

was simulated by enriching nine mesocosms with nutrient-rich deep-water. The pCO$_2$ levels in these mesocosms ranged from 400μatm, to 1500μatm. Then, the phytoplankton community bloomed (Phase II) until nutrient depletion. At this point, the Post-bloom (Phase III) began. All the mesocosms showed similar trends in Chloropyll_a (Chl_a) and Biomass (B) during these three phases (Taucher et al. (2018)). In the mesocosms with elevated pCO$_2$, three changes were noted: (1) cell abundances of picocyanobacteria, *Synechococcus sp.* increased; (2) interspecific shifts favouring the large diatom species, *Guinardia strata* and the acrylic-acid producing Prymmnesiophyceae, *Phaeocystis globose*; and (3) the harmful algal species (HAS), *Vicicitus globosus* proliferated (Taucher et al. (2018); Hernández-Hernández et al. (2018); Riebesell et al. (2018)). *V. globosus* disrupted the plankton community in these mesocosms, inhibiting the growth of micro and mesozooplankton, and increasing the Chl_a retention time in the water column (Taucher et al. (2018); Riebesell et al. (2018); Algueró-Muñiz et al. (2019)).

Here, we assessed how ocean acidification impacted the oligotrophic nano and microplankton respiratory metabolism during the simulated deep-water upwelling event. During the different stages of the phytoplankton bloom, shifts in the community, ranging from an autotroph-dominated community to a heterotroph-dominated one, was detected from the changes in the ratio between Potential Respiration rate (Φ) and Chl_a. Accordingly, we focused on the effects of simulated upwelling on microplankton metabolism and its relationship with the shifts in the microplankton composition.

As Φ is a measurement of the plankton catabolic metabolism (see Chapter 1, section 1.3.3), and as Chl_a is related to photosynthetic capacity in photautotrophs, we expect the Φ/Chl_a ratio to behave as follows:

– Low Φ/Chl_a values should represent photoautotroph dominance, due to a high levels of Chl_a or low levels of ETS activity, in the plankton community. During the bloom phase, the lowest Φ/Chl_a values in the experiment, were expected.

– High Φ/Chl_a values should represent higher ETS activity and low Chl_a levels and would indicate a heterotroph-dominated plankton community.

– Finally, intermediate Φ/Chl_a values should reflect a balanced plankton community where photoautotrophic and heterotrophic metabolism coexist.

In addition, the coexistence of both photosynthetic and heterotrophic pathways in the same organism (mixotrophy) that arose in both planktonic algae and protozoa, challenge the classic conception of a pure auto- or heterotroph marine food web (Sanders (1991); Stoecker (1999); Caron (2016); Stoecker et al. (2017)). However, the mixotrophic effects on the food web

structure, on the trophic transfer efficiency, and on the vertical carbon flux (Fc) have been omitted in ecosystem models until recently (Sanders (1991); Caron (2016); Ward and Follows (2016)).

In plankton communities, harmful algal species (HAS) were thought to be strictly photoautotrophic until the last decade, when Burkholder et al. (2008) highlighted mixotrophy as the major mode of nutrition among these organisms. In the oligotrophic waters, mixotrophy not only functions well, but is particularly advantageous, as organisms find the potentially limiting nitrogen and phosphate much more concentrated in microbial prey (usually bacteria) than in the water column (Sanders (1991)). Although mixotrophy is thought to impact positively on the food web (Ward and Follows (2016)), when HAS is dominant, the impact may be negative due to the toxic effects on micro and mesozooplankton, and on higher levels of the food chain. These effects may also impact negatively on Fc.

As said before, in this experiment, elevated CO_2 treatments resulted in proliferation of HAS, *V. globosus*, that disrupted the plankton community (Riebesell et al. (2018)). Even though *V.globosus* has been cultured, strictly as a photoautotroph, in the literature (Chang et al. (2012); Chang (2015)), we hypothesize that mixotrophy is the major form of nutrition for this HAS. The combination of the oligotrophic environment and mixotrophy may be a key factor for the HAS proliferation in these areas and this may lead to a disrupted food-web with low Fc.

5.2 Material and Methods

5.2.1 Experimental design

A 55-day in situ mesocosm experiment was carried out in Gando Bay, on the east coast of Grand Canary Island (Spain), during autumn (October-November 2014). Nine $35m^3$-mesosocosms, with increasing partial pressure CO_2 (pCO_2) treatments ranging from ambient levels to on average 1140μatm, were deployed in order to study the physical, ecological, and biogeochemical responses before, during and after a simulated upwelling event. The detailed description of the study site, experimental design, key events, overall sampling and measurements was reported in Taucher et al. (2017).

5.2.2 Sampling

Seawater was collected every two days during phase I and III and every day during phase II using the depth-integrated water-sampler (IWS, HYDRO-BIOS, Kiel) taking in a total volume of 5L uniformly distributed over the

mesocosms depth (0-13m in every mesocosm, and in the Atlantic as a reference level). An average volume of 60-70L per mesocosms was collected.

The water column plankton community between 0.7 and 50μm was sampled for metabolic assays every four days during phase I and III and every two days during phase II, as an aliquot (2-5L) from the IWS sampling per mesocosms. It was filtered through a 50μm net before passing through a GF/F glass fiber filter (Whatman 0.7μm nominal pore size) until the filter was saturated (always before 1h of filtration). Samples were frozen in liquid nitrogen and stored at -80ºC until their treatment in the laboratory. There, samples were homogenized at 0-4°C in 0.1M phosphate buffer, by a Teflon$^{\circledR}$ 2mL-pestle PYREX$^{\circledR}$ Potter-Elvehjem tissue grinder (homogenizer) at 2600rpm for 2 min. Crude homogenates were centrifuged (0-4°C) at 4000rpm for 10 min.

5.2.3 Nutrients, Chlorophyll *a* (Chl_*a*) and Water-column community composition

The overall data related to the nutrient variability, Chl_*a*, and the water-column community composition (both phytoplankton and microzooplankton) used in the interpretation and discussion of the results of this study were reported by Taucher et al. (2017); Hernández-Hernández et al. (2018) and Algueró-Muñiz et al. (2019).

Chl_*a* in the IWS was measured from HPLC analyses. Subsamples were homogenated in acetone using glass beads in a cell mill. They were centrifuged at 5200rpm for 10min at 4ºC. The supernadant was filtered (0.2μm PTFE filters, VWR International) and used to determine the phytoplankton pigment concentration in a Thermo Scientific HPLC Ultimate 3000 with an Eclipse XDB-C8 3.5 u 4.6 x 150 column. CHEMTAX software (Mackey et al. (1996)) was used to classify phytoplankton on the base of taxon-specific pigment ratios. Every 8 days, subsamples from the IWS were used to determine the microzooplankton abundances. Samples were immediately fixed with acidic Lugol (1-2%) solution and stored in the dark in 250mL brown glass bottles. To identify and count the microzooplankton, the Utermöhl (1931) technique was applied using an inverted microscope (Axiovert 25, Carl Zeiss) (Algueró-Muñiz et al. (2019)).

5.2.4 Potential respiration

Potential respiration (Φ) was determined from ETS activity (Packard and Williams (1981); Packard and Christensen (2004)) incorporating the modifications described in Kenner and Ahmed (1975) and Gómez et al. (1996). The original assay (Packard (1971)) is descended from a classical succinate-INT reductase assay (Nachlas et al. (1960)) in which the maximum velocity

is assured by saturating the reaction with the reactants. The ETS measurements were made on the centrifuged supernadant from the metabolic assay samples (see section 5.2.2).

The absorbance increase of the INT-formazan at 490nm was continuously monitored spectrophotometrically at 18°C in 1cm path-length cuvettes for 8min. The regression line of absorption versus time was used to calculate the ETS activity and potential respiration rates (Φ) after Packard and Christensen (2004). The tetrazolium salt, INT (p-Iodonitrotetrazolium Violet, Sigma #I8377) was reduced by the respiratory ETS enzymes, replacing O_2 as the electron acceptor (Lester and Smith (1961); Smith and McFeters (1997)). INT accepts two electrons whereas O_2 would accept four. Thus, the INT-formazan production rate ($\delta INT/\delta t$) is stoichiometrically related by a factor of 2 to ETS activity ($\delta e^-/\delta t$) and by a factor of 0.5 to Φ. In other words, $\delta e^-/\delta t = 2 \cdot \delta INT/\delta t$ and $\Phi = 0.5 \cdot \delta INT/\delta t$ were Φ is in units of μmol O_2, if INT is in μmols. Blanks were run without the ETS substrates in order to subtract the contribution of the background non-enzymatic and enzymatic reduction of the INT (Maldonado et al. (2012)). Φ was reported in μmol O_2 min^{-1}(mL of homogenate)$^{-1}$ units. To convert to μLO_2 min^{-1}(mL of homogenate)$^{-1}$, multiply by 22.4 μL μmol^{-1}.

5.2.5 Biomass and Net Productivity

Biomass content (B) was determined from samples kept for enzyme activities by the protein method of Lowry et al. (1951) modified by Rutter (1967) using bovine serum albumin (BSA) as the standard. Biomass was reported in mg of protein L^{-1}.

Net productivity[1] (P_N) was determined by calculating the first derivative of the B time-series. Thus, $P_N = \delta B^-/\delta t$. Positive values reflected a net protein formation (formation processes exceeded the combination of "losses" caused by remineralization, grazing, and sinking). On the other hand, negative values of P_N indicated a net loss of proteinaceous biomass.

5.2.6 Data Analysis and Statistics

The Mann-Whitney test was used to compare Φ, B and Chl_a distributions between the different mesocosmos (Hollander et al. (2013)).

Integrative analysis per phase and mesocosm was applied to the area below the data curves by trapezoidal integration using the trapz function of the pracma R-Cran package (Borchers (2017)).

---

[1] We use the term "productivity" instead of "production" because the temporal scale of these data are lower than a year. If these results were extrapolated to higher scales, we should express the results in terms of "Net production"

CHAPTER 5. Chapter 5: Metabolic responses of subtropical North Atlantic
microplankton after a simulated deep-water upwelling event.

86

5.3 Results

5.3.1 Responses to CO_2-treatments under low-nutrient conditions.

During the oligotrophic phase, all the mesocosms behaved in the same way.
The Φ/Chl_a ratio reflected a mesocosm shift towards a weaker photoautotroph community inside the mesocosms. Whereas average values between
2.0 and 4.7 $\mu LO_2 h^{-1} \mu g$ Chl_a^{-1} were obtained in the Atlantic samples,
mesocosms resulted in higher values, ranging between 3.4 and 8 $\mu LO_2 h^{-1} \mu g$
Chl_a^{-1} (Fig.5.1, I).
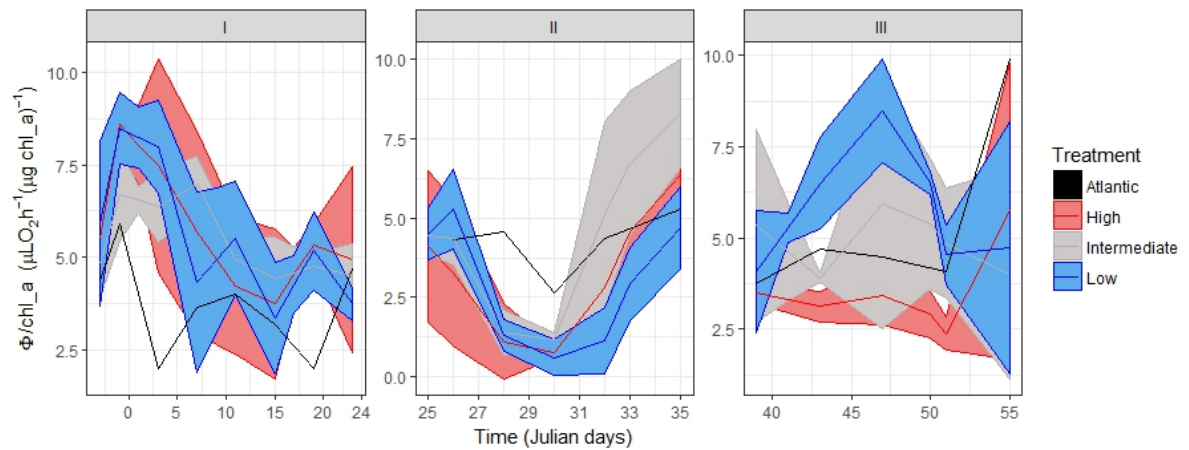
Figure 5.1: Potential respiration per Chl_a during Phase I: Oligotrophic phase;
Phase II: Bloom phase after deep-water addition; and Phase III: Post-bloom phase
after nutrient-depletion.

According to Hernández-Hernández et al. (2018) the phytoplankton community evolved from a cyanobacteria-dominated community to a mixed one in
all the mesocosms: diatoms, prymnesiophytes, crypsophytes and cyanobacteria. Besides, microplankton (mainly aloricate ciliates and dinoflagellates)
remained in low concentrations (Algueró-Muñiz et al. (2019)). Nanoplankton dominated the biomass (50%) but not the Chl_a (30%) (Hernández-Hernández et al. (2018)), which led to a more heterotrophic community.

Throughout the entire phase, P_N remained around 0 mg of proteins $L^{-1} d^{-1}$
until the last two days. Then, the community was fuelled by a natural nutrient
addition from a Sahara-dust deposit event ("Calima") (Fig.5.2, I). Considering the integral analysis of the mesocosms' biomass and metabolic capacity
($\int_{t=0}^{t=23} Chl\_a, \int_{t=0}^{t=23} B, \int_{t=0}^{t=23} \Phi$), no significant CO_2-related effects were observed during this phase (Fig.5.3, I).
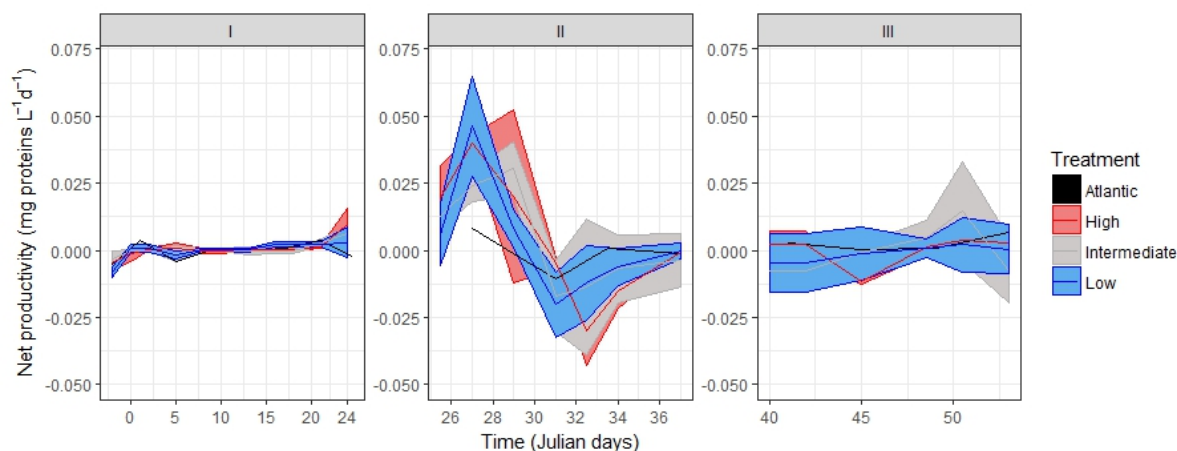
Figure 5.2: P$_N$ of the microplankton community, as the first derivative of biomass, during Phase I: Oligotrophic phase; Phase II: Bloom phase after deep-water addition; and Phase III: Post-bloom phase after nutrient-depletion. Note that negative values reflects the net loss of biomass, when the combination of sinking, remineralization and grazing outnumbers the biomass production by both autotrophs and heterotrophs

5.3.2 Responses during the deep-water addition event.

The deep-water addition on T24 (Day 24) resulted on a phytoplankton bloom between T28 (Day 28) and T30 (Day 30) in all the mesocosms (Taucher et al. (2017); Hernández-Hernández et al. (2018); Taucher et al. (2018)). During the bloom, the average Φ/Chl_a ratio drop to the lowest values in the whole experiment ($<1.7\mu LO_2 h^{-1}\mu g$ Chl_a^{-1} in all the mesocosms) due to the photoautotroph-dominated community. The lowest average values occurred during the diatom bloom in T30, ranging from 0.6 to $1.2\mu LO_2 h^{-1}\mu g$ Chl_a^{-1} among the mesocosms (Fig.5.1, II).

Even though all the mesocosms behaved in a similar way during the bloom, afterwards, until nutrient depletion, the plankton communities evolved differently. The integral analysis of Chl_a, Φ and B (as protein) in Phase II ($\int_{t=25}^{t=37}\Phi, \int_{t=25}^{t=37}Chl\_a, \int_{t=25}^{t=37}B$) in the communities dominated by the microphytoplankton, showed a positive trend with increasing pCO$_2$ levels (Fig.5.3, II). However only the relationship between Φ and pCO$_2$ was found to be clearly positive, being particularly strong after extracting the data of M2 and M8, the most acidified mesocosms. Both M2 and M8 developed a harmful algal species (HAS), *Vicicitus globosus* at the end of Phase II that disrupted the community. These two mesocosms reached the lowest micro- and mesozooplankton levels observed during the entire whole experiment (Riebesell et al. (2018); Algueró-Muñiz et al. (2019)) because zooplankton was outcompeted by the presence of *V. globosus* (Riebesell et al. (2018)).

In contrast, microzooplankton, dominated by dinoflagellates, proliferated in
the intermediated mesocosms (M3,M4 and M7) at the end of hase II, where
the HAS did not grow (Algueró-Muñiz et al. (2019)).

Surprisingly, even though the microzooplankton did not develop in meso-
cosms M2 and M8, Φ reached as high values in M2 and M8 ($5.3\pm0.7\mu LO_2h^{-1}L^{-1}$)
at the end of Phase II as in mesocosms M3, M4 and M7 ($4.7\pm1.1\mu LO_2h^{-1}L^{-1}$),
where microzooplankton bloomed (Fig.5.3, II; Appendix D).

P_N was maximum between one and two days before the Chl_a peak in all
the mesocosms (0.039 ± 0.013 mg proteins $L^{-1}d^{-1}$) (Fig.5.2,II). On the other
hand, during the 24h after the peak (Fig.5.2), the combination of remineral-
ization, grazing, and sinking processes resulted in an average biomass net-
loss of -0.023 ± 0.008 mg proteins $L^{-1}d^{-1}$. Note that, if Primary Produc-
tivity[2] (PP) data were available, we could combine both measurements (ex-
pressed in terms of mgC $L-1d-1$) in order to calculate the Biomass Loss
(BL) in the system (P_N=PP-BL).
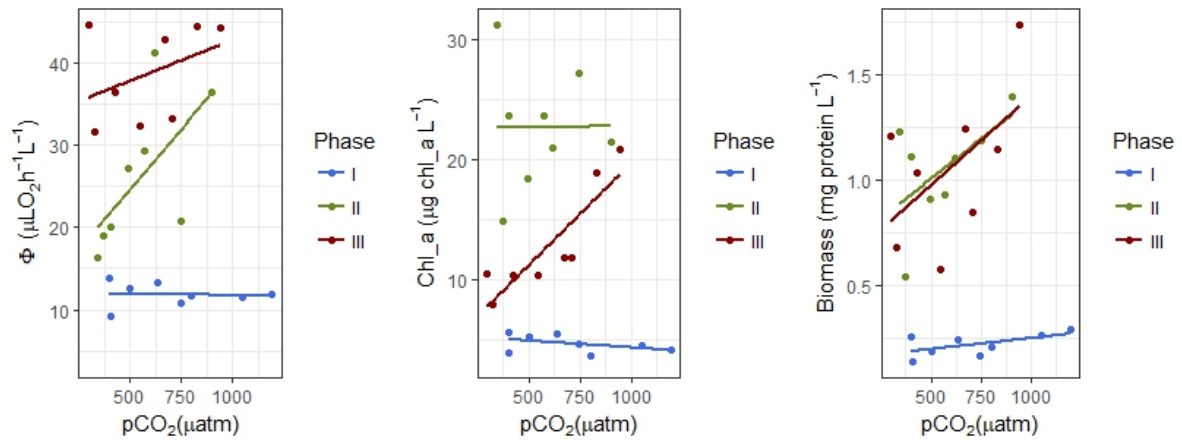
Figure 5.3: Integral analysis of Potential respiration, Chl_a and Biomass by phase
of experiment and treatment. Note that every point symbolizes the integral of each
parameter by the related phase in the mesocosm with the CO_2-treatment reflected
in the x-axis. Blue colour represents Phase I, green represents Phase II, and Phase
III is represented in red.

---

[2]We use the term "productivity" instead of "production" because the temporal scale of these data
are lower than a year. If these results were extrapolated to higher scales, we should express the results
in terms of "Primary production"

5.3.3 Responses to the CO_2-treatments during the nutrient depletion phase.

After the nutrient depletion, the communities differed among the treatments. The Φ/Chl_a ratio resulted in maximum values when the microzooplankton, dominated by dinoflagellates, peaked in both low pCO_2 (M1, M5 and M9) and intermediate pCO_2 mesocosms (M3, M4 and M7) (Fig.5.1, III; Algueṙ-Muñiz et al. (2019)). Here, values rose sharply up to 10 $\mu LO_2 h^{-1} \mu g$ Chl_a^{-1}. In addition, as we have seen before, in M2 and M8, high pCO_2 levels fuelled the Chrysophyceae community dominated by *V. globosus* (Taucher et al. (2018); Riebesell et al. (2018)). This HAS had a significantly negative effect on the dinoflagellates but not on the diatoms. They had a longer retention time in biomass, probably due to the lack of grazing (Taucher et al. (2018)). The Φ/Chl_a ratio ($4.1\pm1.5 \mu LO_2 h^{-1} \mu g$ Chl_a^{-1} [3]) remained between 2.5 and $7 \mu LO_2 h^{-1} \mu g$ Chl_a^{-1}, reflecting a weaker heterotrophic community. However, although these values are lower than those related to dinoflagellate-dominated communities, they are not as low as expected for a photoautotroph dominated community ($<1.7 \mu LO_2 h^{-1} \mu g$ Chl_a^{-1} during the phytoplankton bloom in Phase II). The values ($4.1\pm1.5 \mu LO_2 h^{-1} \mu g$ Chl_a^{-1}) are closer to those of the mixed community from the surrounded Atlantic water ($4.3\pm1.73 \mu LO_2 h^{-1} \mu g$ Chl_a^{-1}), or the former community in Phase I from all the mesocosms (between 3.4 and $8 \mu LO_2 h^{-1} \mu g$ Chl_a^{-1}).

Besides, changes in the communities did not impact P_N during the Post-Bloom phase. Although it was more variable than in Phase I, P_N trends were to stay close to the minimum in all the mesocosms (Fig.5.2, III). This suggests that, after the bloom and the nutrient depletion, the community tended to reach a steady state close to the one in Phase I.

Finally, the integral analysis in B and Φ ($\int_{t=39}^{t=55} B, \int_{t=39}^{t=55} \Phi$) did not find a significant relationship with pCO_2 (Fig.5.3, III), particularly after extracting the M2 and M8 data linked to the HAS-disrupted community. The integral analysis in Chl_a ($\int_{t=39}^{t=55} Chl\_a$) illustrated a clearly positive relationship with pCO_2 during this phase. However, this result is linked to the disrupted communities by the *V. globosus* presence in M2 and M8. Once these data were extracted, just a slightly positive pCO_2 effect on phytoplankton biomass was found.

---

[3] Averaged value from Day 35 (T35, nutrient depletion (Taucher et al. (2017)) to Day 47 (T47, the *V. globosus* community dropped (Riebesell et al. (2018))

5.4 Discussion

5.4.1 The use of the Φ/Chl_a ratio as an index of autotrophic, mixotrophic or heterotrophic dominance in the microplankton community.

The electron transport system (ETS) is an ubiquitous catabolic pathway used to generate energy in all cells, in the form of adenosine triphosphate (ATP). Even though the autotrophs use other pathways to obtain energy from inorganic resources or light throughout anabolic pathways, they also use this type of catabolism when those energy resources are limited. Thus, we have considered the ETS as a proxy for the catabolic metabolism in plankton communities. In contrast, the anabolic pathway of photosynthesis relays on the Chl_a to capture solar energy. As photoautotrophs are the dominant autotrophs in the euphotic zone, where this experiment was carried out, we used Chl_a as a proxy of the anabolic metabolism in this community. Here, we had the chance to follow the Φ/Chl_a relationship through the community changes related to the simulated deep-water upwelling and the subsequent diatom bloom and nutrient depletion that occurred in all the mesocosms.

The Atlantic water microplankton community is composed of *Prochlorococcus* and *Synechococcus*-type cyanobacteria, picoeukaryotes, nanoeukaryotes, diatoms (Hernández-Hernández et al. (2018); Taucher et al. (2018)), ciliates (aloricate and loricate) and dinoflagellates (athecate and thecate) (Algueró-Muñiz et al. (2019)). The reference Φ/Chl_a ratio from the mixed Atlantic waters community varied around $4.3 \pm 1.7 \mu LO_2h^{-1} \mu g \, Chl\_a^{-1}$ throughout the 55 days experiment. However, this ratio was higher in all 9 mesocosms ($5.6 \pm 2 \mu LO_2h^{-1} \mu g \, Chl\_a^{-1}$) from the very beginning of the experiment. This mesocosm-enhanced effect was related to the shift in the microplankton towards a more heterotrophic dinoflagellate community. These Φ/Chl_a results in a mixed community were consistent with those obtained from the Φ and Chl_a measurements found in the literature when the ETS activities were to converted to ETS activity as it is currently measured (Christensen and Packard (1979)). The upwelled waters of Baja California were characterized by a Φ/Chl_a ratio of $3.28 \mu LO_2h^{-1} \mu g \, Chl\_a^{-1}$ (Packard et al. (1974)). The upwelled waters off Northwest African were characterized by a Φ/Chl_a ratio of $2.5\text{-}4.1 \mu LO_2h^{-1} \mu g \, Chl\_a^{-1}$ (Packard (1979))).

In the mesocosms, this ratio also reflected the shift towards a phytoplankton bloom between T28 (Day 28) and T30 (Day 30), dropping to values lower than $1.7 \, \mu LO_2h^{-1} \mu g \, Chl\_a^{-1}$ in all the mesocosms ($1.1 \pm 0.6 \mu LO_2h^{-1} \mu g \, Chl\_a^{-1}$). These results were consistent with those reported at the Chl_a maximum of the Western Mediterranean Sea ($0.3 \mu LO_2h^{-1} \mu g \, Chl\_a^{-1}$ (Martinez et al. (1990))) and in the Barents Sea ($0.7 \mu LO_2h^{-1} \mu g \, Chl\_a^{-1}$ (Mar-

tinez (1991))). They are slightly higher than those for the euphotic-zone community in eutrophic waters of the Taiwan Strait (0.02-1.6 $\mu LO_2 h^{-1} \mu g$ Chl_a^{-1} (Bangqin et al. (2005))) and those in the Gulf of Maine (0.5-0.9 $\mu LO_2 h^{-1} \mu g$ Chl_a^{-1} (Packard and Williams (1981))). They are also similar to those from different bloom conditions (0.3-1.9$\mu LO_2 h^{-1} \mu g$ Chl_a^{-1}) in the phytoplankton from the Nova Scotian shelf (Packard et al. (2000)). From this evidence, we can consider that Φ/Chl_a ratios lower than 2.5 $\mu LO_2 h^{-1} \mu g$ Chl_a^{-1} to reflect a mainly photoautotrophic microplankton community.

In the plankton community of our mesocosms, during the nutrient depletion and the post-bloom phases, there was great variability in the community development and in the evolution of the Φ/Chl_a ratio. However, similar Φ/Chl_a ratios were found in those mesocosms where the microzooplankton bloomed (M3, M4, M7, the intermediate-pCO$_2$ mesocosms; and M1, M5 and M9, the low-pCO$_2$ mesocosms). First, the microzooplankton, dominated by small thecate and large athecate dinoflagellates (Algueró-Muñiz et al. (2019)), bloomed in the intermediate mesocosms at the end of Phase II (T32 (Day 32) and T35 (Day 35) in M3 and M4, and during T35 (Day 35) and T37 (Day 37) in M7), when values of 7.6±1.5$\mu LO_2 h^{-1} \mu g$ Chl_a^{-1} were attained. This dinoflagellate community also bloomed in the weakly acidified mesocosms during Phase III (T43 (Day 43) and T47 (Day 47) in M1, M5 and M9), when Φ/Chl_a ratio was high (7.5±1.6$\mu LO_2 h^{-1} \mu g$ Chl_a^{-1}). From the benchmark, we consider that Φ/Chl_a ratios higher than 7$\mu LO_2 h^{-1} \mu g$ Chl_a^{-1} reflected dominance of a heterotrophic microplankton community.

Lower Φ/Chl_a ratios of around 4.1±1.5$\mu LO_2 h^{-1} \mu g$ Chl_a^{-1} were found in the high-pCO$_2$ mesocoms (M2 and M8) at the end of Phase II and during the main part of Phase III. At that time, the presence of *V. globosus* disrupted the community. However, even though the microzooplankton did not proliferate, and the Chl_a retention time was higher in these mesocosms, the Φ/Chl_a ratio was not as low as expected for a photoautotroph-dominated community. Indeed, it reflected a mixed community (or a mixotroph-dominated one), closer to the reference values in the Atlantic surrounded waters (4.3±1.7 $\mu LO_2 h^{-1} \mu g$ Chl_a^{-1}). Note that, during the last days of the experiment, the aloricate ciliates bloomed in M2. This made the Φ/Chl_a ratio soar up to 8.6$\mu LO_2 h^{-1} \mu g$ Chl_a^{-1}, indicating a heterotroph-dominated community.

5.4.2 Acidification, mixotrophy and the development of *Vicicitus globosus*

As said before, one of the main effects of acidication in the high pCO$_2$ mesocosms (M2 and M8) was the proliferation of *V. globosus*. This was clear after nutrient depletion until T47 (Day 47). In the literature, this HAS has been

assessed and cultured as a pure autotrophic organism. However, if *V. globosus* is considered a pure autotroph HAS, that negatively impacts microzooplankton, a low Φ/Chl_*a* would be expected (<2.5 μLO$_2$h^{-1}μg Chl_*a*$^{-1}$). However, this was not observed. During nutrient depletion until the disappearance of *V. globosus*, higher Φ/Chl_*a* were noted ($4.1\pm1.5\mu$LO$_2$h^{-1}μg Chl_*a*$^{-1}$). These values are similar to those attained in the mixed oligotrophic community of the surrounded Atlantic waters (4.3 ± 1.7 μLO$_2$h^{-1}μg Chl_*a*$^{-1}$), suggesting that the community in M2 and M8 is a mixed or a mixotroph-dominated one. As said in the introduction, in the oligotrophic waters, mixotrophy is particularly advantageous, as organisms find the potentially limiting nutrient much more concentrated in the prey than in the water column (Sanders (1991)). So, could *V. globosus* be a mixotroph?

First of all, *V. globosus* was able to maintain its population during nutrient depletion, when other pure autotrophs, such as diatoms, dropped to their minimum because of nutrient deficiency. In contrast, *V. globosus* was able to maintain its population for at least 12 more days. This Dycthyochales is the only one of its class that lacks pyrenoids. In addition, its haploid form has less pigment than other Dycthyochales (Chang et al. (2012)). The pyrenoid is a sub-cellular body used in photoautotrophs to optimize the performance of RuBisCo by concentrating CO_2 in the chloroplast (Badger et al. (1998)). When pyrenoids are absent, RuBisCo is forced to work barely at a quarter of its maximum velocity because of normally low environmental CO_2 concentrations. In comparison with other phytoplankton species, *V. globosus* has an inefficient photosynthetic system under ambient pCO_2. To survive these normal conditions, it has developed heterotrophic pathways to obtain a variety of organic compounds and energetic molecules to supplement its retarded photosynthesis. In addition, when pCO_2 levels rise, *V. globosus*´s photosynthetic system would be less inefficient, facilitating its proliferation and outcompeting other phytoplankton species. This is our hypothesis why *V. globosus* had a positive relationship with increasing pCO_2 levels.

Furthermore, *V. globosus* is a shape-shifter. It is able to change from a flagellated-shape to an amoeboid-shape and back in minutes. As it was considered an autotroph, this shape-shifting was reported in relation to the reproduction pathways (Chang et al. (2012)). However, we suggest that one of the *V. globosus*' nutritive pathways may be bacterivory. In addition, *V. globosus* has a cytotoxic effect on the membranes of both diatoms and microzooplankton (Chang (2015)). It destroys the cells and releases dissolved organic matter to the seawater. For the bacterial community, this DOC excretion may impact positively on the bacterial community. Consequently, *V. globosus* could feed on bacteria and maintain its community even under low-nutrients conditions.

To sum up, *V. globosus* is more a mixotroph than a photoautotroph. This is suggested from the Φ/Chl_*a* results in the *V. globosus*-disrupted commu-

nities, considering *V. globosus*'s normally inefficient photosynthetic system and its shape-shifting ability.

5.5 Conclusion

We used the Φ/Chl_a ratio to monitor the metabolic changes in the microplankton community during the effects of a simulated upwelling of enriched deep-water. Where its range fell indicated three different conditions.

- For Φ/Chl_a values between 0 and 2.5 μLO$_2$h^{-1} μg Chl_a^{-1}, the plankton community was dominated by photoautotrophs. The lowest ratios (<1.7μLO$_2$h^{-1} μg Chl_a^{-1}) were attained during the phytoplankton bloom. These values had also been reported in the open ocean at the depths of the Ch_a maximum, or in the euphotic zone of highly eutrophic regions.

- For Φ/Chl_a values between 2.5 and 7.5 μLO$_2$h^{-1} μg Chl_a^{-1}, the plankton community appeared mixed or was a community where mixotrophs dominated.

- For Φ/Chl_a values higher than 7.5 μLO$_2$h^{-1} μg Chl_a^{-1}, the plankton community indicated microzooplankton proliferation. When heterotrophic dinoflagellates dominated de community, Φ/Chl_a soared to 10μLO$_2$h^{-1} μg Chl_a^{-1}.

In addition, ro strengthen our analysis of the KOSMOS timecourses, we measured the Leibnizian first-derivative of the biomass per time P$_N$. This derivative advanced the quantification and monitoring of the plankton dynamics when ^{14}C fixation and biomass loss measurements were not available. During the oligotrophic phase, P$_N$ was minimum. However, in the bloom phase, between 24-48h before the Chl_a-peak, P$_N$ reached a maximum. During the post-bloom phase, P$_N$ tended towards minimum values similar to those in the original oligotrophic phase. When P$_N$ negative values were observed, they facilitated the calculation of biomass-loss processes in the ecosystem. The highest net loss of biomass in the mesocosms occurred during the 24h after the Chl_a-peak.

In contrast, the Newtonian integral analysis of Chl_a, Φ, and B, for the different phases and mesocosms, allowed the assessment of the accumulated acidification effects on the community. A clearly positive relationship was found between Φ and pCO$_2$ during the bloom phase. This correlation was stronger when HAS were absent. On the contrary, HAS presence led to a positive relationship between Chl_a and pCO$_2$ during the post-bloom phase. Apart from the reduction of grazing on the phytoplankton community due to the presence of *V.globosus*, we suggest that *V.globosus*' photosynthetic system, whose lack of pyrenoid made it inefficient in low pCO$_2$ environments,

CHAPTER 5. Chapter 5: Metabolic responses of subtropical North Atlantic
microplankton after a simulated deep-water upwelling event.

94

was stimulated in the high pCO$_2$ mesocosms, leading to acidification´s positive impact on Chl_a.

Finally, the Φ/Chl_a results in the communities were *V. globosus* bloomed; *V.globosus*' inefficient photosynthetic system and its shape-changing ability suggest that it is a mixotroph more than a photoautotroph.

To sum up, the development of Φ/Chl_a ratios with the use of Liebnizian differential and Newtonian integral analysis advances our knowledge and understanding of the plankton community dynamics at both the ecosystem and the species scale.

Chapter 6

Chapter 6: Conclusions

*The pursuit of curiosity about the
basic facts of nature has proven, with
few exceptions throughout the history
of medical science, to be the route by
which the successful drugs and
devices of modern medicine were
discovered.*

Arthur Kornberg

6.1 Developing the assay for NADP-IDH activity as a tool to detect CO_2 production in cells

An enzyme assay for isocitrate dehydrogenase (NADP-IDH) in zooplankton and microplankton, based on the reduction of $NADP^+$, was developed. The rates of NADPH formation (μmol NADPH min^{-1} mL^{-1}) were obtained kinetically at 340nm. Activities in μmol of NADPH were based on a molar extinction coefficient (ε) of 5.42 mL μmol^{-1}cm^{-1}. In our hands, the maximum NADP-IDH activity (V_{max}) in marine plankton samples was attained in 0.1M phosphate buffer at pH 8.2 (pKa_1=7.6 and pKa_2=8.8), by adding 6mM $MgCl_2$, 0.3mM $NADP^+$ and 2mM DL-trisodium isocitrate.

The apparent Michaelis-Menten *Km* values for the substrates in crude homogenates at pH 8.5 and 18ºC were 271$\pm$63 μM for isocitrate and 18$\pm$3 μM for $NADP^+$. Arrhenius plots for NADP-IDH in mesozooplankton samples and porcine heart yielded similar Energies of activation, 20.4 Kcal mol^{-1} and 21.4 Kcal mol^{-1}, respectively. Thus, although there seems to be an adaptation to homoeothermic conditions allowing high activity at higher temperatures, a common basic structure seems to have been maintained even after millions of years of evolution.

6.2   The assessment of mesozooplankton potential CO_2 production from NADP-IDH measurements.

Considering all the CO_2-producing enzymes and normalising their activities by NADP-IDH activity, the potential CO_2 production (Ψ_{NADP}, in μmol CO_2 h^{-1} mg of protein^{-1}) was calculated as 2.94·NADP-IDH in microplankton and mesozooplankton samples. Without considering biosynthesis, the ratio between the purely respiratory CO_2 production (Respiratory Ψ_{NADP}) and the potential O_2 consumption is 1.47, indicating that the enzymatic pathways related to the organic carbon oxidation phase of cellular respiration is prepared to exceed the requirements of the ETS. This may serve as an advantage when, eventually, the organism has a high energy requirement. Once this requirement is met, NAD(P)H excess may be redirected to biosynthesis by the IDH substrate cycle of Sazanov and Jackson.

From our calculations, Ψ_{NADP} always exceeded the physiological R_{CO2} rate. This is in harmony with theory because the physiological rate should not exceed the potential. We predict that, from our measurements in the North Eastern Subtropical Atlantic, the R_{CO2}/Ψ_{NADP} ratios for open ocean mesozooplankton samples will fall between 0.3 and 0.4, whereas the ratios for a mixed microplankton community will fall between 0.2 and 0.3. However, we recommend the use of physiological R_{CO2}, if available, to develop accurate R_{CO2}/Ψ_{NADP} ratios for every region, experiment or case.

6.3   The assessment of the relationship between R_{CO2} and NADP-IDH activity

CO_2 production rates (R_{CO2}) were measured in *Leptomysis lingvura* to compare with the potential CO_2 production rates, proxied here for the first time by the NADP$^+$-dependent isocitrate dehydrogenase activity (NADP-IDH).

Nutrition prior to sampling, has a significant impact on the respiratory enzymatic activity of *L. lingvura*. Although higher activities normalised per biomass were found in bloom communities than in post-bloom communities, an average R_{CO2}/NADP-IDH ratio of 0.12 was obtained on well-fed mysids from both communities. This result was only slightly higher in nutrient-limited mysids (0.16). This value well characterizes the physiological response of *L. lingvura*.

Sex differences did not significantly alter enzymatic activities nor the ratios of respiratory physiology to enzyme activity. Starvation for longer than 12h decreased the R_{O2}/Φ ratios, whereas it increased the R_{CO2}/NADP-IDH ratios, leading to higher RQs. Our interpretation is that energy production is diminished whereas lipid synthesis and anti-oxidation are strengthened.

Incubation of mysids longer than 12h mixes starvation and circadian effects.
We recommend incubations between 4 and 6 hours in future ecophysiological studies. This will reduce the circadian influences.

6.4 Assessing variations in the microplankton autotrophy-heterotrophy ratio using enzyme analysis

We used the Φ/Chl_a ratio to monitor the metabolic changes in the microplankton community during the effects of a simulated upwelling of enriched deep-water.

- Values between 0 and 2.5 $\mu LO_2 h^{-1}$ μg Chl_a^{-1} were attained when the community was dominated by photoautotrophs. The lowest results (<1.7) were reached during the phytoplankton bloom. These values had also been reported at the depths of the Ch_a maximum in the ocean, or at the euphotic zone in highly eutrophic regions.
- Values between 2.5 and 7 $\mu LO_2 h^{-1}$ μg Chl_a^{-1} represented a mixed community (or a community where mixotrophs were dominant).
- Values higher than 7 were related to the microzooplankton proliferation. When heterotrophic dinoflagellates were dominant in the community, Φ/Chl_a soared up to $10 \mu LO_2 h^{-1}$ μg Chl_a^{-1}.

Net productivity (P_N) measurements as the biomass first derivative per time strengthened the quantification and the monitoring of this process when ^{14}C fixation measurements were not available. Negative values allowed the quantification of the biomass-loss processes in the ecosystem.

The integral analysis per time and mesocosms of Chl_a, Φ and B allowed the assessment of the acidification effects on the community during the oligotrophic, bloom and post-bloom phases. A significant positive relationship was found between Φ and pCO$_2$ during the bloom phase. In addition, a positive relationship between Chl_a and pCO$_2$ during the post-bloom phase was also found.

During the post-bloom phase of the experiment, a harmful algal species (HAS, *Vicicitus globosus*) proliferated in the most acidified mesocosms. From the Φ/Chl_a results in these communities (similar to those related to a mixed one); an inefficient photosynthetic system at current pCO$_2$ levels (it lacks pyrenoid); and the ability to quickly change from a flagellate-shaped microorganism to an amoeboid-shaped one, we suggest that *V. globosus* is a mixotroph more than a photoautotroph.

To sum up, the development of Φ/Chl_a ratios strengthens the knowledge of the community metabolic state, not only from an ecosystem scale, but also from a species scale.

Chapter 7

Chapter 7: Future research.

*One never notices what has been done;
one can only see what remains to be done.*
Marie Curie

– Independent measurements of cytosolic and mitochondrial NADP-IDH may improve our knowledge about IDH's role in lipid-synthesis and in the cell's ROS scavenging capacity.

– Other CO_2-producing enzymes in plankton should be investigated in order to elucidate the relationships among their activities, activators and inhibitors and to accurately model the total potential plankton CO_2 production.

– Further research, on the relationship between R_{CO2} and NADP-IDH, on how different environmental factors (such as age, pO_2, T, circadian rhythm, etc.) impact this relationship, and on the in-cell substrates availability, is still needed.

– New models based on measurements of NADP-IDH, isocitrate and $NADP^+$ to predict R_{CO2} should be developed and tested with R_{CO2} measurements from plankton incubations.

– Vertical R_{CO2} profiles based on NADP-IDH measurements throughout the water column should be made in order to calculate and appraise F_C. In other words, the calculations should be compared with other F_C measurements (i.e. F_C from sediment traps), noting that different time scales must be considered during this comparison.

– In order to develop an average R_{CO2}/NADP-IDH ratio (or linear regression) to be used over a large-scale, further R_{CO2} and NADP-IDH measurements should be widely made on oceanographic campaigns. Over shorter scales, different measurements should be made under oligotrophic and eutrophic conditions in different regions and in different seasons.

99

– Measurements of heterotrophic metabolism (both Φ and/or NADP-IDH) should be made during oceanographic campaigns on a regular basis in order to promote comparison with autotroph proxies (i.e. Chl_a) and to assess the community metabolic state and its relationship with environmental factors.

Chapter 8

Chapter 8: Resumen en español.

Los "midiclorianos" son criaturas microscópicas que se encuentran dentro de todos los seres vivos en simbiosis. Sin "midiclorianos" la vida no podría existir y no conoceríamos la Fuerza. Cuanto más nivel de "midiclorianos" tenga un ser vivo, más aptitud tiene para usar la Fuerza.
Star Wars Episodio I. George Lucas. Estraído, en referencia a las mitocondrias, del libro "Power,Sex, Suicide" de Nick Lane.

8.1 Introducción

Debido a las emisiones por la combustión de fuentes de energía fósiles, los niveles de CO_2 atmosféricos han aumentado exponencialmente en los últimos 250 años (Doney and Schimel (2007)). El océano puede considerarse un sumidero de este CO_2, ya que su concentración aquí es menor que en la atmósfera, y posee una comunidad de organismos autótrofos que fijan CO_2 para producir materia orgánica (producción primaria). Sin embargo, en la columna de agua, esta nueva materia orgánica en forma de carbono orgánico particulado (POC) es consumida por organismos heterótrofos tanto para crecer como para generar energía por medio de la respiración. De este modo, parte del CO_2 previamente fijado, vuelve al océano. Dependiendo de las tasas de respiración en la columna de agua y su magnitud frente a las de producción primaria, esta producción de CO_2 puede reducir el flujo de CO_2

atmósfera-océano hasta quedar en equilibrio, o incluso ser una fuente de CO_2 en algunas regiones. Por ello, para estimar adecuadamente el papel del océano en este balance, es necesario conocer tanto las tasas de producción primaria como las de respiración.

Desde un punto de vista oceanográfico, la producción primaria y la función de los organismos fotosintéticos en las capas más superficiales del océano ha sido ampliamente estudiada. Por el contrario, la respiración fue durante muchos años derivada de estas tasas de producción primaria. Desde los años 30, la realización de largos periodos de incubación ha permitido la medición directa y el seguimiento de las tasas de consumo de O_2 de organismos vivos (R_{O2}) (Waksman and Carey (1935); Johnson (1936)). Sin embargo, estas técnicas requieren mucho tiempo de incubación, con lo que la tasa de obtención de datos es muy baja para los estudios oceanográficos. Asimismo, requieren que los organismos se encuentren en buen estado fisiológico. Esto no siempre es viable, especialmente en el estudio de aguas profundas donde suelen quedar gravemente dañados durante el muestreo. Además, el propio proceso de incubación hace que los organismos puedan sufrir durante la manipulación de las muestras o que, dentro de las botellas, puedan encontrarse en densidades de población superiores a las existentes en el medio natural (Fernández-Urruzola et al. (2011); Bondyale-Juez et al. (2017)). Por ello, a partir de los años 70 se desarrollaron técnicas basadas en la medición de la actividad de las enzimas responsables de esa respuesta fisiológica: las enzimas del sistema de transporte de electrones (ETS) (Packard (1971)). Estas medidas aportan información sobre la capacidad máxima de consumo de O_2 de los organismos (Φ) (King and Packard (1975)). La utilización de estas técnicas bioquímicas ha permitido aumentar las tasas de obtención de datos, así como obtener medidas del océano profundo. Debido a que son medidas del estado metabólico del organismo, requieren del análisis de su relación con la respuesta fisiológica real en cada momento (R_{O2}). Durante décadas se ha analizado y observado la variabilidad del ratio R_{O2}/Φ (Hernández-Leon and Gómez (1996); Martínez et al. (2010); Herrera et al. (2011b); Osma et al. (2016a,b)). Los mismos factores ambientales y fisiológicos que influyen sobre R_{O2}, son los responsables de la variabilidad de R_{O2}/Φ (Hernández-Leon and Gómez (1996)). De entre todos, la disponibilidad de nutrientes parece tener un papel fundamental.

Lo cierto es que las enzimas, responsables últimas de la respuesta fisiológica, catabolizan las reacciones en función de la disponibilidad de sus sustratos a nivel celular. Esta idea, transformada en ecuación por Michaelis-Menten, es la base de los modelos cinéticos enzimáticos (Enzymatic Kinetic Model, EKM) (Packard et al. (1996b); Packard and Gómez (2008); Aguiar-González et al. (2012); Osma et al. (2016b)). Su aplicación al ETS, midiendo a su vez la concentración de sus sustratos principales (NADH y NADPH) y su afinidad por ellos (mediante las constantes cinéticas o *Km*) ha permitido el

cálculo del consumo de O_2 de diferentes organismos marinos de la manera más precisa hasta la fecha (Packard and Gómez (2008); Osma et al. (2016b)).

Todos estos avances se han centrado en la respiración desde el punto de vista del consumo de O_2. Sin embargo, para el adecuado estudio de la función del océano en los flujos de carbono, es necesario conocer la producción de CO_2 asociada a la respiración (R_{CO2}). Debido a la dificultad de la medición directa R_{CO2} en la columna de agua, generalmente se han utilizado los denominados Coeficientes Respiratorios (Respiratory Quotient, RQ, moles producidos de CO_2 por mol consumido de O_2) sobre los valores de R_{O2}. Lamentablemente, este coeficiente puede ser muy variable (Berggren et al. (2012); Romero-Kutzner et al. (2015)). Esta variabilidad, sumada a la ya existente en los ratios R_{O2}/Φ, esenciales en el estudio del océano profundo, hace que se requiera una mejora en las técnicas de análisis de R_{CO2}.

Al igual que en el caso del consumo de O_2, R_{CO2} puede ser estudiado a partir de la medición una de las enzimas responsables de la producción de CO_2. Dentro de todas las enzimas implicadas, la Isocitrato Dehidrogenasa (IDH) es la responsable de la producción de la primera molécula de CO_2 dentro del ciclo de Krebs. En base al cofactor que requieren, se pueden clasificar dos isoenzimas: (1) la dependiente de $NADP^+$ (NADP-IDH) y (2) la dependiente de NAD^+ (NAD-IDH) (Kornberg and Pricer (1951); Gálvez and Gadal (1995)). La NADP-IDH se encuentra tanto en procariotas como en eucariotas, está presente en el citosol con funciones relacionadas con la síntesis lipídica (Koh et al. (2004)), y es mucho más estable que la NAD-IDH para su medición (Plaut (1970, 1962)). Además, se encuentra relacionada con la formación de la especie reducida de glutatión, implicada en funciones antioxidantes de la célula (Jo et al. (2001)). Debido a su ubicuidad y a su participación en los distintos procesos catabólicos, hace que estudios en diferentes organismos hayan observado una actividad de NADP-IDH significativamente mayor que la de la NAD-IDH (Colman (1975); Alp et al. (1976); Denton et al. (1978)). Estas características hacen de la NADP-IDH la enzima idónea sobre la que desarrollar un nuevo método para el cálculo de la producción de CO_2 en la columna de agua. Por ello, en los años 90 se llevaron a cabo estudios en bacterias marinas analizando el R_{CO2}/NADP-IDH y desarrollando un EKM específico (Packard et al. (1996a); Roy and Packard (2001)). Sin embargo, no ha sido hasta la presente tesis cuando se ha conseguido adaptar esta metodología a la comunidad planctónica (Tames-Espinosa et al. (2018)) (ver capítulo 2).

Aun siendo una de las enzimas responsables de la producción de CO_2 de la célula, la NADP-IDH no es la única. Otras enzimas relacionadas directa o indirectamente con el ciclo de Krebs (como la piruvato deshidrogenasa (PDH), la alfa-ketogluratato deshidrogenasa (KGDH), la enzima málica (ME) o la fosfoenolpiruvato carboxiquinasa (PEPCK)) también producen CO_2 en diferentes proporciones cada vez que se activa el ciclo. Asimismo,

otras enzimas relacionadas con el crecimiento o la síntesis de lípidos y ácidos grasos también colaboran en el aumento de la producción de CO_2 en momentos puntuales del desarrollo de los organismos. Debido a ello, parte de la presente tesis se ha centrado en la relación entre la NADP-IDH y la producción total de CO_2 en base a los estudios existente hasta la fecha (ver capítulo 3).

En conclusión, este estudio se centra en el desarrollo y aplicación de un nuevo método enzimático para el análisis de la producción potencial de CO_2 asociada a la comunidad planctónica. Para ello, se han definido los siguientes objetivos:

- Objetivo 1: La medición de la máxima actividad de una de las enzimas principales en la producción de CO_2 en la comunidad planctónica: la NADP-IDH. Partiendo de la metodología existente, aplicada a otros organismos, se ha optimizado la misma adaptándola al micro y meso-zooplancton (ver capítulo 2).

- Objetivo 2: Modelización de la producción máxima de CO_2 de la comunidad planctónica en base a la actividad de la NADP-IDH. Para ello, se han analizado las relaciones entre la NADP-IDH y las actividades de las principales enzimas productoras de CO_2 (ver capítulo 3).

- Objetivo 3: Análisis de la relación R_{CO2}/NADP-IDH. La respuesta fisiológica de este proceso, la R_{CO2}, es la que finalmente impacta en los ciclos biogeoquímicos. Este estudio se ha llevado a cabo por medio de incubaciones del misidáceo *Leptomysis lingvura* (ver capítulo 4).

Estos tres primeros objetivos permiten mejorar el conocimiento existente de uno de los procesos esenciales en el flujo de carbono en la columna de agua. Asimismo, la posibilidad de analizar este tipo de parámetros en muestras de gran profundidad puede suponer una nueva fuente de conocimiento directo sobre los procesos metabólicos de los ecosistemas batipelágicos.

Por otra parte, no hay que olvidar que el estudio de la respiración desde un punto de vista enzimático es un indicador de la estructura que la comunidad planctónica posee para la obtención catabólica de energía. Debido a ello, la medición de Φ o de la NADP-IDH puede utilizarse, en combinación con otros parámetros relacionados con la producción primaria (por ejemplo la Chl_a), para la determinación del grado de autotrofía o heterotrofía de una comunidad. Este tipo de estudios complementan la aplicación de las medidas enzimáticas como forma de cuantificar otros procesos que se dan en los ecosistemas, tales como la cuantificación del Flujo de Carbono vertical (*Fc*, Packard et al. (2015)), el cálculo de la eficiencia en la regeneración de nutrientes (NRE,Packard et al. (2015)) o la cuantificación de la producción de energía heterotrófica (HEP, Packard et al. (2015)). Por ello, se ha añadido un cuarto objetivo a esta tesis, donde se muestra la posible utilización

de estas técnicas para monitorizar los cambios metabólicos en la comunidad microplanctónica.

- – Objetivo 4: Análisis del cambio del grado de autotrofía-heterotrofía existente en una comunidad microplanctónica en condiciones oligotróficas tras la influencia de un afloramiento de agua profunda. Para ello, se ha utilizado Φ como la técnica bioquímica relacionada con el metabolismo catabólico y la medición de la Chl_a como el parámetro oceanográfico relacionado con la fotoautotrofía. De esta manera, se ha analizado el nivel de consumo de O_2 por mg de Chl_a a lo largo de los 55 días de duración del experimento. Además, se ha estudiado el impacto de la acidificación oceánica en estos resultados y su relación con las variaciones en la comunidad (ver capítulo

8.2   Metodología General

8.2.1   Muestreo de mesozooplancton y conservación de las muestras.

Las muestras de mesozooplancton (50-200μm y 200-2000μm) fueron recogidas en Sardina del Norte (Gáldar, Gran Canaria) por medio del arrastre de una red WP2 por tres buzos con escafandra autónoma, en una profundidad nunca superior a los 10m y siempre a más de un metro del lecho marino. Tras ser almacenados en contenedores de plástico para su traslado al laboratorio, las muestras se fraccionaron pasándolas por una columna de filtración con mallas de 2000μm , de 200μm y 50μm. Las muestras fueron recogidas con cuidado de las mallas de 200μm y 50μm y almacenadas en tubos Microvials$^{\textregistered}$ de 2mL a -80ºC, para los posteriores análisis enzimáticos y de biomasa.

8.2.2   Muestreo microplancton y conservación de las muestras.

El microplancton (0,7-50μm) se muestreó en las aguas de la playa de las Alcaravaneras (Las Palmas de Gran Canaria). Las muestras de agua se almacenaron en contenedores de 25L para su traslado al laboratorio. Una vez allí, se pasaron por una malla de 50μm antes de filtrarlas por un GF-F con un poro de 0,7μm hasta su saturación (aproximadamente 4L por filtro o un máximo de 1h de filtrado). Posteriormente, la muestra recogida en el filtro fue congelada y almacenada a -80ºC.

Para el experimento llevado a cabo en el capítulo 5, se utilizó un equipo de muestreo de agua integrada por profundidad (IWS, HYDRO-BIOS, Kiel) que recogía volúmenes de 5L de una mezcla homogénea de la

columna de agua (0-13m) en cada mesocosmos, muestreando entre 60 y 70L por mesocosmos y día. De esos volúmenes, se tomó una alícuota de entre 2 y 5L representativa de cada mesocosmos. Las muestras se pasaron por una malla de 50μm antes de ser filtradas por un GF-F con un poro de 0,7μm hasta su saturación (un máximo de una hora de filtración). Posteriormente, fueron congeladas en Nitrógeno líquido y almacenadas a -80ºC hasta su análisis en el laboratorio.

8.2.3   Muestreo y cultivos de *Leptomysis lingvura*.

Los muestreos de *L. lingvura* para su cultivo se realizaron a finales del otoño de 2017 y a finales de otoño de 2018 en Taliarte (Telde, Gran Canaria). Se realizaron buceos con escafandra autónoma en la zona de contacto entre los fondos arenosos y el veril rocoso a una profundidad de entre 5 y 10m. Se utilizaron redes de mano con una apertura de malla de 500μm y unos contenedores de plástico para almacenar los individuos asegurando el intercambio de agua con el entorno durante el tiempo de muestreo. Una vez capturados se trasladaron al laboratorio donde se mantuvieron en cultivo conforme a Herrera et al. (2011a). Para ello se utilizaron cuatro tanques de 40L con agua de mar filtrada, interconectados entre sí formando un sistema con un volumen de recirculación de 6L/h. El sistema además incluía un tanque de 70L de filtrado biológico por bacterias nitrificantes (BIO DIGEST, 1 ampolla cada 15 días), así como por minifiltros en cada uno de los tanques. Esto, junto a la renovación del 25% del agua cada semana, aseguró que los niveles de NH_4^+, NO_2^- y NO_3^- se mantuvieran por debajo de 0,1, 0,02 y 0,2 mg L^{-1} (Lussier et al. (1988)). La alimentación se basó en dos tomas diarias de *Artemia sp.* proveniente de cultivos secundarios. Tras un mínimo de una semana de aclimatación de los cultivos, se seleccionaron los individuos que fueron objeto del estudio de tasas respiratorias (ver capítulo 4) en incubaciones durante diferentes periodos de tiempo o bajo distintas condiciones de alimentación. Tras la incubación se recogieron las muestras con cuidado con una malla de 50μm y se almacenaron en Microvials® a -80ºC, hasta su análisis.

8.2.4   Medición de NADP-IDH.

Una vez en el laboratorio, las muestras de microzooplancton fueron homogeneizadas en 0,1M de buffer fosfato por medio de un sistema con varilla de teflón® en un recipiente de 2mL (PYREX® Potter-Elvehjem) a 2600rpm durante 2 min. El mesozooplancton y los misidáceos se homogeneizaron por medio de sonicación durante 45sec al 70% de la amplitud en un procesador ultrasónico Vibracell VCX 130 Sonics®.

Los homogeneizados resultantes fueron centrifugados a 4000rpm durante 10min entre 0-4ºC. Nada más finalizar la centrifugación, se realizaron los ensayos enzimáticos sobre los sobrenadantes obtenidos.

La actividad de la NADP-IDH se midió siguiendo la metodología descrita por Tames-Espinosa et al. (2018), desarrollada en el capítulo 2 de la presente tesis doctoral. La actividad de la NADP-IDH se obtiene siguiendo el aumento de la absorbancia del NADPH (340nm) cinéticamente durante 1200sec, a 18ºC en una cubeta de 1cm de anchura transparente a la longitud de onda ultravioleta con un espectrofotómetro Cary 100 UV-Visible. El β-NADP$^+$ (SIGMA #N0505, de aquí en adelante NADP$^+$) se reduce por la NADP-IDH a NADPH mientras se decarboxila el DL-trisodio-isocitrato (SIGMA #I1252; de aquí en adelante isocitrato) a α-cetoglutarato. Los blancos se realizan sin añadir isocitrato para extraer los valores del resultado asociados a reacciones no enzimáticas o de aquellas enzimas no relacionadas con la NADP-IDH. El aumento de la absorbancia adquiere forma de regresión lineal, cuya pendiente es considerada la actividad de la NADP-IDH. La actividad de NADP-IDH se ha expresado tanto en μmol NADPH min^{-1} (mL de homogeneizado)$^{-1}$ como en μmol CO$_2$ min^{-1} (mL de homogeneizado)$^{-1}$ (ambas unidades son estequiométricamente equivalentes). Para pasarlo a uLCO$_2$min^{-1}(mL de homogeneizado)$^{-1}$ se debe multiplicar por 22,4μL μmol^{-1}.

8.2.5 Optimización de parámetros para la medición de la V$_{max}$ de NADP-IDH en la comunidad planctónica.

Para asegurar la medición de la velocidad máxima de reacción (V$_{max}$) de NADP-IDH se determinaron las concentraciones óptimas del substrato (isocitrato), del cofactor (NADP$^+$) y del cofactor mineral (MgCl$_2$), así como su pH óptimo. Asimismo, se estudió la dependencia de esta velocidad con la temperatura, y se comprobó la relación lineal existente con la biomasa. Otros aspectos, como el tiempo e intensidad óptimas de centrifugación de las muestras durante la preparación de los homogeneizados, así como la estabilidad de éstos también fueron estudiados para asegurar la reproducibilidad del ensayo y la emisión de la máxima señal de la reacción. En todos los casos se utilizó la metodología definida en la sección 8.2.4 para medir la actividad en muestras de 0,7-50μm, 50-200μm y de 200-2000μm. Las distintas especificaciones para cada parámetro pueden consultarse en la sección 2.2 del capítulo 2). Por otra parte, la sensibilidad al buffer, el coeficiente de extinción, la precisión del ensayo y la interpretación de las diferentes respuestas espectrofotométricas se encuentran recogidas en el Apéndice A de la presente tesis doctoral.

8.2.6 Medición del consumo máximo de O_2 (Φ) en la comunidad planctónica.

La respiración potencial basada en el consumo de O_2 se determinó por medio del análisis de la actividad del sistema de transporte de electrones, ETS, en el sobrenadante de las muestras homogeneizadas y centrifugadas (Packard (1971), incorporando las modificaciones descritas por Kenner and Ahmed (1975) para el fitoplancton y por Owens and King (1975) y Gómez et al. (1996) para el zooplancton). El aumento de la absorbancia asociada al INT-formazán (490nm) fue monitorizado a 18ºC en cubetas de plástico de 1cm de anchura, transparentes a esta longitud de onda. Siguiendo la metodología de Packard and Williams (1981) se estimó la actividad potencial del ETS, así como el consumo potencial de O_2, en base a la recta de regresión del aumento de la absorbancia a 490nm por tiempo. Durante el proceso, la sal de tetrazolium (INT, p-Iodonitrotetrazolium Violet, Sigma #I8377) es reducida por las enzimas respiratorias presentes en el ETS, sustituyendo al O_2 como aceptor de electrones. El INT capta 2 electrones mientras que el O_2 requiere 4 para reducirse. Por ello, la tasa de producción del INT-formazán equivale estequiométricamente a dos veces la actividad del ETS y a 0,5 al consumo potencial de O_2. El consumo potencial de O_2 se ha expresado en $\mu molO_2h^{-1}$(mg de proteína)$^{-1}$. Para pasarlo a uLO_2h^{-1}(mg de proteína)$^{-1}$ se debe multiplicar por 22,4μL μmol^{-1}.

8.2.7 Medición del consumo de O_2 fisiológico en base a la aplicación de los ratios R_{O2}/Φ a las mediciones de Φ.

Cuando no se encuentran disponibles las medidas de consumo de O_2 fisiológico (R_{O2}), es común utilizar los ratios R_{O2}/Φ presentes en la literatura, para obtener R_{O2} a partir de las medidas de Φ tanto para el micro como para el mesozooplancton (Cleland (1967); Hernández-Leon and Gómez (1996); Packard and Codispoti (2007); Osma et al. (2016c)). Aquí hemos aplicado tres ratios distintos, asociado a tres escenarios diferentes, para aplicarlos sobre las muestras de mesozooplancton. En el caso del microplancton, se ha definido un cuarto escenario específico. La descripción de los cuatro escenarios, así como sus valores, se encuentra recogida en la Tabla 3.1 del capítulo 3. En todos los casos, se obtiene R_{O2} con la Eq.8.1:

$R_{O2}=\Phi\cdot(R_{O2}/\Phi)$ (8.1)

Donde R_{O2} es el consumo de O_2 fisiólogico, Φ es el consumo de O_2 potencial, y (R_{O2}/Φ) es el ratio a aplicar. Ambas tasas se expresan en las mismas unidades, bien en base al volumen de agua o en base a la biomasa (bien μmol O_2 h^{-1} L^{-1}; o bien μmol O_2 h^{-1} (mg de

proteína)$^{-1}$), por ello el ratio entre ellas es adimensional, pudiendo publicarse el resultado en tanto por uno o en tanto por ciento para una mejor comprensión.

8.2.8 Medición de la producción de CO_2 fisiológica (R_{CO2}) teórica en base a la aplicación de RQ ratios a los resultados en R_{O2}

A partir de los valores de R_{O2} obtenidos tanto por medio de incubaciones como con la aplicación de R_{O2}/Φ, se ha calculado R_{CO2} tal y como se expresa en la Eq.8.2. Para ello, se barajaron distintas posibilidades incluyendo la aplicación de ratios de Redfield (Packard and Gómez (2013)) o distintos cocientes respiratorios (RQs) (Mayzaud et al. (2005); Berggren et al. (2012); Romero-Kutzner et al. (2015), de forma que se abarcara un amplio rango de condiciones fisiológicas.La descripción de las tres condiciones, así como sus valores, se encuentra recogida en la Tabla 3.1 del capítulo 3.

$R_{CO2}=R_{O2}\cdot R_{CO2:O2}$ (8.2)

Donde $R_{CO2:O2}$ es la conversión aplicada en cada escenario en la Tabla 3.1. Las tasas de respiración se expresan en las mismas unidades, bien en base al volumen de agua, bien en base a la biomasa (μmol del gas h^{-1} L^{-1} o μmol del gas h^{-1} (mg de proteína)$^{-1}$), de tal forma que el ratio aplicado se medirá en moles de CO_2 por mol de O_2.

8.2.9 Medición del consumo de O_2 (R_{O2}) fisiológico en incubaciones de *L. lingvura*.

La tasa de consumo de O_2 se midió sobre incubaciones de tres individuos en botellas de 60mL de agua de mar filtrada (por triplicado). Se utilizaron los optodos Presens$^{®}$ 1-Channel Fibox 4 con sensores tipo PSt3. Se seleccionaron cuatro sensores: uno en el interior de cada una de las tres botellas de incubación y un cuarto en el interior de la botella blanco. Se realizó una medida de la concentración de O_2 en cada botella tres veces cada 15 min durante un tiempo máximo de incubación de 120 min (Bondyale-Juez et al. (2017)). La concentración de O_2 obtenida por el optodo se expresa en μmol O_2 L^{-1}. El descenso de la concentración de O_2 en el tiempo, eliminando los datos de los primeros 30 min, puede modelarse con líneas de regresión cuya pendiente es negativa. En nuestro caso la pendiente (α) es la variación de μmol O_2 L^{-1} min^{-1}. Para obtener la tasa de respiración de los organismos se debe transformar este valor en μmol O_2 h^{-1}, utilizando el volumen de la botella de incubación (V) expresado en L, tal y como se

recoge en la Eq.8.3:

R_{O2}= - (α)· V·60 (8.3)

Siendo α la pendiente de la línea de regresión obtenida, V el volumen de la botella de incubación en L y 60 los minutos que tiene una hora. Una vez aplicada la Eq.8.3, R_{O2} se expresa en μmol O_2 h^{-1}.

8.2.10   Medición de la producción de CO_2 (R_{CO2}) fisiológica en incubaciones de *L. lingvura*.

Debido a los requerimientos de volumen de muestra de la técnica de medición de CO_2 (250mL en cada medida), se ha realizado una medición de punto final sobre incubaciones de diez individuos en botellas de 1L (por triplicado) con una duración de entre 4 y 24h dependiendo del objetivo de cada experimento (ver capítulo 4). La producción de CO_2 por los organismos impacta en el sistema de carbonatos del agua de mar, dando lugar a un incremento del Carbono inorgánico Total (TC). Por ello, y tras comprobar que la alcalinidad no variaba durante el periodo de incubación, se consideró el incremento de TC una medida directa de la producción de CO_2. Se midió la concentración de TC en el agua de mar filtrada al inicio de la incubación (por triplicado, TC_0), en botellas con individuos al final de la incubación (por triplicado, TC_e) y en botellas sin individuos al final de la incubación (blancos, por triplicado, $TC_{e-blank}$). Para la determinación de TC se utilizó el Sistema VINDTA 3C de determinación coloumétrica (Mintrop et al. (2000)) con una precisión de $\pm1,0$ μmol L^{-1} (www.MARIANDA.com). Con los valores de concentración de TC obtenidos, la tasa de producción de CO_2 en μmol CO_2 h^{-1} se obtiene por medio de la Eq.8.4:

R_{CO2}= ((TC_e-TC_0)-($TC_{e-blank}$-TC_0))·V / t (8.4)

Siendo V el volumen de incubación en L (en el presente caso, 1L en todas las botellas) y t el tiempo de incubación expresado en h. Con ello, R_{CO2} se expresa en μmol O_2 h^{-1}.

8.2.11   Medición de la biomasa en términos de contenido proteínico.

El contenido proteico en biomasa se ha determinado en los mismos sobrenadantes en los que se han realizade los ensayos enzimáticos. Para ello, se ha utilizado el método de Lowry et al. (1951) modificado por Rutter (1967) usando albúmina de serum bovino (BSA) como estándar de calibración. La biomasa se expresa en mg de proteína (mL de homogeneizado)$^{-1}$. Conociendo el volumen total de homogeneizado y

el volumen de agua que representa la muestra (en L) se puede expresar también como mg de proteína L^{-1}.

8.2.12 Medición de la productividad neta

La productividad neta se ha medido aplicando la primera derivada a la biomasa en las series temporales obtenidas en el experimento KOS-MOS GC 2014. Los resultados positivos de esta primera derivada son indicador del proceso de producción neta de biomasa en el tiempo, esto es, la productividad neta. Sin embargo, los valores negativos implican que los procesos de remineralización, precipitado y pastoreo (grazing) son mayores que la producción de biomasa en el tiempo, resultando en una pérdida neta de biomasa en determinados periodos de tiempo.

8.3 Principales resultados y discusión

8.3.1 Optimización de la medición de la actividad de la NADP-IDH en la comunidad planctónica.

En el curso de esta tesis doctoral se ha desarrollado una metodología para medir la actividad de la NADP-IDH en el plancton. Para ello se han determinado las concentraciones necesarias del substrato, cofactor y cofactor metálico para asegurar la medición de la velocidad máxima de la reacción (*Vmax*). Los valores óptimos en la cubeta para la comunidad planctónica (de 0,7 a 2000μm) fueron 2mM para el isocitrato, 0,3mM para el $NADP^+$ y 6mM para el $MgCl_2$. Las constantes de Michaelis-Menten (*Km*s) se obtuvieron tanto por los gráficos de Michaelis-Menten (Fig.2.1) como con la linearización de Hanes-Woolf, resultando en $271\pm63\mu$M para el isocitrato y $18\pm3\mu$M para el $NADP^+$. La *Vmax* se alcanzó con un pH de 8,19 (Fig.2.2), reduciéndose a la mitad cuando éste era menor que 7,62 o mayor que 8,75 (*pKa*s). Si bien la temperatura óptima para esta enzima fue de 28ºC en el mesozooplancton y de 39ºC en la NADP-IDH proveniente de corazón de cerdo, ambas necesitaron similares Energías de activación (*Ea*) (20,4 Kcal mol^{-1} y 21,4Kcal mol^{-1} respectivamente) (Fig.2.3). Esto ha permitido el desarrollo de una ecuación de Arrhenius precisa a la hora de calcular la actividad a diferentes temperaturas (Eq.2.8 en el capítulo 2). Además, el Q_{10} (entre 15 y 25ºC) de la NADP-IDH del mesozooplancton fue 1,98.

Por otra parte se comprobó la relación lineal existente entre la actividad enzimática y la biomasa (Fig.2.4), asegurando que la dilución de una muestra no afecta a la actividad de la NADP-IDH normalizada por mg de proteína (con una desviación estándar del 3,5%). El límite de

detección de este nuevo método fue de 8±2 μg de proteína mL^{-1} para el microplancton y de 10±2 μg de proteína mL^{-1} para el mesozoo-plancton.

El nivel de centrifugación impactó de manera significativa en las muestras filtradas por GF/F (en nuestro caso, el microplancton) (Fig.2.5). En estos casos, una fuerza mayor que 1500g debe mantenerse por más de 2min para asegurar que se alcanza la *Vmax*. Sin embargo, las muestras que fueron sonicadas (mesozooplancton), no sufrieron cambios significativos asociados a la centrifugación. No obstante, ya que los blancos de las muestras sin centrifugar daban valores muy negativos que influían en el resultado final, se recomienda una centrifugación de al menos 375g durante 2min. Una vez centrifugadas, observamos que las muestras sufrían una pérdida del 1,1% de NADP-IDH por cada 10 min (Fig.2.6). Si se analizan durante la primera media hora tras la centrifugación, la pérdida de la actividad no será mayor del 3%.

8.3.2 Producción máxima de CO_2 de la comunidad planctónica a partir de la medición de la actividad de la NADP-IDH (Ψ_{NADP}).

La NADP-IDH es una de las principales enzimas productoras de CO_2, pero no es la única. Por ejemplo, la producción de CO_2 en el ciclo de Krebs será la suma del CO_2 producido por la piruvato deshidrogenasa (PDH$_{CO2}$), por la α-cetoglutarato deshidrogenasa (KGDH$_{CO2}$), por la enzima málica (ME$_{CO2}$), por la fosfoenolpiruvato carboxiquinasa (PEPCK$_{CO2}$) y por las isoenzimas isocitrato deshidrogenasas (IDH KC$_{CO2}$) (Fig.1.1). Gracias al trabajo de Walsh and Koshland (1984) en *Escherichia coli* pudimos relacionar la actividad de cada una de ellas con la actividad de la IDH KC$_{CO2}$, tal y como se refleja en las ecuaciones Eq.3.4 y Eq.3.5 del capítulo 3. Según esta aproximación, la producción potencial de CO_2 asociada al ciclo de Krebs, es 3,57 veces la actividad de la IDH KC$_{CO2}$.

Sin embargo, la IDH KC$_{CO2}$ en los organismos eucariotas[1] se encuentra en la mitocondria y está compuesta por dos isoenzimas: una dependiente del NAD$^+$ (NAD-IDH) y otra dependiente del NADP$^+$ (NADP-IDH) (Eq.8.5). Por otra parte, la medición de la NADP-IDH no sólo incluye la enzima mitocondrial (NADP-IDH$_{mit}$), sino también una NADP-IDH presente en el citosol (NADP-IDH$_{out}$) (Eq.8.6). Para poder calcular la producción total de CO_2 del organismo a partir de nuestras medidas de NADP-IDH debíamos encontrar la forma de relacionar estos

---

[1]Los organismos procariotas sólo poseen una isoenzima, la NADP-IDH, careciendo de la NAD-IDH. Además, carecen de mitocondria. Por ello, en su caso, la producción máxima de CO_2 puede calcularse sustituyendo directamente la IDH KC$_{CO2}$ por la actividad de la NADP-IDH. La producción máxima de CO_2 sería 3,57 veces la NADP-IDH.

valores.

IDH KC = NADP-IDH$_{mit}$ + NAD-IDH$_{mit}$(8.5)

NADP-IDH= NADP-IDH$_{out}$ + NADP-IDH$_{mit}$ (8.6)

Para ello, utilizamos los resultados obtenidos por Alp et al. (1976) en crustáceos, para la CS (que se encuentra en la mitocondria), la NAD-IDH (que se encuentra en la mitocondria) y la NADP-IDH (que, al igual que el caso de nuestro método, incluye tanto la mitocondrial como la citosólica). En primer lugar, a partir de los datos aportados por Walsh and Koshland (1984), establecimos la relación entre la CS y la IDH KC$_{CO2}$ (Eq.8.7), donde la IDH KC$_{CO2}$ es 0,72 veces la actividad de la CS en el ciclo de Krebs.

CS= 1.39·IDH KC

IDH KC= 0.72·CS (8.7)

Combinando las tres ecuaciones (Eq.8.5,Eq.8.6, y Eq.8.7) Se puede extraer la fracción de la NADP-IDH que no se encuentra a nivel mitocondrial (Eq.8.8):

NADP-IDH$_{out}$ = NADP-IDH - (IDH KC - NAD-IDH)(8.8)

Una vez calculados los valores de cada enzima a partir de los resultados de Alp et al. (1976) (ver Tabla 3.2 en el capítulo 3), procedimos a su normalización por la actividad medida de NADP-IDH (ver Tabla 3.3 en el capítulo 3). Por medio de esta relación se puede calcular la producción de CO_2 de cada enzima a partir de la medición de la NADP-IDH.

Teniendo en cuenta todo lo anterior, determinamos que la producción total de CO_2 debe incluir tanto la relacionada con el ciclo de Krebs, como la que sucede en el citosol asociada a la biosíntesis (Eq.8.9).

Ψ= KC$_{CO2}$ + NADP-IDHout$_{CO2}$(8.9)

Combinando esta ecuación con la Eq.8.5, obtenemos la Eq.8.10.

Ψ= 3.57 · (NADP-IDHmit+NAD-IDH)+NADP-IDHout(8.10)

Finalmente, incluyendo los ratios medios obtenidos a partir de los datos de Alp et al. (1976) en la Tabla 3.3, podemos relacionar estas actividades a la NADP-IDH (Eq.8.11).

Ψ_{NADP}= 3.57·(0.65·NADP-IDH + 0.07·NADP-IDH)+ 0.38·NADP-IDH

Ψ_{NADP}= 2.94·NADP-IDH (8.11)

En base a la aplicación de este modelo lineal a las mediciones de NADP-IDH en muestras de mesozooplancton y microzooplancton, la producción potencial de CO_2 fue de 42,1±10,9 10^{-3} μmol CO_2 min^{-1} (mg protein)$^{-1}$ y 53,5±9,5 10^{-3} μmol CO_2 min^{-1} (mg protein)$^{-1}$ respectivamente, hasta 1.7 veces el valor de Φ en las mismas muestras (26,6±4,8 10^{-3} μmol O_2 min^{-1} (mg protein)$^{-1}$ en el mesozooplancton y 42,7±9,1 10^{-3} μmol O_2 min^{-1} (mg protein)$^{-1}$ en el microplancton). Si sólo se tiene en cuenta la producción de CO_2 asociada al ciclo de Krebs (Respiratory Ψ_{NADP}), ésta es 1.47 veces superior a Φ, lo que indica que la estructura enzimática asociada con la oxidación de las moléculas de carbono orgánico está preparada para superar las demandas del ETS.

8.3.3   Desarrollo de los ratios teóricos R_{CO2}/ Ψ_{NADP}.

Una vez determinado el valor de Ψ_{NADP} en nuestras muestras a partir de la medición de la actividad de NADP-IDH, necesitamos conocer la R_{CO2} para el estudio de los ratios R_{CO2}/Ψ_{NADP}.

Para ello, medimos Φ en las mismas muestras en las que medimos Ψ_{NADP}. En la literatura pudimos encontrar distintos ratios R_{O2}/Φ asociados a diferentes escenarios (ver Tabla 3.1 en capítulo 3). De esta manera determinamos el consumo de O_2 (R_{O2}) que tendría esa comunidad en los diferentes escenarios (ver Fig.3.3a). Estos valores oscilaron entre 11 y 25 10^{-3} μmol O_2 min^{-1} (mg protein)$^{-1}$ en el mesozooplancton, siendo 11,1±2,4 10^{-3} μmol O_2 min^{-1} (mg protein)$^{-1}$ en el microplancton (Fig.3.3a).

A partir de la aplicación de distintos cocientes respiratorios (RQs) sobre los valores obtenidos de R_{O2} (ver Tabla 3.1), obtuvimos los valores de R_{CO2} en 12 condiciones diferentes (9 para el mesozooplancton y 3 el microplancton; ver Fig.3.3b). Los valores de R_{CO2} obtenidos oscilaron entre 8 y 30 10^{-3} μmol CO_2 min^{-1} (mg protein)$^{-1}$ en el mesozooplancton y entre 6 y 18 10^{-3} μmol CO_2 min^{-1} (mg protein)$^{-1}$ en el microplancton.

En base a estos valores y a Ψ_{NADP} analizamos los ratios R_{CO2}/Ψ_{NADP}, que variaron entre 0,17 y 0,86 para el mesozooplancton y entre 0,12 y 0,32 para el microplancton (Tabla 3.4). Teniendo en cuenta las condiciones asociadas a una comunidad muestreada en las Islas Canarias durante la primavera, estimamos que el ratio a utilizar para nuestras muestras debe ser de entre 0,3 y 0,4 para el mesozooplancton y entre 0,2 y 0,3 para el microplancton. No obstante, siempre que sea posible, se debe determinar el ratio específico en cada región, campaña, o comunidad, combinando la medición fisiológica de R_{CO2} y la medición de Ψ_{NADP}. De esta manera el ratio utilizado será más representativo del objeto de estudio en cada momento.

8.3.4 Estudio de los efectos de la inanición, las diferencias sexuales y el estado trófico de la comunidad en la producción de CO_2 del misidáceo *L. lingvura*

Siguiendo la recomendación del punto anterior, medimos las tasas de producción de CO_2 (R_{CO2}) en distintas incubaciones de *L. lingvura* y las comparamos con la producción máxima de CO_2 de la NADP-IDH. Para analizar su variabilidad en relación a diferentes factores biológicos y ambientales, se llevaron a cabo comparaciones entre: 1) una comunidad en estado de bloom y una en estado post-bloom; 2) entre machos y hembras bien alimentados; y 3) entre hembras bien y mal alimentadas.

Ratios R_{CO2}/ IDH en incubaciones de machos y hembras de *L. lingvura*, así como en distintos estadios de inanición.

Durante los experimentos realizados no se evidenciaron diferencias significativas entre machos y hembras en niguno de los parámetros estudiados: ni en la Φ (con un valor medio de 0,6$\pm$0,12 μmol O_2 h^{-1} (mg protein)$^{-1}$) o ni en la NADP-IDH (con un valor medio de 0,97$\pm$0,17 μmol CO_2 h^{-1} (mg protein)$^{-1}$), ni en los ratios R_{O2}/Φ (en torno a 0,35 para los organismos bien alimentados) o R_{CO2}/NADP-IDH (en torno a 0,12).

Dentro de los experimentos realizados sobre la comunidad bloom, observamos las variaciones del ratio R_{CO2}/NADP-IDH durante 24h tras haber sido alimentados. Este ratio se mantuvo en una media de 0,13$\pm$0,04 durante las primeras 12h, pero se redujo a 0,08$\pm$0,01 en las incubaciones más largas (Fig.4.8). Debido a que la actividad de *L. lingvura* sigue un ritmo circadiano (Herrera et al. (2011b)), consideramos que éste influye en los resultados observados en las incubaciones más largas. Por ello, recomendamos no realizar incubaciones superiores a las 6 horas en estudios con *L. lingvura*.

Por otra parte, el grado de inanición sí que afectó a la respuesta fisiológica (ver Fig.4.6). Los valores de R_{O2}/Φ descendieron a 0,27$\pm$0,08 entre las hembras que se encontraban tras 12h de inanición, mientras que el R_{CO2}/NADP-IDH ascendió a 0,16$\pm$0,06. Esta diferencia en la respuesta fisiológica hizo que el RQ casi se doblara durante la inanición, pasando de valores en torno a 0,6 a valores superiores a 1 mol CO_2 mol O_2^{-1} (ver Fig.4.7). Este incremento en el RQ durante las primeras horas de la inanición ha sido reportado en otras ocasiones en bacterias (Romero-Kutzner et al. (2015)), en eufausiáceos (Mayzaud et al. (2005)), o en lepidópteros (Kozhantshikov (1938)). Este aumento es debido a que: 1) Durante la inanición se mantiene el metabolismo asociado a la síntesis de lípidos estructurales Jansen et al. (1966); Aster

and Moon (1981); Zara et al. (2000), reduciéndose el consumo de O_2 mientras que se mantiene o incluso se refuerza la producción de CO_2 por biosíntesis. 2) Durante la síntesis lipídica a partir de hidratos de carbono se produce O_2, reduciéndose aún más el consumo neto de O_2 (Kozhantshikov (1938)).

En base a lo anterior, nosotros hipotetizamos que durante la inanición los nutrientes se utilizan principalmente para el mantenimiento de la estructura celular, en detrimento a la generación de energía. Esta suposición es coherente con el estudio realizado por Teruya et al. (2019) en seres humanos. En él observaron que durante la inanición, se veía una regulación positiva de algunos marcadores metabólicos relacionados con la gluconeogénesis y la protección ante moléculas oxidantes[2]).

Efectos del estado trófico de la comunidad durante el muestreo sobre las actividades enzimáticas y el ratio R_{CO2}/NADP-IDH

Las condiciones tróficas en las que se encontraba la comunidad de *L. lingvura* durante el muestreo tuvieron un impacto significativo sobre las actividades enzimáticas relacionadas con la respiración. Las actividades de Φ y de la NADP-IDH fueron significativamente mayores en las hembras provenientes de la comunidad en "bloom" que en aquellas provenientes de la comunidad "post-bloom" (1,04±0,14 μmol O_2 h^{-1} (mg protein)$^{-1}$ y 1,96±0,09 μmol CO_2 h^{-1} (mg protein)$^{-1}$ respectivamente en la comunidad "bloom"; y 0,58±0,12μmol O_2 h^{-1} (mg protein)$^{-1}$ y 0,97±0,19μmol CO_2 h^{-1} (mg protein)$^{-1}$ en la comunidad "post-bloom") (Fig.4.1 en el Capítulo 4). Los resultados de Φ obtenidos son coherentes con los encontrados en la literatura, al encontrarse dentro de los valores publicados por Osma et al. (2016c) para el mesozooplancton de Canarias (1,47±0,76μmol O_2 h^{-1} (mg protein)$^{-1}$). A su vez, son mayores que los publicados por Bondyale-Juez et al. (2017) para una comunidad de *L. lingvura* muestreada en el momento más cálido y oligotrófico del año 2015 (0,25±0,06 μmol O_2 h^{-1} mg of protein^{-1}), y menores que los publicados por Herrera et al. (2011b) para una comunidad de *L. lingvura* muestreada al final de la primavera (1,53±0,43 μmol O_2 h^{-1} mg of protein^{-1}).

El ratio NADP-IDH/Φ, con valores de entre 1,5 y 2,2 mol CO_2 mol $O_2$$^{-1}$ y sin diferencias significativas entre ambas comunidades, muestra que el proceso de descarboxilación está preparado para exceder ampliamente la demanda del sistema de transporte de electrones en el caso de que el misidáceo requiera un aporte extra de energía.

---

[2]Tal y como se comenta en la introducción, se ha demostrado que la NADP-IDH está involucrada en la producción del NADPH necesario para la producción de glutatión reducido, esencial en la protección celular ante especies de oxígeno reactivo (ROS) (Jo et al. (2001)

A su vez, el ratio R_{CO2}/NADP-IDH se mantuvo en torno a 0,12 en ambas comunidades. Este valor puede resultar muy bajo si lo comparamos con los ratios R_{O2}/Φ (0,81 en Bondyale-Juez et al. (2017), entre 0,66 y 1 en Herrera et al. (2011b)). Sin embargo, es similar a los obtenidos en otros procesos asociados a la remineralización, como el ratio de excreción de NH_4^+ frente a la actividad de la GDH (0,11$\pm$0.05 en Fernández-Urruzola et al. (2011)).

Por otra parte, nótese que este ratio está basado en la comparación directa entre R_{CO2} y NADP-IDH, no entre R_{CO2} y la producción total de CO_2 tal y como se calculó en la sección anterior (Ψ_{NADP}). Al ser Ψ_{NADP} 2,94 veces NADP-IDH, los ratios R_{CO2}/Ψ_{NADP} obtenidos en estas comunidades de *L.lingvura* fueron aproximadamente 0,04. Este valor es sensiblemente inferior a los ratios teóricos obtenidos en el capítulo 3. Esto es debido a que, por un lado, la respuesta fisiológica obtenida durante estos experimentos, también para el caso del consumo de O_2, fue menor de lo esperado (R_{O2}/Φ entre 0,27 y 0,35). Si tenemos en cuenta que los RQ obtenidos sí son coherentes con los valores de la literatura, las causas que implicaron la reducción de la respuesta fisiológica en términos de consumo de O_2, también afectaron a la producción de CO_2. Por otra parte, los ratios teóricos fueron calculados sobre una comunidad mixta de mesozooplancton, dominada por copépodos. En ellos la proporción Ψ_{NADP}/Φ fue de 1,7mol CO_2 mol O_2^{-1}. Por el contrario, en *L.lingvura* observamos una proporción media de Ψ_{NADP}/Φ de 4,8 mol CO_2 mol O_2^{-1} (NADP-IDH/Φ=1,63$\pm$0,4 mol CO_2 mol O_2^{-1}).

El descenso de la respuesta fisiológica junto con una actividad de NADP-IDH superior a la esperado son los responsables de unos valores de R_{CO2}/Ψ_{NADP} más bajos de lo esperado inicialmente. Por todo ello se recomienda, siempre que sea posible, medir de manera combinada estos parámetros en cada estudio (al menos R_{CO2} y NADP-IDH, siendo recomendable su comparación con R_{O2} y Φ). De esta manera, se podrán aplicar ratios específicos de cada campaña, región o comunidad, sobre resto de las muestras de cada estudio. Asimismo, se generará una base de datos que permitirá ahondar en la relación entre estos parámetros y el correcto desarrollo de modelos cinéticos bisustrato (EKM).

8.3.5 Variaciones del valor del ratio Φ/Chl_*a* y su relación con la composición de la comunidad microplanctónica en términos de dominancia de fotoautótrofos, heterótrofos o mixótrofos.

Gracias al experimento KOSMOS GC 2014 (ver capítulo 5 desarrollado en la Bahía de Gando (Gran Canaria) en el otoño de 2014 pudi-

mos observar las variaciones del ratio Φ/Chl_a asociado a la comunidad microplanctónica, tanto en condiciones oligotróficas, como bajo la influencia de un afloramiento de agua profunda rica en nutrientes y en condiciones posteriores, monitorizando los cambios en la comunidad.

Durante los primeros 24 días se mantuvieron condiciones oligotróficas, y pudimos observar un cambio en la comunidad asociado a la propia instalación de los mesocosmos (Fig.5.1, I). Los valores de Φ/Chl_a obtenidos en la comunidad de las aguas circundantes fueron de entre 2 y 4,7 $\mu LO_2 h^{-1}$ μg Chl_a^{-1}, mientras que en los mesocosmos ascendieron a valores de entre 3,4 y 8 $\mu LO_2 h^{-1}$ μg Chl_a^{-1}. Este cambio está asociado a la transformación de una comunidad dominada por cianobacterias a una mixta, donde el nanoplancton heterótrofo y mixótrofo domina la biomasa Hernández-Hernández et al. (2018). La productividad neta se mantuvo alrededor de 0 mg proteína L^{-1} d^{-1} (Fig.5.2, I). La integral de Φ, Chl_a y B para cada mesocosmos a lo largo de toda esta fase no mostró ningún efecto asociado al aumento de pCO_2 (Fig.5.3, I).

Tras la simulación del afloramiento de agua profunda se produjo un bloom de fitoplancton en todos los mesocosmos entre los días 28 y 30 (Taucher et al. (2017); Hernández-Hernández et al. (2018); Taucher et al. (2018)). Esto dió lugar a los valores más bajos de Φ/Chl_a de todo el experimento (Fig.5.1, II), debido a la dominancia de la comunidad fotoautótrofa en el microplancton ($1,1\pm0,6\mu LO_2 h^{-1}$ μg Chl_a^{-1}). Durante esta fase, la productividad neta fue máxima entre uno y dos días antes del pico de Chl_a ($0,039\pm0,013$ mg proteína L^{-1} d^{-1} (Fig.5.2, II). Sin embargo, 24 horas después del pico de Chl_a, los procesos de remineralización, pastoreo ("grazing") y sedimentación dieron lugar a una pérdida neta de biomasa de $-0,023\pm0,008$ mg proteína L^{-1} d^{-1} (Fig.5.2, II). En esta fase, a diferencia de la anterior, se empezaron a observar ciertas tendencias relacionadas con los distintos niveles de pCO_2. Si bien la Chl_a, Φ y B aumentaron a mayor pCO_2, sólo se puede considerar significativa la relación positiva entre Φ y pCO_2 (Fig.5.3, II). Esta relación es especialmente clara tras extraer los datos asociados a aquellos mesocosmos en los que la proliferación de un alga tóxica (harmful algal species, HAS), *Vicicitus globosus*, impidió el desarrollo del microzooplancton (y del mesozooplancton) (Riebesell et al. (2018); Algueró-Muñiz et al. (2019)).

Una vez que se agotaron los nutrientes, la comunidad microplanctónica evolucionó de manera diferente. Se alcanzaron los valores máximos de Φ/Chl_a cuando el microzooplancton, dominado por dinoflagelados, proliferó en los mesocosmos con tratamientos de pCO_2 bajos o intermedios (hasta 10 $\mu LO_2 h^{-1}$ μg Chl_a^{-1}). Sin embargo, en los meso-

cosmos más ácidos, la proliferación de *V.globosus* hizo que Φ/Chl_a se mantuviera más bajo (entre 2,5 y 7 μLO$_2$h^{-1} μg Chl_a^{-1}) (Fig.5.1, III). Sin embargo estas variaciones entre los distintos mesocosmos no afectaron a su productividad neta. Tras los efectos del bloom de diatomeas y el agotamiento posterior de los nutrientes, la productividad neta tendió a un estado de equilibrio similar al de la fase oligotrófica en todos los casos (Fig.5.2, III), solo que con mayor variabilidad en esta fase.

El análisis integral de Chl_a^{-1}, Φ y B en esta última fase no muestra una relación significativa con el aumento pCO$_2$, especialmente si se extraen los valores asociados a los mesocosmos en los que *V.globosus* proliferó (Fig.5.3, III). Sin embargo, considerando estos valores, Chl_a^{-1} sí tiene una relación positiva con la acidificación. La proliferación de *V.globosus* en condiciones de alta pCO$_2$ puede estar asociada al refuerzo de su actividad fotosintética asociado a una mayor concentración de CO$_2$ en el entorno. Al carecer de pirenoide, su sistema fotosintético es ineficiente en condiciones normales, sin embargo queda reforzado en condiciones de alta pCO$_2$. En océanos donde HAS similares a *V.globosus* formen parte de la comunidad, el aumento de pCO$_2$ puede resultar en una relación positiva con la Chl_a debido al refuerzo de este tipo de sistema fotosintético carente de pirenoide, ineficiente en las condiciones actuales de pCO$_2$. Asimismo, la ausencia de microzooplancton (y mesozooplancton) reduce el grazing sobre cianobacterias y diatomeas, lo que genera una mayor retención de Chl_a en el medio (Riebesell et al. (2018); Taucher et al. (2018); Alguero-Muñiz et al. (2019)).

8.4 Conclusiones

8.4.1 El desarrollo de un método para determinar la actividad de la NADP-IDH en el plancton como una de las principales enzimas responsables de la producción de CO$_2$

Durante el desarrollo de esta tesis creamos un método enzimático para determinar la actividad de la NADP-IDH en el zooplancton y el microplancton. Este método se basa en monitorizar la reducción de NADP$^+$ a NADPH durante la reacción de decarboxilación del isocitato a α-cetoglutarato, catalizada por esta enzima. Las tasas de producción de NADPH (μmol NADPH min^{-1} mL^{-1}) se obtienen espectrofotométricamente siguiendo el aumento de la absorbancia a 340nm en el tiempo. Para porder expresar la actividad en μmol de NADPH se utiliza un coeficiente de extinción molar (ε) de 5,42 mL μmol^{-1}cm^{-1}. En nuestras condiciones de laboratorio, conseguimos alcanzar la velocidad máxima

de reacción (V_{max}) en la comunidad planctónica con un buffer fosfato 0,1M a pH 8.2 (*pKa*$_1$=7,6 and *pKa*$_2$=8,8), con unas concentraciones en la cubeta de 6mM de $MgCl_2$, 0,3mM de $NADP^+$ y 2mM de isocitrato DL-trisódico.

La afinidad de la NADP-IDH con sus sustratos se obtuvo determinando las constantes aparentes de Michaelis-Menten (*Km*s). A un pH de 8.5 y a 18ºC el *Km* del isocitrato fue 271$\pm$63 μM y el del $NADP^+$, 18$\pm$3 μM.

A partir de la representación de Arrhenius tanto de la actividad de la NADP-IDH proveniente del mesozooplancton como de la proveniente del corazón de cerdo, observamos que la energía de activación (*Ea*) es muy similar (20,4 Kcal mol^{-1} y 21,4 Kcal mol^{-1} respectivamente). Esto indica que, si bien existen diferencias entre los organismos homeotermos o poiquilotermos en cuanto a su óptimo de temperatura, una estructura básica similar, a nivel celular, parece haberse mantenido a lo largo de la evolución de las distintas especies. Asimismo, permite el desarrollo de una ecuación de Arrhenius precisa para la comparación de actividades medidas a distintas temperaturas.

8.4.2   El estudio de la produccion máxima de CO_2 del mesozooplancton a partir de las mediciones de NADP-IDH

Por otra parte, hemos calculado la producción máxima de CO_2 del mesozooplancton teniendo en cuenta otras enzimas productoras de CO_2 y normalizando su actividad por la NADP-IDH. La producción máxima de CO_2 derivada de la NADP-IDH (Ψ_{NADP}) es 2,94·NADP-IDH para muestras mixtas de mesozooplancton.

Durante el desarrollo del modelo de Ψ_{NADP} observamos que no sólo el metabolismo respiratorio, sino también la biosíntesis, afectan a la producción de CO_2. Sin embargo, al analizar el metabolismo respiratorio, observamos que la producción máxima de CO_2 asociada al ciclo de Krebs (Ψ_{NADP} Respiratorio), excede en 1,47 veces el consumo máximo de O_2 asociado al ETS. Esto indica que la estructura enzimática asociada con la oxidación de las moléculas de carbono orgánicos está preparada para superar las demandas del ETS. Esto puede ser una ventaja cuando el organismo tiene una alta demanda de energía. Una vez que se han alcanzado los niveles de energía requeridos, el exceso de NADPH puede ser redirigido hacia la biosíntesis lipídica.

Cuando comparamos Ψ_{NADP} con la tasa de producción de R_{CO2} obtenida a partir de la medición de Φ y su conversión con los distintos ratios publicados en la literatura observamos que en todos los casos Ψ_{NADP} es mayor que R_{CO2}. Este resultado es acorde con el concepto teórico ya que una tasa fisiológica nunca debería superar la capacidad máx-

ima del organismo. Por ello Ψ_{NADP} puede ser considerada la capacidad máxima de producción de CO_2 en la comunidad planctónica marina. De nuestros cálculos en el Atlántico Subtropical Nordeste, estimamos que los ratios R_{CO2}/Ψ_{NADP} para el zooplancton oscilarán entre 0,3 y 0,4, siendo entre 0,2 y 0,3 en una comunidad microplanctónica. Sin embargo, recomendamos medir las tasas R_{CO2} siempre que sea posible y desarrollar los propios R_{CO2}/Ψ_{NADP} específicos para cada región, experimento o situación.

8.4.3 El estudio de la relación entre R_{CO2} and la actividad de la NADP-IDH

Al desarrollar los ratios $R_{CO2}/$NADP-IDH en *L. lingvura* observamos que:

* El estado nutricional en el que se encuentre la comunidad en el momento de muestreo tiene un impacto significativo en la actividad enzimática respiratoria de *L. lingvura*.

* Aunque la actividad de la NADP-IDH fue mayor en la comunidad "bloom" que en la "post-bloom", el ratio $R_{CO2}/$NADP-IDH tuvo unos valores medios de 0,12 en ambas comunidades para aquellos individuos que se encontraban bien alimentados. Durante el periodo de inanición, este valor ascendía levemente hasta 0,16. Debido a estos valores se mantienen en comunidades diferentes, se puede decir que caracterizan la relación entre la respuesta fisiológica y la actividad metabólica de *L. lingvura*.

* Las diferencias entre machos y hembras no reflejaron diferencias significativas ni en las actividades enzimáticas ni en los ratios relacionados con la respuesta fisiológica.

* La inanición durante más de 12h da lugar a un descenso en el ratio R_{O2}/Φ, y a un aumento en el ratio $R_{CO2}/$NADP-IDH. Esto dió lugar a un aumento de los valores del RQ durante la inanición. Nuestra interpretación es que los requerimientos de producción de energía se limitan durante la inanición mientras que la síntesis lipídica y de los sistemas de protección ante moléculas oxidantes se refuerzan.

* La incubación de los misidáceos por más de 12h no permite identificar claramente los efectos de la inanición, ya que se mezclan con la influencia del ritmo circadiano en la producción de CO_2. Para evitarlo, recomendamos incubaciones de entre 4 y 6 horas en los futuros estudios con *L. lingvura*.

8.4.4 La aplicación de una técnica enzimática para el estudio de las variaciones en el estado autotrófico-heterotrófico de la comunidad microplanctónica

La monitorización del ratio Φ/Chl_a durante los cambios metabólicos de una comunidad debidos a la influencia de un afloramiento de aguas profundas cargadas de nutrientes permite concluir lo siguiente:

* Valores de entre 0 y 2,5 $\mu LO_2 h^{-1}$ μg Chl_a^{-1} son los resultantes en una comunidad dominada por fotoautótrofos. Durante el bloom de diatomeas este ratio obtuvo valores inferiores a 1,7. Valores similares se han reportado en la literatura para zonas muy eutróficas o en el máximo de Chl_a de la columna de agua.

* Valores de entre 2,5 y 7,5 $\mu LO_2 h^{-1}$ μg Chl_a^{-1} son valores asociados bien a una comunidad mixta, bien a una comunidad dominada por mixótrofos.

* Valores superiores a 7,5 $\mu LO_2 h^{-1}$ μg Chl_a^{-1}. Son valores relacionados con la proliferación de microzooplancton. Durante el experimento, en el momento en el que los dinoflagelados heterótrofos dominaron la comunidad, se alcanzaron valores de hasta $10 \mu LO_2 h^{-1}$ μg Chl_a^{-1}.

El cálculo de la productividad neta como la primera derivada de la biomasa por tiempo permite identificar este proceso en aquellos casos en los que no existan medidas de fijación de ^{14}C. Asimismo, los valores negativos de este parámetro, permiten cuantificar el resultado neto de la combinación de los ditintos procesos de pérdida de biomasa en el ecosistema.

El uso del análisis integral por fase y mesocosmos de los parámetros oceanográficos Chl_a, Φ y B permite la identificación de los efectos de la acidificación. Se observa una relación positiva claramente significativa entre Φ y pCO_2 en los casos en los que la ausencia de HAS permite la proliferación de la comunidad microzooplantónica. En los casos en los que se produce una proliferación de HAS, la Chl_a también recibe un impacto positivo con el aumento de pCO_2, bien por la reducción del grazing sobre las diatomeas y cianobacterias, bien por la proliferación del sistema fotosintético asociado a las HAS, carente de pirenoide e ineficiente en condiciones de bajo pCO_2.

Appendix A

Appendix A. NADP-IDH assay extended information

A.1 Buffer studies

An enzymatic assay is performed on buffered reaction mixtures containing cofactors and effectors. Here, the optimum combination between buffer and the main cationic effectors (Mg^{2+} or Mn^{2+}) was obtained from ten different experiments that were run at 18°C, pH 8.5, 4mM isocitrate, 0.08mM $NADP^+$ and 2mM $MgCl_2$ on five different concentrations of purified NADP-IDH from porcine heart (I2002, Sigma Aldrich) (zooplankton samples were not used here in order to maintain the same sample conditions in every experiment). Preliminary tests were performed to determine the range of purified NADP-IDH concentrations needed to optimize this study. The response in the enzyme activity was analysed for different combinations of buffer, cationic effector (Kornberg and Pricer (1951); Munilla-Moran and Stark (1989)) and the presence of lysozyme in the homogenisation buffer (Berdalet et al. (1995a)): (1) 25mM MOPS, 2mM $MgCl_2$ and 0.167mg mL^{-1} lysozyme (SIGMA L6876); (2) 25mM MOPS and 2mM $MgCl_2$; (3) 25mM MOPS, 2mM $MnCl_2 \cdot 4H_2O$ (PANREAC 131410) and 0.167mg mL^{-1} lysozyme; (4) 25mM MOPS and 2mM $MnCl_2 \cdot 4H_2O$; (5) 0.1M phosphate buffer, 2mM $MgCl_2$ and 0.167mg mL^{-1} lysozyme; (6) 0.1M phosphate buffer and 2mM $MgCl_2$; (7) 0.1M TRIS 2mM $MgCl_2$ and 0.167mg mL^{-1} lysozyme; (8) 0.1M TRIS and 2mM $MgCl_2$; (9) 0.1M TRIS, 2mM $MnCl_2 \cdot 4H_2O$ and 0.167mg mL^{-1} lysozyme; (10) 0.1M TRIS and 2mM $MnCl_2 \cdot 4H_2O$. Results were based on triplicate measurements. NADP-IDH activity was reported in μmol NADPH min^{-1}(mL of homogenate)$^{-1}$ units.

NADP-IDH activity in phosphate buffer resulted to be 45.88% higher than the next higher activity (in MOPS) for the same dilute enzyme so-

lution in the lowest concentration (the closest to zooplankton samples, 1 μmol NADPH min^{-1} mL^{-1} in the X axis of Fig.A.1). No results for Mn^{2+}-phosphate buffer were obtained because Mn^{2+} reacted with the phosphate to give a Mn$_3$(PO$_4$)$_2$ precipitate, resulting in a competing chemical reaction among the reagents that prevented correct readings of the spectrophotometer. Given the reactivity of Mn^{2+} with phosphate buffer, Mn^{2+} was eliminated and Mg^{2+} was selected as the metal cation for this assay.
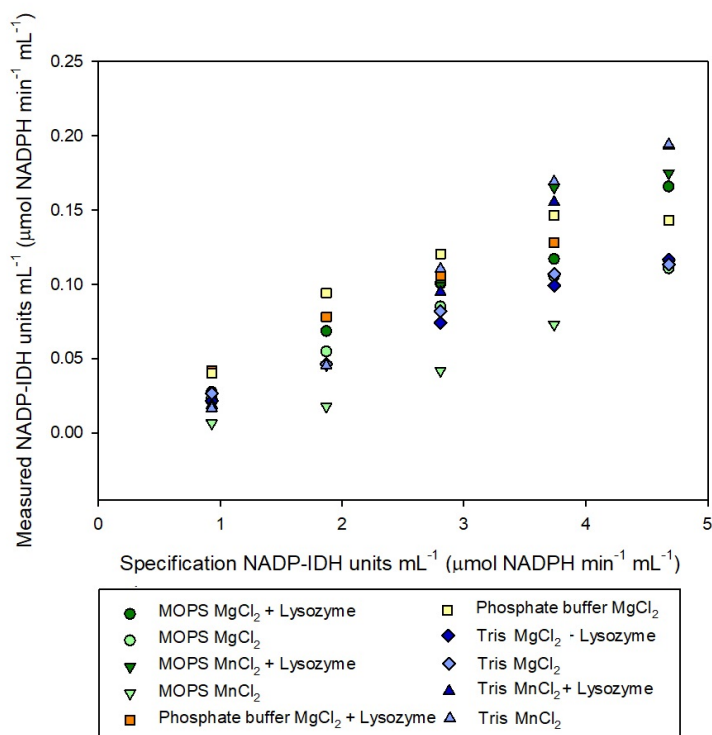
Figure A.1: Buffer effects on NADP-IDH activity

A.2   Molar extinction coefficient (ε) studies

This assay is based on spectrophotometry, the Beer-Lambert law, and the absorbance at 340nm (A_{340}), all of which go to determine the concentration of NADPH (Section 3.2.2). To accomplish this we needed to determine the molar extinction coefficient (ε) for the NADPH in our specific reactant solution. The molar extinction coefficient (ε) is a measurement of the attenuation of light, at a specific wavelength, due

to a molar concentration of the target chemical species. It quantifies the relationship between the light absorbance and the concentration of the chemical species. Thus, ε for the NADPH was analysed at pH 8.5 and 18°C by measuring absorbance at 340nm (A_{340}) under simulated reaction conditions and simulated blank conditions. Ten different concentrations of NADPH, ranging from 0.08 to 40μM, were prepared with three solutions: (1) phosphate buffer 0.1M, 2mM isocitrate and 3.3mM MgCl$_2$; (2) phosphate buffer 0.1M and 3.3mM MgCl$_2$; and (3) only phosphate buffer 0.1M. Results were based on triplicate measurements. The molar extinction coefficient was reported in absortivity units mL μmol^{-1} cm^{-1}.

Reported NADPH ε in the literature is 6.2 L mmol^{-1} cm^{-1} (Morris and Redfearn (1969)), which was measured at pH 7.5 in a solution different from the buffer in our NADP-IDH assay. In our hands, Fig.A.2, the increase of absorbance per mmol L^{-1} of NADPH was similar for the three experiments (5.21 L mmol^{-1} cm^{-1} for the phosphate buffer, 5.35 L mmol^{-1} cm^{-1} for the phosphate buffer with MgCl$_2$ and 5.42 L mmol^{-1}cm^{-1}, for the phosphate buffer with MgCl$_2$ and isocitrate). Our reaction solution is similar to the third buffer, so we will use an ε of 5.42L mmol^{-1} cm^{-1} in our calculations. If we were to use an ε from the literature (6.2 L mmol^{-1} cm^{-1}) we would introduce an error of 12.6%.
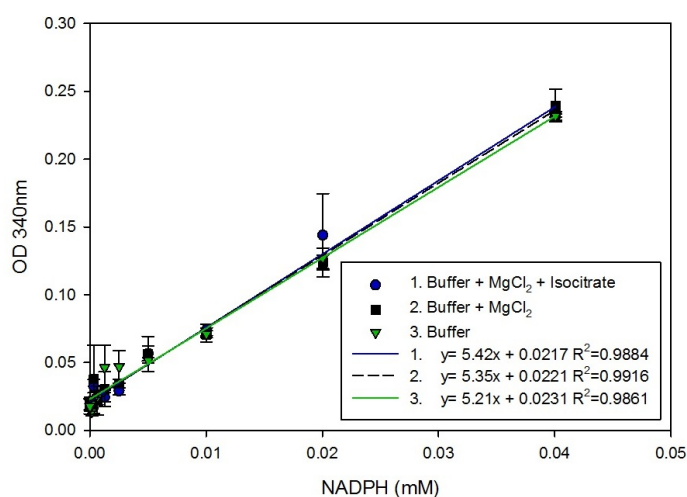
Figure A.2: NADPH molar extinction coefficient, in three different buffer combinations.

Note that the ε increased with the complexity of the buffer solution. So, testing the ε related to product measurements on the solution where re-

action is happening, would be a good practice to reduce error in future measurements.

A.3   Kinetics

The NADP-IDH activity related to the substrate concentration showed a rectangular hyperbolic relationship for isocitrate, $NADP^+$ and $MgCl_2$, following the expression represented in Eq.A.1.

$\%V_{max}=a\cdot[S]/(y_0+[S])$ (A.1)

The values of "a" which represents the V_{max} (in this case, the $\%$ of V_{max}); and "y_0", which represents the K_m, are shown in Table A.1.

Table A.1: Michaelis-Menten hyperbolic curves for isocitrate, $NADP^+$ and $MgCl_2$ affinity in marine plankton samples. K_m is in mM units. For isocitrate, V_{max}=0.038 in mesozooplankton; 0.031 in microzooplankton; and 0.002 in microplankton. For $NADP^+$, V_{max}=0.029 in mesozooplankton; 0.019 in microzooplankton; and 0.001 in microplankton. For $MgCl_2$, V_{max}=0.010 in mesozooplankton; 0.009 in microzooplankton; and 0.00002 in microplankton. V_{max} is in μmol NADPH min^{-1} (mL homogenate)$^{-1}$ units.

Size-fractionated sample / Substrate	a ($\%V_{max}$)	y_0 (K_m)	r^2	p-value
Mesozooplankton / isocitrate	109.34	0.225	0.987	<0.0001
Microzooplankton / isocitrate	109.25	0.270	0.985	<0.0001
Microplankton / isocitrate	96.99	0.203	0.962	<0.0001
Average values for isocitrate	105.20	0.232±0.034	NA	NA
Mesozooplankton / $NADP^+$	102.75	0.024	0.926	<0.0001
Microzooplankton / $NADP^+$	93.45	0.023	0.930	0.0001
Microplankton / $NADP^+$	96.83	0.020	0.981	<0.0001
Average values for $NADP^+$	97.68	0.022±0.007	NA	NA
Mesozooplankton / $MgCl_2$	142.94	2.189	0.976	0.0135
Microzooplankton / $MgCl_2$	133.70	2.198	0.968	0.0243
Microplankton / $MgCl_2$	106.11	2.542	0.930	0.0395
Average values for $MgCl_2$	127.58	2.310±0.201	NA	NA

NADP-IDH dependences on isocitrate were not significantly different among these samples (F test, $F_{(4,63)}$=1.73, p=0.01). On the other hand, dependence on $NADP^+$ showed significant differences among the three size-fractions (F test, $F_{(4,69)}$=6.85, p=0.01). Even though the regressions were different, the average K_m and optimum values in both experiments can be properly used in our assay in order to obtain the V_{max} for the whole plankton community. Furthermore, although there are significant differences in the NADP-IDH and $MgCl_2$ affinity among

the samples (F test, $F_{(4,114)}$=2.75, p=0.01), the optimal value obtained by inspection of Fig.2.1, can be properly used for our assay in order to obtain the V_{max} for the whole plankton community (6mM $MgCL_2$ for the whole community).

We applied three main linearisation techniques to evaluate the K_ms of isocitrate, $NADP^+$ and $MgCl_2$. In the Hanes-Woolf linearisation, substrate concentration [S] was plotted against concentration per enzymatic activity ([S]/V). The V_{max} was obtained from the inverse of the slope (a) (V_{max} = 1/a), whereas K_ms were equal to the ratio of the Y intercept (y_0) and a (K_m = y_0/a) (Suelter et al. (1985)). In the case of the Lineweaver-Burk method, the inverse of the substrate (1/[S]) was plotted against the inverse of the activity (1/V), so the V_{max} was the inverse of y_0 (V_{max}=1/y_0) and K_m = a/y_0. Finally, using the Eadie-Hofstee methodology we plotted V/[S] against V, where the V_{max} = y_0 and K_m =-y_0/a. K_m was reported in mmol of substrate, and V_{max} in μmol NADPH min^{-1}(mL of homogenate)$^{-1}$ units (Suelter et al. (1985)).
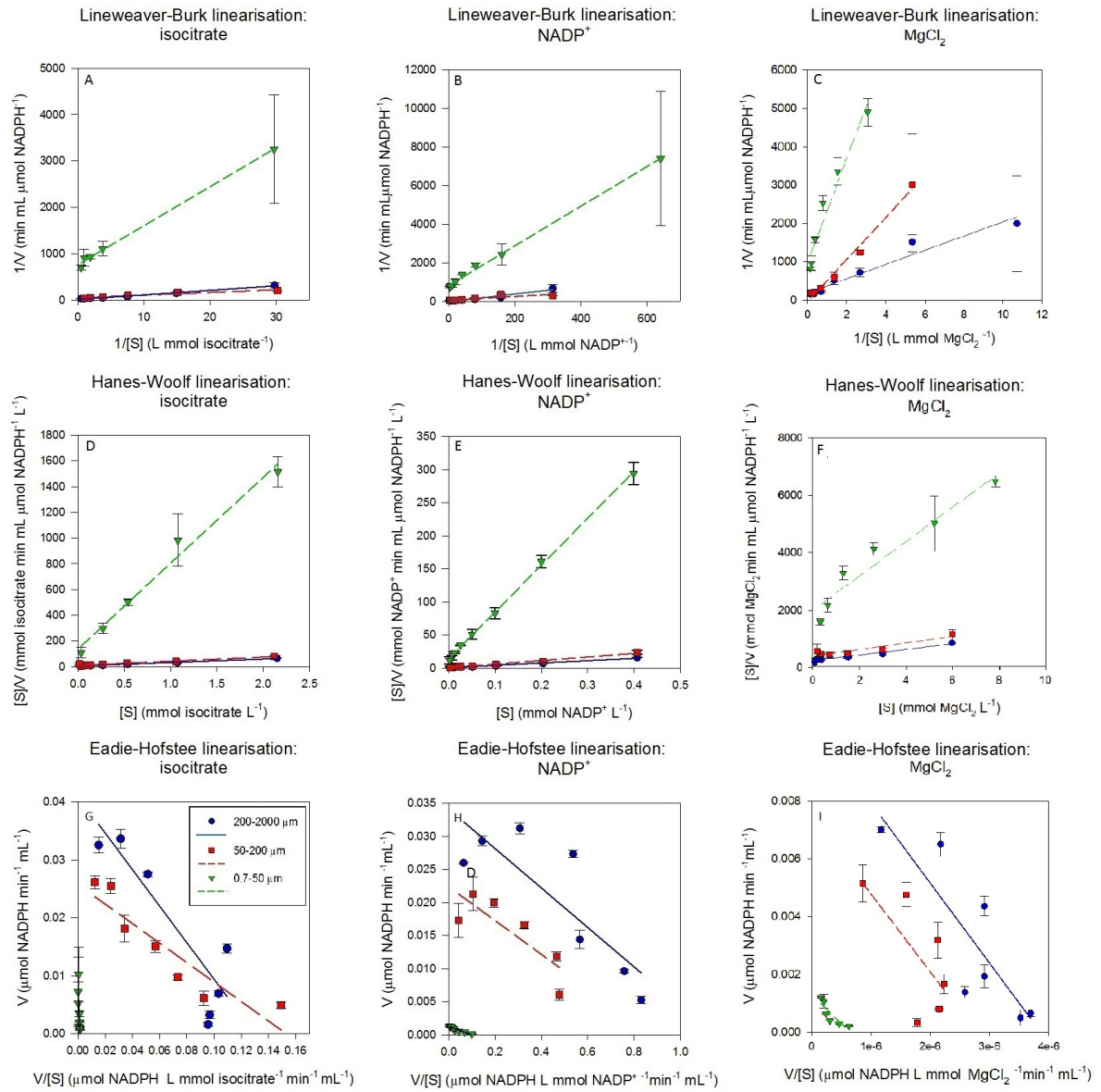
Figure A.3: Hanes-Woolf, Lineweaver-Burk and Eadie-Hofstee linearisations to determine the affinity (K_m) of NADP-IDH for isocitrate, NADP$^+$ and MgCl$_2$ in marine-plankton samples. The symbols in the key of panel G apply to all six panels.

Finally, Hanes-Woolf linearisation was the most accurate to our data base for both isocitrate, NADP $^+$ and MgCl$_2$ (p<0.01). The apparent Kms of 271$\pm$63μM of isocitrate, 18$\pm$3μM of NADP$^+$ and 3060$\pm$643μM of MgCl$_2$ are consistent with those obtained by Michaelis-Menten hyperbolic regressions.

A.4   pH effects

Michaelis-Menten constants are affected by pH levels that impact ionisation around the enzyme active site. Thus, the conformations of the active site, the binding of substrate to the enzyme, and/or the transformation from substrates to products may be altered. This ionisation is sensitive to the chemical solution, shifting the pK_a values in relation to the nature of the buffer solution (Whitaker (1993)). Although we have not checked the K_ms for every pH condition, during the pH experiments we maintained concentrations of isocitrate and NADP$^+$ high enough to broadly saturate the enzyme at pH 8.5, assuming the V$_{max}$ was reached at every experimental pH level. Finally, a pH of 8.2 (Fig.2.2) resulted to be the marine NADP-IDH optimum, with pK_as at 7.62 and 8.75. For Fig.2.2, results were normalised by V$_{max}$ and reported as a percentage.

A.5   Temperature effects: Development of the Arrhenius equation

Another reason for determining the Arrhenius relationship between NADP-IDH activity and T, is to correct measurements when environmental T is different from the measurement T. If plankton samples were assayed at the in-situ T from a low temperature environment, there is a risk that the NADP-IDH signal would fall below the limit of detection. Accordingly, enzyme activities are measured at T above the in-situ one (Packard (1971)) and converted back to the activity at in-situ T using the Arrhenius equation (Fig.2.3) (Packard (1971)). This equation is equivalent to Van,t Hoff equation (Atkin and de Paula (2006)), as expressed on Eq.A.2, A.3 and A.4:

$\ln(K_2/K_1) = (Ea/R)\cdot((1/T_1)-(1/T_2))$ (A.2)

Taking anti-logarithms we obtained the ratio of the rate constants:

$K_2/K_1 = \exp((Ea/R)\cdot((1/T_1)-(1/T_2)))$ (A.3)

Then, we transposed to solve for the in-situ rate:

$$K_2 = K_1 \cdot exp((Ea/R) \cdot ((1/T_1) - (1/T_2))) \quad (A.4)$$

where: K_2 is the in-situ reaction rate and K_1 is the measured reaction rate at T_2 (in-situ T) and T_1 (measurement T) respectively, in μmol NADPH min^{-1} mL^{-1}; Ea is the energy of activation in Kcal mol^{-1}; R is the molar gas constant in Kcal mol^{-1} $^{\circ}$K^{-1}; and T_1 and T_2 are temperatures in $^{\circ}$K.

In the case of the marine plankton NADP-IDH, with an Ea of 20.39 Kcal mol^{-1} NADP-IDH activity for the in-situ T (T_i) is obtained by applying Eq.A.5:

$$NADP\text{-}IDH(T_i) = NADP\text{-}IDH(T_m) \cdot exp((20.39/R) \cdot (1/T_m - 1/T_i)) \quad (A.5)$$

where: NADP-IDH(T_i) is NADP-IDH activity at in-situ temperature; NADP-IDH(T_m) is NADP-IDH activity at temperature in the spectrophotometric cuvette during measurement; R is $1.9872 \cdot 10^{-3}$ Kcal mol^{-1} $^{\circ}$K^{-1}; T_m is temperature in the spectrophotometric cuvette during measurement in $^{\circ}$K; and T_i in-situ temperature in $^{\circ}$K.

A.6   Precision studies

The precision of this assay was tested on four different solutions of porcine heart NADP-IDH (I2002, Sigma Aldrich). These solutions where made by diluting the original solution (93.6units of NADP-IDH mL^{-1}), resulting in four solutions which ranged from 0.0004 to 0.25 units of NADP-IDH mL^{-1} which were reported in specification units (*UsIDH*, *i.e.*, μmol NADPH min^{-1} (mL of homogenate)$^{-1}$). Ten duplicates were used for every solution. Note that one unit (U) of enzyme activity was defined as the amount of sample able to catalyse the production of 1μmol NADPH in 1 min.

Precision was scaled by using the standard deviation with the optimum pH and ligands from previous experiments (pH 8.2, 6mM MgCl$_2$, 2.1mM isocitrate and 0.2mM NADP$^+$). The measurement was made at 37.5ºC for comparison with the theoretical characteristics of pure porcine heart NADP-IDH (specification sheet I2002 by Sigma Aldrich). Results were tested in ten samples for every solution and reported as measured units (*UmIDH*), in μmol NADPH min^{-1} (mL of homogenate)$^{-1}$.

The average standard deviation was 1.2nmol NADPH min^{-1}, ranging from 0.6nmol in the two lower values, to 2nmol NADPH min^{-1} in the most concentrated ones (Fig.A.4). On a percentage basis, except for the lowest value, where it represented 25% of the sample value, the standard deviation was less than 3.5% for the samples with more than 25nmol NADPH min^{-1}, dropping to 1.73% for the highest concentration (Fig.A.4).

Using our new NADP-IDH assay we also measured the activity of the Sigma-Aldrich porcine-heart NADP-IDH. We used the same pH and T as those specified in the Sigma-Aldrich specification sheet (pH=7.4; T=37.5ºC), and found 39.3% of the theoretical activity (Fig.A.4). When we measured the activity at pH 8.2 (optimum value in Fig.2.2) we found 48.2% (Fig.A.4) of the theoretical activity. The use of pure-porcine NADP-IDH activity to normalise the method is useful to compare with other samples, organisms and methodologies. In our hands, one unit (μmol NADPH min^{-1}) of NADP-IDH activity in marine plankton homogenates, was equivalent to 2.08 pure porcine-heart NADP-IDH units, by applying the equation obtained from Fig.A.4 and Eq.A.6. This equation pertains to the optimum conditions of our new NADP-IDH method:

UmIDH=0.48 · UsIDH + 0.0029 (A.6)

where *UmIDH* refers to NADP-IDH activity units as measured by the new method, and *UsIDH* refers to the specification NADP-IDH activity
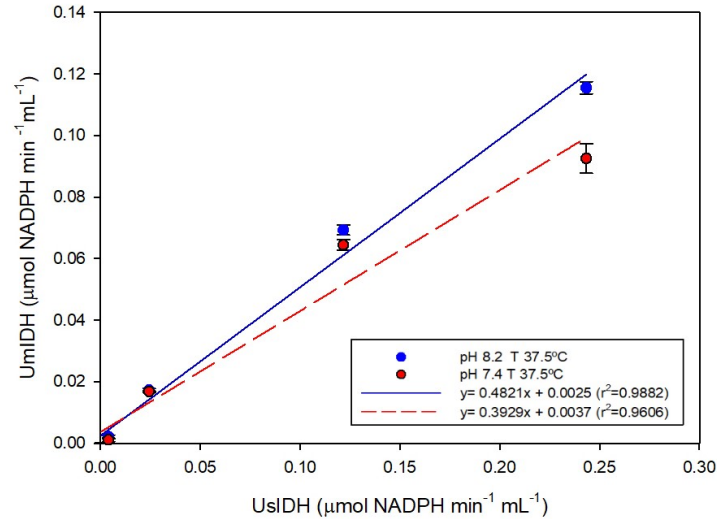
Figure A.4: Porcine-heart NADP-IDH activity measured by the marine-plankton NADP-IDH assay at pH:8.2 and pH:7.4

units as calculated for the pure porcine-heart NADP-IDH solutions.

In the linear range of Fig.A.4, which describes the increase in NADP-IDH activity as a function of enzyme concentration, it is clear that the substrate concentrations are sufficient to maintain maximum activity until 0.25 *UsIDH* units of NADP-IDH (which represents a measured value of 0.12UmIDH with our methodology). Samples from the Canary Islands plankton never reached such a high value, so they were always in the linear range. For future plankton samples, if a pilot test were to show activity above 0.12 *UmIDH* μmol NADPH min^{-1}mL^{-1}, the homogenate would need dilution.

A.7 Understanding changes in the NADP-IDH spectrophotometrical response

A linear A_{340} increasing (Fig.A.5(A)) is expected when NADP-IDH is catalysing the reaction at V$_{max}$. However, in marine plankton samples, some conditions may change this linearity as follows:

1 Low Biomass samples (Fig.A.5(B)). Under these conditions, the rate of NADPH formation is low, and the signal was not detectable for the first 500s. The NADP-IDH activity, in this case, is under the limit of detection. If more biomass is not available, sensitivity can be obtained by raising the reaction temperature to 30°C and

applying the Arrhenius equation to correct the activity to that of the in-situ T (Eq. 17).

2 T effects (Fig.A.5(C)). Depending on the difference between the laboratory T and the spectrophotometer read-out T, the reaction temperature will lag until thermal equilibrium is reached in the cuvette. We monitored T in the cuvette over time and for 8 to 46°C range, and found that steady-state was reached after 450s. We suggest that enzyme activity measurements should be made only after this lag-period (7.5 min). If the plateau zone is reached within the first 500s, the cuvette might not have reached the equilibrium T. In this case, we suggest repeating the measurement with a diluted sample. Given the importance of T and all the problems with maintaining it in the cuvette, we also suggest measuring T in the cuvette at the end of the reaction.

3 High Biomass samples (Fig.A.5(D)). The optimum values for NADP-IDH substrates reported on this study have proved to work well for the biomass levels found in plankton samples around the Canary Islands archipelago. Eventually, the reagents are completely consumed when the A_{340} reaches 0.8. After that point, the reaction becomes non-linear, underestimating the V_{max}.

4 Blank effects (Fig.A.5(E)). Working with natural homogenates, instead of pure enzyme extracts, rises interference from other enzymes oxidizing the produced NADPH. Although this effect is not usually significant because these enzymes are not supplied with their other substrates, eventually, some samples will produce negative blanks that could significantly increase the results. Particle sinking in the cuvette due to low centrifugation may also affect the measurements in this way (Section 3.5). To minimise the sedimentation effect we recommend centrifugation (at least 2 min at 1000rpm for zooplankton samples, or 10min at 4000rpm for microplankton samples collected on 0.7GF/F filters). If the condition persists, even after the centrifugation, and the blank remains negative, a background reaction is likely real and has to be taken into account.

During the T and pH experiments, great differences in the slopes (the velocity of the reaction) at different levels of T or pH were observed (Fig. A.6) Higher slopes were observed near the optimum values. Temperatures shown in Fig. A.6 represent final T in the cuvette. When this temperature was close to the temperature of the lab (around 21°C), we obtained the same slope for 1500s, throughout the measurement. However, when the reaction temperatures were far from the laboratory T, time was needed for the cuvette to reach thermal equilibrium. As said before, we have observed that 500s ensures a good measurement at the
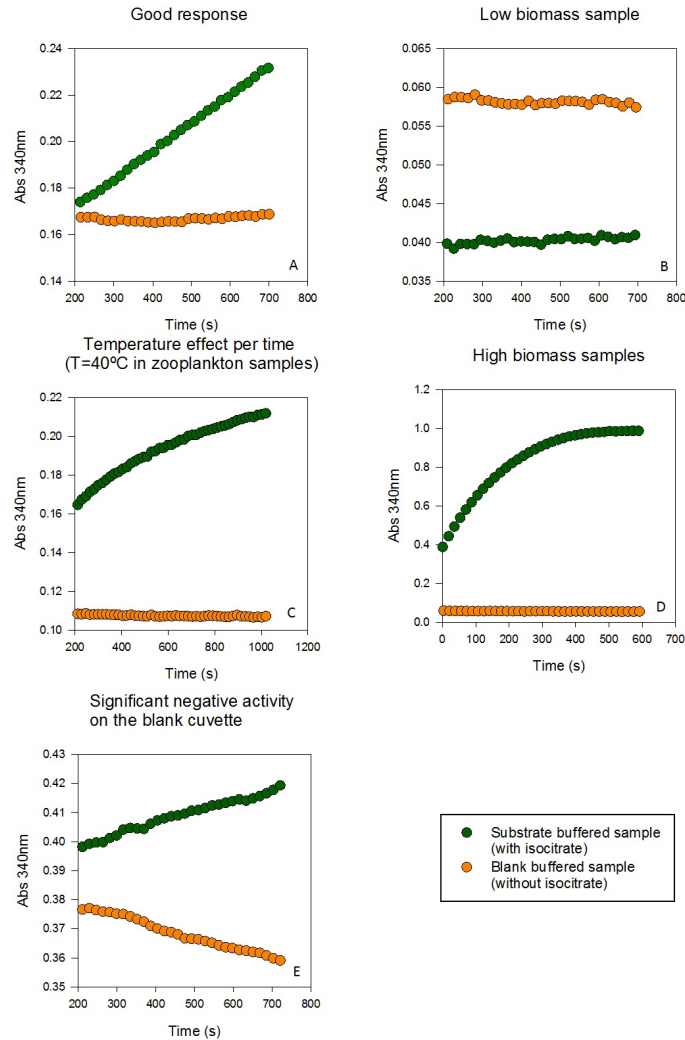
Figure A.5: Spectrophotometrical response of NADP-IDH activity, following the A_{340} per time of the substrate and blank buffered cuvettes, under conditions that affect the signal during the measurement

selected temperature. Furthermore, when T higher than 30ºC is used, denaturation of the enzyme becomes a factor that needs to be considered (Fig.A.6(a)).

Thus, cuvette temperature should be measured before the assay is initiated, to make sure that the target temperature has been reached after the cuvette has been placed into the thermostatted cell holder of the

spectrophotometer.
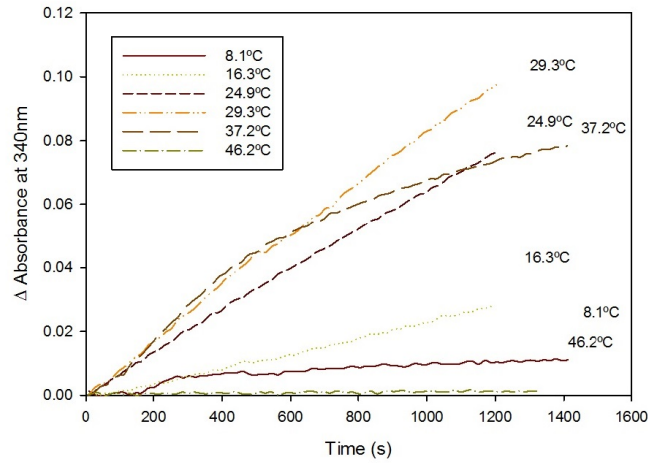
[a]
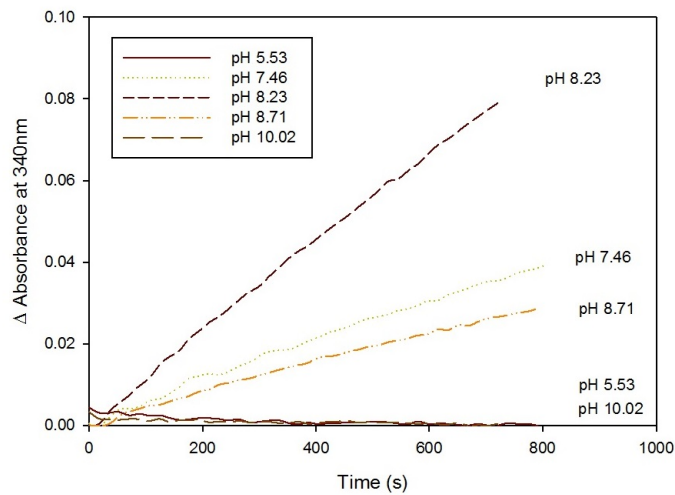
[b]

Figure A.6: Kinetic responses of NADP-IDH to different levels of T and pH. (a) Temperature effects on NADP-IDH activity by the kinetic assay. (b) pH effects on NADP-IDH activity by the kinetic assay.

Appendix B

Appendix B. NADP-IDH thermodynamic factors

The thermodynamic parameters were calculated applying the equations of Arrhenius, Eyring and Low *et al.* (1973) Arrhenius (1889); Laidler (1984); Eyring (1935); Dixon and Webb (1979); Low et al. (1973). The Arrhenius equation describes the dependence of the rate of a chemical reaction on the absolute temperature, as expressed in Eq.B.1 Arrhenius (1889):

$k_{IDH}{=}A{\cdot}exp(-E_a/(R{\cdot}T))$(B.1)

where: k_{IDH} is the NADP-IDH activity related to the temperature in mol NADPH s^{-1}(kg of protein)$^{-1}$; A is the preexponential frequency factor, a unique value, in mol NADPH s^{-1}(kg of protein)$^{-1}$, for each chemical reaction defined by the rate due to collision frequency when reactants are in the correct orientation; Ea is the energy of activation in Kcal mol^{-1}; T is the absolute temperature in ^{o}K and R is the universal molar gas constant in Kcal mol^{-1} ^{o}K^{-1} (1.9872$\cdot$ 10^{-3} Kcal mol^{-1} ^{o}K^{-1}). The Ea and A were obtained from the Arrhenius plot (Fig. 2.3), where the ln(k_{IDH}) is plotted against 1/T and T is in 10^{-3} ^{o}K units. Eq.B.2 describes the linear regression from this Arrhenius plot (y=a$\cdot$x +y$_0$), where x is 1/T and y$_0$ is ln(k_{IDH}):

ln(k_{IDH})=ln(A)-(E_a/R)$\cdot$(1/T)(B.2)

E_a is related to the slope (a) of this linear regression, so a=-E_a/R. A is obtained from the intercept on the y axis (y$_0$=ln(A)). The enthalpy of activation (ΔH^*), in Kcal mol^{-1}, was calculated from the E_a as represented on Eq.B.3 Low et al. (1973):

$\Delta H^*{=}E_a$-$R{\cdot}$T (B.3)

Here, R is 1.9872$\cdot$10^{-3} Kcal mol^{-1} ^{o}K^{-1}, as above, and T is the stan-

dard temperature of 25°C, expressed in °K (298°K).

ΔH^* also was obtained by combining the definition of Gibbs free energy (ΔG^*) (Eq.B.4) and the Eyring equation Eyring (1935); Dixon and Webb (1979) (Eq.B.5), resulting in Eq.B.6 and B.7:

$$\Delta G^* = \Delta H^* - T \cdot \Delta S^* \quad \text{(B.4)}$$

$$k_{IDH} = (N_A \cdot k_B \cdot T / N_A \cdot h) \cdot \exp(-\Delta G^*/(R \cdot T)) \quad \text{(B.5)}$$

$$k_{IDH}/T = (k_B/h) \cdot \exp(-\Delta H^*/(R \cdot T)) \cdot \exp(\Delta S^*/R) \quad \text{(B.6)}$$

$$\ln(k_{IDH}/T) = \ln(k_B/h) + (\Delta S^*/R) - (\Delta H^*/R) \cdot (1/T) \quad \text{(B.7)}$$

where: k_{IDH} is the NADP-IDH activity related to the temperature in mol NADPH s^{-1}(kg of protein)$^{-1}$; T in °K; k_B is the Boltzman constant in cal °K^{-1} (3.29·10^{-27} cal °K^{-1}); h is the Planck constant in cal s (1.58·10^{-37} cal s). Note that these two constants are atomic constants. Thus, in order to transform them into the molar scale, both have been multiplied by Avogadro's number (N_A) in Eq.B.5. ΔG^* is the Gibbs free energy at standard conditions in Kcal mol^{-1}, ΔH^* is the enthalpy of activation at standard conditions in Kcal mol^{-1} and ΔS^* is the entropy of activation at standard conditions in Kcal mol^{-1} °K^{-1}. ΔH^* is related to the slope (a) of this linear regression, so a=$-\Delta H^*/R$, and ΔS^* is obtained from the intercept on the y axis ($y_0 = \ln(k_B/h) + \Delta S^*/R$).

For comparison, ΔG^*, ΔH^* and ΔS^* were also calculated from the expressions reported by Low *et al.* (1973) represented in Eq.B.3, B.4 and B.8 Low et al. (1973). As the molecular weight of the enzyme NADP-IDH was needed for this method, these expressions were only applied to pure NADP-IDH from porcine heart (I2002, Sigma Aldrich), with a molecular weight (MW) of 57800 g mol^{-1} (60KDa Dixon and Webb (1979)). We calculated the ΔG^* from Eq.B.4. To do that, we also obtained ΔH^* from Eq.B.3, and ΔS^*, from Eq.B.8:

$$\Delta S^* = 4.576 \cdot (log(k_{IDH}) - 10.753 - log(T) + Ea/(4.576 \cdot T))(\text{B.8})$$

For this expression $k_{IDH} = NADP\text{-}IDH*MW$, where *NADP-IDH* is the NADP-IDH activity in mol NADPH s^{-1}(kg of protein)$^{-1}$ units, and MW is the NADP-IDH molecular weight in kg mol^{-1} units, so k_{IDH} is in s^{-1}.

Note that the results related to energy are reported in cal. To convert to Joules (J), multiply the result by 4.184 J cal^{-1}. Furthermore, all the constants used here are in molar units instead of atomic units, in order to be consistent with most of the chemical, biochemical and biological research since Arrhenius (1915) Arrhenius et al. (1915). Furthermore, molar units are more appropriate for all scientific fields other

than atomic physics Feynman et al. (2011). This is because all these fields deal with large numbers of atoms or molecules in the range of Avogadro´s number ($6.02 \cdot 10^{23}$), i.e. molar quantities, whose chemical characteristics reflect their means described by Boltzmann distribution function Eggers Jr et al. (1964); Moore (1972). We chose not to use the atomic units of electron-volts because all of our measurements are made on a molar-scale.

The thermodynamic factors related to the NADP-IDH activity were calculated for both zooplankton and porcine heart NADP-IDH. The energy of activation (*Ea*), the frequency factor (*A*), the enthalpy of activation at 25ºC (ΔH^*), the entropy of activation at 25ºC (ΔH^*) and the Gibbs free energy (ΔG^*), calculated by the Arrhenius, Eyring, and Low *et. al* methodology when possible Arrhenius et al. (1915); Eyring (1935); Low et al. (1973), are reported in Table B.1.

Table B.1: NADP-IDH thermodynamic factors.

Sample origin	Marine Plankton	Porcine Heart
Ea Arrhenius (Kcal mol^{-1})	20.40	21.40
A Arrhenius (mol NADPH s^{-1} (kg of protein)$^{-1}$)	$2.19 \cdot 10^{11}$	$1.60 \cdot 10^{13}$
ΔH^* Arrhenius (Kcal mol^{-1})	19.81	20.76
ΔH^* Eyring (Kcal mol^{-1})	19.88	20.76
ΔS^* Eyring (Kcal mol^{-1} K^{-1})	$-8.59 \cdot 10^{-3}$	$-8.74 \cdot 10^{-5}$
ΔG^* Eyring (Kcal mol^{-1})	22.44	20.79
ΔS^* Low *et al.* (Kcal mol^{-1} K^{-1})	Not Available	7.97 ± 0.19
ΔG^* Low *et al.* (Kcal mol^{-1})	Not Available	18.39 ± 0.06

F test and an independent *t* test were conducted to compare the Arrhenius *Ea* and ΔH^* between poikilothermic (marine plankton) and homoeothermic (porcine heart) organism samples. Although linear regressions were significantly different (*F* test, $F_{(2,37)} = 4.64$, $p = 0.05$), there was not a significant difference between the regression coefficients (*t* test, $t(39) = 0.0773$, $p = 0.05$). These results suggested that, for NADP-IDH, although the frequency factor (*A*) was different, the Energy of activation (*Ea*) and the other thermodynamic factors derived from it (ΔH^*, ΔS^*, ΔG^*) were not significantly different between the

two types of organisms.

Appendix C

Appendix C. *Leptomysis lingvura* dataset

Table C.1: Respiratory rates measured in a bloom community of *L. lingvura*. Note that both NADP-IDH and CO_2 production rates (R_{CO2}) are expressed in μmolCO$_2$ h^{-1} mg protein^{-1} units.

Bloom Community (2017)				R_{CO2}	NADP-IDH
Incubation	Sex	Starvation	Triplicate		
4 h	Females	Well-Fed	1	0.160	1.815
4 h	Females	Well-Fed	2	0.404	1.928
4 h	Females	Well-Fed	3	0.308	2.095
8 h	Females	Well-Fed	1	0.165	1.933
8 h	Females	Well-Fed	2	0.301	1.977
8 h	Females	Well-Fed	3	0.235	1.995
12 h	Females	Well-Fed	1	0.340	2.108
12 h	Females	Well-Fed	2	0.244	2.123
12 h	Females	Well-Fed	3	0.247	2.148
16 h	Females	Well-Fed	1	0.205	2.665
16 h	Females	Well-Fed	2		
16 h	Females	Well-Fed	3	0.256	2.830
24 h	Females	Well-Fed	1	0.208	2.813
24 h	Females	Well-Fed	2	0.179	2.147
24 h	Females	Well-Fed	3	0.150	1.992

Table C.2: Respiratory rates measured in a post-bloom community of *L. lingvura*. Note that both NADP-IDH and CO_2 production rates (R_{CO2}) are expressed in $\mu molCO_2$ h^{-1} mg protein^{-1} units; and both Φ and O_2 consumption rates (R_{O2}) are expressed in $\mu molO_2$ h^{-1} mg protein^{-1} units.

Post-Bloom Community (2018)				R_{CO2}	NADP-IDH	R_{O2}	Φ
Incubation	Sex	Starvation	Triplicate				
1-O_2	Females	Well-Fed	1		0.862	0.187	0.447
1-O_2	Females	Well-Fed	2		0.972	0.179	0.531
1-O_2	Females	Well-Fed	3		0.735	0.157	0.486
1-CO_2	Females	Well-Fed	1	0.073	1.310		0.754
1-CO_2	Females	Well-Fed	2	0.143	0.996		0.687
1-CO_2	Females	Well-Fed	3	0.128	0.934		0.604
2-O_2	Females	Starved	1		0.955	0.159	0.388
2-O_2	Females	Starved	2		0.979	0.133	0.594
2-O_2	Females	Starved	3		0.921	0.124	0.624
2-CO_2	Females	Starved	1	0.132	0.791		0.525
2-CO_2	Females	Starved	2		1.217		0.534
2-CO_2	Females	Starved	3	0.135	1.009		0.610
3-O_2	Males	Well-Fed	1		1.220	0.256	0.571
3-O_2	Males	Well-Fed	2		0.888	0.224	0.876
3-O_2	Males	Well-Fed	3		1.085	0.193	0.638
3-CO_2	Males	Well-Fed	1	0.104	1.078		0.573
3-CO_2	Males	Well-Fed	2	0.094	0.927		0.774
3-CO_2	Males	Well-Fed	3	0.160	0.910		0.781
4-O_2	Males	Non-starved	1		0.734	0.143	0.536
4-O_2	Males	Non-starved	2		0.543	0.134	0.641
4-O_2	Males	Non-starved	3		0.915	0.146	0.428
4-CO_2	Males	Non-starved	1	0.202	0.798		0.596
4-CO_2	Males	Non-starved	2	0.081	0.960		0.627
4-CO_2	Males	Non-starved	3	0.171	1.032		0.633

Appendix D

Appendix D. KOSMOS GC 2014 Main dataset

Table D.1: Potential respiration (Φ) during the Oligotrophic phase (Phase I) in the KOSMOS GC 2014 experiment. Mesocosms have been classified as Low, Intermediate or High depending on the pCO$_2$ levels of the treatment. Note that Φ is expressed in μLO$_2$h^{-1}L^{-1} units. To convert to "per protein" units, use the data on table D.4.

Φ		I: Oligotrophic phase (day)							
Treatment	Mesocosm	-3	-1	3	7	11	15	19	23
Low	M1	0.595	0.477	0.641	0.644	1.023	0.543	0.660	0.496
High	M2	0.460	0.369	0.852	0.339	0.362	0.656	0.780	0.675
Intermediate	M3	0.347	0.513	0.467	0.678	0.680	0.599	0.774	0.711
Intermediate	M4	0.438	0.470	0.452	0.589	0.509	0.526	0.720	0.674
Low	M5	0.381	0.440	0.716	0.640	0.706	0.328	0.780	0.697
Intermediate	M7	0.318	0.302	0.486	0.598	0.486	0.328	0.674	0.713
High	M8	0.427	0.486	0.396	0.736	0.650	0.273	0.734	0.756
Low	M9	0.440	0.601	0.418	0.186	0.497	0.340	0.768	0.601
Atlantic	Atlantic	0.350	0.302	0.440	0.272	0.273	0.215	0.267	0.314

Table D.2: Potential respiration (Φ) during the Bloom phase (Phase II) in the KOSMOS GC 2014 experiment. Mesocosms have been classified as Low, Intermediate or High depending on the pCO_2 levels of the treatment. Note that Φ is expressed in $\mu L O_2 h^{-1} L^{-1}$ units. To convert to "per protein" units, use the data on table D.5.

Φ		II: Bloom Phase (day)				
Treatment	Mesocosm	26	28	30	32	35
Low	M1	2.483	3.529	1.285	1.496	2.167
High	M2	2.392	1.043	1.490	2.254	5.174
Intermediate	M3	2.766	2.107	1.622	4.708	3.515
Intermediate	M4	2.190	5.044	2.398	6.194	5.845
Low	M5	2.724	4.254	0.855	1.229	2.683
Intermediate	M7	2.373	4.652	2.197	2.779	4.220
High	M8	2.631	4.494	1.257	5.136	6.321
Low	M9	2.477	3.733	0.152	0.441	3.277
Atlantic	Atlantic	0.467	0.388	0.234	0.465	0.565

Table D.3: Potential respiration (Φ) during the Post-bloom phase (Phase III) in the KOSMOS GC 2014 experiment. Mesocosms have been classified as Low, Intermediate or High depending on the pCO_2 levels of the treatment. Note that Φ is expressed in $\mu L O_2 h^{-1} L^{-1}$ units. To convert to "per protein" units, use the data on table D.6.

Φ		III: Post-bloom Phase (day)				
Treatment	Mesocosm	39	43	47	51	55
Low	M1	1.691	1.995	2.214	1.659	2.419
High	M2	4.573	3.371	2.032	1.524	3.837
Intermediate	M3	1.692	1.647	1.409	2.658	3.071
Intermediate	M4	4.189	1.657	1.811	2.048	1.443
Low	M5	2.548	2.146	2.339	3.146	0.408
Intermediate	M7	4.080	1.952	2.793	3.100	1.736
High	M8	4.672	3.331	2.309	1.926	2.377
Low	M9	4.001	2.548	2.606	2.257	3.506
Atlantic	Atlantic	0.328	0.459	0.711	0.631	1.978

Table D.4: Biomass (B) during the Oligotrophic phase (Phase I) in the KOSMOS GC 2014 experiment. Mesocosms have been classified as Low, Intermediate or High depending on the pCO_2 levels of the treatment. Note that B is expressed in mg protein L^{-1} units.

B		I: Oligotrophic phase (day)							
Treatment	Mesocosm	-3	-1	3	7	11	15	19	23
Low	M1	0.027	0.012	0.018	0.006	0.005	0.007	0.021	0.031
High	M2	0.022	0.009	0.011	0.008	0.010	0.013	0.017	0.023
Intermediate	M3	0.025			0.008	0.009	0.015	0.013	0.018
Intermediate	M4	0.021	0.013		0.009	0.014	0.010	0.005	0.019
Low	M5	0.026	0.005	0.012	0.005		0.006	0.013	0.024
Intermediate	M7	0.014	0.004	0.002	0.009		0.006	0.008	0.023
High	M8	0.022		0.009	0.018	0.014		0.013	0.017
Low	M9	0.019	0.006	0.003		0.006	0.003	0.012	0.016
Atlantic	Atlantic	0.018	0.007	0.022	0.005	0.006	0.005	0.009	0.023

Table D.5: Biomass (B) during the Bloom phase (Phase II) in the KOSMOS GC 2014 experiment. Mesocosms have been classified as Low, Intermediate or High depending on the pCO_2 levels of the treatment. Note that B is expressed in mg protein L^{-1} units.

B		II: Bloom Phase (day)				
Treatment	Mesocosm	26	28	30	32	35
Low	M1	0.029	0.079	0.079	0.047	0.050
High	M2	0.079	0.163	0.158	0.146	0.067
Intermediate	M3	0.054	0.096	0.134	0.103	0.091
Intermediate	M4	0.040	0.101	0.170	0.161	0.078
Low	M5	0.024	0.140	0.162	0.141	0.089
Intermediate	M7	0.042	0.082	0.159	0.096	0.111
High	M8	0.040	0.116	0.201	0.195	0.154
Low	M9	0.054	0.165	0.192	0.124	0.099
Atlantic	Atlantic	0.016	0.032	0.030	0.009	0.010

Table D.6: Biomass (B) during the Post-bloom phase (Phase III) in the KOSMOS GC 2014 experiment. Mesocosms have been classified as Low, Intermediate or High depending on the pCO_2 levels of the treatment. Note that B is expressed in mg protein L^{-1} units.

B		III: Post-bloom Phase (day)				
Treatment	Mesocosm	39	43	47	51	55
Low	M1	0.038	0.063	0.034	0.030	0.049
High	M2	0.071	0.094	0.044	0.066	0.095
Intermediate	M3	0.042	0.035	0.041	0.026	0.043
Intermediate	M4	0.107	0.041	0.023	0.072	0.045
Low	M5	0.087	0.026	0.067	0.095	0.055
Intermediate	M7	0.085	0.064	0.066	0.119	0.039
High	M8	0.144	0.137	0.095	0.089	0.081
Low	M9	0.110	0.089	0.065	0.053	0.080
Atlantic	Atlantic	0.005	0.015	0.017	0.020	0.047

Table D.7: Chlorophyll *a* (Chl_*a*) during the Oligotrophic phase (Phase I) in the KOSMOS GC 2014 experiment. Mesocosms have been classified as Low, Intermediate or High depending on the pCO_2 levels of the treatment. Note that Chl_*a* is expressed in μg L^{-1} units. To convert to "per protein" units, use the data on table D.4.

Total Chl_*a*		I: Oligotrophic phase (day)							
Treatment	Mesocosm	-3	-1	3	7	11	15	19	23
Low	M1	0.071	0.053	0.069	0.103	0.161	0.107	0.140	0.130
High	M2	0.081	0.046	0.089	0.091	0.124	0.127	0.159	0.213
Intermediate	M3	0.068	0.044	0.072	0.087	0.122	0.132	0.154	0.192
Intermediate	M4	0.078	0.058	0.084	0.088	0.119	0.096	0.149	0.125
Low	M5	0.075	0.060	0.091	0.124	0.110	0.127	0.122	0.169
Intermediate	M7	0.084	0.049	0.066	0.094	0.099	0.100	0.156	0.161
High	M8	0.081	0.053	0.073	0.097	0.117	0.119	0.128	0.113
Low	M9	0.105	0.067	0.061	0.119	0.132	0.143	0.173	0.185
Atlantic	Atlantic	0.080	0.051	0.220	0.075	0.068	0.068	0.136	0.067

Table D.8: Chlorophyll a (Chl_a) during the Bloom phase (Phase II) in the KOS-MOS GC 2014 experiment. Mesocosms have been classified as Low, Intermediate or High depending on the pCO$_2$ levels of the treatment. Note that Chl_a is expressed in μg L^{-1} units. To convert to "per protein" units, use the data on table D.5.

| Total Chl_a | | II: Bloom phase (day) | | | | |
Treatment	Mesocosm	26	28	30	32	35
Low	M1	0.3838	1.9067	1.0872	0.6553	0.3506
High	M2	1.4529	4.0160	1.6453	1.3349	0.8758
Intermediate	M3	0.7153	3.5005	1.2707	0.8083	0.4436
Intermediate	M4	0.5618	3.2992	1.8301	0.8133	0.5730
Low	M5	0.5048	3.4288	1.5563	1.3006	0.6894
Intermediate	M7	0.4477	2.3366	2.3752	1.4558	0.6201
High	M8	0.5371	2.2904	2.0110	1.2962	0.9296
Low	M9	0.6218	4.5137	2.5883	2.2726	0.8154
Atlantic	Atlantic	0.1081	0.0847	0.0892	0.1065	0.1067

Table D.9: Chlorophyll a (Chl_a) during the Post-Bloom phase (Phase III) in the KOSMOS GC 2014 experiment. Mesocosms have been classified as Low, Intermediate or High depending on the pCO$_2$ levels of the treatment. Note that Chl_a is expressed in μg L^{-1} units. To convert to "per protein" units, use the data on table D.6.

| Total Chl_a | | III:Postbloom Phase (day) | | | | |
Treatment	Mesocosm	39	43	47	51	55
Low	M1	0.7304	0.2513	0.2182	0.4631	0.3497
High	M2	1.2395	0.9873	0.7085	0.7447	0.4449
Intermediate	M3	0.7393	0.4303	0.4046	0.4195	0.4210
Intermediate	M4	0.6270	0.4098	0.4024	0.6174	0.5299
Low	M5	0.5920	0.3764	0.3075	0.6406	0.5428
Intermediate	M7	0.5786	0.5112	0.2835	0.6345	0.8797
High	M8	1.4283	1.1776	0.5760	0.7102	0.8263
Low	M9	0.7103	0.4357	0.3379	0.4422	0.5378
Atlantic	Atlantic	0.0871	0.0977	0.1593	0.1553	0.1992

Appendix E

Appendix E. Abbreviations

Table E.1: Summary of the symbols used to identify the parameters (1/2).

Parameter	Definition
A	Preexponential frequency factor
A_{340}	Absorbance at 340nm
Acon	Aconitase
ATP	Adenosine triphosphate
B	Biomass
$\mathbf{B}_{340}$	A_{340} increase per time of the absorbance at 340nm in the blank assay
Biosynthetic Ψ_{NADP}	Potential CO_2 production related to biosynthesis
Chl_a	Chlorophyll a
CS	Citrate synthase
χ	Empirical relationship between physiological CO_2 production and potential O_2 consumption
Δ_{340}	A_{340} increase per time
ΔH^*	Enthalpy of activation at standard conditions
Δ_{NADPH}	$[NADPH]$ increase per time
DOC	Dissolved organic carbon
Ea	Energy of activation
EKM	Enzyme kinetic model
ETS	Electron transport system
ε	Extinction coefficient
Fc	Carbon flux
Fum	Fumarase
Φ	Potential O_2 consumption based on ETS
HEP	Heterotrophic energy production
$\mathbf{IDH_{KC}}$	IDH isoenzymes linked to the Krebs cycle
$\mathbf{IDH_{KC}}_{CO2}$	CO_2 production related to IDH isoenzymes linked to the Krebs cycle
INT	2-(p-iodophenyl)-3-(p-nitrophenyl)-5-phenyl tetrazolium chloride (tetrazolium salt)
$\mathbf{K_1}$	Velocity constant at T1
$\mathbf{K_2}$	Velocity constant at T2
KC	Krebs cycle
$\mathbf{KC}_{CO2}$	CO_2 production related to the Krebs cycle
KGDH	α-ketoglutarate dehydrogenase
$\mathbf{KGDH}_{CO2}$	CO_2 production related to α-ketoglutarate dehydrogenase
$\mathbf{k}_{IDH}$	NADP-IDH activity related to temperature
K_m	Michaelis-Menten constant

Table E.2: Summary of the symbols used to identify the parameters (2/2).

Parameter	Definition
MDH	Malate dehydrogenase
ME	Malic enzyme
MTE	Metabolical theory of ecology
ME_{CO2}	CO_2 production related to the malic enzyme
NAD-IDH	NAD^+-dependent isocitrate dehydrogenase
NADP-IDH	$NADP^+$-dependent isocitrate dehydrogenase
$NADP\text{-}IDH_{mit}$	NADP-IDH isoenzyme linked to the mitochondria
$NADP\text{-}IDH_{out}$	NADP-IDH isoenzymes outside the mitochondria
$NADP\text{-}IDHout_{CO2}$	CO_2 production related to the NADP-IDH isoenzymes outside the mitochondria
NADP-IDH(Ti)	NADP-IDH activity at in-situ T
NADP-IDH(Tm)	NADP-IDH activity at T during measurement
NRE	Nutrient regeneration efficiency
P_N	Net productivity
PEPCK	Phosphoenolpyruvate carboxykinase
$PEPCK_{CO2}$	CO_2 production related to phosphoenolpyruvate carboxykinase
PDH_{CO2}	CO_2 production related to pyruvate dehydrogenase
POC	Particulte organic carbon
Ψ	Potential CO_2 production
Ψ_{NADP}	Potential CO_2 production based on NADP-IDH
Q_{10}	Temperature coefficient
R	Universal molar gas constant
Respiratory Ψ_{NADP}	Potential CO_2 production related to the respiratory metabolism
R_{CO2}	Physiological CO_2 production
R_{CO2}/NADP-IDH	Ratio between physiological CO_2 production and potential CO_2 production of the NADP-IDH
R_{CO2}/Ψ_{NADP}	Ratio between physiological and potential CO_2 production
R_{O2}	Physiological O_2 consumption
R_{O2}/Φ	Ratio between physiological and potential O_2 consumption
RQ	Respiratory Quotient
SuccDH	CO_2 Succinate dehydrogenase
[S]	Substrate concentration
T	Temperature
T_i	In-situ temperature
T_m	Inside-cuvette temperature during measurement
V_c	Final volume in the cuvette
V_h	Volume of the sample-homogenate added into the cuvette
V_s	Total volume of the sample-homogenate
V_{max}	Maximum velocity of an enzyme-catalysed reaction

Bibliography

Aguiar-González, B., Packard, T.T., Berdalet, E., Roy, S., Gómez, M., 2012. Respiration predicted from an enzyme kinetic model and the metabolic theory of ecology in two species of marine bacteria. Journal of Experimental Marine Biology and Ecology 412, 1–12.

Ahmed, S., Kenner, R., King, F., 1976. Preservation of enzymic activity in marine plankton by low-temperature freezing. Marine Chemistry 4, 133–139.

Alberty, R.A., Goldberg, R.N., 1992. Standard thermodynamic formation properties for the adenosine 5'-triphosphate series. Biochemistry 31, 10610–10615.

Algueró-Muñiz, M., Horn, H.G., Alvarez-Fernandez, S., Spisla, C., Aberle, N., Bach, L.T., Guan, W., Achterberg, E.P., Riebesell, U., Boersma, M., 2019. Analyzing the impacts of elevated-CO_2 levels on the development of a subtropical zooplankton community during oligotrophic conditions and simulated upwelling. Frontiers in Marine Science 6, 61.

Alp, P.R., Newsholme, E.A., Zammit, V.A., 1976. Activities of citrate synthase and NAD^+-linked and $NADP^+$-linked isocitrate dehydrogenase in muscle from vertebrates and invertebrates. Biochemical Journal 154, 689–700.

Aranguren-Gassis, M., Teira, E., Serret, P., Martínez-García, S., Fernández, E., 2012. Potential overestimation of bacterial respiration rates in oligotrophic plankton communities. Marine Ecology Progress Series 453, 1–10.

Arístegui, J., Denis, M., Almunia, J., Montero, M.F., 2002a. Water-column remineralization in the Indian sector of the Southern Ocean during early spring. Deep Sea Research Part II: Topical Studies in Oceanography 49, 1707–1720.

Arístegui, J., Duarte, C.M., Agustí, S., Doval, M., Álvarez-Salgado, X.A., Hansell, D.A., 2002b. Dissolved organic carbon support of respiration in the dark ocean. Science 298, 1967–1967.

Arístegui, J., Harrison, W.G., 2002. Decoupling of primary production and community respiration in the ocean: implications for regional carbon studies. Aquatic Microbial Ecology 29, 199–209.

Arístegui, J., Montero, M.F., 1995a. Plankton community respiration in Bransfield Strait (Antarctic Ocean) during Austral spring. Journal of Plankton Research 17, 1647–1659.

Arístegui, J., Montero, M.F., 1995b. The relationship between community respiration and ETS activity in the ocean. Journal of plankton research 17, 1563–1571.

Arístegui, J., Montero, M.F., 2005. Temporal and spatial changes in plankton respiration and biomass in the Canary Islands region: the effect of mesoscale variability. Journal of Marine Systems 54, 65–82.

Ariza, A., Garijo, J., Landeira, J., Bordes, F., Hernández-León, S., 2015. Migrant biomass and respiratory carbon flux by zooplankton and micronekton in the subtropical Northeast Atlantic Ocean (Canary Islands). Progress in Oceanography 134, 330–342.

Arrhenius, S., 1889. Über die reaktionsgeschwindigkeit bei der inversion von rohrzucker durch säuren. Zeitschrift für physikalische Chemie 4, 226–248.

Arrhenius, S., et al., 1915. Quantitative laws in biological chemistry. G. Bell and Sons, Ltd.

Aster, P.L., Moon, T.W., 1981. Influence of fasting and diet on lipogenic enzymes in the American eel, *Anguilla rostrata* LeSueur. The Journal of nutrition 111, 346–354.

Atamanchuk, D., Tengberg, A., Thomas, P.J., Hovdenes, J., Apostolidis, A., Huber, C., Hall, P.O., 2014. Performance of a lifetime-based optode for measuring partial pressure of carbon dioxide in natural waters. Limnology and Oceanography: Methods 12, 63–73.

Atkin, P., de Paula, J., 2006. Atkins' physical chemistry. WH Freeman and Company Books , p747–755.

Badger, M.R., Andrews, T.J., Whitney, S., Ludwig, M., Yellowlees, D.C., Leggat, W., Price, G.D., 1998. The diversity and coevolution of Rubisco, plastids, pyrenoids, and chloroplast-based CO_2-concentrating mechanisms in algae. Canadian Journal of Botany 76, 1052–1071.

Bangqin, H., Huasheng, H., Xiangzhong, X., Yuan, L., 2005. Study on respiratory electron transport system (ETS) of phytoplankton in Taiwan Strait and Xiamen Harbour. Chinese Journal of Oceanology and Limnology 23, 176–182.

Barton, E., Arístegui, J., Tett, P., Cantón, M., García-Braun, J., Hernández-León, S., Nykjaer, L., Almeida, C., Almunia, J., Ballesteros, S., et al., 1998. The transition zone of the Canary Current upwelling region. Progress in Oceanography 41, 455–504.

Berdalet, E., Packard, T., Lagacé, B., Roy, S., St-Amand, L., Gagné, J.P., 1995a. CO_2 production, O_2 consumption and isocitrate dehydrogenase in the marine bacterium *Vibrio natriegens*. Aquatic Microbial Ecology 9, 211–217.

Berdalet, E., Packard, T.T., Lagacé, B., Roy, S., St-Amand, L., Gagné, J.P., 1995b. CO_2 production, O_2 consumption, isocitrate dehydrogenase and electron transport system activities in the marine bacterium *Pseudomonas nautica*. Aquatic Microbial Ecology 9, 211–217.

Berggren, M., Lapierre, J.F., Del Giorgio, P.A., 2012. Magnitude and regulation of bacterioplankton respiratory quotient across freshwater environmental gradients. The ISME journal 6, 984–993.

Bondyale-Juez, D.R., Packard, T.T., Viera-Rodríguez, M.A., Gómez, M., 2017. Respiration: comparison of the Winkler technique, O_2 electrodes, O_2 optodes and the respiratory electron transport system assay. Marine Biology 164, 226.

Borchers, H.W., 2017. pracma: Practical Numerical Math Functions. URL: `https://CRAN.R-project.org/package=pracma`. r package version 2.0.4.

Braden-Behrens, J., Yan, Y., Knohl, A., 2017. A new instrument for stable isotope measurements of C^{13} and O^{18} in CO_2-instrument performance and ecological application of the Delta Ray IRIS analyzer. Atmospheric Measurement Techniques 10, 4537–4560.

Buesseler, K.O., Boyd, P.W., 2009. Shedding light on processes that control particle export and flux attenuation in the twilight zone of the open ocean. Limnology and Oceanography 54, 1210–1232.

Burkholder, J.M., Glibert, P.M., Skelton, H.M., 2008. Mixotrophy, a major mode of nutrition for harmful algal species in eutrophic waters. Harmful algae 8, 77–93.

Caron, D.A., 2016. Mixotrophy stirs up our understanding of marine food webs. Proceedings of the National Academy of Sciences 113, 2806–2808.

Castro, J., 1995. Mysids and euphasiids in the diet of *Scomber japonicus* houttuyn, 1782 off the Canary Islands. Boletin-Instituto Espanol de Oceanografia 11, 77–86.

Chance, B., 1965. Reaction of oxygen with the respiratory chain in cells and tissues. The Journal of General Physiology 49, 163–188.

Chance, B., Williams, G.R., 1956. The respiratory chain and oxidative phosphylation. Advances in Enzymology 17, 65–134. File: Author file (Chance).

Chang, F., 2015. Cytotoxic effects of *Vicicitus globosus* (Class Dictyochophyceae) and *Chattonella marina* (Class Raphidophyceae) on rotifers and other microalgae. Journal of Marine Science and Engineering 3, 401–411.

Chang, F.H., McVeagh, M., Gall, M., Smith, P., 2012. *Chattonella globosa* is a member of Dictyochophyceae: reassignment to *Vicicitus* gen. nov., based on molecular phylogeny, pigment composition, morphology and life history. Phycologia 51, 4.

Christensen, J., Owens, T., Devol, A., Packard, T., 1980. Respiration and physiological state in marine bacteria. Marine Biology 55, 267–276.

Christensen, J.P., Packard, T.T., 1979. Respiratory electron transport system activities in phytoplankton and bacteria: Comparison of methods. Limnology and Oceanography 24, 576–583.

Clark, J., Greenbaum, A., Slater, T., 1965. Effects of tetrazolium salts on oxidative phosphorylation in rat-liver mitochondria. Biochemical Journal 94, 651.

Cleland, W., 1967. Enzyme kinetics. Annual Review of Biochemistry 36, 77–112.

Colman, R.F., 1975. Mechanisms for the oxidative decarboxylation of isocitrate: Implications for control. Advances in Enzyme Regulation 13, 413–433.

Corral, J., 1970. Contribución al conocimiento del plancton de Canarias. Publicaciones de la Faculdad de Ciencias. University of Madrid (Seccion de Biologicas), Serie A 129, 343.

Craig, H., 1971. The deep metabolism: oxygen consumption in abyssal ocean water. Journal of Geophysical Research 76, 5078–5086.

Czyzewska, U., Tylicki, A., Siemieniuk, M., Strumilo, S., 2012. Changes of activity and kinetics of certain liver and heart enzymes of hypothyroid and T_3-treated rats. Journal of Physiology and Biochemistry 68, 345–351.

Dam, H.G., Roman, M.R., Youngbluth, M.J., 1995. Downward export of respiratory carbon and dissolved inorganic nitrogen by diel-migrant mesozooplankton at the JGOFS Bermuda time-series station. Deep Sea Research Part I: Oceanographic Research Papers 42, 1187–1197.

Darnis, G., Fortier, L., 2012. Zooplankton respiration and the export of carbon at depth in the Amundsen Gulf (Arctic Ocean). Journal of Geophysical Research: Oceans 117.

Denton, R.M., Richards, D.A., Chin, J.G., 1978. Calcium ions and the regulation of NAD^+-linked isocitrate dehydrogenase from the mitochondria of rat heart and other tissues. Biochemical Journal 176, 899–906.

Dixon, M., Webb, E.C., 1979. Enzymes, Third edition.

Domingues, P., Turk, P., Andrade, J., Lee, P., 1999. Culture of the mysid, *Mysidopsis almyra* (Bowman),(Crustacea: Mysidacea) in a static water system: effects of density and temperature on production, survival and growth. Aquaculture research 30, 135–143.

Doney, S.C., Fabry, V.J., Feely, R.A., Kleypas, J.A., 2009. Ocean acidification: the other CO_2 problem. Annual Review of Marine Science 1, 169–192.

Doney, S.C., Schimel, D.S., 2007. Carbon and climate system coupling on timescales from the Precambrian to the Anthropocene. Annual Review Environment and Resources 32, 31–66.

Ducklow, H.W., Doney, S.C., . What is the metabolic state of the oligotrophic ocean? A debate. Annual Review of Marine Science .

Eddelbuettel, D., François, R., Allaire, J., Ushey, K., Kou, Q., Russel, N., Chambers, J., Bates, D., 2011. Rcpp: Seamless R and C++ integration. Journal of Statistical Software 40, 1–18.

Eggers Jr, D., Gregor, N., Halsey, G., Rabinovitch, B., 1964. Physical Chemistry. Wiley, New York, N. Y.

El-Mansi, E., Holms, W., 1989. Control of carbon flux to acetate excretion during growth of escherichia coli in batch and continuous cultures. Microbiology 135, 2875–2883.

Eppley, R.W., Peterson, B.J., 1979. Particulate organic matter flux and planktonic new production in the deep ocean. Nature 282, 677–680.

Eyring, H., 1935. The activated complex in chemical reactions. The Journal of Chemical Physics 3, 107–115.

Ferguson, R.L., Buckley, E., Palumbo, A., 1984. Response of marine bacterioplankton to differential filtration and confinement. Applied and Environmental Microbiology 47, 49–55.

Ferguson, S.J., 2010. ATP synthase: from sequence to ring size to the P/O ratio. Proceedings of the National Academy of Sciences 107, 16755–16756.

Fernández-Urruzola, I., Osma, N., Gómez, M., Montesdeoca-Esponda, S., Packard, T.T., 2016. Building a model of ammonium excretion in two species of marine zooplankton based on glutamate dehydrogenase kinetics. Marine Ecology Progress Series 550, 83–99.

Fernández-Urruzola, I., Packard, T.T., Gómez, M., 2011. GDH activity and ammonium excretion in the marine mysid, *Leptomysis lingvura*: effects of age and starvation. Journal of Experimental Marine Biology and Ecology 409, 21–29.

Feynman, R.P., Leighton, R.B., Sands, M., 2011. Six not-so-easy pieces: Einstein's relativity, symmetry, and space-time. Basic Books.

Fisher, H.F., 1964. A limiting law relating the size and shape of protein molecules to their composition. Proceedings of the National Academy of Sciences of the United States of America 51, 1285.

Fruton, J.S., Simmonds, S., 1958. General Biochemistry. second edition ed., John Wiley Sons, Inc., New York.

Gálvez, S., Gadal, P., 1995. On the function of the nadp-dependent isocitrate dehydrogenase isoenzymes in living organisms. Plant Science 105, 1–14.

Giering, S.L., Sanders, R., Lampitt, R.S., Anderson, T.R., Tamburini, C., Boutrif, M., Zubkov, M.V., Marsay, C.M., Henson, S.A., Saw,

K., et al., 2014. Reconciliation of the carbon budget in the ocean's twilight zone. Nature 507, 480.

del Giorgio, P.A., le B. Williams, P.J., 2005. Respiration in aquatic systems. Oxford University Press, London,.

Gómez, M., Fernández-Urruzola, I., Herrera-Ulibarri, A., Maldonado-Uribe, F., Martínez, I., Osma, N., Packard, T.T., 2011. The R/ETS ratio: Where we are now. Poster in 5th International Zooplankton Production Symposium ICES PICES .

Gómez, M., Torres, S., Hernández-León, S., 1996. Modification of the electron transport system (ETS) method for routine measurements of respiratory rates of zooplankton. South African Journal of Marine Science 17, 15–20.

Hernández-Hernández, N., Bach, L.T., Montero, M.F., Taucher, J., Baños, I., Guan, W., Espósito, M., Ludwig, A., Achterberg, E.P., Riebesell, U., et al., 2018. High CO_2 under nutrient fertilization increases primary production and biomass in subtropical phytoplankton communities: a mesocosm approach. Frontiers in Marine Science 5, 213.

Hernández-Leon, S., Gómez, M., 1996. Factors affecting the respiration/ETS ratio in marine zooplankton. Journal of Plankton Research 18, 239–255.

Hernández-León, S., Gomez, M., Arístegui, J., 2007. Mesozooplankton in the Canary Current System: The coastal–ocean transition zone. Progress in Oceanography 74, 397–421.

Hernández-León, S., Putzeys, S., Almeida, C., Bécognée, P., Marrero-Díaz, A., Arístegui, J., Yebra, L., 2019. Carbon export through zooplankton active flux in the Canary Current. Journal of Marine Systems 189, 12–21.

Herrera, A., Gómez, M., Molina, L., Otero, F., Packard, T., 2011a. Rearing techniques and nutritional quality of two mysids from Gran Canaria (Spain). Aquaculture Research 42, 677–683.

Herrera, A., Packard, T., Santana, A., Gómez, M., 2011b. Effect of starvation and feeding on respiratory metabolism in *Leptomysis lingvura* (GO Sars, 1866). Journal of Experimental Marine Biology and Ecology 409, 154–159.

Hollander, M., Wolfe, D.A., Chicken, E., 2013. Nonparametric statistical methods. volume 751. John Wiley & Sons.

Ikeda, T., Fay, E.H., 1981. Metabolic activity of zooplankton from the Antarctic Ocean. Marine and Freshwater Research 32, 921–930.

Ikeda, T., Kanno, Y., Ozaki, K., Shinada, A., 2001. Metabolic rates of epipelagic marine copepods as a function of body mass and temperature. Marine Biology 139, 587–596.

Ikeda, T., Sano, F., Yamaguchi, A., Matsuishi, T., 2006. Metabolism of mesopelagic and bathypelagic copepods in the Western North Pacific Ocean. Marine Ecology Progress Series 322, 199–211.

Isla, J.A., Perissinotto, R., 2004. Effects of temperature, salinity and sex on the basal metabolic rate of the estuarine copepod *Pseudodiaptomus hessei*. Journal of Plankton Research 26, 579–583.

Jansen, G., Hutchison, C., Zanetti, M., 1966. Studies on lipogenesis in vivo. effect of dietary fat or starvation on conversion of ^{14}C glucose into fat and turnover of newly synthesized fat. Biochemical Journal 99, 323.

Jenkins, W.J., 1982. Oxygen utilization rates in North Atlantic subtropical gyre and primary production in oligotrophic systems. Nature 300, 246–248.

Jo, S.H., Son, M.K., Koh, H.J., Lee, S.M., Song, I.H., Kim, Y.O., Lee, Y.S., Jeong, K.S., Kim, W.B., Park, J.W., et al., 2001. Control of Mitochondrial Redox Balance and Cellular Defense against Oxidative Damage by Mitochondrial NADP^{+}-dependent Isocitrate Dehydrogenase. Journal of Biological chemistry 276, 16168–16176.

Johnson, F.H., 1936. The oxygen uptake of marine bacteria. Journal of Bacteriology 31, 547.

Johnson, K., Sieburth, J.M., leB Williams, P., Brändström, L., 1987. Coulometric total carbon dioxide analysis for marine studies: automation and calibration. Marine Chemistry 21, 117–133.

Johnson, K., Wills, K., Butler, D., Johnson, W., Wong, C., 1993. Coulometric total carbon dioxide analysis for marine studies: maximizing the performance of an automated gas extraction system and coulometric detector. Marine Chemistry 44, 167–187.

Jumars, P.A., 2007. Vertical and Horizontal Migrations Affect Local and Integrated Water-Column Scattering Strengths. Technical Report. Maine Uniersity at Walpole Darling Marine Center.

Jurado-Ruzafa, A., González-Lorenzo, G., Jiménez, S., Sotillo, B., Acosta, C., Santamaría, M., 2019. Seasonal evolution of small

pelagic fish landings index in relation to oceanographic variables in the Canary Islands (Spain). Deep Sea Research Part II: Topical Studies in Oceanography 159, 84–91.

Kadenbach, B., Goebell, H., Klingenberg, M., 1964. Differential action of thyroid hormones on enzyme levels of the DPN and TPN specific isocitrate dehydrogenase. Biochemical and Biophysical research Communications 14, 335–339.

Karl, D.M., . Solar energy capture and transformation in the sea. Elementa Science of the Anthropogene 2, 000021.

Kenner, R., Ahmed, S., 1975. Measurements of electron transport activities in marine phytoplankton. Marine Biology 33, 119–127.

Ketchum, B.H., 1957. The effects of the ecological system on the transport of elements in the sea. The Effects of Atomic Radiation on Oceanography and Fisheries. National Research Council, Washington, DC , 52–59.

King, F.D., Packard, T.T., 1975. The effect of hydrostatic pressure on respiratory electron transport activity in marine zooplankton. Deep-Sea Research 22, 849–854.

Kiørboe, T., Møhlenberg, F., Hamburger, K., 1985. Bioenergetics of the planktonic copepod *Acartia tonsa*: relation between feeding, egg production and respiration, and composition of specific dynamic action. Marine Ecology Progress Series 26, 85–97.

Kitsos, M.S., Tzomos, T., Anagnostopoulou, L., Koukouras, A., 2008. Diet composition of the seahorses, *Hippocampus guttulatus* cuvier, 1829 and *Hippocampus hippocampus* (L., 1758)(Teleostei, Syngnathidae) in the Aegean Sea. Journal of Fish Biology 72, 1259–1267.

Koh, H.J., Lee, S.M., Son, B.G., Lee, S.H., Ryoo, Z.Y., Chang, K.T., Park, J.W., Park, D.C., Song, B.J., Veech, R.L., et al., 2004. Cytosolic $NADP^+$-dependent Isocitrate Dehydrogenase Plays a Key Role in Lipid Metabolism. Journal of Biological Chemistry 279, 39968–39974.

Kornberg, A., 1991. For the love of enzymes: The odyssey of a biochemist. Harvard University Press.

Kornberg, A., Pricer, W., 1951. Di-and triphosphopyridine nucleotide isocitric dehydrogenases in yeast. Journal of Biological Chemistry 189, 123–136.

Kozhantshikov, I., 1938. Carbohydrate and fat metabolism in adult lepidoptera. Bulletin of Entomological Research 29, 103–114.

Kühlbrandt, W., 2015. Structure and function of mitochondrial membrane protein complexes. BMC biology 13, 89.

Laidler, K.J., 1984. The development of the Arrhenius equation. Journal of Chemical Education 61, 494.

Lane, N., 2006. Power, sex, suicide: mitochondria and the meaning of life. Oxford University Press.

Lane, N., 2010. Life ascending: the ten great inventions of evolution. Profile books.

Lawrence, J.M., 1976. Patterns of lipid storage in post-metamorphic marine invertebrates. American Zoologist 16, 747–762.

Lee, R.F., Hagen, W., Kattner, G., 2006. Lipid storage in marine zooplankton. Marine Ecology Progress Series 307, 273–306.

Lefévre, D., Denis, M., Lambert, C.E., Miquel, J.C., 1996. Is DOC the main source of organic remineralization in the ocean water column. Journal of Marine Systems 7, 281–291.

Lester, R.L., Smith, A.L., 1961. Studies on the electron transport system XXVIII. the mode of reduction of tetrazolium salts by beef heart mitochondria; Role of Coenzyme Q and other lipids. Biochimica et Biophysica Acta 47, 475–496.

Low, P.S., Bada, J.L., Somero, G.N., 1973. Temperature adaptation of enzymes: roles of the free energy, the enthalpy, and the entropy of activation. Proceedings of the National Academy of Sciences 70, 430–432.

Lowry, O.H., Rosebrough, N.J., Farr, A.L., Randall, R.J., et al., 1951. Protein measurement with the folin phenol reagent. Journal of Biological Chemistry 193, 265–275.

Lussier, S.M., Kuhn, A., Chammas, M.J., Sewall, J., 1988. Techniques for the laboratory culture of *Mysidopsis* species (Crustacea: Mysidacea). Environmental Toxicology and Chemistry: An International Journal 7, 969–977.

MacDonald, M.J., 2002. Differences between mouse and rat pancreatic islets: succinate responsiveness, malic enzyme, and anaplerosis. American Journal of Physiology - Endocrinology and Metabolism 283, E302–E310.

Mackey, M., Mackey, D., Higgins, H., Wright, S., 1996. CHEMTAX-a program for estimating class abundances from chemical markers: application to HPLC measurements of phytoplankton. Marine Ecology Progress Series 144, 265–283.

Maldonado, F., Packard, T., Gómez, M., 2012. Understanding tetra-zolium reduction and the importance of substrates in measuring respiratory electron transport activity. Journal of Experimental Marine Biology and Ecology 434, 110–118.

Markwell, M.A.K., Haas, S.M., Tolbert, N., Bieber, L., 1981. Protein determination in membrane and lipoprotein samples: Manual and automated procedures, in: Methods in Enzymology. Elsevier. volume 72, pp. 296–303.

Marshall, S., Nicholls, A., Orr, A., 1935. On the biology of *Calanus finmarchicus*. part VI. oxygen consumption in relation to environmental conditions. Journal of the Marine Biological Association of the United Kingdom 20, 1–27.

Martin, J.H., Knauer, G.A., Karl, D.M., Broenkow, W.W., 1987. VER-TEX: carbon cycling in the Northeast Pacific. Deep Sea Research Part A. Oceanographic Research Papers 34, 267–285.

Martínez, I., Gómez, M., Packard, T.T., 2010. Potential respiration is a better respiratory predictor than biomass in young *Artemia salina*. Journal of Experimental Marine Biology and Ecology 390, 78–83.

Martinez, R., 1991. Biomass and respiratory ETS activity of microplankton in the Barents Sea. Polar Research 10, 193–200.

Martinez, R., Arnone, R.A., Velasquez, Z., 1990. Chlorophyll a and respiratory electron transport system activity in microplankton from the surface waters of the Western Mediterranean. Journal of Geophysical Research: Oceans 95, 1615–1622.

Martínez-García, S., Fernández, E., Aranguren-Gassis, M., Teira, E., 2009. In vivo electron transport system activity: a method to estimate respiration in natural marine microbial planktonic communities. Limnology and Oceanography: Methods 7, 459–469.

Mauchline, J., 1980. The biology of mysids. Advances in Marine Biology 18, 3–369.

Mayzaud, P., Boutoute, M., Gasparini, S., Mousseau, L., Lefevre, D., 2005. Respiration in marine zooplankton - the other side of the coin: CO_2 production. Limnology and Oceanography 50, 291–298.

McCave, I., 1975. Vertical flux of particles in the ocean, in: Deep Sea Research and Oceanographic Abstracts, Elsevier. pp. 491–502.

Millero, F.J., 2006. Chemical oceanography. volume 30. CRC press.

Mintrop, L., Pérez, F.F., González-Dávila, M., Santana-Casiano, J.M., Körtzinger, A., 2000. Alkalinity determination by potentiometry: Intercalibration using three different methods. Ciencias Marinas 26, 23–27.

Moon, T.W., Hochachka, P., 1971. Temperature and enzyme activity in poikilotherms. Isocitrate dehydrogenases in rainbow-trout liver. Biochemical Journal 123, 695–705.

Moore, W.J.W.J., 1972. Physical chemistry, Fourth edition. Prentice-Hall.

Moran, L.A., Horton, H.R., Scrimgeour, K.G., Perry, M.D., 2012. Principles of biochemistry. Pearson Boston.

Morris, J., Redfearn, E., 1969. Vitamins and coenzymes, in: Data for Biochemical Research. Clarendon Press Oxford, pp. 123–167.

Munilla-Moran, R., 1994. Biochemical studies in marine species II. NADP$^+$-dependent isocitrate dehydrogenase from turbot (*Scophthalmus maximus* l.) larvae. Comparative Biochemistry and Physiology Part B: Comparative Biochemistry 107, 61–68.

Munilla-Moran, R., Stark, J., 1989. Biochemical studies in marine species I. NADP$^+$-dependent isocitrate dehydrogenase from turbot liver (*Scophthalmus maximus* l.). Comparative Biochemistry and Physiology Part B: Comparative Biochemistry 93, 823–828.

Munk, W.H., 1966. Abyssal recipes, in: Deep Sea Research and Oceanographic Abstracts, Elsevier. pp. 707–730.

Nachlas, M.M., Margulies, S.I., Seligman, A.M., 1960. A colorimetric method for the estimation of succinic dehydrogenase activity. The Journal of Biological Chemistry 235, 499–503.

Nelson, D.L., Cox, M.M., 2008. Lehninger principles of biochemistry, Fifth Edition. W.H. Freeman and Company.

Nicholls, D., Garland, P., 1969. The control of isocitrate oxidation by rat liver mitochondria. Biochemical Journal 114, 215–225.

Ochoa, S., 1943. Efficiency of aerobic phosphorylation in cell-free heart extracts. The Journal of Biological Chemistry 151, 493–505.

Olano, J., de Arriaga, D., Busto, F., Soler, J., 1995. Kinetics and thermostability of NADP-Isocitrate Dehydrogenase from *Cephalosporium acremonium*. Applied and Environmental Microbiology 61, 2326–2334.

Osma, N., Aristizabal, M., Fernández-Urruzola, I., Packard, T.T., Gómez, M., 2016a. Influence of starvation on respiratory metabolism and pyridine nucleotide levels in the marine dinoflagellate *Oxyrrhis marina*. Protist 167, 136–147.

Osma, N., Fernández-Urruzola, I., Gómez, M., Montesdeoca-Esponda, S., Packard, T.T., 2016b. Predicting in vivo oxygen consumption rate from ETS activity and bisubstrate enzyme kinetics in cultured marine zooplankton. Marine Biology 163, 146.

Osma, N., Fernández-Urruzola, I., Packard, T., Postel, L., Gómez, M., Pollehne, F., 2014. Short-term patterns of vertical particle flux in Northern Benguela: a comparison between sinking POC and respiratory carbon consumption. Journal of Marine Systems 140, 150–162.

Osma, N., Maldonado, F., Fernández-Urruzola, I., Packard, T.T., Gomez, M., 2016c. Variability of respiration and pyridine nucleotides concentration in oceanic zooplankton. Journal of Plankton Research 38, 537.

Otero-Ferrer, F., Molina, L., Socorro, J., Fernández-Palacios, H., Izquierdo, M., Herrera, R., 2012. Effect of different live prey on spawning quality of short-snouted seahorse, *Hippocampus hippocampus* (Linnaeus, 1758). Journal of the World Aquaculture Society 43, 174–186.

Owens, T., King, F., 1975. The measurement of respiratory electron-transport-system activity in marine zooplankton. Marine Biology 30, 27–36.

Packard, T., 1971. The measurement of respiratory electron transport activity in marine phytoplankton. Journal of Marine Research 29, 235–244.

Packard, T., 1979. Respiration and respiratory electron-transport activity in plankton from the Northwest African upwelling area. Journal of Marine Research 37, 711–742.

Packard, T., Berdalet, E., Blasco, D., Roy, S., St-Amand, L., Lagacé, B., Lee, K., Gagne, J., 1996a. CO_2 production predicted from isocitrate dehydrogenase activity and bisubstrate enzyme kinetics in the

marine bacterium *Pseudomonas nautica*. Aquatic Microbial Ecology 11, 11–19.

Packard, T., Berdalet, E., Blasco, D., Roy, S., St-Amand, L., Lagacé, B., Lee, K., Gagnó, J.P., 1996b. Oxygen consumption in the marine bacterium *Pseudomonas nautica* predicted from ETS activity and bisubstrate enzyme kinetics. Journal of Plankton Research 18, 1819–1835.

Packard, T., Blasco, D., MacIsaac, J., Dugdale, R., 1971a. Variations of nitrate reductase activity in marine phytoplankton. Scientia Marina: Investigacion Pesquera 35, 209.

Packard, T., Chen, W., Blasco, D., Savenkoff, C., Vezina, A., Tian, R., St-Amand, L., Roy, S., Lovejoy, C., Klein, B., et al., 2000. Dissolved organic carbon in the Gulf of St. Lawrence. Deep Sea Research Part II: Topical Studies in Oceanography 47, 435–459.

Packard, T., Healy, M., Richards, F., 1971b. Vertical distribution of the activity of the respiratory electron transport system in marine plankton 1. Limnology and Oceanography 16, 60–70.

Packard, T., Minas, H., Owens, T., Devol, A., 1977. Deep-sea metabolism in the Eastern tropical North Pacific Ocean, in: Oceanic sound scattering prediction. Plenum Press New York, pp. 101–116.

Packard, T., Osma, N., Fernández-Urruzola, I., Codispoti, L., Christensen, J., Gómez, M., 2015. Peruvian upwelling plankton respiration: calculations of carbon flux, nutrient retention efficiency, and heterotrophic energy production. Biogeosciences 12, 2641–2654.

Packard, T., Williams, P., 1981. Rates of respiratory oxygen-consumption and electron-transport in surface seawater from the Northwest Atlantic. Oceanologica Acta 4, 351–358.

Packard, T.T., Christensen, J., 2004. Respiration and vertical carbon flux in the Gulf of Maine water column. Journal of Marine Research 62, 93–115.

Packard, T.T., Codispoti, L., 2007. Respiration, mineralization, and biochemical properties of the particulate matter in the Southern Nansen Basin water column in April 1981. Deep Sea Research Part I: Oceanographic Research Papers 54, 403–414.

Packard, T.T., Devol, A.H., King, F.D., 1975. The effect of temperature on the respiratory electron transport system in marine plankton. Deep-Sea Research 22, 237–249.

Packard, T.T., Gómez, M., 2008. Exploring a first-principles-based model for zooplankton respiration. ICES Journal of Marine Science 65, 371–378.

Packard, T.T., Gómez, M., 2013. Modeling vertical carbon flux from zooplankton respiration. Progress in Oceanography 110, 59–68.

Packard, T.T., Harmon, D., Boucher, J., 1974. Respiratory electron transport activity in plankton from upwelled waters. Tethys 6, 213–222.

Paul, A.J., Bach, L.T., Schulz, K.G., Boxhammer, T., Czerny, J., Achterberg, E.P., Hellemann, D., Trense, Y., Nausch, M., Sswat, M., et al., 2015. Effect of elevated CO_2 on organic matter pools and fluxes in a summer Baltic Sea plankton community. Biogeosciences 12, 6181–6203.

Pentecost, A., 1999. Analysing environmental data. Prentice Hall.

Plaut, G.W., 1970. DPN-linked isocitrate dehydrogenase of animal tissues. Current Topics in Cellular Regulation 2, 1–27.

Plaut, G.W.E., 1962. Isocitric dehydrogenase (TPN-linked) from pig heart (revised procedure). Academic Press, New York. volume V of *Methods in Enzymology*. pp. 645–651.

Przibram, H., 1923. Temperatur und Temperatoren im Tierreiche: Beiträge zu einer quantitativen Biologie XXI-XXX. F. Deuticke.

Rakusa-Suszczewski, S., McWhinnie, M.A., Cahoon, M., 1976. Respiration of the Antarctic copepod, *Rhincalanus gigas* 1. Limnology and Oceanography 21, 763–765.

Redfield, A.C., 1934. On the proportions of organic derivatives in sea water and their relation to the composition of plankton. University Press, Liverpool. James Johnstone Memorial Volume, pp. 177–192.

Riebesell, U., Aberle-Malzahn, N., Achterberg, E.P., Algueró-Muñiz, M., Alvarez-Fernandez, S., Arístegui, J., Bach, L.T., Boersma, M., Boxhammer, T., Guan, W., et al., 2018. Toxic algal bloom induced by ocean acidification disrupts the pelagic food web. Nature Climate Change 8, 1082.

Riebesell, U., Schulz, K.G., Bellerby, R., Botros, M., Fritsche, P., Meyerhöfer, M., Neill, C., Nondal, G., Oschlies, A., Wohlers, J., et al., 2007. Enhanced biological carbon consumption in a high CO_2 ocean. Nature 450, 545–548.

Riley, G.A., 1951. Oxygen, phosphate, and nitrate in the Atlantic Ocean. Bingham Oceanographic Collection Bulletin 13, 1–169.

Rivkin, R.B., Legendre, L., 2001. Biogenic carbon cycling in the upper ocean: effects of microbial respiration. Science 291, 2398–2400.

Romero-Kutzner, V., Packard, T.T., Berdalet, E., Roy, S., Gagné, J.P., Gómez, M., 2015. Respiration quotient variability: bacterial evidence. Marine Ecology Progress Series 519, 47–59.

Roy, S., Packard, T., 2001. CO_2 production rate predicted from isocitrate dehydrogenase activity, intracellular substrate concentrations and kinetic constants in the marine bacterium *Pseudomonas nautica*. Marine Biology 138, 1251–1258.

Roy, S.O., Packard, T.T., 1998. NADP-Isocitrate Dehydrogenase from *Pseudomonas nautica*: Kinetic Constant Determination and Carbon Limitation Effects on the Pool of Intracellular Substrates. Applied and Environmental Microbiology 64, 4958–4964.

Rutter, W., 1967. Protein determination in embryos, in: Methods in Developmental Biology. Crowell New York, pp. 671–683.

Sachs, L., 2012. Applied statistics: a handbook of techniques. Springer Science & Business Media.

Salvato, B., Cuomo, V., Di Muro, P., Beltramini, M., 2001. Effects of environmental parameters on the oxygen consumption of four marine invertebrates: a comparative factorial study. Marine Biology 138, 659–668.

Sanders, R.W., 1991. Mixotrophic protists in marine and freshwater ecosystems. The Journal of Protozoology 38, 76–81.

Sazanov, L., Jackson, J., 1994. Proton-translocating transhydrogenase and NAD-and NADP-linked isocitrate dehydrogenases operate in a substrate cycle which contributes to fine regulation of the tricarboxylic acid cycle activity in mitochondria. FEBS letters 344, 109–116.

Schmoker, C., Hernández-León, S., Calbet, A., 2013. Microzooplankton grazing in the oceans: impacts, data variability, knowledge gaps and future directions. Journal of Plankton Research 35, 691–706.

Segel, I.H., 1975. Enzyme kinetics: behavior and analysis of rapid equilibrium and steady state enzyme systems. Wiley New York.

Seiwell, H., 1937. Consumption of oxygen in sea water under controlled laboratory conditions. Nature 140, 506.

Seiwell, H., Seiwell, G.E., 1938. The sinking of decomposing plankton in sea water and its relationship to oxygen consumption and phosphorus liberation. Proceedings of the American Philosophical Society , 465–481.

Simčič, T., Brancelj, A., 2006. Effects of pH on electron transport system (ETS) activity and oxygen consumption in *Gammarus fossarum*, *Asellus aquaticus* and *Niphargus sphagnicolus*. Freshwater Biology 51, 686–694.

Škorjanc, D., Pette, D., 1998. Kinetic versus endpoint measurement for quantitative histochemical determination of enzyme activity in muscle fibers. Journal of Histochemistry & Cytochemistry 46, 275–276.

Smajgl, D., Böhm, F., Eisenhauer, A., Taubner, I., Mandic, M., 2018. New analytical approach in monitoring of CO_2 cycle in aquatic ecosystems. Poster in Ocean Sciences Meeting 2018, ASLO AGU .

Smith, J.J., McFeters, G.A., 1997. Mechanisms of int (2-(4-iodophenyl)-3-(4-nitrophenyl)-5-phenyl tetrazolium chloride), and ctc (5-cyano-2, 3-ditolyl tetrazolium chloride) reduction in escherichia coli k-12. Journal of Microbiological Methods 29, 161–175.

Stoecker, D.K., 1999. Mixotrophy among dinoflagellates 1. Journal of Eukaryotic Microbiology 46, 397–401.

Stoecker, D.K., Hansen, P.J., Caron, D.A., Mitra, A., 2017. Mixotrophy in the marine plankton. Annual Review of Marine Science 9, 311–335.

Suelter, C.H., et al., 1985. Practical guide to enzymology. Wiley.

Suess, E., 1980. Particulate organic carbon flux in the oceans: Surface productivity and oxygen utilization. Nature 288, 260–263.

Sverdrup, H.U., Johnson, M.W., Fleming, R.H., et al., 1942. The Oceans: Their physics, chemistry, and general biology. volume 7. Prentice-Hall New York.

Takahashi, T., Broecker, W.S., Langer, S., 1985. Redfield ratio based on chemical data from isopycnal surfaces. Journal of Geophysical Research: Oceans 90, 6907–6924.

Tames-Espinosa, M., Martínez, I., Romero-Kutzner, V., Bondyale-Juez, D.R., Packard, T.T., Gómez, M., 2018. $NADP^+$-dependent isocitrate dehydrogenase activity in marine plankton. Marine Chemistry 204, 86–94.

Taucher, J., Arístegui, J., Bach, L.T., Guan, W., Montero, M.F., Nauendorf, A., Achterberg, E.P., Riebesell, U., 2018. Response of subtropical phytoplankton communities to ocean acidification under oligotrophic conditions and during nutrient fertilization. Frontiers in Marine Science 5, 330.

Taucher, J., Bach, L.T., Boxhammer, T., Nauendorf, A., Achterberg, E.P., Algueró-Muñiz, M., Arístegui, J., Czerny, J., Esposito, M., Guan, W., et al., 2017. Influence of ocean acidification and deep water upwelling on oligotrophic plankton communities in the subtropical North Atlantic: Insights from an in situ mesocosm study. Frontiers in Marine Science 4, 85.

Teruya, T., Chaleckis, R., Takada, J., Yanagida, M., Kondoh, H., 2019. Diverse metabolic reactions activated during 58-hr fasting are revealed by non-targeted metabolomic analysis of human blood. Scientific Reports 9, 854.

Utermöhl, v.H., 1931. Neue wege in der quantitativen erfassung des plankton.(mit besonderer berücksichtigung des ultraplanktons.) mit 4 abbildungen im text. Internationale Vereinigung für theoretische und angewandte Limnologie: Verhandlungen 5, 567–596.

Villegas-Mendoza, J., Cajal-Medrano, R., Maske, H., 2015. INT (2-(4-iodophenyl)-3-(4-nitrophenyl)-5-(phenyl) tetrazolium chloride) is toxic to prokaryote cells precluding its use with whole cells as a proxy for in vivo respiration. Microbial Ecology 70, 1004–1011.

Waksman, S.A., Carey, C.L., 1935. Decomposition of organic matter in sea water by bacteria: I. Bacterial multiplication in stored sea water. Journal of Bacteriology 29, 531–543.

Walker, J.E., 1992. The NADH: ubiquinone oxidoreductase (complex I) of respiratory chains. Quarterly Reviews of Biophysics 25, 253–324.

Walsh, K., Koshland, D.E., 1984. Determination of flux through the branch point of two metabolic cycles. the tricarboxylic acid cycle and the glyoxylate shunt. Journal of Biological Chemistry 259, 9646–9654.

Ward, B.A., Follows, M.J., 2016. Marine mixotrophy increases trophic transfer efficiency, mean organism size, and vertical carbon flux. Proceedings of the National Academy of Sciences 113, 2958–2963.

Whitaker, J.R., 1993. Principles of enzymology for the food sciences. volume 61. CRC Press.

Wieckowski, M.R., Giorgi, C., Lebiedzinska, M., Duszynski, J., Pinton, P., 2009. Isolation of mitochondria-associated membranes and mitochondria from animal tissues and cells. Nature Protocols 4, 1582–1590.

Williams, P.J.l.B., Quay, P.D., Westberry, T.K., Behrenfeld, M.J., 2013. The oligotrophic ocean is autotrophic. Annual Review of Marine Science 5, 535–549.

Williamson, J.R., Cooper, R.H., 1980. Regulation of the citric acid cycle in mammalian systems. FEBS letters 117, K73–K85.

Winkler, L.W., 1888. The determination of dissolved oxygen in water. Berlin DeutChem Gas 21, 2843–2855.

Woods, C.M., 2005. Growth of cultured seahorses (*Hippocampus abdominalis*) in relation to feed ration. Aquaculture International 13, 305–314.

Yakir, D., da SL Sternberg, L., 2000. The use of stable isotopes to study ecosystem gas exchange. Oecologia 123, 297–311.

Zara, V., Palmieri, L., Giudetti, A., Ferramosca, A., Capobianco, L., Gnoni, G.V., 2000. The mitochondrial tricarboxylate carrier: unexpected increased activity in starved silver eels. Biochemical and Biophysical Research Communications 276, 893–898.

Declaration

I herewith declare that I have produced this work without the prohibited assistance of third parties and without making use of aids other than specified; notions taken over directly or indirectly from other sources have been identified as such. This work has not previously been presented in identical or similar form to any examination board. The dissertation work was conducted from 2014-2019 under the supervision of Prof.María M.Gomez Cabrera and Dr.Theodore T. Packard at the University of Las Palmas de Gran Canaria.

This dissertation was finished writing in Las Palmas de Gran Canaria on 15 of May of 2019.

María Teresa Tames Espinosa